ELUCIDATING THE ANTI-CANCER MECHANISM OF LOW DENSITY LIPOPROTEIN-MEDIATED DELIVERY OF DOCOSAHEXAENOIC ACID TO HEPATOCELLULAR CARCINOMA CELLS

APPROVED BY SUPERVISORY COMMITTEE

Ian Corbin, Ph.D.

Kathlynn Brown, Ph.D.

John Minna, M.D.

Joyce Repa, Ph.D.

DEDICATION

I wish to thank the numerous people who contributed to helping me complete this work. First and foremost, I would like to thank my mentor, Dr. Ian Corbin, for his guidance through the entirety of this project. His constant optimism, enthusiasm, and mentorship made it possible for me to continue through the challenges of research and created a safe environment for me to grow as a scientist. He also gave me many opportunities to work on aspects of our lab's research that would benefit me in pursuit of my career path into clinical laboratory assay design. He has been a continual source of support, wisdom, and knowledge. I am incredibly grateful for his open-door policy that allowed me to bounce ideas off of him and fostered my growth as a researcher.

I would also like to thank the current and past members of the Corbin Laboratory for their help on my research and my colleagues in the Advanced Imaging Research Center for their support. I would like to thank Tim Van Treuren and Esther Kim for their friendship and aid on many experiments during their time in the lab. I would also like to thank Dr. Xiadong Wen and Archana Dilip for their help with experiments when I first joined the lab. I would like to thank Dr. Rohit Mulik for being my nanoparticle-making machine and being a great research partner. I would like to give a

special thanks to Marilyn Jimmerson for knowing the answers to all my questions about department resources and for being a continual source of good cheer.

This work would not be possible without the help of my Thesis Committee members. Dr. Kathylnn Brown was a fantastic committee chair who provided great suggestions on how to improve my research and for providing advice about pursuing a career in science. Dr. Joyce Repa was a great resource for many of my research projects in terms of opening her lab to me so I could learn how to do mouse liver perfusions, providing reagents and Balb/C mice, and for providing help with the statistical analysis of my data. Lastly, I would like to thank Dr. John Minna for his unique perspectives on medicine and what is needed to get my research into a clinical setting.

Lastly, I would like to thank my family, my friends, and my husband, Eric Moss, for their constant support during my education. My parents ensured I had an education that fostered a love of learning through discovery and exploration. They were always willing to listen to my frustrations when “science didn’t like me” and have always encouraged me to pursue my education and my future career goals. My husband’s gentle encouragement urging me to finish my Ph.D. has been the greatest help during this journey and I look forward to many more journeys with him as we continue our lives together.

ELUCIDATING THE ANTI-CANCER MECHANISM OF LOW DENSITY LIPOPROTEIN-MEDIATED DELIVERY OF DOCOSAHEXAENOIC ACID TO HEPATOCELLULAR CARCINOMA CELLS

by

LACY REYNOLDS MOSS

DISSERTATION

Presented to the Faculty of the Graduate School of Biomedical Sciences

The University of Texas Southwestern Medical Center at Dallas

In Partial Fulfillment of the Requirements

For the Degree of

DOCTOR OF PHILOSOPHY

The University of Texas Southwestern Medical Center at Dallas

Dallas, Texas

Degree Conferral August, 2015

ELUCIDATING THE ANTI-CANCER MECHANISM OF LOW DENSITY LIPOPROTEIN-MEDIATED DELIVERY OF DOCOSAHEXAENOIC ACID TO HEPATOCELLULAR CARCINOMA CELLS

Publication No. 2

Lacy Reynolds Moss, Ph.D., MLS(ASCP)

The University of Texas Southwestern Medical Center at Dallas, 2015

Supervising Professor: Ian R. Corbin, Ph.D.

Hepatocellular carcinoma is a lethal malignancy with few effective therapy options. New selective treatments are urgently needed to destroy hepatocellular carcinoma cells without harming the surrounding normal hepatocytes. Recently, docosahexaenoic acid has been shown to possess promising anticancer properties. The Corbin laboratory has incorporated docosahexaenoic acid into low density lipoprotein nanoparticles (LDL-DHA) as a means to transport these fatty acids to cancer cells. To test LDL-DHA's efficacy, immortalized mouse normal liver (TIB-73) and isogeneic malignant liver (TIB-75) cell lines were compared. Cell

viability and co-culture experiments demonstrated that TIB-75 cells were more sensitive to LDL-DHA than TIB-73 cells. LDL-DHA enters into cells through LDL receptor-mediated endocytosis to the lysosomes. LDL-DHA treatment increased dichlorofluorescein fluorescence in TIB-75 cells over TIB-73 cells, and generation of reactive oxygen species by menadione sensitized TIB-73 cells to LDL-DHA. Importantly, TIB-75 cells were rescued from LDL-DHA cytotoxicity when antioxidants specific for removing lipid peroxide species were added indicating that lipid peroxidation was critical for LDL-DHA cytotoxicity. LDL-DHA also caused lysosomal membrane permeability of only the TIB-75 cells. Subsequent studies showed that only the LDL-DHA treated TIB-75 cells lose their mitochondrial membrane potential. Mitochondrial reactive oxygen species were elevated in TIB-75 cells following LDL-DHA treatment, and TIB-73 cells were sensitized to LDL-DHA after decoupling of mitochondrial respiration. LDL-DHA treatment also caused DNA damage selectively in the TIB-75 cells. When the Fenton reaction, an iron-catalyzed reaction that generates hydroxyl radicals and lipid peroxide species, was blocked by iron chelation, TIB-75 showed less LDL-DHA cytotoxicity, lipid peroxidation, and lysosome leaking. Studies conducted in human hepatocellular carcinoma cells (FOCUS, Hep3B, and Huh7) on LDL-DHA cytotoxicity, lysosome permeability, and mitochondrial reactive oxygen species production confirmed the findings seen in TIB-75 cells following LDL-DHA treatment. Furthermore, primary human hepatocytes were not sensitive to LDL-DHA treatment. In conclusion, these studies have shown that LDL-DHA is selectively cytotoxic to hepatocellular carcinoma cells and that iron-catalyzed lipid peroxidation sets off a subcellular chain of events resulting in increased reactive oxygen species, lysosome permeability,

mitochondrial dysfunction, DNA damage, and, ultimately, cell death in hepatocellular carcinoma cells.

TABLE OF CONTENTS

PRIOR PUBLICATIONS

"Reynolds, L., Mulik, R., Wen, X., Dilip, A., & Corbin, I. (2014). Low-density lipoprotein-mediated delivery of docosahexaenoic acid selectively kills murine liver cancer cells. *Nanomedicine,* doi: 10.2217/NNM.13.187"

LIST OF FIGURES

LIST OF TABLES

LIST OF APPENDICES

LIST OF ABBREVIATIONS

AA – Arachidonic Acid

AFB_1 – Aflotoxin-B_1

AIF – Apoptosis-Inducing Factor

ALT – Alanine Aminotransferase

AO – Acridine Orange

AP-1 – Activating Protein-1

AST – Aspartate Aminotransferase

ATP – Adenine Triphosphate

BSA – Bovine Serum Albumin

CCCP – Carbonyl Cyanide *m*-Chlorophenyl Hydrazone

CD – Circular Dichroism

CICD – Caspase-Independent Cell Death

COX – Cyclooxygenase

DCF-DA – Dichlorofluoroscein Diacetate

DCF – Dichlorofluoroscein

DFO – Deferoxamine

DHA – Docosahexaenoic Acid

DHE – Dihydroethidium

DMPC – l-α-dimyristoylphosphatidylcholine

DNA – Deoxyribonucleic Acid

EDTA – Ethylenediaminetetraacetic Acid

EGF – Epidermal Growth Factor

EPA – Eicosapentaenoic Acid

ERK – Extracellular Signal-Related Kinase

ETC – Electron Transport Chain

FFA – Free Fatty Acid

FST – Ferrostatin-1

GPx – Glutathione Peroxidase

GSH – Reduce Glutathione

GSSG – Oxidized Glutathione

HBV – Hepatitis B Virus

HCC – Hepatocellular Carcinoma

HCV – Hepatitis C Virus

HIF-1 – Hypoxia Inducible Factor-1

HNE – 4-Hydroxynonenal

HNF-α – Hepatocyte Nuclear Factor-α

HSA – Human Serum Albumin

IMM – Inner Mitochondrial Membrane

LDL – Low Density Lipoprotein

LMP – Lysosome Membrane Permeability

LNAC – N-Acetyl-L-Cysteine

LOX – Lipooxygenase

LPO – Lipid Peroxides or Peroxidation

LXR – Liver X Receptor

MDA – Malondialdehyde

MD-B – Menadione Bisulfite

MDR-1 – Multi-Drug Resistant Gene-1

MMP – Mitochondrial Membrane Potential

MOMP – Mitochondrial Outer Membrane Permeabilization

NAFLD – Non-Alcoholic Fatty Liver Disease

NASH – Non-Alcoholic Steatohepatitis

NF-κB – Nuclear Factor Kappa-Light-Chain-Enhancer of Activated B-Cells

Nrf2 – NF-E2-Related Factor 2

NQO1 – NAD(P)H:Quinone Oxidoreductase 1

OA – Oleic Acid

OMM – Outer Mitochondrial Membrane

PARP – Poly-ADP-Ribose Polymerase

PDGF – Platelet Derived Growth Factor

PEG – Polyethylene Glycol

PEI – Percutaneous Ethanol Injection

PPAR – Peroxisome Proliferator-Activated Receptor

PUFA – Polyunsaturated Fatty Acid

RF – Radiofrequency Ablation

RNA – Ribonucleic Acid

ROS – Reactive Oxygen Species

RSL – Ras-Selective Lethal

SIH – Salicyl-Aldehyde Isonicotinoyl Hydrazone

SOD – Superoxide Dismutase

SREBP – Sterol Regulatory Element-Binding Protein

TACE – Transarterial Chemoembolization

TBARS – Thiobarbituric Acid Reactive Substance

TCA – Tricarboxylic Acid

TIGAR – TP53-Induced Glycolysis and Apoptosis Regulator

TMRM – Tetramethylrhodamine Methyl Ester

TMS – Tetramethylsilane

TNF-α – Tumor Necrosis Factor-α

TO – Trioleic Acid/Triolein

TSP – Trimethylsilyl Propanoic Acid

VDAC – Voltage Dependent Anion Channel

VEGF – Vascular Endothelial Growth Factor

CHAPTER ONE
Introduction

The Research Problem: Its Purpose and Significance

Background of the problem

Hepatocellular carcinoma (HCC), or primary liver cancer, arises from malignant transformation of hepatocytes within the liver. It is the fifth most common cancer in the world and is the third leading cause of cancer-related deaths worldwide (Zhu, 2006). Treatment of hepatocellular carcinoma (HCC) has faced many challenges over the years and effective treatments for HCC are sadly lacking. A main problem surrounding HCC treatment is that HCC develops from chronic liver injury, inflammation, and repair resulting from many chronic liver diseases, such as alcoholic cirrhosis, non-alcoholic fatty liver disease (NAFLD), hepatotoxin exposure, and chronic infection with Hepatitis B Virus (HBV) or Hepatitis C Virus (HCV) (Bruix *et al.*, 2004; Farazi & DePinho, 2006; Gomaa *et al.*, 2008; Wang *et al.*, 2002).The vast range of HCC etiologies create many different tumorigenic mutations (Wang *et al.*, 2002), which hampers the widespread use of therapies that target a particular oncogenic pathway. Additionally, these patients have an expansive collection of background liver diseases and compromised liver function, which limits the use of more general cytotoxic chemotherapies as these could cause liver failure and death (Zhu, 2006). While there are some effective therapeutic options for HCC patients with early stage HCC,

such as resection, liver transplant, and percutaneous tumor treatments, therapeutic options for intermediate to late-stage HCC are very limited (El-Serag *et al.*, 2008). Currently, >80% of HCC patients are diagnosed with intermediate/late stage HCC (Zhu, 2006) and these patients can have a median survival as little as three to four months (Llovet & Bruix, 2008). The current standard of care for late stage HCC is sorafenib, a Raf kinase inhibitor, and it is able to improve survival by only three months (Llovet *et al.*, 2008). There is a desperate need for effective therapies that can selectively kill HCC cells without harm to the surrounding liver.

One way to approach cancer treatment is to take advantage of one of the "Hallmarks of Cancer" proposed by Hanahan and Weinberg (Hanahan & Weinberg, 2011). In addition to the original six hallmarks, the emerging hallmark that cancer cells deregulate cellular energetics is important in HCC. Additionally, HCC also utilizes the tumor-enabling characteristics of inflammation and genome instability and mutation. Oxidative stress is an important part of inflammation and more reactive oxygen species (ROS) are produced when cellular energetics, particularly in the mitochondria, are deregulated to promote tumorigenesis (Reuter *et al.*, 2010; Ward & Thompson, 2012).Low to moderate levels of reactive oxygen species promote tumorigenesis, cell cycle progression, cell-to-cell adhesion, metabolism, motility, angiogenesis, proliferation, and survival in cancer cells (Liou & Storz, 2010; Ozben, 2007). However, high levels of reactive oxygen species induce apoptosis and necrosis in cancer cells; interestingly, many chemotherapies generate ROS as part of their mechanism of action (Ozben, 2007; Pelicano *et al.*, 2004). Based on this information,

treatment of HCC with a therapeutic that generates oxidative stress in the HCC cells and not the normal cells would be ideal to minimize cytotoxicity to the liver tissue.

A promising molecule for the treatment of HCC is docosahexaenoic acid (DHA), which is an ω-3polyunsaturated fatty acid (PUFA) found in fish oil. DHA has been touted for decades for its beneficial effects on cardiovascular health and brain development (Horrocks & Yeo, 1999). More recently, DHA has been studied for its cancer preventative properties. Studies to date have shown that *in vitro* DHA is able to kill cancer cells from a variety of tissue types: breast (Kang *et al.*, 2010; Kim *et al.*, 2009; Larsson *et al.*, 2004; Sun *et al.*, 2011), colon (Chen & Istfan, 2000; Toit-Kohn *et al.*, 2009), lung (Serini *et al.*, 2008), leukemia (Miura *et al.*, 2004; Yamagami *et al.*, 2009), gastric (S. E. Lee *et al.*, 2009; H. Sun *et al.*, 2013; Wu *et al.*, 2010), and liver (C. Y. Lee *et al.*, 2010; Lim *et al.*, 2009; S. N. Sun *et al.*, 2013). The large number of double bonds in DHA's chemical structure makes it vulnerable to lipid peroxidation particularly in cancer cells that have increased ROS levels (Ding & Lind, 2007; Ding *et al.*, 2004; Gotoh *et al.*, 2002; Merendino *et al.*, 2005; Siddiqui *et al.*, 2008; Stoll, 2002) and intralysosomal iron storage (Toyokuni, 2014). Importantly, some studies have shown that DHA might even reduce some forms of chronic liver disease (Fernandez *et al.*, 1997; Sekiya *et al.*, 2003; Valenzuela *et al.*, 2012) based on its ability to inhibit the pro-inflammatory action of the cyclooxygenase (COX) and lipoxygenase (LOX) enzymes (Calder, 2006; Massaro *et al.*, 2006; Ringbom *et al.*, 2001), inhibit tumor-necrosis factor-α (TNF-α) (Weylandt *et al.*, 2011), and inhibit lipid peroxidation and DNA damage in normal hepatocytes (Gonzalez-Periz *et al.*, 2006). Because DHA works not only by generating ROS

in cancer cells, but also by inhibiting pro-inflammatory and pro-tumorigenic pathways, it may be an ideal therapeutic agent for HCC and experiments aimed to investigate how it differentially affects malignant and non-malignant cells are needed.

The main problem that is faced with using DHA *in vivo* as a therapeutic for cancers is its low saturation (≈12.5 μM) in plasma (Arterburn *et al.*, 2006; Conquer & Holub, 1998) and apparent saturation well below the therapeutic doses used in the *in vitro* studies (> 50 μM). Several groups have looked into the use of liposomes (Ichihara *et al.*, 2011) or small unilamellar vesicles (Jenski *et al.*, 1995; Kafrawy *et al.*, 1998) to carry DHA, but these are less than ideal for many reasons including poor bioavailability and stability, large particle size subject to removal by the mononuclear phagocytic system, and, in some cases, cytotoxicity from the liposome vehicle. One study enriched low density lipoprotein (LDL) with ω-3 PUFAs by feeding African Green Monkeys a fish-oil enriched diet for three years and they showed that this LDL was more cytotoxic to cancer cells *in vitro* than ω-3 PUFAs delivered by albumin (Edwards *et al.*, 2004). Dietary enrichment of LDL with ω-3 PUFAs is significantly hampered by low PUFA loading and the large time and expense required to attain this LDL. Importantly, dietary enrichment of LDL with DHA may not be sufficient to be cytotoxic to an established tumor. In order to overcome the problems with delivering cytotoxic doses of DHA *in vivo*, the Corbin laboratory incorporated DHA into LDL by the core reconstitution method (Reynolds *et al.*, 2014). With LDL now serving as a delivery vehicle DHA will enter the cancer cells by LDL receptor-mediated endocytosis and be shuttled to the lysosome rather than by diffusion into the cytosol as a free fatty acid. LDL-

mediated transport is likely to bring out important changes in DHA's cytotoxicity and mechanism of action in HCC and liver cells that need to be studied.

Statement of the problem

Research to date on the anti-cancer properties of DHA have focused on the effects of DHA (either solubilized with ethanol or conjugated to albumin) following its diffusion across the cell's plasma membrane. When DHA enters the cell by diffusion it is channeled along various pathways, which include transport out of the cell by fatty acid binding transporters, β-oxidation in the mitochondria and peroxisomes, incorporation into phospholipids, and energy storage as a triglyceride (Berg, 2007; Jump *et al.*, 2008; Le Borgne, 2012; Sampath & Ntambi, 2005). DHA in cancer cells is prone to lipid peroxidation and DHA and its metabolites can inhibit various cell pathways important for tumorigenesis and proliferation (Calviello *et al.*, 2007; Hardman *et al.*, 2002; Kang *et al.*, 2010; Lim *et al.*, 2009; Stoll, 2002; Xue *et al.*, 2014). Few studies, if any, have examined how the metabolism and cancer-selective cytotoxicity of DHA changes when it enters the cells via receptor-mediated endocytosis into the lysosome. Even the researchers that used hybrid liposomes of DHA did not examine the differences in cytotoxicity and mechanism of action between liposomal DHA delivery and free DHA (Ichihara *et al.*, 2011; Tanaka *et al.*, 2008), but rather focused on the differences between liposomes with or without DHA. Furthermore, these studies failed to examine how normal cells responded to the DHA liposomes or ω-3 PUFA-enriched LDL.

The research problem of this thesis work addressed the gaps in the literature regarding how DHA delivered by LDL (LDL-DHA) to the lysosome is more cytotoxic to HCC cells than DHA delivered by albumin, whether LDL-DHA is able to selectively kill HCC cells and spare the non-malignant liver cells, and what mechanisms of selective anticancer toxicity may be induced by LDL-DHA nanoparticles in HCC cells.

Purpose of the research

Studies into DHA's ability to kill established tumors *in vivo* have been hindered by DHA's low solubility in plasma, such that any further attempts to utilize DHA *in vivo* will require a system to deliver cytotoxic doses of DHA to tumors. Future research into DHA as an anti-cancer therapy should study DHA's cytotoxicity when it enters via endocytosis and how this changes DHA's intracellular effects on malignant and non-malignant cells. The general purpose of this research was to examine the cancer-selective cytotoxicity of LDL-mediated delivery of DHA in HCC and non-malignant liver cells. The specific purpose of this research was, first, to examine the inherent differences between syngeneic malignant and non-malignant liver cells before and after LDL-DHA treatment to determine what alterations in malignant cells make them more susceptible to LDL-DHA cytotoxicity, and, second, to examine intracellular changes in oxidative stress and organelle integrity following DHA's delivery via receptor-mediated endocytosis or diffusion.

Significance of the research

The study of LDL-DHA as a cancer-selective therapeutic agent in HCC is important because HCC has a very poor prognosis and limited therapeutic options especially in patients with liver disease and/or late-stage HCC. This research is significant for the field of cancer treatments as dose-limiting cytotoxicity is a problem faced in the treatment of many cancers including HCC using traditional chemotherapeutics. DHA has been shown to be cytotoxic to cancers from many tissues *in vitro*, but the *in vivo* studies, especially as an adjuvant to standard of care chemotherapy in humans, have had mixed results due to insufficient delivery of DHA *in vivo* (Berquin *et al.*, 2008; Biondo *et al.*, 2008; Bougnoux *et al.*, 2009; Fauser *et al.*, 2011; Merendino *et al.*, 2013; Murphy *et al.*, 2011). If DHA is to ever be considered an effective adjuvant or stand-alone therapy option for cancer treatment, DHA delivery *in vivo* will need to be increased substantially. LDL-DHA delivery offers a unique solution to reach high DHA concentrations *in vivo*, but delivery to the lysosome may change DHA's cytotoxicity in cancer and in the normal tissues. If it is shown that LDL-DHA has cancer-selective cytotoxicity, then LDL-DHA could be a stand-alone therapeutic or an adjuvant to standard of care in a host of different malignancies. This research could be further expanded in the future to study the *in vivo* efficacy of LDL-DHA in HCC and in other malignancies. Delivery of DHA by diffusion results in an increase in ROS and inhibition of multiple pro-tumorigenic pathways, which makes DHA unique among current cancer treatments and it could reduce the development of drug resistance in cancer cells. These actions may be changed by lysosomal delivery of DHA, so previous research done by other groups on DHA's anti-cancer properties may not apply. Probing the mechanism of action of LDL-DHA's cytotoxicity in cancer and normal cells is important to determine how lysosomal

delivery of DHA changes its cytotoxicity profile. It is important to study not only DHA's anti-cancer effects, but also its effects on normal tissue since a major requirement for HCC treatments is to avoid harming the surrounding liver tissue. The field of cancer research is currently divided as to whether the use of pro-oxidants or antioxidants in cancer treatments are best to enhance drug cytotoxicity or reduce side effects, respectively (Ozben, 2007; Pelicano *et al.*, 2004). Studying the inherent differences between malignant and non-malignant tissues and their sensitivity to oxidative stress can give important insight as to why a ROS-producing treatment, such as DHA, selectively kills malignant cells and how LDL delivery could enhance their cytotoxicity. This knowledge can have broad utility to researchers studying cancer therapeutics or nanoparticle delivery systems in order to show how drug delivery into the cell can exploit inherent differences between malignant and non-malignant tissues. Importantly, the use of DHA, a naturally-occurring fatty acid, to treat cancer may elicit more research into the anti-cancer properties of other naturally-occurring molecules that have been neglected due to problems with delivering cytotoxic doses *in vivo*.

Research Aims, Hypotheses, and Design

Treatment and test groups

In order to examine the selective cytotoxicity of DHA on HCC and normal liver cells, cells were treated with LDL-DHA along with vehicle and untreated controls. The vehicle controls for LDL-DHA were native LDL, LDL-Oleic Acid (LDL-OA) or LDL-Triolein (LDL-TO) and cells were treated with an equivalent amount of these vehicles based on LDL-DHA's

protein content. In some experiments, human serum albumin conjugated to DHA (HSA-DHA) was used to test for differences between DHA delivery via endocytosis or diffusion and equal concentrations of DHA were used in both LDL-DHA and HSA-DHA groups.

The main cell lines used in these experiments were syngeneic non-malignant and malignant mouse hepatocyte cell lines. TIB-73 cells (BNL CL.2) are SV-40 immortalized fetal hepatocytes derived from Balb/C mice and TIB-75 cells (BNL 1ME A.7R.1) are malignant cells that were chemically transformed from TIB-73 cells (Patek *et al.*, 1978). The TIB-73 and TIB-75 cells were obtained from ATCC and maintained in DMEM plus 10% fetal bovine serum (FBS), and primary BALB/c mouse hepatocytes were obtained from liver perfusion isolation and cultured according to the protocol by Katsura *et al* (2002) to maintain their differentiated state.

In order to test whether the experimental findings observed in TIB-73 and TIB-75 cells translated over to human HCC cells. The following human cell lines were used: Hep3B (HB-8064), a hepatocellular carcinoma cell line positive for Hepatitis B virus derived from a juvenile male; Huh7 (JCRB Cell Bank, JCRB0403), a well-differentiated hepatocellular carcinoma cell line derived from an adult male; and FOCUS (cell line established by the Quaroni lab), a poorly differentiated hepatocellular carcinoma cell line positive for Hepatitis B virus (He *et al.*, 1984). Hep3B, Huh7, and FOCUS cells were treated with LDL-DHA, LDL-OA, HSA-DHA, or media. The use of these three cell lines enabled the study of LDL-DHA efficacy and metabolism in a spectrum of HCC derived from different liver disease

states. Additionally, primary human hepatocytes were used in one experiment to test for LDL-DHA and LDL-OA cytotoxicity and they were cultured according to the supplier's recommendations to maintain their differentiated state. The difficulty and cost associated with primary human hepatocytes precluded their use in the mechanistic studies of LDL-DHA's cytotoxicity.

Methodology overview

All cell lines were grown to 80-90% confluency and serum starved for six to eighteen hours prior to treatment with LDL-DHA, LDL vehicles, or HSA-DHA to minimize variation in results due to differences in treatment time or cell growth phases. Cells within an experiment were always treated with the same batch of LDL-DHA or vehicle to minimize variation in results due to batch differences. Following treatment, samples were tested simultaneously to minimize between-assay variations, and sample values were normalized to cell number or cell protein as necessary. In assays where between-run variation was high, samples were normalized to untreated controls to allow for comparison between runs. All experiments were repeated a minimum of three times and, where possible, triplicate samples were tested in each assay to control for within-assay variations. Where possible, standard curves or a positive and/or negative control were included in assays to ensure the assays were working properly. Sample data collection and analysis was conducted identically for samples regardless of cell type or treatment group to remove user bias, which is a particular problem in microscopy image and flow cytometry data analysis. Data was analyzed by *t*-test or ANOVA corrected for multiple comparisons as appropriate to determine statistical

significance. These controls in methodology were designed to minimize error variance, extraneous variance, and confounding variables in the experimental design so the results of these experiments can be considered reliable upon peer-review.

Aim 1: Determination of LDL-DHA's physicochemical properties, LDLR binding and uptake, and escape from the lysosome

The first sub-aim was to determine the physicochemical properties of LDL-DHA and the other LDL nanoparticles compared to native LDL in terms of changes to ApoB-100 secondary structure, particle diameter, particle surface charge, phospholipid content, and lipid cargo loading. The rationale for this experiment was to ensure that reconstitution of LDL with DHA did not significantly alter the native LDL structure to impact binding to LDL receptors on cells. It was hypothesized that LDL-DHA would maintain similar characteristics to native LDL.

The second sub-aim was to measure LDL receptor (LDLR) protein expression levels along with LDLR binding affinity and specificity to native LDL and LDL-DHA in both TIB-73 and TIB-75 cells. The first rationale for this experiment was to determine if TIB-73 and TIB-75 cells have different LDLR protein expression and uptake of LDL since many cancer cells over-express LDLR. An increased LDL-DHA cytotoxicity in TIB-75 cells could then be due to increased uptake (Firestone, 1994). The second rationale was to determine the LDLR binding affinity and specificity to native LDL and reconstituted LDL nanoparticles in order to determine if the reconstitution procedure altered LDL-DHA binding to LDLR. It was

hypothesized that TIB-75 cells would have slightly higher LDLR expression and internalization than TIB-73 cells and that LDL reconstitution with DHA would have minimal effects on LDLR binding compared with native LDL.

The third sub-aim to be evaluated in this research was to investigate the endocytosis and shuttling of native LDL and LDL-DHA to the lysosome in TIB-73 and TIB-75 cells. The rationale for this experiment was to show that LDL-DHA enters the TIB-73 and TIB-75 cells through receptor-mediated endocytosis to the lysosome, rather than by some other pathway. It was hypothesized that both native and LDL-DHA would colocalize strongly with the lysosome in both TIB-73 and TIB-75 cells.

The final sub-aim was to determine whether inhibition of LDL degradation in the lysosome blocked LDL-DHA cytotoxicity in TIB-75 cells. The rationale for this experiment was to determine how LDL-DHA is degraded in the lysosome or if LDL-DHA degradation was even necessary for LDL-DHA cytotoxicity in TIB-75 cells. It was hypothesized that blocking lysosome acidification and lysosome protease activity would inhibit LDL-DHA cytotoxicity in TIB-75 cells.

Aim 2: Establish the selective cytotoxicity of LDL-DHA on HCC cells over normal hepatocytes in vitro *and the mode of cell death*

The first sub-aim of this research was to determine the therapeutic window of LDL-DHA and HSA-DHA cytotoxicity in a panel of mouse and human HCC and hepatocyte cells. The

rationale was to show that DHA may be a safe and effective therapeutic alternative for patients with HCC by establishing that DHA was more toxic to cancer cells than normal cells over a range of treatment doses. Additionally, this research sought to demonstrate that LDL-DHA was equally effective or more effective than HSA-DHA at inducing cytotoxicity in HCC cells. It was hypothesized that both LDL-DHA and HSA-DHA would be more cytotoxic to the HCC cells than the normal liver cells to create a therapeutic window for treatment, and that the LDL-DHA would have a lower IC_{50} than HSA-DHA in the HCC cells.

The second sub-aim was to examine the selective cytotoxicity of LDL-DHA on HCC cells and hepatocytes when they were co-cultured to simulate *in vivo* conditions. The rationale for this experiment was to establish that LDL-DHA would maintain its selective cytotoxicity to HCC cells even in the presence of normal hepatocytes. This experiment simulated *in vivo* conditions since both the HCC and normal hepatocytes would be exposed side-by-side to LDL-DHA's potential cytotoxic effects. It was hypothesized that LDL-DHA would maintain its selective cytotoxicity to HCC cells when they were cocultured and the non-malignant cells would remain unharmed by the adjacent HCC cell death.

The third sub-aim was to determine the mode of cell death induced by LDL-DHA in HCC and normal liver cells. The rationale for these experiments were to determine if LDL-DHA treatment caused activation of apoptosis, necrosis, autophagy, or some other cell death pathway especially since free DHA has been shown to induce apoptosis *in vitro* by other

investigators (Kang *et al.*, 2010; Lim *et al.*, 2009; Toit-Kohn *et al.*, 2009). It was hypothesized that LDL-DHA would cause cell death in HCC cells by a combination of apoptosis and necrosis as both cell death pathways can be induced by oxidative stress.

Aim 3: Determination of the role of ROS in LDL-DHA cytotoxicity in HCC and normal liver cells

The first sub-aim was to measure the baseline levels of different reactive oxygen species in TIB-73 and TIB-75 cells and their baseline levels of different antioxidants. The rationale for these experiments was to examine the inherent differences between HCC and normal liver cells in terms of their initial oxidative stress and ability to respond to increased oxidative stress. It was hypothesized that TIB-75 cells would have higher ROS levels and lower antioxidant capacity than TIB-73 cells at baseline.

The second sub-aim was to determine how LDL-DHA treatment affects ROS levels in HCC and normal liver cells. The rationale for this experiment was based on the previous literature on DHA which showed that DHA mediates anticancer cytotoxicity by increasing ROS and lipid peroxidation (Ding & Lind, 2007; Ding *et al.*, 2004; Gotoh *et al.*, 2002; Merendino *et al.*, 2005; Siddiqui *et al.*, 2008; Stoll, 2002). It was hypothesized that LDL-DHA treatment would increase ROS/lipid peroxide production in the human HCC cells compared to untreated controls and TIB-75 cells would also have a higher increase in ROS/lipid peroxide production compared to TIB-73 cells following LDL-DHA treatment.

The last sub-aim was to determine which ROS species are necessary for the cytotoxic action of LDL-DHA in HCC cells by treating TIB-75 cells with antioxidants to remove superoxide radicals, hydrogen peroxide, and lipid peroxide species or by inducing ROS to increase TIB-73 cell sensitivity to LDL-DHA. The rationale behind this experiment was to determine which ROS species are critical for LDL-DHA cytotoxicity. It was hypothesized that hydrogen peroxide and lipid peroxides would be critical for LDL-DHA cytotoxicity in TIB-75 cells and that increasing ROS would sensitize TIB-73 cells to LDL-DHA cytotoxicity.

Aim 4: Determination of LDL-DHA's subcellular effects on lysosome integrity, mitochondrial function, and DNA damage

The first sub-aim was to determine the effects that LDL-DHA and HSA-DHA have on lysosome membrane integrity in HCC and normal liver cells. The rationale for conducting this experiment was based on the premise that when LDL-DHA is delivered to the lysosome, DHA can affect the fluidity and permeability of cell membranes (Stillwell *et al.*, 1993). Furthermore, lipid peroxidation has been tied to increasing lysosomal membrane permeability (LMP) (Johansson *et al.*, 2010). It was hypothesized that LDL-DHA rather than HSA-DHA would cause LMP in HCC cells and that the normal liver cells would not have LMP with LDL-DHA treatment.

The second sub-aim was to determine the effect of LDL-DHA on mitochondrial membrane potential (MMP) in TIB-73 and TIB-75 cells and the role of mitochondrial ROS production in LDL-DHA sensitivity in HCC and normal liver cells. The rationale behind this series of

experiments was that DHA is known to incorporate into cardiolipin in the mitochondria and change ROS production and mitochondrial function due to changes in membrane fluidity and peroxidation caused by DHA (Gogvadze *et al.*, 2008; Hong *et al.*, 2002; Ng *et al.*, 2005; Siddiqui *et al.*, 2008; Watkins *et al.*, 1998). It was hypothesized that TIB-75 cells treated with LDL-DHA would have loss of MMP and increased mitochondrial ROS production and these findings would not be observed in TIB-73 cells. It was also hypothesized that increasing mitochondrial ROS production in TIB-73 cells prior to LDL-DHA treatment could increase their sensitivity to LDL-DHA.

The last sub-aim was to determine the effect of LDL-DHA on DNA damage in TIB-73 and TIB-75 cells. The rationale for this experiment was based on the previous literature which shows that lipid peroxide species and their metabolites can form damaging adducts with DNA (Cao *et al.*, 1995; Valko *et al.*, 2007). It was hypothesized that LDL-DHA treatment would induce DNA damage in TIB-75 and not TIB-73 cells due to the increased lipid peroxidation and ROS present in TIB-75 cells.

Aim 5: Determination of the effect of iron chelation on LDL-DHA cytotoxicity, lipid peroxidation, and lysosomal and mitochondrial damage

The first sub-aim explored whether iron chelation reduced the cytotoxic effects of LDL-DHA in TIB-73 and TIB-75 cells. The rationale behind this experiment is based on the importance of labile iron in catalyzing the Fenton reaction. The Fenton reaction generates hydroxyl radicals or lipid peroxide species in the presence of labile iron and ROS (hydrogen peroxide

or superoxide radical) (Valko *et al.*, 2007). Lysosomes contain a large pool of labile iron and are hot spots for the Fenton reaction to occur. Iron storage in the lysosomes is increased in proliferative and metabolically active cells, as there is more protein turnover and organelle autophagy (Boya & Kroemer, 2008; Dixon & Stockwell, 2014; Toyokuni, 2014). Given the importance of the Fenton reaction in lipid peroxidation and its localization to the lysosome, it was important to explore the role of iron chelation as a potential mediator of LDL-DHA cytotoxicity in HCC cells. It was hypothesized that iron chelation by deferoxamine (DFO) would rescue cytotoxicity of LDL-DHA in TIB-75 cells.

The second sub-aim was to look at the role of DFO on lipid peroxidation in TIB-73 and TIB-75 cells with or without LDL-DHA treatment. The rationale behind this was to show that iron chelation can effectively prevent lipid peroxidation occurring from the Fenton reaction in these cells. It was hypothesized that DFO pretreatment would reduce lipid peroxidation following LDL-DHA treatment in TIB-73 and TIB-75 cells.

The final sub-aim determined the beneficial effects of iron chelation by DFO in TIB-73 and TIB-75 cells on LMP and MMP loss after LDL-DHA treatment. The rationale behind these experiments was based on the fact that lipid peroxidation can permeabilize lysosome membranes and affect mitochondrial function; conversely, blocking lipid peroxidation by iron chelation could ameliorate LDL-DHA's negative effects on these organelles. It was hypothesized that DFO pretreatment would reverse LMP and MMP loss caused by LDL-DHA.

Assumptions, Limitations, and Delimitations of the Research

Assumptions that were made in this research were that the TIB-73 and TIB-75 cells differ in sensitivity to LDL-DHA based only on the genetic mutations in TIB-75 cells that make it malignant. Because TIB-75 cells were chemically transformed from TIB-73 cells, many mutagenic events occurred that may or may not contribute to TIB-75 cells malignancy and their sensitivity to LDL-DHA. Furthermore, TIB-73 cells are an immortalized fetal hepatocyte cell line, which may not behave in the same way to LDL-DHA as primary adult hepatocytes. In order to account for this assumption, primary Balb/C hepatocytes were tested for their sensitivity to LDL-DHA and they were found to be less sensitive to LDL-DHA than TIB-73 cells so it was assumed that the observations made in TIB-73 are largely applicable to primary hepatocytes.

For the LDL-DHA mechanistic studies in human liver cells, only HCC cell lines were investigated due to expense and difficulty associated with the primary human hepatocytes. In the future, perhaps an immortalized human hepatocyte cell line (equivalent to TIB-73) could be obtained and compared with FOCUS, Hep3B, and Huh7 cells to study the mechanisms facilitating LDL-DHA's anticancer effects. One limitation of this study was that it did not probe the mechanism of lysosome membrane permeability and mitochondrial dysfunction caused by LDL-DHA and their individual roles in cell death and it was assumed that lipid peroxidation of DHA played a major role in these events. A final limitation to this study was

that the mode of cell death caused by LDL-DHA was not explored in depth beyond treatment with cell death inhibitors. In the future, studies should look for biological markers, such as caspase cleavage and Bcl-2 family member activation and localization, following LDL-DHA treatment.

While this research did examine the cytotoxicity and mechanism differences between LDL-DHA and HSA-DHA to some extent, the main purpose of this research was to examine LDL-DHA in HCC and normal cells. This meant that some experiments in this research did not include HSA-DHA as a variable. Notably, the effect of HSA-DHA in the human HCC cells was limited to a dose-response curve and subsequent experiments looking into DHA's effects on lipid peroxidation and organelle integrity did not include HSA-DHA, even though Hep3B cells showed a marked sensitivity to HSA-DHA. A second major delimitation on this research was that it did not cover the role of LDL-DHA or HSA-DHA on activating or inhibiting different cell signaling pathways and nuclear transcription factors. These signaling processes can be explored in future experiments. A final delimitation to the scope of this research was the limited number of organelles that were studied, future studies should also investigate the effects of LDL-DHA treatment on the endoplasmic reticulum and peroxisome compartments.

CHAPTER TWO
Review of the Literature

Hepatocellular Carcinoma: Etiology, Pathogenesis, and Current Treatments

Hepatocellular carcinoma (HCC), also known as primary liver cancer, arises from malignant transformation of hepatocytes within the liver. It is the fifth most common cancer in the world and is the third leading cause of cancer-related deaths worldwide (Zhu, 2006). Within the United States, the annual incidence of HCC has increased from 3.1 to 5.1 cases per 100,000 between 1992 to 2005 with an estimated 80% increase over the past two decades (Gomaa *et al.*, 2008). The liver cancer mortality rates in the United States rose similarly from 3.3 to 4.0 deaths per 100,000. Models based on the incidence of chronic Hepatitis C infection, a main risk factor for HCC development, predict that HCC incidence will continue to rise in the upcoming decades (Altekruse *et al.*, 2014; Research, 2011). The following section will explore the causes of HCC development and the limitations of the current standard of care for HCC patients.

Hepatocellular carcinoma develops from chronic inflammation and repair

The liver is the main organ responsible for drug detoxification in the mammal. The liver is responsible for metabolic activation and elimination of toxic chemicals, including ethanol, and their intermediates. These chemicals or reactive oxygen species (ROS) generated from

their metabolism may induce liver damage and increase the risk of hepatocellular carcinoma (Sakurai *et al.*, 2008). Many environmental factors affect the development of HCC but a main characteristic from these environmental factors is the development of chronic hepatitis and/or cirrhosis. Chronic hepatitis and cirrhosis, arise from persistent injury to the liver which results in a continual cycle of liver cell death, regeneration and activation of Kupffer cells (resident macrophages in the liver) and other immune cells (Sakurai *et al.*, 2008). Hepatocytes are regenerated to maintain liver mass, but this continual regeneration after repeated injury makes them more prone to mutation especially when cell checkpoints become compromised. This results in preneoplastic lesions that become progressively more dysplastic and proliferative as more damage, inflammation, and repair occur in the liver. These dysplastic lesions grow in size, neovascularize via the hepatic artery, dedifferentiate and become truly malignant, and eventually these cells metastasize to surrounding organs (Figure 1-1) (Bruix *et al.*, 2004). Chronic Hepatitis B Virus (HBV) and Hepatitis C Virus (HCV) infection account for more than 80% of HCC cases worldwide (X. W. Wang *et al.*, 2002). Risk of HCC development with chronic HBV or HCV infection increases 1000-times if liver cirrhosis is also present (Gomaa *et al.*, 2008). Of the 170 million people with HCV, around 20–30% will develop cirrhosis and once cirrhosis is established one third of those HCV-infected patients will develop HCC (3-5% annual incidence) (Llovet & Bruix, 2008). Epidemiological studies estimate that it takes ≈29 years from time of HCV infection to development of HCC (Gomaa *et al.*, 2008). Chronic HBV infections provide a 100-fold relative risk for developing HCC and a 2-6% annual incidence in cirrhotic patients (Llovet & Bruix, 2008). It is not clear whether virus infection with HBV or HCV itself initiates tumor

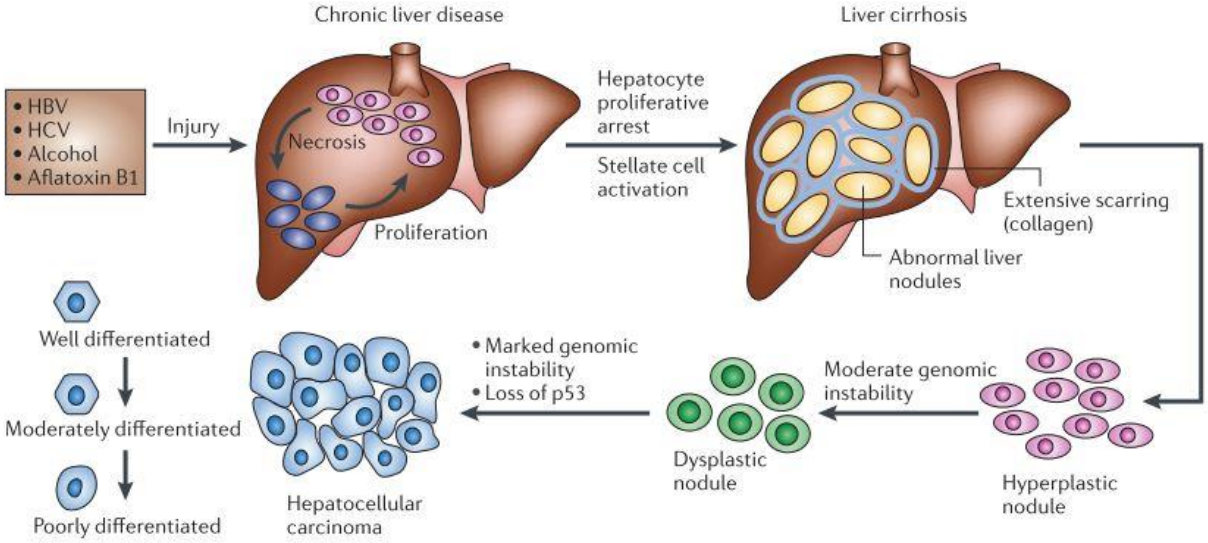

Figure 1-1: Histopathological development of hepatocellular carcinoma

After hepatocyte injury caused by any number of factors (HBV, HCV, AFB_1, alcohol, lipotoxicity), there is hepatocyte necrosis followed by proliferation. Continuous cycles of damage, inflammation, and repair promote liver disease resulting in abnormal nodule formation surrounded by collagen deposition and scarring. Hyperplastic nodules result that are prone to genomic instability and further progress to dysplastic nodules. Given time and more genomic alterations, these dysplastic nodules will result in hepatocellular carcinoma and become progressively more dedifferentiated and malignant. Adapted by permission from Macmillan Publishers Ltd: [NATURE REVIEWS CANCER] (Farazi & DePinho), copyright (2006).

formation or whether the inflammation resulting from the immune response to the viral infection causes tumor formation. Both HBV and HCV infections cause inflammation that result in free radicals, chemokines, and cytokines release causing DNA damage (Hussain *et al.*, 2007). DNA damage resulting from inflammation is normally resolved through the p53 pathway. The HBx gene of HBV reduces nucleotide excision repair in the cells and binds to p53 and inactivates p53-dependent activities (Hussain *et al.*, 2007). Additionally, HBx blocks p53-mediated apoptosis and deregulates cell cycle check point controls in infected cells. Chronic HBV and HCV infections cause upregulation of Tumor Necrosis Factor-α,

Interferon-γ, and Interleukin-1, which results in activation of iNOS, a protein involved production of DNA-damaging nitric oxide radicals (Hussain *et al.*, 2007). Nitric oxide radical production also activates cyclooxygenase-2 resulting in release of prostaglandin E2 which inhibits the apoptotic pathway and activates the WNT pathway (Hussain *et al.*, 2007). In addition to WNT pathway changes, approximately half of patients with HCC have Akt/mTOR signaling pathway activation (Llovet & Bruix, 2008). All of these actions cumulatively create an environment in the liver that is prone to proliferation and DNA damage with no way to repair that damage or to induce apoptosis, which leads to hepatocarcinogenesis.

In western countries, over 90% of patients with HCC also have liver cirrhosis. In Asia and Africa, greater than half of the HCC cases have cirrhotic livers (Gomaa *et al.*, 2008). A major causative agent for HCC development in these developing regions is environmental exposure to aflotoxin-B_1 (AFB_1), a mycotoxin produced by Aspergillus *spp* that commonly contaminates food (corn, rice, peanuts, and legumes) in developing countries. AFB_1 increases risk for HCC development through a point mutation of codon 249 (G:C to T:A transversion) of TP53, a tumor suppressor gene. In areas with high AFB_1 exposure, as much as 40% of HCC cases are attributable to AFB_1. AFB_1 can cause oxidative and nitrosative stress and lipid peroxidation (LPO) may indirectly cause TP53 249 codon mutations (Gomaa *et al.*, 2008; Hussain *et al.*, 2007).

Additional risk factors independent of HBV or HCV infection or toxin exposure for development of HCC include diabetes mellitus, non-alcoholic fatty liver disease (NAFLD), non-alcoholic steatohepatitis (NASH), iron and copper deposition, and alcoholic cirrhosis (Bruix *et al.*, 2004; Gomaa *et al.*, 2008). NAFLD is contributing more to HCC development as obesity and metabolic syndrome increases in the United States. NAFLD and the more severe NASH are defined as intrahepatic accumulation of free fatty acids and triglycerides resulting in hepatocyte injury and apoptosis due to cytokine induction and oxygen radical generation. The lipotoxicity induced by free fatty acid and triglyceride accumulation and their subsequent peroxidation in hepatocytes promotes liver fibrosis and cirrhosis and in some cases HCC (Farazi & DePinho, 2006).

Background liver damage limits therapeutic options for hepatocellular carcinoma

Current standard of care for early stage HCC (patients with a single lesion < 5 cm or three or fewer lesions that are < 3 cm) is tumor resection, liver transplantation or percutaneous tumor treatment. These interventions are considered curative yielding a 50-70% survival after five years. Unfortunately, even after successful resection or tumor ablation, 50% of patients will have tumor recurrence or *de novo* tumor formation within three years. Patients with intermediate stage HCC (multinodular asymptomatic lesions > 5 cm without vascular invasion) are treated not only based on tumor size, number of nodes, but also based on liver function. Patients with sufficient liver function may receive trans-arterial chemoembolization (TACE), percutaneous ethanol injection (PEI), or radiofrequency ablation (RF) of the tumor

nodules and if the nodules respond well, then resection of the remaining tumor is possible. After these interventions, the five year survival is 40-70%, but that survival is largely dependent on liver function and initial tumor node size. Recently, the use of radioembolization using radioactive yttrium-90-labeled microspheres has been used in the treatment of primary and metastatic hepatic cancers, but only patients with sufficient liver function (albumin >3g/dL and bilirubin <2.0 mg/dL) are candidates for this treatment. Use of radioembolization has less toxic side effects with similar or slightly improved patient outcomes compared to TACE (Kennedy & Salem, 2010; Salem *et al.*, 2011). Most HCC patients (>80%) are diagnosed with an advanced stage of disease which presents with symptomatic multinodular lesions, poor liver function, and vascular or extrahepatic spread (Zhu, 2006). In the case of patients with advanced stage HCC, the median survival is 3-4 months and currently only sorafenib, a multi-kinase inhibitor, is approved as treatment in these patients. Sorafenib treatment extends survival approximately 3 months (Llovet & Bruix, 2008). Unfortunately, patients with advanced HCC are not candidates for resection or liver transplant (El-Serag *et al.*, 2008), and traditional chemotherapy has many adverse side effects that are intolerable in patients with liver disease. To date, a wide range of systemic chemotherapies (doxorubicin, VP-16, mitoxantrone, cisplatin, paclitaxel, capecitabine, gemcitabine, ironotecan, nolatrexed, and irofulven) have been studied to improve clinical outcomes in HCC, but none of these agents, singly or in combination, significantly improved patient survival and combined therapy attempts increased adverse side effects (Zhu, 2006). Another hurdle to treating HCC is the heterogeneity of tumors between patients because of the many etiologies and risk factors leading to hepatocarcinogenesis (hepatitis, cirrhosis,

NAFLD, etc.), which makes it difficult to design universally-applicable, targeted chemotherapies for HCC. Furthermore, HCC tumors are inherently chemoresistant because of their expression of the multi-drug resistant gene-1 (MDR-1).

Overall the efficacy of current therapies available for HCC is largely dependent on the stage at diagnosis and the liver function of the patient. Given that there are limited treatment options for the majority of patients diagnosed with HCC, it is critical to develop therapeutic options that are selectively cytotoxic to the tumor and not the surrounding liver.

Docosahexaenoic Acid: A Cancer-Fighting Omega-3 Free Fatty Acid

A prospective cohort study conducted in Japan (n = 90,296) found that increased fish consumption lowered the incidence of HCC even in high-risk populations with chronic HBV and HCV infections (Sawada *et al.*, 2012). One candidate for a nontoxic and effective therapy for HCC is the ω-3 polyunsaturated fatty acid (PUFA), docosahexaenoic acid (DHA, ω-3 22:6; 4, 7, 10, 13, 16, 19). DHA is a naturally-occurring fatty acid that is commonly found in cold water fish and has been studied for many years as a cancer preventative agent, but little is known about its effect on established tumors. Problems with the use of DHA as a cancer therapy lie in difficulties with delivery of sufficient doses of DHA and understanding how DHA is selectively killing cancer cells while leaving normal cells unharmed. The following section will review what is known about DHA from its structure, transport, metabolism, health benefits, anti-cancer properties and challenges with *in vivo* delivery.

The unique structure of docosahexaenoic acid

DHA consists of 22 carbons and 6 double bonds at carbons 4, 7, 10, 13, 16, and 19 (Figure 3-1A). The length and high number of double bonds makes DHA unique among other naturally produced free fatty acids (FFA) because it is metabolized differently than shorter free fatty acids and is more vulnerable to LPO due to its high degree of unsaturation. The length and unsaturation also make its structure more fluid so that its incorporation into phospholipids affects membrane permeability, fluidity, and lipid raft formation, all of which have important effects on different areas of cell regulation (Bruno *et al.*, 2007; Shaikh *et al.*, 2009; Stillwell *et al.*, 2005). DHA also exerts biological effects by altering eicosanoid metabolism, gene expression, protein trafficking, and cell signaling (Shaikh *et al.*, 2009). These effects will be explored in greater detail later in this review.

Normal intracellular uptake of docosahexaenoic acid

Long chain fatty acids like DHA are predominantly transported in the plasma bound to albumin. Albumin has at least 7 fatty acid binding sites and usually only 1-2 of those sites are occupied at a time. One hypothesis for the entry of long-chain fatty acids into the cells is by free diffusion. In this model, ionized long chain fatty acids dissociate from albumin, and flip into the outer leaflet of the plasma membrane so that the charged carboxylic head aligns with the water interface of the membrane and the hydrophobic tail aligns with the fatty acid tail of the phospholipid. From that position, the fatty acid can flip to the inner membrane and into the cell cytoplasm where it either remains free to flip out of the cell once again or is trapped

intracellularly by enzymes such as acyl-CoA synthase, caveolin-1, fatty acid transport proteins (Guo *et al.*, 2006; Kamp & Hamilton, 2006). This model is regulated by a concentration gradient of free fatty acids across the membrane. A second hypothesis claims that free fatty acids bound to albumin are taken up by the cell via an unspecified transport protein where albumin binds to its receptor and transfers the free fatty acids to cytosolic fatty acid binding protein (FABP) for transport in the cell (Kamp & Hamilton, 2006). DHA is present at 50 mol% in the phospholipids of brain, sperm, and retina cells and as low as 5 mol% in phospholipids of other cell types. Dietary supplementation with DHA will increase its inclusion in tissues that normally have low DHA levels (Stillwell *et al.*, 2005).

Metabolism of docosahexaenoic acid

Hepatocytes are able to take up large amounts of fatty acids from the circulation for oxidation and lipid synthesis. Once inside the cell, fatty acids have a variety of fates. Fatty acids can be esterified into membrane phospholipids, stored as triglycerides, or be transported to the mitochondria or peroxisomes for oxidation (Berg, 2007; Le Borgne, 2012). Long chain fatty acids (>20 carbons), such as DHA, can undergo β-oxidation in the peroxisomes or mitochondria whereas shorter chain fatty acids are oxidized solely in the mitochondria (Stoll, 2002). Experimental studies show that initial β-oxidation of DHA occurs preferentially in the peroxisomes (Madsen *et al.*, 1999). Before undergoing β-oxidation, fatty acids are activated to an acyl-CoA form in the cytosol by an ATP-dependent reaction catalyzed by acyl-CoA synthases. Once in the acyl-CoA form, fatty acids are transported to the mitochondria or peroxisome. Mitochondrial β-oxidation's main function is to provide

energy and produces $FADH_2$, NADH, and acetyl CoA through many series of β-oxidation steps (Berg, 2007; Le Borgne, 2012). On the other hand, oxidation that occurs in the peroxisome is for detoxification and production of bioactive molecules and yields hydrogen peroxide instead of $FADH_2$ after the first reaction and generates other unique oxidation products that may inhibit carcinogenesis (Berg, 2007; Le Borgne, 2012). DHA can also be oxidized in microsomes after four oxidation steps utilizing microsome cytochrome P-450 monooxygenases (VanRollins *et al.*, 1984). In hepatocytes, only a small amount of fatty acids will undergo β-oxidation, and the rest will be assimilated into polar and neutral lipids or shuttled to the nucleus to interact with transcription factors (Jump *et al.*, 2008). The cyclooxygenase- (COX) and lipooxygenase- (LOX) mediated oxidation of PUFAs can form metabolites (eg. prostaglandins, thromboxanes, leukotrienes, epoxy and hydroxy fatty acid metabolites) that affect cell signaling and gene expression. DHA can also interact directly as a ligand for nuclear transcription factors (NF-κB, PPAR family, SREBP, HNF-α, and LXR) to affect cell signaling and gene transcription (Sampath & Ntambi, 2005).

Besides β-oxidation, fatty acids can be incorporated into membrane phospholipids using the enzymes of the acyl-CoA:1-acyl GPC acyltransferase system. These enzymes can selectively add certain fatty acids over others. Polyunsaturated fatty acids can also be added to phospholipids preferentially at the *sn*-2 position (Stillwell et al., 2005) and thus affect cell signaling by modifying membrane permeability, fluidity, and composition of lipid rafts (Corsetto et al., 2011; Stillwell et al., 2005). Additional evidence suggests that fatty acids can affect cell signaling without having to enter the cell by their regulation of G-protein-coupled

plasma membrane receptors (Jump *et al.*, 2008). DHA is also preferentially added to cardiolipin, a phospholipid of the inner mitochondrial membrane, after cellular uptake, and its enrichment in cardiolipin can have important effects on the electron transport chain (ETC) and mitochondrial reactive oxygen species production (Watkins *et al.*, 1998).

Safety and health benefits of docosahexaenoic acid

The health benefits of DHA in normal cells and tissues have been studied for decades. Dietary consumption of DHA up to 7.5 g/day does not have any deleterious effects in adults (Lien, 2009). DHA has been shown to protect fibroblasts, macrophages, renal epithelial cells, and retinal ganglion cells *in vitro* from the deleterious effects of oxidative stress by a variety of mechanisms including: inhibition of COX, xanthine oxidase, and inducible nitric oxide synthase, suppression of nitric oxide production, stimulation of GSH and antioxidant enzymes, and radical scavenging (Arab *et al.*, 2006; Y. J. Kim & Chung, 2007; Komatsu *et al.*, 2003; Shimazawa *et al.*, 2009). DHA consumption also results in lower arachidonic acid (AA, ω-6 20:4) levels since DHA and its derivatives compete with AA for binding to COX and LOX proteins. Furthermore, DHA is inserted into phospholipids preferentially over AA (Arterburn *et al.*, 2006). This results in reduced inflammation since the pro-inflammatory prostaglandins, thromboxanes, and leukotrienes are not produced by the COX and LOX pathways from AA (Massaro *et al.*, 2006; Ringbom *et al.*, 2001) and instead anti-inflammatory products are produced such as D-series resolvins, docosatrienes and neuroprotectins (Calder, 2006). There is some concern that increased DHA consumption will increase the risk for LPO, but studies have been inconclusive. An *in vitro* study conducted in

human vascular endothelial cells showed that DHA treatment caused a 3-4 fold increase in conjugated dienes formation, a LPO indicator, but these cells also exhibited a concomitant increase in glutathione peroxidase activity (Crosby *et al.*, 1996). One study showed that DHA consumption in a rat model increased LPO in the cell membranes of the liver and kidneys *in vivo* (Kubo *et al.*, 1997), but a subsequent study using a more precise measure of LPO showed that LPO did not increase significantly *in vivo* (Mori, 2004). Because DHA treatment has been associated with increases in GSH and antioxidant enzymes, healthy cells with their multiple layers of antioxidant protection should be able to successfully remove any reactive oxygen or lipid peroxide species resulting from DHA and its metabolism without effort (Visioli *et al.*, 2012). Furthermore, some LPO products of DHA, notably 18-HEPE and 17-HDHA, have important anti-cancer effects due to their ability to inhibit tumor necrosis factor-α (TNF-α), resulting in down-regulation of pro-inflammatory and pro-proliferative pathways (Weylandt *et al.*, 2011). Another study showed that oxidized ω-3 fatty acids react directly with Keap1, the negative regulator of NF-E2-related factor 2 (Nrf2), initiating Keap1dissociation from Cullin3 which allows Nrf2, a master regulator of antioxidant gene expression, to enter the nucleus and upregulate a cell's antioxidant defense system (Gao *et al.*, 2007; Kusunoki *et al.*, 2013).

Because hepatocellular carcinoma is associated with background liver disease, it is important to examine the literature for DHA's effects in the non-malignant liver tissue to make sure that high doses of DHA will not further damage liver function. Non-alcoholic fatty liver disease is associated with depletion of ω-3 PUFAs and a subsequent increase in the ω-6:ω-3

ratio and in oxidative stress (Valenzuela *et al.*, 2012; Videla *et al.*, 2004). Mice on a high fat diet develop steatohepatitis and insulin resistance, but supplementation with ω-3 PUFAs (DHA and EPA) increased GSH and reduced fat accumulation in the liver, insulin resistance and IL-6, IL-1β, and TNF-α expression back to control levels (Valenzuela *et al.*, 2012). In a study using ob/ob mice that are prone to obesity and steatohepatitis, administration of fish oil (24.8% DHA and 8.1% EPA) resulted in both lower liver triglyceride content and alanine aminotransferase (ALT, an enzyme associated with liver damage) through repression of SREBP-1and subsequent repression of the lipogenic genes fatty acid synthase and stearoyl-CoA desaturase (Sekiya *et al.*, 2003). A study using mice with chemically-induced cirrhosis showed no benefit on liver steatosis by histological examination after ω-3 PUFA treatment, but a decrease in liver fibrosis was observed (Fernandez *et al.*, 1997). As mentioned previously, DHA-derived mediators, 18-HEPE and 16-HDHA, down-regulate TNF-α in the liver, which blocks the inflammation and proliferation associated with steatohepatitis and hepatocarcinogenesis (Weylandt *et al.*, 2011). Additional DHA-derived lipid intermediates termed resolvins (17*S*-hydroxy-DHA) and protectins (protectin-D1) prevented liver damage by inhibiting DNA damage, COX-2 mRNA, prostaglandin-E2 production, and LPO *in vitro* when CC-1 hepatocytes were challenged with hydrogen peroxide, as well as *in vivo* in mice treated with carbon tetrachloride to induce necroinflammatory liver injury (Gonzalez-Periz *et al.*, 2006). DHA and EPA can also regulate liver lipogenesis, insulin sensitivity and glycolysis by acting as regulators of transcription factors PPAR-α, SREBP, HNF-α, LXR, ChREBP, MLX, and farnesoid X receptor indicating that DHA may have beneficial effects on prevention or amelioration of NAFLD, NASH, steatohepatitis, and diabetes mellitus

(Jump *et al.*, 2008; Masterton *et al.*, 2010). DHA, EPA, and AA at 100 μM doses inhibited the replication of HCV *in vitro* (Leu *et al.*, 2004). The mechanism of this inhibition has not been elucidated, but reducing viral replication could reduce the inflammation and cirrhosis associated with chronic HCV infection and prevent progression to HCC. A study examined a small cohort of patients with chronic HBV infection and determined that COX-2 is overexpressed in these patients even after loss of HBsAg and seroconversion following antiviral therapy (Cheng *et al.*, 2002). Because COX-2 activity promotes production of mutagenic and tumorigenic prostanoids, angiogenesis, cell proliferation, and immune evasion, DHA inhibition of COX-2 in patients with chronic HBV might mitigate the virus's deleterious effects. Overall, the research to date points to DHA as a benign agent to normal hepatocytes and it might even prevent further liver damage and hepatocarcinogenesis.

Anti-cancer properties of docosahexaenoic acid

DHA has many anti-cancer properties that work on a variety of pathways and by many mechanisms. The major anti-cancer properties of DHA will be reviewed below. DHA has been tested as a cytotoxic agent *in vitro* and *in vivo* in a variety of different cancer types including breast (Kang *et al.*, 2010; J. Kim *et al.*, 2009; Larsson *et al.*, 2004; H. Sun *et al.*, 2011), colon (Chen & Istfan, 2000; Toit-Kohn *et al.*, 2009), lung (Serini *et al.*, 2008), leukemia (Miura *et al.*, 2004; Yamagami *et al.*, 2009), gastric (S. E. Lee *et al.*, 2009; H. Sun *et al.*, 2013; Wu *et al.*, 2010), and liver cancer (C. Y. Lee *et al.*, 2010; Lim *et al.*, 2009; S. N. Sun *et al.*, 2013).

The large number of double bonds in DHA's chemical structure makes it vulnerable to LPO, which will increase cellular levels of lipid peroxides particularly in cancer cells (Ding & Lind, 2007; Ding *et al.*, 2004; Gotoh *et al.*, 2002; Merendino *et al.*, 2005; Siddiqui *et al.*, 2008; Stoll, 2002) since cancer cells have altered antioxidant systems and ROS production in order to promote proliferation. Aldehyde derivatives of LPO have also been shown to slow tumor growth (Siddiqui *et al.*, 2008). DHA also down-regulates GPx-4 expression making cancer cells more sensitive to oxidative stress from LPO (Ding & Lind, 2007). GPx-4 protects cells against damage from LPO because it can act on phospholipid hydroperoxides. In contrast, GPx is upregulated *in vitro* in human vascular epithelial cells and *in vivo* in the livers of healthy mice treated with fish oil, which illustrates the different effects ω-3 PUFAs may have on cancer and normal cells (Sneddon *et al.*, 2003; Takahashi *et al.*, 2002). As part of the propagation of LPO, superoxide radical production increases thereby changing superoxide levels. Superoxide production has also been shown to be increased by DHA in HT-29 colon cancer cells by DHA's enrichment in the cardiolipin of the mitochondria, which causes a disruption of electron transfer chain efficiency (Watkins *et al.*, 1998). In addition to increasing superoxide production, DHA can also inhibit superoxide dismutase-1 (SOD-1) independent of LPO via the PPARα pathway (Tuller *et al.*, 2009). Cancer cells sensitive to DHA cytotoxicity have decreased SOD-1 expression indicating that SOD-1 may be an important enzyme in determining DHA sensitivity (Ding *et al.*, 2004). Other antioxidant modulators that are negatively affected by DHA in cancer cells are catalase (Hardman *et al.*, 2002) and intracellular levels of reduced glutathione (GSH) (Cepinskas *et al.*, 1994; Gotoh *et al.*, 2002; Merendino *et al.*, 2005). Notably, DHA and EPA are able to activate Nrf2 in

HepG2 cells (Gao *et al.*, 2007), which may be used to modulate the deleterious effects of DHA treatment in these cells. Other anti-cancer mechanisms attributed to DHA include: COX-2 inhibition and the subsequent repression of proinflammatory arachidonic acid-derived prostaglandins (Chen & Istfan, 2000; Larsson *et al.*, 2004; Lim *et al.*, 2009; Y. Sun *et al.*, 2002), cell cycle arrest (Gotoh *et al.*, 2002; C. Y. Lee *et al.*, 2010; H. Sun *et al.*, 2013), interleukin-1β and interleukin-6 cytokine suppression (Park *et al.*, 2009), epidermal growth factor receptor suppression (Corsetto *et al.*, 2011), β-catenin inhibition (Lim *et al.*, 2009; Xue *et al.*, 2014), TNF-α inhibition by DHA metabolites (Skender *et al.*, 2012; Weylandt *et al.*, 2011), and N-Myc inhibition (C. Y. Lee *et al.*, 2010).

In addition to increasing ROS and inhibiting antioxidants in cancer cells, DHA is also able to induce apoptosis in many cancer types. An *in vitro* and *in vivo* study using MCF-7 breast cancer cells demonstrated that treatment with DHA in ethanol creates oxidative stress in the tumor cells and apoptosis is induced by procaspase-8 cleavage (Corsetto *et al.*, 2011; Kang *et al.*, 2010) and DHA decreased EGFR and Bcl-2 expression (Corsetto *et al.*, 2011). It was also reported that 30 μM DHA conjugated to bovine serum albumin (BSA) was capable of inducing apoptosis in MCF-7 cells through syndecan-1 and the subsequent inhibition of MEK, ERK, and Bad phosphorylation *in vitro* and *in vivo* (H. Sun *et al.*, 2011). DHA was also able to induce apoptosis *in vitro* in multiple lung cancer lines by inhibiting the MAPK/ERK pathways (Serini *et al.*, 2008). HCC commonly exhibits COX-2 and β-catenin activation. One study examined DHA's cytotoxicity in COX-2 negative colorectal cancer cells (HCT116 and SW480) and observed caspase-3 dependent apoptosis along with

increased proteasomal degradation of β-catenin, inhibition of β-catenin's nuclear translocation, and decreased expression of TCF-β-catenin pathway proteins: survivin, matrix metalloproteinase-7, PPAR-δ, and vascular endothelial growth factor (Calviello *et al.*, 2007). A similar observation was made in HCC cells (Hep3B, Huh7, and HepG2) treated with DHA. These cells were sensitive to DHA in a time- and dose-dependent manner and DHA treatment caused loss of prostaglandin-E2 expression by COX-2 inhibition, which reduced prostaglandin-E2's activation of β-catenin resulting in β-catenin degradation and apoptosis through procaspase-9 and PARP cleavage (Lim *et al.*, 2009). On the other hand, HT-29 colon adenocarcinoma cells were sensitive to apoptosis by DHA treatment based on increased LPO rather than COX-2 inhibition (Chen & Istfan, 2000).

DHA apoptosis induction in cancer cells has also been attributed to p53 activation, Bax expression, cytochrome c release from the mitochondria, caspase-3 cleavage, and PARP (Poly-ADP-Ribose Polymerase) cleavage (S. E. Lee *et al.*, 2009; Toit-Kohn *et al.*, 2009). Induction of apoptosis by DHA might be dependent on the Bax:Bak ratio in some cancer cells, which is supported by studies done by many groups (Chiu *et al.*, 2004; Miura *et al.*, 2004; H. Sun *et al.*, 2013; S. N. Sun *et al.*, 2013; Yamagami *et al.*, 2009). Ultimately, DHA-induced apoptosis in cancer seems to be attributed to many different pathways and the pathway used might be dependent on cell type tested and the heterogeneity of the cell population, DHA dose and delivery, and the length of the treatment. Variations in these factors make it difficult to attribute a single mechanism to DHA's induction of apoptosis.

Combination of DHA with traditional chemotherapy has also been studied and shows promise to increase cancer cytotoxicity while minimizing toxic side effects and this topic has been reviewed previously ((Biondo *et al.*, 2008). The main mechanisms found for increased susceptibility to chemotherapies with DHA treatment can be grouped into the following categories: LPO of DHA and inhibition of GPx activity to increase cytotoxicity of ROS-inducing chemotherapies (Hardman *et al.*, 2002; Vibet *et al.*, 2008), DHA prevents efflux of chemotherapy drugs (Das & Madhavi, 2011; Kuan *et al.*, 2011), DHA alters membrane-associated signal transduction (Corsetto *et al.*, 2011; Schley *et al.*, 2005; Shaikh *et al.*, 2009; Stillwell *et al.*, 2005), DHA decreases NF-κB activity (Schley *et al.*, 2005), and DHA alters expression of apoptotic and antiapoptotic proteins (Chen & Istfan, 2000; Chiu *et al.*, 2004; Wu *et al.*, 2010).

Challenges with delivery of docosahexaenoic acid to tumors

A major challenge that has plagued researchers with using DHA as a cancer treatment is their inability to deliver cytotoxic doses *in vivo* since DHA is not particularly soluble in blood. Studies looking at dietary supplementation with DHA have shown that serum concentrations of non-esterified DHA are limited to ≈12.5 μM once DHA supplementation is above two grams per day (Arterburn *et al.*, 2006; Conquer & Holub, 1998). Meanwhile, studies conducted *in vitro* typically require DHA concentrations above 50 μM to kill cancer cells, and some studies reported concentrations as high as 280 μM are needed. A variety of approaches have been used by other groups to try to deliver cytotoxic doses of DHA *in vivo*. The use of emulsions of fish oil have been used in the clinic as parenteral nutrition (≈3 g

DHA/10 g of total fatty acids) ("Omegaven ", 1999), but emulsions only exhibit a moderate improvement in short-term absorption compared to DHA administered orally as an oil (Garaiova *et al.*, 2007; Raatz *et al.*, 2009; Schuchardt & Hahn, 2013). Delivering DHA as a mono- or di- acyl glyceride has been hypothesized to improve absorption in the digestive track because DHA will form micelles that might be more readily absorbed by enterocytes (Schuchardt & Hahn, 2013). As mentioned previously, DHA is transported in serum bound to albumin and albumin is a major antioxidant *in vivo* (Roche *et al.*, 2008). An interesting study looking at how albumin modulates DHA cytotoxicity in human HCC showed that both the addition of exogenous albumin and intracellular albumin overexpression reduced DHA cytotoxicity and DCF fluorescence in HepG2 cells. Furthermore, the same study showed that knockdown of albumin expression using siRNA in Huh7 and Hep3B cells increased both DHA cytotoxicity and DCF fluorescence (Kanno *et al.*, 2011).

In one report, investigators loaded DHA fatty acid or DHA ethyl ester into hybrid liposomes composed of l-α-dimyristoylphosphatidylcholine (DMPC) and Tween 80 and showed that incorporation of DHA significantly enhanced the cytotoxicity of the hybrid liposomes in a variety of cancer cells from >300 μM to <100 μM through an apoptosis mediated pathway and that this cytotoxicity was rescued by vitamin E (Tanaka *et al.*, 2008). The group expanded this study of hybrid liposomes loaded with DHA to an *in vivo* mouse model of metastatic liver cancer and showed increased apoptosis in the tumor and survival of the mice treated with DHA in the hybrid liposome versus treatment with the hybrid liposome alone (Ichihara *et al.*, 2011). These studies did not look at the cytotoxicity of DHA by itself in the

cancer cell lines so no conclusions can be made as to whether hybrid liposome delivery increases DHA cytotoxicity, but they did show that effective delivery of DHA via hybrid liposome is possible both *in vitro* and *in vivo*. A problem with the use of hybrid liposomes is that their size ranged from 50-210 nm and they could be recognized as foreign by the immune system, which would make them subject to removal by the mononuclear phagocytic system *in vivo*.

Studies have also been published where DHA was incorporated into small unilamellar vesicles made of phosphatidylcholine, and vesicles made with DHA rather than other fatty acids had cytotoxic properties to cancer cells (Jenski *et al.*, 1995; Kafrawy *et al.*, 1998). A study conducted in 2004 examined the differential cytotoxicity of ω-3 PUFAs to cancer cells when delivered by LDL or albumin. In order to obtain LDL with ω-3 PUFAs, the researchers fed African Green monkeys a fish oil-enriched diet for three or more years and then isolated their LDL which had a composition of ≈22% ω-3 PUFAs. Despite the low doses of ω-3 PUFAs in the LDL, delivery by LDL was more cytotoxic to MCF-7 and PC-3 cells and changed gene expression patterns differently than albumin delivery of EPA. This study failed to account for the changes that DHA inclusion in the LDL had on cytotoxicity and gene expression since only EPA was used in the albumin delivery arm (Edwards *et al.*, 2004). Despite this failure to account for DHA's unique anti-cancer properties, this study still illustrates the potential benefits of delivering DHA to cancer cells via a lipoprotein.

Low Density Lipoprotein Structure and Use as a Therapy Delivery Platform

Normally, LDL consists of a large belt-like ApoB-100 protein that binds to cell receptors and stabilizes the phospholipid monolayer. The phospholipid monolayer is intercalated with free cholesterol and surrounds a liquid core composed of cholesterol esters and a small quantity of triglycerides (Figure 2-1) (Corbin *et al.*, 2011; Hevonoja *et al.*, 2000; Shen *et al.*, 1977). The use of LDL as targeted carriers for chemotherapy drugs has been explored in some depth by other groups since many cancer cells overexpress LDL receptor in order to acquire the cholesterol needed for their proliferation though LDLR internalization rate may not be increased (Firestone, 1994). LDL is more advantageous as a carrier than a liposome or emulsion formulation because it is non-immunogenic, small enough to escape the mononuclear phagocytic system, and it will be directed to cells that overexpress LDLR. Loading chemotherapy drugs into LDL generally increases the cytotoxicity of the drug while reducing side effects from systemic free drug delivery (Firestone, 1994; Kader & Pater, 2002), but there are a variety of problems that may be faced such as insufficient drug loading,

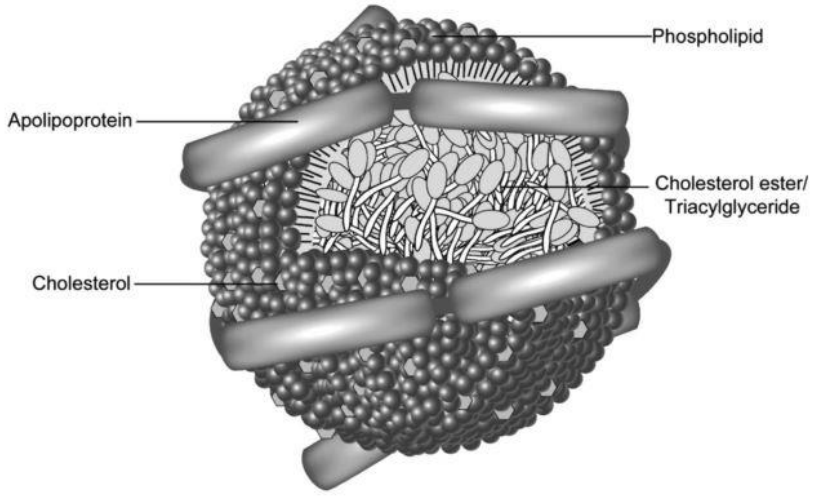

Figure 2-1: Structure of low density lipoprotein

Used with permission from John Wiley & Sons, Inc.: [Nanoplatform-Based Molecular Imaging: Chapter 18 "Lipoprotein-Based Nanoplatforms for Cancer Molecular Imaging"], (Corbin *et al.*), copyright (2011).

lysosomal trapping, and the drug may leak from the lipoprotein before reaching its target and cause damage to normal cells (Firestone, 1994; Shaw & Shaw, 1991).

In general, drugs can be associated with LDL by three main mechanisms by direct conjugation to the amino acid residues of the ApoB-100 protein, by intercalation into the phospholipid monolayer, or by loading into the lipophilic core of the LDL via the reconstitution method (Corbin *et al.*, 2011; Firestone, 1994; Krieger, 1986). Drug conjugation onto the ApoB-100 amino acid residues creates a stable delivery system, but it is severely dose-limited as excessive drug-conjugation will impair binding of ApoB-100 to LDL receptor. Intercalation of drugs into the phospholipid membrane is also limited to drug dose and the drug can be exchanged into nearby membranes leading to off-target effects and reduced cytotoxicity. Core loading provides the largest drug delivering ability, but it is important to load drugs with lipophilic moieties so they will not leak from the core (Corbin *et al.*, 2011; Firestone, 1994). Because DHA is not cytotoxic to normal cells and it is lipophilic, delivery by LDL is ideal.

CHAPTER THREE
Methodology

MATERIALS AND METHODS

Nanoparticle Preparation, Composition, and Binding Analysis

Low Density Lipoprotein Isolation by Sequential Ultracentrifugation

Plasma in EDTA from a hypercholesterolemic patient was obtained from Parkland Hospital. Low Density Lipoprotein was isolated from the plasma using the method described by Lund-Katz *et al* (Lund-Katz *et al.*, 1998). Briefly, the plasma (~45 mL) was aliquoted to 75-mL polycarbonate ultracentrifuge tubes (Thermo Scientific, Cat #314460) and then layered with 5-6 mL of a 1.006 g/mL density solution of 2 mM EDTA and 0.2 M NaCl (pH 7.4) and the tubes were balanced by mass. The plasma and density solution was spun in a Sorvall Discovery 90SE ultracentrifuge in a T647.5 fixed-angle rotor at 35,000 rpm for 22 hours at 4°C. After ultracentrifugation the top layer containing VLDL and chylomicrons was discarded along with the middle clear layer. The bottom layer containing LDL and HDL was collected and its density was adjusted to 1.063 g/mL with potassium bromide. The density-adjusted LDL+HDL fraction was aliquoted into 10-mL polycarbonate bottles (Beckman, Cat #355603) and refrigerated for at least 1 hour at 4°C, then ~2-3 mL of a KBr density solution of 1.063 g/mL was layered on top and the tubes were balanced by mass. The tubes were spun at 40,000 rpm for 22 hours at 4°C in a Sorvall T890 fixed-angle rotor. After ultracentrifugation, the top LDL layer was collected and the bottom HDL layer was

discarded. The LDL was stored in high salt solution at 4°C. Prior to use, the LDL was dialyzed in a 25 mm width 12-14,000 MWCO dialysis tubing (VWR Scientific, Cat# 25225-226) overnight at 4°C in 1 Liter of 10 mM tris-HCl, 150 mM NaCl, 1 mM EDTA, pH 7.5 buffer solution. Protein concentration of the dialyzed LDL was measured by Bradford or Lowry Assay according to the manufacturer's protocol.

Preparation of LDL-DHA

Incorporation of DHA (Nu-Chek Prep, INC) into LDL was performed by the reconstitution (core-loading) method (Krieger *et al.*, 1979). Briefly, lyophilized LDL was subjected to organic extraction with heptane. Following the extraction, DHA in heptane was added to the LDL residue and the sample was allowed to sit at 4°C for 90 min. Thereafter, heptane was removed by evaporation and the dried residue was resuspended in 10 mM Tricine buffer. After an overnight incubation at 4°C, LDL samples were clarified by low-speed centrifugation and stored under N_2 atmosphere at 4°C. Control LDL Nanoparticles: Throughout these studies, various LDL particles were used as controls. These included native LDL, as an overall control vehicle, LDL reconstituted with oleic acid (LDL-OA), or LDL reconstituted with oleic acid triglyceride (triolein) (LDL-TO).

Preparation of HSA-DHA

Human serum albumin (HSA; 5 % w/v) was dissolved in 1 ml of 75mM KCl solution (pH = 7.4). DHA in ethanol (0.125 % w/v; final concentration) was added to the HSA solution,

vortexed briefly and incubated at 37˚C for 1 hour. Samples were then filtered through 0.2 μm syringe filter and stored under N_2 atmosphere at 2-8˚C until further use.

Apoprotein Secondary Structure

Far-UV circular dichroism (CD) spectroscopy of LDL nanoparticles was recorded using a Jasco J-810 CD spectrometer. The CD spectra were recorded at 25°C with a 1 nm step size from 260 to 195 nm. The data was collected over three consecutive scans and averaged. Readings were normalized to protein concentration and expressed as molar ellipticity. Estimates of apoB-100 protein secondary structure was determined using Dichroweb CDSSTR software package.

Nuclear Magnetic Resonance Spectroscopy

Samples were diluted with deuterated solvents (D_2O, $CDCl_3$, or deuterated ethanol) and spiked with 100 μg of an internal standard of trimethylsilyl propanoic acid (TSP) or tetramethylsilane (TMS) for aqueous or organic solvents, respectively. Spectra were acquired on a ^1H Varian 600 MHz nuclear magnetic resonance spectrometer (NMR) at 37°C for at least 256 scans. NMR spectra were analyzed on ACD/NMR Processor software. Briefly, spectra underwent zero filling, exponential signal-to-noise correction, Fourier Transform, and then baseline correction. Peaks of interest were highlighted using the peak picking tool and integrated to determine concentration relative to the internal standard.

Nanoparticle Composition and Physicochemical Properties Measurement

Cholesterol was measured in LDL nanoparticles using a commercial kit according to the manufacturer's directions (BioVision). Phospholipid content was measured using a commercial kit according to the manufacturer's directions (Wako). The size distribution and polydispersity indices (PDI) of LDL nanoparticles were evaluated by dynamic light scattering (DLS) measurements at 25°C, and the zeta potential was measured in Tricine buffer at pH 8.4 using a Zetasizer Nano (ZEN3500, Malvern Instruments, UK). All measurements were performed in at least triplicate readings.

Preparation of Low Density Lipoprotein labeled with DiI

Dialyzed LDL was labeled with 1,1'- Dioctadecyl-3,3,3',3'-tetramethylindocarbocyanine iodide (DiI) lipophilic dye by the following method. 10 mg of dialyzed LDL was diluted to a 5 mg/mL solution with milli-Q water in a conical tube and then 150 µg of DiI in DMSO (from a 30 mg/mL DiI in DMSO stock) was added. The LDL-DiI solution was gently mixed, the tube was covered in foil and incubated overnight at 37°C. The density of the LDL-DiI was then adjusted to 1.080 g/mL with potassium bromide and aliquoted to 10-mL polycarbonate bottles (Beckman, Cat 355603) and refrigerated for at least 1 hour at 4°C, then 2-3 mL of a 1.063 g/mL density solution was layered on top and the tubes were balanced by mass. The tubes were spun at 40,000 rpm for 22 hours at 4°C using a Sorval Discovery 90SE in a T890 fixed-angle rotor. After ultracentrifugation, the top LDL-DiI layer was collected and filtered through a 25 mm, 0.45 um surfactant free cellulose acetate syringe filter (Nalgene, Cat # 190-2545). After filtration, the LDL-DiI was stored at 4°C in the dark in high salt. Prior to use, the LDL-DiI was dialyzed in 25 mm width 12-14,000 MWCO dialysis

tubing (VWR Scientific, Cat # 25225-226) overnight in the dark at 4°C in 1 liter of 10 mM tris-HCl, 150 mM NaCl, 1 mM EDTA, pH 7.5 buffer solution. Protein concentration of the dialyzed LDL was measured by Lowry Assay according to the manufacturer protocol. The LDL-DiI specific activity was determined by extracting the DiI from LDL using 750 µL of 2:1 chloroform:methanol plus 300 µL water with LDL-DiI (0.094, 0.88, 0.375, 0.75, 1.5, 3.0, 6.0 µg/mL of LDL-DiI) followed by centrifuging at 2000 rpm for 1 minute and collecting the bottom chloroform layer for fluorescent analysis. Fluorescence measurement of 400 µL of solution was performed on the Hitachi F7000 fluorescence spectrophotometer with a 520 nm excitation and 570 nm emission in a 10 mm ultraviolet cuvette (VWR Scientific, Cat # 414004-229). The extracted LDL-DiI fluorescence was compared to the fluorescence on a standard curve of 400 µL of DiI in isopropanol (20, 40, 60, 80, 100, 120, and 140 ng/mL DiI). The DiI in isopropanol standard curve was no longer linear after 80 ng/mL DiI and the LDL-DiI in chloroform standard curve was truncated after it exceeded the linear fluorescence of the DiI in isopropanol standard curve.

Low Density Lipoprotein Receptor (LDLR) Binding Affinity Assay

For the binding assays, cells were incubated with LDL-DiI/LDL-DHA-DiI (10 µg/ml) in serum free DMEM culture medium for 2 hours at 4°C with or without excess native LDL (500 µg). Because receptors are not internalized at 4°C, only binding of the ligand to the cell surface receptors is measured. After washing with PBS, 1 mL of isopropanol was added to each well and the plates were rocked for 15 minutes in the dark. The isopropanol extract of DiI was transferred to a tube and centrifuged for 15 minutes at 3000 rpm. Thereafter, the DiI

fluorescence signal was determined using a Hitachi F7000 spectrofluorometer (excitation at 520 nm and an emission scan from 530 nm to 630 nm). Cells were dissolved with Cell Lysis Reagent (1g/L sodium dodecyl sulfate in 0.1 M NaOH) for protein determination. The calculated bound LDL-DiI in µg/mL was normalized to cellular protein in mg/mL. Parallel experiments were performed at 37° C to measure total association of LDL-DiI/LDL-DHA-DiI (bound and internalized) with the cells. The amount of internalized LDL particle was calculated by subtracting the 4°C binding values from the measure of total association at 37°C. To calculate specific versus non-specific receptor binding, the fluorescence intensity of the treated cells was compared to the standard curve of LDL-DiI in chloroform to determine the LDL-DiI in µg/mL taken up by each well. The calculated LDL-DiI uptake in µg/mL was normalized to cellular protein in mg/mL for both the LDL-DiI treated (total binding) and LDL-DiI plus native LDL treated cells (non-specific binding). This normalized fluorescent data was analyzed on GraphPad Prism 6 software using the nonlinear regression fit for one site receptor binding using total and non-specific binding data to obtain the K_D (µg/mL of LDL-DiI) and B_{max} (µg LDL-DiI/mg cell protein) values for each cell type.

LDL and LDL-DHA Endocytosis to the Lysosome by Confocal Microscopy

TIB-73 and TIB-75 cells were grown to 80-90% confluency in 35mm^2 glass bottom dishes coated with 10 µg/mL fibronectin. The cells were serum starved overnight and then treated with 10 µg/mL of LDL-DHA-DiI or LDL-DiI for 2 hours at 37°C and then stained for 30 minutes with 1µM LysoSensor Green DND-189 (Life Technologies). Cells were imaged at 63x magnification on a Leica LP5 confocal. The green channel measured LysoSensor dye at

488 nm excitation and 505 nm emission. The red channel measured DiI dye at 561 nm excitation and >590 nm emission. Images were deconvoluted using AutoQuant X3 software. Imaris imaging software was used to calculate LysoSensor Green colocalization with red DiI labeled LDL nanoparticles in the cells.

Cell Culture Conditions and Cell Viability Assays

Cell Culture

All cell lines were acquired from the ATCC (Manassas, VA) unless otherwise indicated. The following mouse cell lines were used: the normal mouse hepatocyte cell line TIB-73 (BNL CL.2) and its malignant counterpart TIB-75 (BNL 1ME A.7R.1) were obtained from ATCC. The rat hepatoma cell line H4IIE (CRL-1548) was also used. The following human cell lines were used: Hep3B (HB-8064), a hepatocellular carcinoma cell line positive for Hepatitis B virus derived from a juvenile male; Huh7 (JCRB Cell Bank, JCRB0403), a well-differentiated hepatocellular carcinoma cell line derived from an adult male; and FOCUS (cell line established by the Quaroni lab), a poorly differentiated hepatocellular carcinoma cell line positive for Hepatitis B virus (He *et al.*, 1984). TIB-73, TIB-75, H4IIE, Hep3B, Huh7, and FOCUS cells were cultured in Dulbeco's modified Eagle's medium (DMEM) (Sigma Aldrich, Cat #D6429) supplemented with 10% fetal bovine serum (FBS). All cells were grown at 37°C in an atmosphere of 5% CO_2 in a humidified incubator.

MTS Cell Viability Assay

After treating and incubating the cells for the experiment in 96-well plates, the media were removed and replaced with 100 µL per well of serum-free media mixed with CellTiter 96® AQueous Non-Radioactive Cell Proliferation Assay (Promega Cat #G5421) for ≈4 hours at 37°C according to the manufacturer's instructions. After incubation, the absorbance of the well plates was read at 450 nm on a Molecular Devices ThermoMax M5 microplate reader. The absorbance of a reagent blank well was subtracted from the absorbance for each treatment and control group. The corrected absorbance for each treatment group was divided by the corrected absorbance of an untreated control group to get a cell viability percentage for each treatment.

Co-Culture, Treatment, and lmaging of TlB-73 and TIB-75 Cells

TlB-73 and TlB-75 cells were trypsinized from a parent flask and the cells were counted by BioRad TC-10 Cell Counter. After counting, TIB-73 (40,000 cells per well) and TIB-75 (35,000 cells per well) were aliquoted into separate sterile 1.5-mL eppendorf tubes and the volumes were adjusted to a final volume of 35 µL per well with DMEM with 10% FBS and mixed gently. The tip of a hydrophobic pen (VWR Scientific, Cat # 95042-566) was sprayed with ethanol then used to divide the wells of a sterile 6-well tissue culture plate in half to prevent the cell plus media solution from spreading during plating. To one half of the divided well, 35 µL of TlB-73 cells (40,000 cells) was spread gently over the surface using a sterile P200 pipette tip and this was repeated for all 6 wells. Then 35 µL of TlB-75 cells (35,000 cells) was spread gently over the other half of the wells. The 6-well plate was incubated at 37°C at 5% CO, for 15 minutes before 2 mL of DMEM plus 10% FBS media was added

gently along the sides of the well to minimize cell mixing. Cells were incubated for 3 days to approximately 80% confluence then the cells were serum-starved in serum free DMEM overnight. After serum starvation, the cells were imaged at 10x using the Zeiss Axiovert 100 inverted microscope attached to an Oprotronics Microfire camera utilizing ImageJ software. The cells were then treated in duplicate with 60 μM LDL-DHA, LDL-TO, or serum free DMEM. Cells were imaged again after 24 hours without changing the media and then imaged after 72 hours of treatment in fresh media. After 72 hours of treatment the whole wells were also imaged at 0.63 x 0.8 magnification using the Zeiss Stemi SV 11 dissecting microscope attached to an Optronics Macrofire CCD camera utilizing Pictureframe 2.0 acquisition software.

Cell Death Assay by Annexin-V and Propidium Iodide

Seventy-two hours following LDL nanoparticle treatments (40 μM) cells were stained with the Promokine Apoptotic/Necrotic Cells Detection Kit according to the manufacturer's protocols. The Annexin-V FITC and propidium iodide (PI) double staining method was used to provide read-outs of apoptotic and necrotic cells, respectively. Cells were analyzed by fluorescent microscope (NIKON Eclipse E600 microscope (Nikon, Lewisville, TX)) and flow cytometric analysis (FACScan flow cytometer, Becton Dickson, Mountain View, CA, USA).

Protein Measurement by Western Blot

Cell and tissue proteins were separated on a 10% sodium dodecyl sulfate polyacrylamide gel and transferred to PVDF. Membranes were then probed with antibodies from Santa Cruz against superoxide dismutase 1(SOD-1 ((FL-154), sc-11407), SOD-2 ((FL-122), sc-30080), catalase ((N-17), sc-34280), glutathione peroxidase 4 (GPx-4 (H-90), sc-50497), NOX-4 ((H-300), sc-30141), transferrin ((M-70), sc-30159), and β-actin ((C4) sc-47778). Appropriate HPR-conjugated secondary antibodies were used for detection. Additional antibodies used were against transferrin receptor (CD71 (H68.4), Life Technologies #13-6800), LDL receptor (gift from Dr. Joachim Herz), and ferroportin (SLC40A1, ab85370).

Oxidative Stress Assays

$NADPH/NADP^+$ Assay

$NADPH/NADP^+$ concentrations in cell lysates and tissue samples were determined by using EnzyChrom NADPH/NADP assay kit (BioAssay Systems). The kit is based on a glucose dehydrogenase cycling reaction, in which a tetrazolium dye (MTT) is reduced by NADPH in the presence of phenazine methosulfate. The intensity of the reduced product color measured at 565 nm is proportionate to the $NADPH/NADP^+$ concentration in the sample.

GSH/GSSG Assay

Total soluble GSH and GSSG were measured in cell lysates and tissue homogenates using the enzymatic recycling method.(Rahman *et al.*, 2006) Briefly, about 3×10^6 cells or 40 mg of tissue were homogenized in 10 volumes of cold sulfosalicylic acid (0.6%) plus 0.1%

Triton-X (for cells) or 5% metaphosphoric acid (tissues). Protein was precipitated and the supernatant was used to determine reduced glutathione (GSH) and glutathione disulphide (GSSG). Total glutathione (GSH + GSSG) was determined by spectrometry by measuring the conversion of 5, 5-dithiobis (2- nitrobenzene acid) (DTNB) to the yellow derivative 5′-thio-2-nitrobenzoic acid (TNB), measurable at 412 nm, in the presence of NADPH and GSH reductase. GSSG determination was similar for total glutathione, except that GSH was first derivatized for 1 h with 2-vinylpyridin. Change in absorbance at 412 nm was recorded for 3 min. The GSH level was calculated by subtracting GSSG content from the total glutathione content (GSH = total GSH-2GSSG). Results were expressed in mmol per mg of cell protein and mmol per gram of weight for the tissues.

Fluorescent Spectrophotometric Analysis of Oxidative Stress by DHE Assay

Cells were cultured in 100 mm^2 sterile cell culture dishes in DMEM + 10% FBS media for three days to a confluency of 80%. The cells were then serum-starved overnight in serum free DMEM. After serum starvation, the cells were treated with LDL-DHA, LDL-vehicle (TO or OA), or serum free DMEM for the specified time period (eg. 24 hours, 2 hours then serum free for 22 hours, etc). Following treatment, cells were incubated in 10 mL of serum free DMEM containing 10 µM Dihydroethidium (DHE) (Molecular Probes, Cat #011347) at 37°C for 30 minutes in the dark (one untreated dish per cell type was left unstained to correct for autofluorescence). The cells were washed three times with 5 mL of phosphate buffered saline (PBS) and the plates were scraped in 1 mL acetonitrile and the cells were collected into 1.5-mL eppendorf tubes and put on ice. The cells were sonicated intermittently

(amplitude 10) for 20 second intervals on ice. The cells were spun down at 10,000 rpm for 15 minutes at 4°C and the supernatant was collected into a new eppendorf tube, the remaining cell pellet was resuspended in 1 mL PBS for protein analysis. The tubes were kept on ice in the dark until analysis. The supernatants (400 µl) were analyzed in a 10 mm ultraviolet cuvette (VWR Scientific, Cat #414004-229) on a Hitashi F-7000 fluorescence spectrophotometer with excitation at 490 nm and an emission scan from 520-650 nm (5.0 nm slit excitation and emission slits with 240 nm/min scan speed at 950 volts). After fluorescent analysis of the cell supernatant, the protein was measured by the Bradford Protein Assay. The results are expressed as a fold-change of fluorescent intensity at 570 nm per mg of cell protein with respect to the untreated controls for each cell type.

DHE Flow Cytometry

Huh7, Hep3B, and FOCUS cells were grown to 80-90% confluency in 12-well plates, serum starved overnight, and then treated for 24 hours with 40 µM LDL-DHA or LDL-OA. After treatment, the cells were trypsinized from the plate, pelleted, and then stained with 10 µM dihydroethidium (Molecular Probes, Cat #011347) in PBS at 37°C for 30 minutes in the dark. Cells were stored on ice until analysis on a BD FACSCalibur using channel FL2. The flow cytometry data was analyzed on FlowJo software. Data were gated to remove cellular debris and clumps (FSC versus SSC) and then the single-cell populations were plotted on a FL2 versus FSC cytogram and gated to determine what percentage of cells exhibited increased red fluorescence relative to untreated cells to indicate which cells have greater ROS production following treatment.

Fluorescent Spectrophotometric Analysis of Oxidative Stress by DCF-DA Assay

TlB-73 and TIB-75 cells were cultured in 100 mm^2 sterile cell culture dishes in DMEM + 10% FBS media for three days to a confluency of ~80%. The cells were then serum-starved overnight in serum free DMEM. After serum starvation, the cells were treated with 60 µM LDL-DHA, LDL-TO, or serum free DMEM for 24 hours. Following treatment, cells were incubated in 5 mL of serum free DMEM containing 15 µM carboxy-H_2DCFDA (from a 4 mM carboxy-H_2DCFDA in DMSO stock solution stored under nitrogen) (Invitrogen, Cat# C-400) at 37°C for 1 hour in the dark. The cells were washed three times with 5 mL of phosphate-buffered saline (PBS) and the plates were scraped and the cells were collected into sterile 1.5-mL eppendorf tubes. The cells were centrifuged at 2000 rpm for 5 minutes and the supernatants were removed from the cell pellets. The cell pellets were resuspended in 400 µl of PBS and then sonicated intermittently for 20 sec intervals on ice. The cells were spun down at 10,000 rpm for 10 minutes and the supernatant was collected and diluted with 750 µl of PBS. The tubes were kept on ice in the dark until analysis. The supernatants were analyzed on a Hitashi F-7000 fluorescence spectrophotometer with excitation at 485 nm and an emission scan from 500-560 nm (5.0 nm slit excitation and emission slits with 1200 nm/min scan speed at 700 volts). After fluorescent analysis of the cell supernatant, the protein was measured by the Bradford Protein Assay. The results are expressed as a percentage of fluorescent intensity at 525 nm per mg of cell protein with respect to the untreated controls for each cell type.

DCF-DA Flow Cytometry

TIB-73 and TIB-75 cells were grown to 80-90% confluency in 6-well plates, serum-starved overnight, and then treated for different time periods with 60 µM LDL-DHA. After treatment, the cells were stained with 15 µM 2′,7′-Dichlorofluorescin diacetate (DCF-DA, a cell-permeable non-fluorescent dye that is de-esterified intracellularly and then fluoresces green in the presence of ROS species) (Sigma Cat# D6883) in DMEM for 30 minutes at 37°C. The DCF-DA dye was aspirated from the cells and then they were removed from the plate using 0.25% Trypsin-EDTA followed by DMEM + 10% FBS. Cells were pelleted by centrifugation, washed with PBS, pelleted again and resuspended in 750 µL PBS. Cells were stored on ice until analysis on a BD FACSCalibur using channel FL1. The flow cytometry data was analyzed on FlowJo software. Data were gated to remove cellular debris and clumps (FSC versus SSC) and then the single cell populations were plotted on a FL1 versus SSC cytogram and gated to determine what percentage of cells exhibited increased green fluorescence relative to untreated TIB-73 cells to indicate which cells have greater ROS production following treatment.

FOCUS, Hep3B, and Huh7 cells were grown to 80-90% confluency in 12-well plates, serum starved overnight, and then treated for 24 hours with 60 µM LDL-DHA or LDL-OA. After treatment, the cells were stained with 10 µM 2′,7′-Dichlorofluorescin diacetate (DCF-DA, a cell-permeable non-fluorescent dye that is de-esterified intracellularly and then fluoresces green in the presence of ROS species) (Sigma, Cat# D6883) in DMEM for 20 minutes at 37°C. The DCF-DA dye was aspirated from the cells and then they were removed from the plate using 0.25% Trypsin-EDTA followed by DMEM + 10% FBS. Cells were pelleted by

centrifugation, washed with PBS, pelleted again and resuspended in 750 µL PBS. Cells were stored on ice until analysis on a BD FACSCalibur using channel FL1. The flow cytometry data was analyzed on FlowJo software. Data were gated to remove cellular debris and clumps (FSC versus SSC) and then the single cell populations were plotted on a FL1 versus SSC cytogram and gated to determine what percentage of cells exhibited increased green fluorescence relative to untreated cells to indicate which cells have greater ROS production following treatment.

BODIPY C11 581/591 Flow Cytometry

TIB-73 and TIB-75 cells were grown to 80-90% confluency in 6-well plates and serum starved for 6 hours or overnight. Prior to treatment, cells were stained for 30 minutes at 37°C with 1 µM BODIPY C11 581/591 (Life Technologies, Cat #D-3861) (a cell-permeable dye that is a fatty acid analog that shifts fluorescence from red to green upon oxidation). After staining, the cells were treated at different time points with 60 µM LDL-DHA. Cells were removed from the plate using 0.25% Trypsin-EDTA followed by DMEM + 10% FBS. Cells were pelleted by centrifugation, washed with PBS, pelleted again and resuspended in 750 µL PBS. Cells were stored on ice until analysis on a BD FACSCalibur using channels FL1 and FL3. The flow cytometry data was analyzed on FlowJo software. Data were gated to remove cellular debris and clumps (FSC versus SSC) and then the single cell populations were plotted on a FL1 histogram and gated relative to untreated TIB-73 cells to determine what percentage of cells exhibited increased green fluorescence following treatment.

BODIPY C11 581/591 Confocal Microscopy

Heat Map Images: TIB-73 and TIB-75 cells were grown to 80-90% confluency in 35mm^2 glass bottom dishes coated with 10 µg/mL fibronectin. The cells were serum starved for 8 hours, treated with serum free media or 60 µM LDL-DHA overnight, then dyed with 2 µM BODIPY C11581/591 dye and , a lipid peroxide indicating dye, for 25 minutes at 37°C and the media was replaced prior to imaging. Cells were imaged at 63x magnification on a Leica LP5 confocal. The green channel measured oxidized lipid dye at 488 nm excitation and 510 nm emission. The red channel measured unoxidized lipid dye at 488 nm excitation and 590 nm emission. Images were deconvoluted using AutoQuant X3 software. A MatLab plug-in of the Imaris imaging software was used to create the heat map images by dividing the fluorescence intensity per pixel of the two channels. Dividing the green channel by the red channel shows the oxidized state of the cellular lipids and dividing the red channel by the green channel shows the unoxidized state of the cellular lipids.

Lipid Oxidation Localization to Lysosome: TIB-73 and TIB-75 cells were grown to 80-90% confluency in 35mm^2 glass bottom dishes coated with 10 µg/mL fibronectin. The cells were serum starved for overnight, dyed with 2 µM BODIPY C11 581/591 dye, a lipid peroxide indicating dye, for 25 minutes at 37°C, then treated with serum free media or 60 µM LDL-DHA for 4 hours, then dyed with 75 nM LysoTracker Deep Red for 30 minutes prior to imaging. Cells were imaged at 63x magnification on a Leica LP5 confocal. The green channel measured oxidized lipid dye at 488 nm excitation and 510 nm emission. The red channel measured unoxidized lipid dye at 488 nm excitation and 590 nm emission. An

additional channel measured deep red fluorescence of the LysoTracker dye with 561 nm excitation and >610 nm emission. Images were deconvoluted using AutoQuant X3 software. Imaris imaging software was used to calculate LysoTracker Deep Red colocalization with green oxidized BODIPY C11 581/591 dye in the cells.

Thiobarbituric Acid Reactive Substances Assay

The total amount of lipid peroxidation (LPO) products formed in the cells was determined using the thiobarbituric acid reactive substances (TBARS) method (Erdahl *et al.*, 1991). Briefly, cells were plated to 80% confluency in 100-mm^2 dishes, serum starved overnight, and treated with nanoparticle. After treatment, cells were washed with cold PBS, scraped from the plate, pelleted by centrifugation, and washed with PBS. Cells were resuspended in 200 µL of PBS and sonicated to lyse the cells. The cell lysate (150 µL) was mixed with 330 µL of thiobarbituric acid reactive substances reagent (75 µL of 0.375% (w/v) thiobarbituric acid, 15% (w/v) trichloroacetic acid, 0.25 M HCl and 0.25 mM butylated hydroxytoluene, and 30 µL of 8.5% sodium dodecyl sulfate) and incubated at 95°C for 1 hour, cooled on ice for 15 minutes, and centrifuged at 10,000 rpm for 10 minutes. The absorbance of 200 µL of supernatant was analyzed at 550 nm on a Molecular Devices ThermoMax M5 microplate reader. TBARS was calculated by the extinction coefficient of malondialdehyde of 1.56×10^5 M^{-1} cm^{-1} normalized by the cell protein determined by Bradford assay.

MitoSox Flow Cytometry

TIB-73 and TIB-75 cells were grown to 80-90% confluency in 6-well plates, serum starved for 6 hours, and then treated overnight. Huh7, Hep3B, and FOCUS cells were grown to 80-90% confluency in 12-well plates, serum starved overnight, and then treated for 24 hours. After treatment, the cells were stained for 15 minutes at 37°C with 5 µM MitoSox (Life Technologies, Cat# M36008) (a mitochondrial-targeted dye that fluoresces red when oxidized by superoxide radicals) and 200 nM MitoTracker Green FM (Life Technologies, Cat# M7514) (a green dye that localizes to mitochondria regardless of mitochondrial membrane potential) in DMEM. The dyes were aspirated from the cells and then the cells were removed from the plate using 0.25% Trypsin-EDTA followed by DMEM + 10% FBS. Cells were pelleted by centrifugation, washed with PBS, pelleted again and resuspended in 750 µL PBS. Cells were stored on ice until analysis on a BD FACSCalibur using channels FL1 and FL2. The flow cytometry data was analyzed on FlowJo software. Data was gated to remove cellular debris and clumps (FSC versus SSC) and then the single cell populations were plotted on a FL1 versus FL2 cytogram and gated to determine what percentage of cells exhibited increased red fluorescence relative to untreated cells to indicate which cells have greater mitochondrial ROS production following treatment.

Subcellular Organelle Integrity and Damage Assays

Acridine Orange Staining for Lysosome Integrity by Confocal Microscopy

Cells were seeded to 35 mm^2 glass-bottom dishes coated with 10 µg/mL fibronectin and grown to 80-90% confluency. Cells were serum-starved overnight and then stained with 500

µL of 5 µg/mL acridine orange (Immunochemistry, Cat #6130) in media for 20 minutes at 37°C. Cells were washed with media and then treated for 6 hours with media or 60 µM of LDL-OA or LDL-DHA. After treatment, cells were imaged at 63x magnification on a Leica SP5 confocal microscope. Acridine orange is a cationic dye that localizes to acidic compartments of the cells where it aggregates and shifts its fluorescence from green (488 nm ex/545 nm em) to red (488 nm ex/640 nm em) so that cells with intact lysosomes will have red punctate fluorescence and cells with leaking lysosomes have cytosolic green fluorescence. Images obtained from the confocal microscope were deconvoluted on AutoQuant X3 software and then analyzed on Imaris imaging software. Lysosome leaking was assessed as the loss of red punctate intracellular organelles in the cells.

Acridine Orange Flow Cytometry

TIB-73 and TIB-75 cells were grown to 80-90% confluency in 6-well plates, serum-starved overnight, and then treated for different time periods with 60 µM LDL-DHA. After treatment, the cells were stained with 0.5 µg/mL acridine orange (AO, a cationic dye that becomes sequestered in low pH organelles where it aggregates causing a shift in fluorescence from green to red) (Immunochemistry, Cat #6130) in DMEM (Sigma, Cat #D6429) for 15 minutes at 37°C. The acridine orange dye was aspirated from the cells and then they were removed from the plate using 0.25% Trypsin-EDTA followed by DMEM + 10% FBS. Cells were pelleted by centrifugation, washed with PBS, pelleted again and resuspended in 750 µL PBS. Cells were stored on ice until analysis on a BD FACSCalibur using channels FL1 and FL2. The flow cytometry data was analyzed on FlowJo software. Data was gated to remove

cellular debris and clumps (FSC vs SSC) and then the single cell populations were plotted on a FL2 histogram to determine what percentage of cells exhibited loss of red acridine orange fluorescence which is indicative of cells that lack intact lysosomes.

Magic Red Cathepsin B Detection by Confocal Microscopy

Magic Red Cathepsin B activity (Immunochemistry, Cat # 937) was used to determine lysosome leaking in vitro via confocal microscopy. The Magic Red reagent is a non-cytotoxic substrate that fluoresces red upon cleavage by active cathepsin enzymes. The majority of cathepsin enzymes are localized to the lysosomes therefore Magic Red fluorescence should be punctate. A diffuse Magic Red staining is indicative of lysosome leaking or cathepsin enzyme activity outside of the lysosome. Cells were grown to 80-90% confluency in 35mm2 glass bottom dishes coated with 10 µg/mL fibronectin. Cells were serum starved overnight and then treated with serum free media or 40 µM LDL-DHA or LDL-OA. Cells were treated with 26x Magic Red Cathepsin B reagent for 30 minutes at 37°C and an additional 15 minutes after adding 1 drop of NucBlue (Invitrogen, Cat #R37605) dye. The cells were washed twice with warm DMEM prior to imaging at 63x magnification on a Leica SP5 confocal microscope. The red channel measured Magic Red Cathepsin B fluorescence at 561 nm excitation and 610 nm emission. The blue channel measured NucBlue fluorescence at 360 nm excitation and 460 nm emission. Images were deconvoluted using AutoQuant X3 software. Imaris imaging software was used to adjust image brightness and contrast to visualize Magic Red Cathepsin B fluorescence and distribution in the Z-stack image.

Transmission Electron Microscopy

Cells were grown to 80% confluency, serum-starved overnight and treated with nanoparticle for 24 hours. Following treatment, cells were washed twice with PBS and fixed twice with 2.5% glutaraldehyde in 0.1 M cacodylate buffer for 3 minutes at room temperature. The cells were scraped unidirectionally from the plate and collected into a 1.5-mL microcentrifuge tube and pelleted at 1500 rpm for 5 minutes. The supernatant was removed and fresh fixative was added. Cells were rinsed three times with 0.1 M sodium phosphate buffer for 5 minutes per rinse with centrifugation between rinses. The cells were post-fixed with 1% osmium tetroxide in 0.1 M sodium phosphate buffer at 4°C for 1 hour. Cells were rinsed three times with 0.1 M sodium phosphate buffer and then five times with distilled water. Cells were stained for 2 hours with 4% uranyl acetate in 50% ethanol followed by an additional 2 hour incubation in 2% aqueous uranyl at 4°C in the dark. Following staining, the cells were rinsed with distilled water three times. The cells were dehydrated in a graded series of ethanol (50%, 70%, 85%, 95%, and 100%) for 5 minutes each at room temperature. The cells were further dehydrated twice in propylene oxide. Following dehydration, cells were pelleted and then both the cells and a 2% agarose solution in water were both warmed to 45°C. Once at 45°C, 90 µL of the agarose solution was added to the cell pellet and immediately centrifuged at 1500 rpm for 2 minutes. The cells were infiltrated into the agarose solution three times for 10 minutes under vacuum with 5 minute centrifugation at 7800 rpm between each step. Following each change of agarose solution, the cells were resuspended in fresh agarose with

a plastic stirrer. Thin sections of the agarose-embedded cells on a copper grid were cut on a microtome. Cell morphology was imaged on a transmission electron microscope.

Tetramethylrhodamine Methyl Esther Confocal Microscopy

Tetramethylrhodamine Methyl Ester (TMRM) is a cationic, cell-permeant dye that is sequestered by active mitochondria to monitor mitochondrial membrane potential (MMP) over time *in vitro*. TMRM loses its fluorescence when it is not sequestered in a hyperpolarized environment because of concentration redistribution; therefore, monitoring loss of TMRM fluorescence indicates loss of MMP. To monitor MMP in cell after LDL-DHA treatment, the cells were plated to 80-90% confluency on 35 mm^2 glass bottom dishes coated with 10 µg/mL fibronectin. Cells were serum starved for 8 hours prior to an overnight treatment with 40 µM of LDL-DHA or LDL-OA. Prior to imaging, each dish was stained for 25 minutes at 37°C with 200 nM TMRM (from a 300 µM TMRM stock diluted in DMSO). The media was replaced with 50 nM TMRM dye for imaging to prevent redistribution of the dye. The cells were imaged at 63x magnification on a Leica SP5 confocal microscope at 561 nm excitation and >590 nm emission. Images were deconvoluted using AutoQuant X3 software. Imaris imaging software was used to adjust image brightness and contrast to visualize TMRM fluorescence and distribution in the Z-stack image. ImageJ software was used to threshold pixel intensity to remove background fluorescence and calculate mean pixel intensity of each z-stack.

Tetramethylrhodamine Methyl Ester Flow Cytometry

TIB-73 and TIB-75 cells were grown to 80-90% confluency in 6-well plates, serum starved overnight, and then treated for different time periods with 60 µM LDL-DHA. After treatment, the cells were removed from the plate using 0.25% Trypsin-EDTA followed by DMEM + 10% FBS, pelleted and resuspended in 100 nM Tetramethylrhodamine Methyl Ester (TMRM, a cell-permeant, cationic red-orange dye that is sequestered by active mitochondria) (Life Technologies Cat #T-668) in DMEM for 15 minutes at 37°C. The cells were pelleted by centrifugation, washed with PBS, pelleted again and resuspended in 750 µL PBS. Cells were stored on ice until analysis on a BD FACSCalibur using channel FL2. The flow cytometry data was analyzed on FlowJo software. Data were gated to remove cellular debris and clumps (FSC vs SSC) and then the single cell populations were plotted on a FL2 histogram to determine what percentage of cells exhibited loss of red fluorescence which is indicative of cells without normal mitochondrial membrane potential.

γ-H2AX Immunofluorescence for DNA Damage

TIB-73 and TIB-75 cells were seeded to 80-90% confluency on an 8-chamber glass slide coated with 10 µg/mL fibronectin and serum starved prior to treatment with serum free DMEM, 40 µM LDL-DHA, 60 µM LDL-DHA, or 60 µM LDL-OA for 6 or 18 hours. Following treatment, cells were washed with 500 µL PBS and fixed with 4% paraformaldehyde in PBS on ice for 30 minutes. Following fixation, cells were washed with 500 µL PBS and permeabilized with 0.5% Triton X-100 on ice for 10 minutes. Cells were washed with 500 µL PBS and blocked with 200 µL 5% BSA/PBS for 20 minutes at room temperature. After blocking, the cells were washed with PBS and probed with a 1:1000

dilution in 1% BSA/PBS of Alexafluor 488-conjugated antibody targeted to γ-H2AX (Millipore, Cat #05-636-AF488) overnight at 4°C in a humidified chamber. The primary antibody against γ-H2AX was removed and the cells were washed three times with PBS. The chamber was removed and the slide was coverslipped using ProLong® Gold Antifade Mountant with DAPI (Life Technologies, Cat #P-36931) and sealed with nail polish. Slides were stored at -20°C prior to imaging at 63x magnification on a Leica SP5 confocal microscope using the appropriate excitations and emissions for DAPI and Alexafluor 488. Images were analyzed on Imaris imaging software to adjust brightness and contrast. ImageJ software was used to count both the total number of cells and the number of cells with ≥3 γ-H2AX foci per field of view.

Iron Measurement Assays

Iron Measurement by ICP-MS

Measurement of iron by ICP-MS was adapted from the protocol by Au-Yeung et al (Au-Yeung *et al.*, 2013). Briefly, cells were grown to 80-90% confluency, trypsinized from the plate and pelleted by centrifugation. The pellets were washed twice with PBS and then frozen at -20°C. To prepare the samples for ICP-MS analysis, the pellets were thawed, and resuspended in 5 mL of PBS. Aliquots of 100 µL cell suspension were transferred to a 1.5 mL microcentrifuge tube for protein determination by Bradford assay. The cell suspension was pelleted by centrifugation, supernatant was carefully removed, and the cell pellet was digested in 200 µL of 70% HNO_3 at 90 °C for 4 hours and then diluted with Milli-Q water to

a 2 mL volume. Samples were analyzed on an Agilent 7700x ICP-MS with auto-sampler using argon carrier gas. Iron signal was detected and compared to a 10 ppm standard (Inorganic Ventures, MSFE-10PPM).

Iron Measurement by Ferrozine Assay

TIB-73 and TIB-75 cells were grown to 80-90% confluency and then scraped and pelleted. The cell pellets were lysed with 200 µL of 50 mM NaOH for 2 hours with agitation. The cell lysates were divided and half was incubated with 100 µL of 10 mM HCl and 100 µL of iron releasing reagent (equal volumes of 1.4 M HCl and 4.5% w/v $KMnO_4$ in H_2O) for 2 hours at 60ºC in a fume hood. After cooling, 30 µL of iron detection reagent was added (6.5 mM ferrozine, 6.5 mM neocuproine, 2.5 M ammonium acetate, 1 M ascorbic acid, dissolved in H_2O) for 30 minutes at room temperature. The absorbance of 280 µL of the reaction was measured at 550 nm on a plate reader. The remaining cell lysate was used to measure protein by Bradford assay. Iron concentration of each sample was determined by comparison to a $FeCl_3$ standard curved and normalized to protein.

Iron and Lysosome Colocalization by Confocal Microscopy

TIB-73 and TIB-75 cells were grown to 80-90% confluency in $35mm^2$ glass bottom dishes coated with 10 µg/mL fibronectin. Cells were treated with serum free media or 200 µM deferoxamine (to chelate labile iron as a negative control for iron specificity of the dye) for 3 hours at 37°C, and then stained for 2 hours at 37°C with 500 µL of 20 µM IP1 (a dye that fluoresces green in the presence of labile iron) or 20 µM control dye (a constitutively

fluorescent derivative of IP1). Cells were then stained for 30 minutes at 37°C with 1000 µL 75 nM LysoTracker Deep Red (Life Technologies, Cat # L12492). Cells were then washed and imaged at 63x magnification on a Leica LP5 confocal. The green channel measured IP1 dye fluorescence at 488 nm excitation and 510 nm emission. The red channel measured deep red fluorescence of the LysoTracker dye with 561 nm excitation and >610 nm emission. Images were deconvoluted using AutoQuant X3 software. Imaris imaging software was used to calculate LysoTracker Deep Red colocalization with green IP1 or control dye in the cells. ImageJ software was used to threshold the images to remove background fluorescence and then calculate the mean pixel intensity of the green channel as a semi-quantitative measure of labile iron in the cells.

Silver Sulfide Autometallography

The silver sulfide autometallography protocol was adapted from the protocol by Danscher (Danscher, 1981). All glassware was washed with 1N HCl to remove trace metals and the following solutions were made prior to staining with milli-Q water: 2% glutaraldehyde in 0.1M Na-Cacodylate buffer with 0.1 M sucrose (pH =7.2) buffer; 1% (w/v) ammonium sulfide in 70% ethanol (pH ≈9); 70%, 90% and 100% ethanol in water; Protecting Colloid Solution (0.5 kg crystalline gum Arabic dissolved in 1L milli-Q water for 5 days with intermittent stirring and then filtered through gauze); Citrate Buffer (25.5 g citric acid 1• H20 plus 23.5 g sodium citrate 2• H20 Q.S to 100 mL with milli-Q water); Reducing agent (0.85 g hydroquinone in 15 mL milli-Q water); Silver Ion Supply (0.11 g silver lactate 15 mL milli-Q water, made fresh). TIB-73 and TIB-75 cells were grown to 80-90% confluency on

an 8-chamber glass slide. Cells were washed with PBS and then fixed with 2% glutaraldehyde in 0.1 M Na-Cacodylate buffer with 0.1 M sucrose (pH 7.2) for 2 hours at 22°C. The cells were washed five times with milli-Q water at room temperature and then sulfidated with the 1% (w/v) ammonium sulfide in 70% ethanol (pH ≈9) for 15 minutes at 22°C. The cells are rinsed in milli-Q water for 10 minutes at 22°C. Development to precipitate iron was performed in the dark at 22°C using 200 µl per chamber of a freshly-mixed, physical, colloid-protected developer solution containing silver lactate (Developer Solution: 6 mL Protecting Colloid Solution, 1 mL Citrate Buffer, 1.5 mL Reducing Agent, 1.5 mL Silver Ion Supply). The reaction was performed in the dark at 26°C for about 10-30 minutes (some chambers were stained lightly while others were stained heavily to ensure that delicate traces of metal sulfides were detected). The chambers were dehydrated in 70%, 90%, and then 100% ethanol prior to being coverslipped with the mountant Canada Basalm, which prevents the oxidation of the silver sulfide precipitate from black to white over time. Slides were imaged on an upright brightfield microscope at 10x and 20x magnification using Oprotronics Microfire camera.

Hepatocyte Isolation and Culture

Hepatocyte Isolation and Culture from Mice

For mice, hepatocytes were isolated from Balb/C mice by non-recirculating collagenase perfusion through the inferior vena cava. Livers were perfused *in situ* with 40 mL Gibco Liver Perfusion Medium (Life Technologies, Cat #17703-038) followed by 80 mL of Gibco

Liver Digestion Medium (Life Technologies, Cat #17701-034) at a rate of 3 mL/min. Thereafter, the livers were excised, their capsules removed and the liver cells were liberated in 20 mL of Liver Digest Medium. The liver cell suspension was then filtered with a Falcon cell strainer (70 µm; Becton Dickinson, Bedford, MA), washed with 20 mL of Hepatocyte Wash Medium (Life Technologies, Cat #17704-024), centrifuged at 50 x g for 4 min. The supernatant containing cell debris was removed and the pellet was gently resuspended in 20 mL of Hepatocyte Wash Medium and centrifuged again. The supernatant was removed and the cell pellet was then resuspended in 10 mL of Hepatocyte Wash Medium. The viability of the isolated hepatocytes, as determined by the exclusion of trypan blue, was > 85%. Hepatocytes were plated on collagen coated plates/dishes in DMEM + 10% FBS for 4 hours to attach to the plate and then the media was exchanged for Weymouth supplemented with 5% FBS, 10 mM nicotinamide, 20 ng/ml EGF, 1x insulin, transferrin, selenium, 10^{-7} M dexamethasone, 1% DMSO and 1x antibiotic/antimycotic. The hepatocytes were cultured at 37°C with 5% CO_2 and the media was changed every other day. These culture conditions allow the cells to maintain their proliferative capacity and differentiated functions of mature hepatocytes.

Primary Human Hepatocyte Culture

Primary human hepatocytes were purchased from Zen-Bio (Research Triangle Park, NC) along with Hepatocyte Plating Medium (HM-1) and Hepatocyte Maintenance Medium (HM-2). Vials of hepatocytes (Lot #ZBH1055) were stored in the vapor phase of liquid nitrogen until thawing at 37°C. Dead cells were removed by a 25% Percoll Gradient (11.25 mL cold Hepatocyte Plating Medium with cells, 3.75 mL Percoll, 0.375 mL 10X PBS) and spinning at

100g for 10 minutes at 4°C. The cell pellet was resuspended in 3 mL of warm Hepatocyte Plating Medium and counted in trypan blue on a hemacytometer to determine cell number and viability. The cells were diluted in Hepatocyte Plating Medium to obtain ≈70,000 cells per 125 µL and plated to a collagen-coated 96-well plate. After 6-8 hours, the media was exchanged for Hepatocyte Maintenance Medium. Cells were treated the following morning for 72 hours with increasing doses of LDL-DHA or LDL-OA (0-200 µM).

Treatment of HCC Tumors *in vivo*

Mouse TIB-75 Subcutaneous Tumor Implantation, Measurement, and Treatment

Balb/C mice were injected with 5 x 10^6 TIB-75 cells in sterile PBS subcutaneously on both hindlegs using a 31 gauge needle and syringe. Tumor size was monitored using digital calipers and volume was calculated as (width^2 x length)/2 where length is the largest measurement. Once tumors reached a size greater than 75 mm^3, tumors were injected with 40 µL of saline, 100 µM LDL-DHA or LDL-OA in saline using a 25 gauge needle attached to a 1 mL syringe. Tumors were injected twice a week for two to three weeks and tumor volume was measured prior to each injection. Following treatment, the animals were sacrificed and the tumors were collected and fixed in 10% neutral buffered formalin. Tissue samples were paraffin embedded and stained with hematoxylin and eosin by the University of Texas Southwestern Medical Center Histology Core Facility. The stained slides were imaged at 10x and 20x magnification on a brightfield microscope.

Statistics

Data were analyzed using GraphPad Prism software (GraphPad Prism version 6.00 for Windows, GraphPad Software). Results are expressed as mean ± standard error. Differences are analyzed by *t test* or ANOVA with multiple comparisons, and results are considered significant at a p value ≤ 0.05.

CHAPTER FOUR
Results

LDL-DHA NANOPARTICLE COMPOSITION, CELLULAR UPTAKE, CANCER-SELECTIVE CYTOTOXICITY, AND MECHANISM OF ACTION

Structure and Composition of the LDL-DHA Nanoparticle

The LDL-DHA nanoparticle is similar to native LDL in structure and size

Replacement of the cholesteryl ester/ triacylglycerol core of plasma LDL with DHA (Figure 3-1A), as described by the reconstitution method (Krieger *et al.*, 1979) yields LDL particles that are uniformly loaded with DHA (Figure 3-1B). Compositional analyses were performed to determine phospholipid, cholesterol, lipid loading, size, and charge of the various LDL nanoparticles (Table 1-1). All calculations assumed that there was one copy of the ApoB-100 protein per nanoparticle. The percent protein and DHA recovery from the initial starting materials were 46% and 13%, respectively. In addition, the average lipid (DHA) to protein mass ratio was calculated to be 0.82. These recovery values are in keeping with those cited by Krieger *et al*. Furthermore, the LDL-DHA and LDL-OA nanoparticles were loaded with approximately 1400 free fatty acid molecules per nanoparticle. Similarly, LDL-TO was loaded with 344 triglyceride oleic acid molecules which is equivalent to approximately 1000 molecules of oleic acid. The phospholipid assay showed that LDL-DHA and LDL-OA nanoparticles have less phospholipid in their amphipathic monolayer compared to native LDL and LDL-TO nanoparticles, which may indicate that the free fatty acids have

intercalated into the phospholipid monolayer resulting in a displacement of some phospholipids in the monolayer. Zeta-potential measurements of surface charge of the native and reconstituted LDL nanoparticles were measured and showed that native LDL and LDL loaded with neutral triglyceride oleic acid had surface charges between -8 and -15 mV, whereas reconstitution with free fatty acids significantly lowered surface charge below -20 mV likely due to the carboxylate groups of the free fatty acids. The reduction in surface charge in LDL loaded with free fatty acids further supports the hypothesis that a portion of the negatively charged free fatty acids are intercalating into the phospholipid monolayer of LDL instead of being loaded solely into the core of the LDL. To ensure that the secondary structure of the ApoB-100 protein, the protein that is recognized by LDL receptor and stabilizes the LDL structure, was not altered by reconstitution with DHA, circular dichroism (CD) spectroscopy was utilized and showed that the ApoB-100 protein was not altered (Figure 3-1C). The CD secondary structure readings of apoB-100 in LDL-DHA indicate that it contains 46% α-helix, 28% β-sheet, 6% β-turns, and 20% unordered structure. The protein secondary structure of apoB-100 from native LDL had a similar conformation (49% α-helix, 25% β-sheet, 5% β-turns, and 21% unordered structure). The apoB-100 from LDL-OA and LDL-TO also contained similar secondary conformations. The cholesterol assay showed that native LDL has cholesterol levels similar to those reported in the literature (Hevonoja *et al.*, 2000; Shen *et al.*, 1977) and that the reconstituted LDL nanoparticles had successful removal of cholesterol.

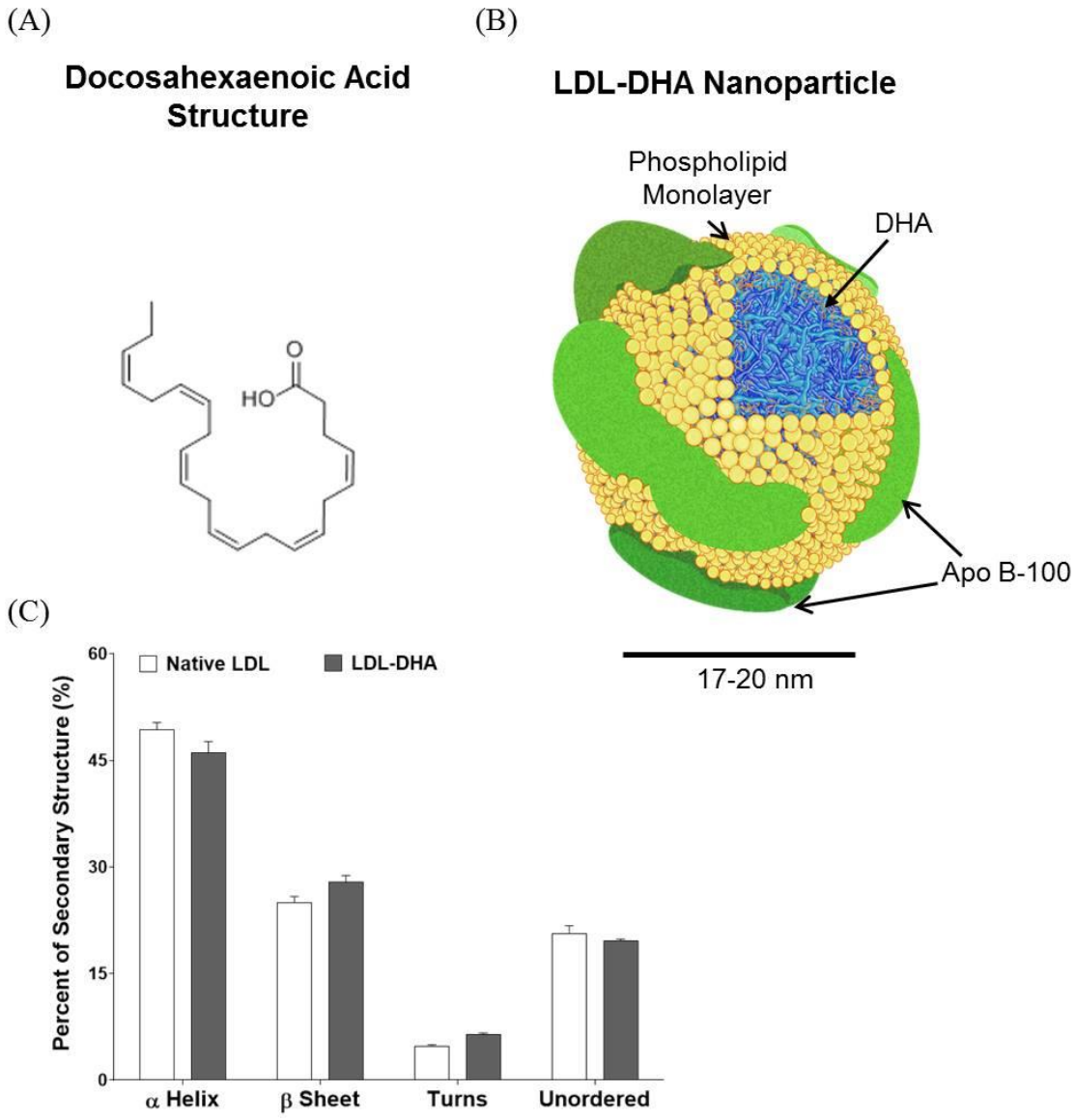

Figure 3-1: Schematic of the LDL-DHA nanoparticle

(A) The chemical structure of docosahexaenoic acid. (**B)** Conceptual figure of the structure of the low density lipoprotein nanoparticle loaded with docosahexaenoic acid. The nanoparticle is 17-20 nm in diameter and is comprised of a phospholipid membrane stabilized by a single ApoB-100 protein. **(C)** Circular dichroism spectroscopy of the secondary protein structure of the ApoB-100 protein of LDL and LDL-DHA at baseline. The ApoB-100 protein of native LDL and LDL-DHA have similar secondary structure.

	Native LDL	LDL-TO	LDL-OA	LDL-DHA
ApoB-100	1	1	1	1
Phospholipid	734 ± 114	862 ± 173	373 ± 79.7	386 ± 113
Cholesterol*	2958 ± 378	ND	ND	ND
Lipid cargo	**	344 ± 26.6	1401 ± 371	1453 ± 92
Diameter (nm)	18.2 ± 0.3	20.3 ± 0.7	20.0 ± 0.9	18.3 ± 0.5
Surface charge	-8.3 ± 0.7	-15.0 ± 2.5	-26.7 ± 6.1	-21.9 ± 3.3

Table 1-1: Composition and physicochemical properties of native LDL and LDL nanoparticles

Cholesterol and Phospholipid values, expressed as molecules per ApoB-100, were obtained from colorimetric assay kits. Lipid cargo was quantified by HPLC compared to a standard curve and values represent the number of molecules per nanoparticle. Particle diameter and surface charge was determined by dynamic light scattering and zeta-potential measurements.
*Total cholesterol includes cholesteryl esters and free cholesterol. Literature values indicate that LDL typically carries between 1300-1600 cholesteryl esters and 500-600 free cholesterol molecules (Hevonoja *et al.*, 2000; Shen *et al.*, 1977).
**LDL also carries about 170 triglyceride molecules. DHA typically makes up only 1% of the total fatty acid composition of LDL (Quilliot *et al.*, 2003).

The diameters of the native LDL and reconstituted nanoparticles were measured by dynamic light scattering and showed that the nanoparticles were approximately 20 nm, which corroborates values given in the literature for native LDL (Scheffer *et al.*, 1998). Transmission electron microscopy micrographs (Appendix A) of native LDL, LDL-DHA, LDL-OA, and LDL-TO all showed LDL's characteristic quasispherical morphology and uniform size distribution which corroborated with the particle size measurements determined by dynamic light scattering.

Another method that was used to study the composition of the native LDL and reconstituted LDL nanoparticles was ^{1}H Nuclear Magnetic Resonance (NMR) spectroscopy (Figure 3-2). The native LDL NMR spectra displayed a unique peak for cholesterol at 0.8 ppm, several resonances from the acyl chain of esterified lipids, as well as the choline head group (3.25 ppm) from the phospholipid monolayer. Reconstitution of LDL with DHA displayed several changes in the NMR spectra as the peaks unique to cholesterol were absent and those unique to carbons 2 and 3 of DHA were present at 2.4 ppm chemical shift. Additionally, the peak of the ω-3 methyl carbon at 0.98 was also present. The NMR spectra were utilized in the lab for quality control to evaluate the overall composition of the LDL-DHA nanoparticle, in addition to the routine chemical assays for protein, phospholipid and DHA determinations.

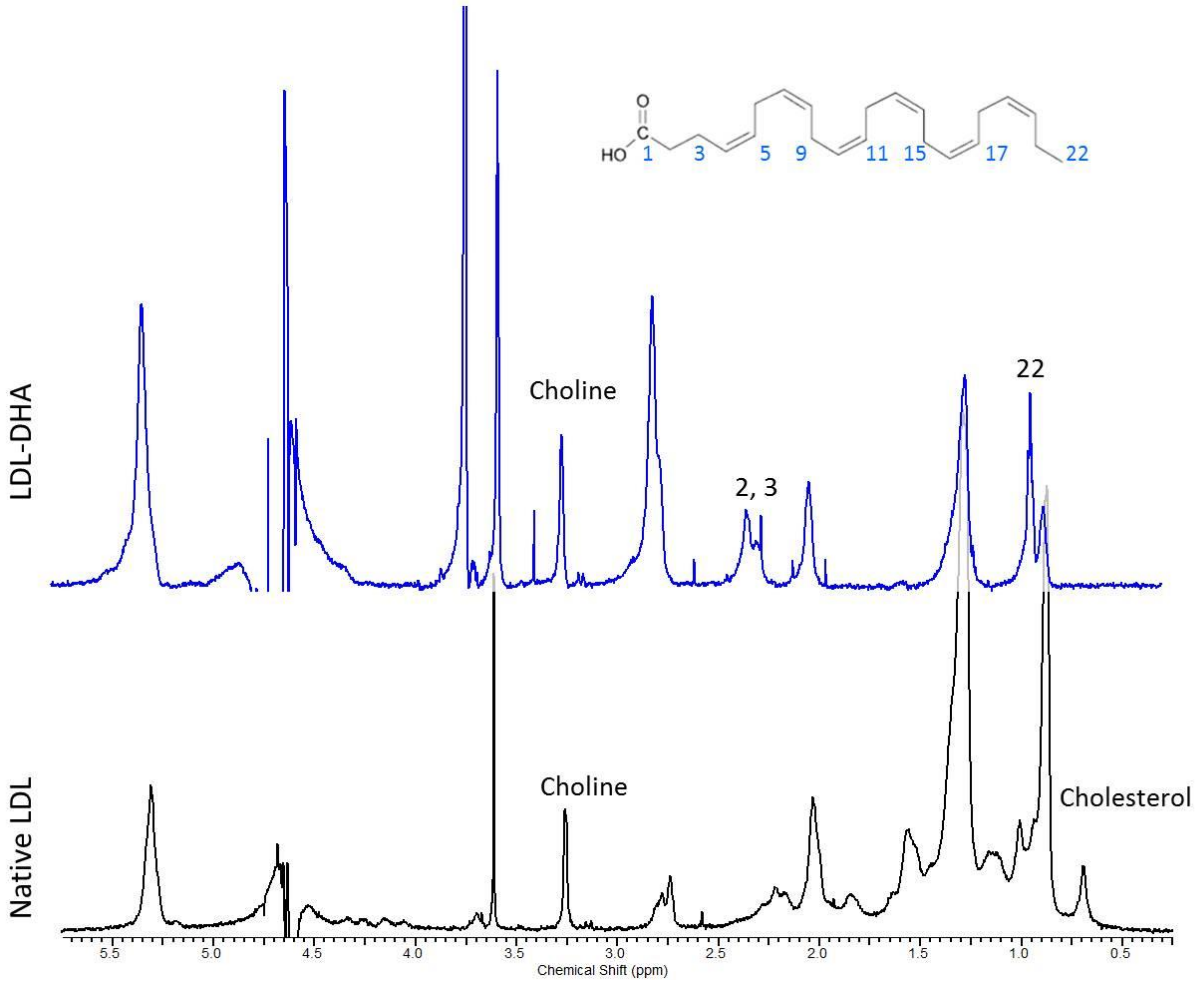

Figure 3-2: NMR spectra of LDL-DHA and native LDL

Proton ^{1}H NMR spectra of (**top**) LDL-DHA which shows the hydrogen peaks unique to DHA which are the methyl hydrogens at the tail (22) and those between the carboxylic head and double bonds (2 and 3) and the hydrogen peaks specific to choline in LDL but the cholesterol peaks are absent. The native LDL spectra **(bottom)** has hydrogen peaks specific to the choline in LDL as well as the cholesterol, the main cargo of native LDL. A 600 T Proton NMR was used.

LDL-DHA Is Internalized via LDLR-Mediated Endocytosis

The following assays were performed to determine the binding and uptake of native LDL and LDL-DHA in each cell line to ascertain whether increased TIB-75 cell cytotoxicity was due to increased uptake of LDL-DHA and whether reconstitution of LDL with DHA changed its binding and uptake by LDL receptor.

LDLR levels in TIB-73 and TIB-75 cells

It was originally hypothesized that TIB-75 cells would have higher LDL receptor levels since cancer cells are commonly cited as upregulating LDL receptor in order to provide cholesterol for the formation of cell membranes necessary for their rapid proliferation. Surprisingly, western blot analysis showed that TIB-73 cells expressed a slightly higher level of LDL receptor protein than TIB-75 cells, but that difference in receptor expression was not significantly different (Figure 4-1). TIB-73 cells may have higher LDL receptor expression than expected because they are also a rapidly dividing immortalized cell line and thus have higher needs for cholesterol than a non-dividing hepatocyte.

TIB-73 and TIB-75 cells have similar LDLR binding affinity and specificity

Since the western blot data showed that there was no significant difference in LDL receptor expression between the two cell lines, the LDL receptor binding and internalization was examined to determine if TIB-75 cells take up more LDL. LDL receptor protein expression levels are not the only determinant of LDL internalization into the cell since the rate of

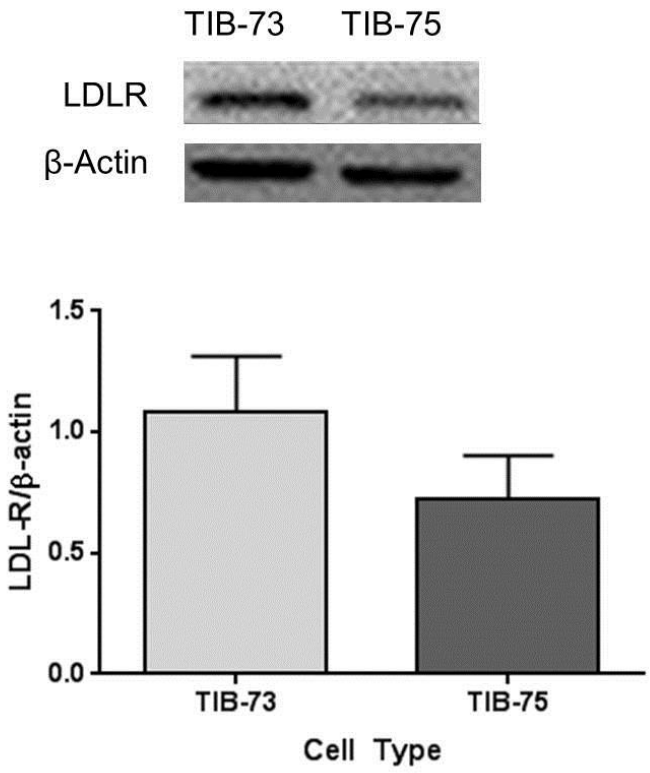

Figure 4-1: LDL receptor expression in TIB-73 and TIB-75 cells

LDL receptor protein levels from TIB-73 and TIB-75 cell lysates were determined by Western Blot and normalized to β-actin protein. TIB-73 and TIB-75 cells had a non-significant different in LDL-Receptor protein expression levels. The experiment was performed by Lacy Moss and Dr. Xiaodong Wen.

receptor recycling and internalization may vary between the two cell lines. To probe the LDL receptor binding affinity and specificity, LDL and LDL-DHA were fluorescently labeled with a carbocyanine dye DiI (1,1'- Dioctadecyl-3,3,3',3'-tetramethylindo-carbocyanine iodide). TIB-73 and TIB-75 cells were treated with 10 µg/mL of LDL-DiI or LDL-DHA-DiI for 2 hours at 4°C or 37°C. Receptor binding to LDL (Figure 4-2-1A) or LDL-DHA (Figure 4-2-1B) was calculated by the fluorescence at 4°C since endocytosis of the receptor is blocked at this temperature. LDL receptor binding was similar between both TIB-73 and TIB-75 cells for native LDL and the LDL-DHA nanoparticle. On the whole, it was observed that LDL-DHA bound to LDL receptor in slightly lower levels than native LDL indicating that the reconstitution of LDL may affect its interaction to LDL receptor. This decrease in binding to LDL receptor may be a result of the lower surface charge of the LDL-DHA nanoparticle. The internalization of LDL and LDL-DHA determined at 37°C showed that TIB-75 cells were able to internalize more native LDL than TIB-73 cells but LDL-DHA internalization by TIB-75 cells was lower. When the same experiment was repeated in the presence of an excess amount of unlabeled LDL (Figure 4-2-1C), it was observed that the binding and internalization of LDL-DiI and LDL-DHA-DiI in TIB-73 cells was sensitive to competitive inhibition by excess LDL at 37°C (p-value = 0.126). This finding shows that TIB-73 cells utilize the LDL receptor to internalize LDL and LDL-DHA. In contrast, TIB-75 cells only responded to competitive inhibition of binding and internalization of LDL and not LDL-DHA. This lack of response to competitive inhibition in TIB-75 cells suggests that TIB-75 cells may be utilizing receptors other than LDL receptor to internalize LDL-DHA (Truong *et al.*, 2000).

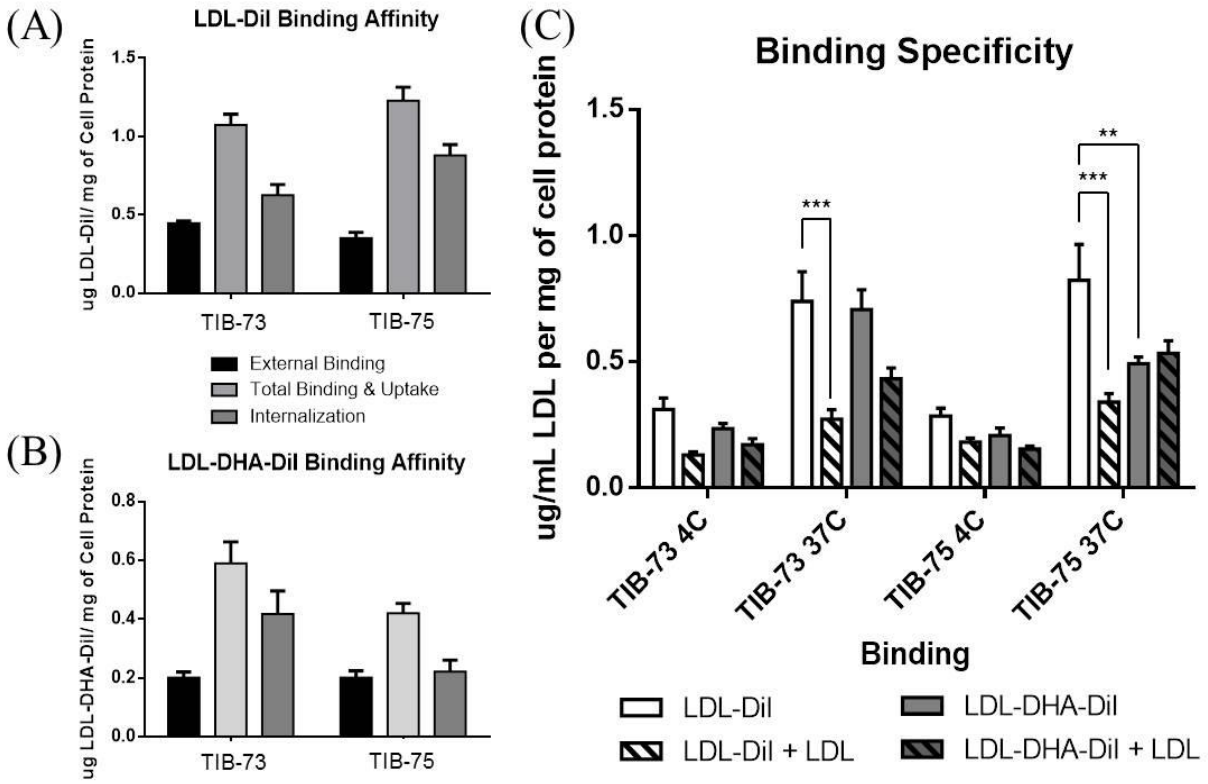

Figure 4-2-1: LDL receptor binding internalization and specificity to LDL and LDL-DHA in TIB-73 and TIB-75 cells

(A-B) External binding and internalization of native LDL and LDL-DHA were determined by treating serum-starved TIB-73 and TIB-75 cells for 2 hours with 10 µg/mL of native LDL or LDL-DHA that were labeled with DiI, a lipophilic carbocyanine dye, at 4°C or 37°C. Following treatment, the DiI was extracted with isopropanol and then the cells were lysed. DiI fluorescence and cell protein concentration of the extract and lysates were measured. External binding of the nanoparticles was calculated from the DiI fluorescence normalized to protein in the cells treated at 4°C. The total binding and uptake was calculated from the DiI fluorescence normalized to protein in the cells treated at 37°C. Internalization was calculated as the difference between the total binding and uptake and external binding. There was not a significant difference between TIb-73 and TIB-75 cells for LDL or LDL-DHA binding, uptake, or internalization. **(C)** LDLR binding specificity of native LDL and LDL-DHA was determined by a competition assay where the cells were treated as in figures A and B but also with an excess of LDL (500 µg/mL). TIB-73 exhibited reduced binding and internalization of native LDL and LDL-DHA indicating their use of the LDL-Receptor. TIB-75 cells also showed reduced binding of native labeled LDL but not of LDL-DHA when excess unlabeled LDL was added. TIB-75 cells may be using receptors other than LDLR to internalize LDL-DHA.

* = p-value ≤0.05, ** = p-value ≤0.01, *** = p-value ≤0.001, **** = p-value ≤0.0001. The error bars represent the standard error of the mean.

Additional experiments were performed where TIB-73 and TIB-75 cells were given increasing doses of LDL-DiI at 4°C and 37°C to determine the maximum ligand binding (B_{max}) and the equilibrium binding constant (K_D) for the LDL receptor in TIB-73 (Figure 4-2-2A) and TIB-75 cells (Figure 4-2-2B). TIB-73 cells generated a binding curve consistent with receptor saturation since the fluorescence increase plateaued at the high doses of LDL-DiI and a linear Scatchard plot was generated. These curves were used to calculate the B_{max} (1.66 ± 0.23 μg/mL LDL-DiI per mg of cell protein) and K_D (16.67 ± 9.22 μg/mL LDL-DiI) of the LDL receptor. The TIB-75 cells never displayed a binding curve consistent with receptor saturation as evidenced by the continual increase in DiI fluorescence and its nonlinear Scatchard plot. Because receptor saturation was never achieved with the dose range given, the B_{max} and K_D could not be determined. This provides further evidence to support that TIB-75 cells are not dependent solely on LDL receptor for endocytosis of LDL.

LDL-DHA is internalized to the lysosome compartment

To confirm that native LDL and LDL-DHA were being internalized to the lysosome by receptor-mediated endocytosis, a confocal microscopy experiment was performed to determine the colocalization of LDL-DiI or LDL-DHA-DiI with the fluorescent LysoSensor labeled lysosomes (Figure 4-3). The colocalization of LDL-DiI and LDL-DHA-DiI with the lysosome was calculated using Imaris software to generate Manders Coefficients, which indicate what percentage of nanoparticles are in the lysosome (Manders M_1) and what percent of lysosomes contain nanoparticles (Manders M_2). If receptor-mediated endocytosis is utilized for LDL and LDL-DHA uptake, then most of the nanoparticle should be in the

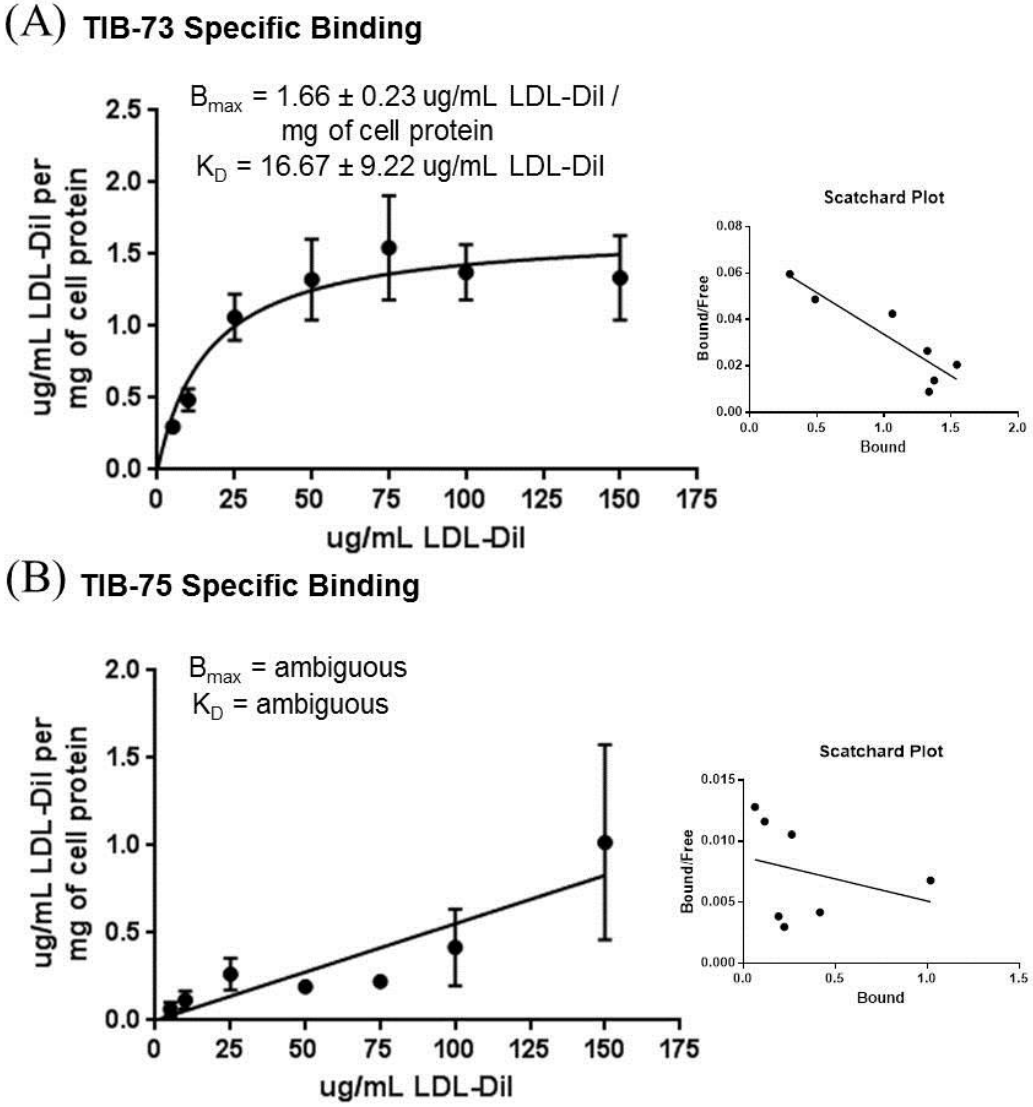

Figure 4-2-2: Receptor binding specificity of TIB-73 and TIB-75 cells to LDL and LDL-DHA

(A-B) Specific binding of the LDLR was measured by treating serum-starved TIB-73 and TIB-75 cells for 2 hours with different doses of native LDL labeled with DiI, a lipophilic carbocyanine dye, with or without an excess amount of native LDL (500 µg/mL) at 4°C or 37°C and extracting DiI fluorescence after treatment. LDL-Receptor binding specificity of native LDL was determined by subtracting the fluorescence of the cells treated with excess native LDL. TIB-73 exhibited reduced binding and internalization of native LDL and LDL-DHA indicating their use of the LDLR. TIB-75 cells also showed reduced binding of native labeled LDL but not of LDL-DHA when excess unlabeled LDL was added.
* = p-value ≤0.05, ** = p-value ≤0.01, *** = p-value ≤0.001, **** = p-value ≤0.0001. The error bars represent the standard error of the mean.

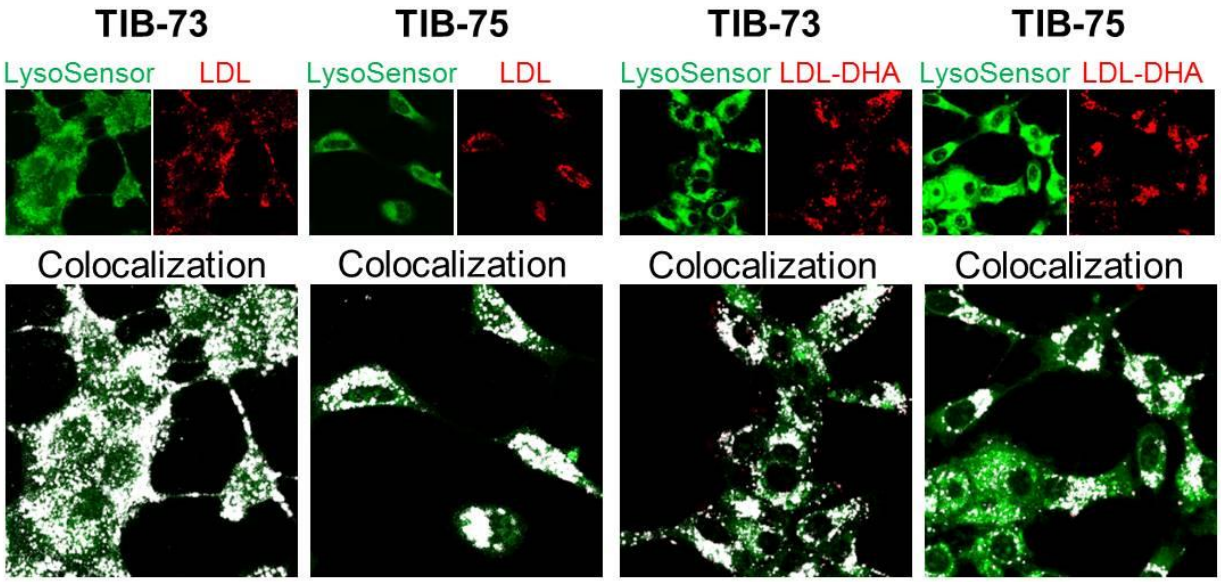

	LDL-DiI		LDL-DHA-DiI	
Cell Type	% of LDL-DiI in Lysosome (Manders M_1)	% of Lysosomes with LDL-DiI (Manders M_2)	% of LDL-DHA-DiI in Lysosome (Manders M_1)	% of Lysosomes with LDL-DHA-DiI (Manders M_2)
TIB-73	94.0 ± 1.9%	31.5 ± 8.6%	71.2 ± 8.6%	40.7 ± 13.5%
TIB-75	91.7 ± 6.6%	39.0 ± 8.6%	81.1 ± 12.4%	43.0 ± 8.0%

Figure 4-3: LDL and LDL-DHA colocalize with the lysosome

TIB-73 and TIB-75 cells were seeded onto glass slides coated with 10 µg/mL fibronectin and treated for 2 hours with LDL and LDL-DHA that were labeled with DiI, a lipophilic carbocyanine dye, and stained with 1 µM LysoSensor Green DND-189. Cells were imaged in z-stacks at 63x on a Leica LP5 confocal microscope. Images were deconvoluted using AutoQuant X3 software and then Imaris software was used to quantify colocalization of the labeled nanoparticles and the LysoSensor Green dye and generate a white mask on the images where the two probes are colocalized. There was not a significant difference in LDL and LDL-DHA colocalization in either TIB-73 or TIB-75 cells.

lysosome (Manders M_1), but it is not expected that all lysosomes will contain nanoparticles (Manders M_2). In the case of LDL-DiI, TIB-73 and TIB-75 cells had ≈94.0% and ≈91.7% of nanoparticle colocalizing with the lysosome, respectively. The colocalization of LDL-DHA nanoparticles with the lysosome was lowered slightly down to ≈71.2% and ≈81.1% for TIB-73 and TIB-75 cells, respectively.

DHA cytotoxicity is not dependent on escape from LDL

The next step after confirming that LDL-DHA was being internalized by receptor-mediated endocytosis to the lysosome was to determine if LDL degradation was necessary for DHA to induce cytotoxicity in TIB-75 cells. This was examined by pretreating TIB-75 cells with agents that inhibited endosome-lysosome or autophagosome fusion, lysosome acidification, or cysteine and serine protease activity. At the onset of this set of experiments, it was hypothesized that blocking LDL degradation, by inhibiting lysosome acidification, would be sufficient to rescue TIB-75 cells from LDL-DHA cytotoxicity. TIB-75 cells were pretreated with ammonium chloride (a weak base that raises lysosome acidity and prevents lysosome-phagosome fusion) and then dosed with 60 μM LDL-DHA for 24 hours. After treatment, TIB-75 cells were still sensitive to LDL-DHA after ammonium chloride treatment even after factoring in the decrease in viability seen with ammonium chloride treatment alone (Figure 4-4-1A). To overcome the potential for LDL-DHA cytotoxicity by endosome-phagosome fusion, a different lysosome acidification inhibitor was utilized. The second inhibitor of LDL degradation utilized was chloroquine, which is a lysosomotropic agent that blocks endosome acidification and ultimately prevents endosome-lysosome fusion, autophagosome formation,

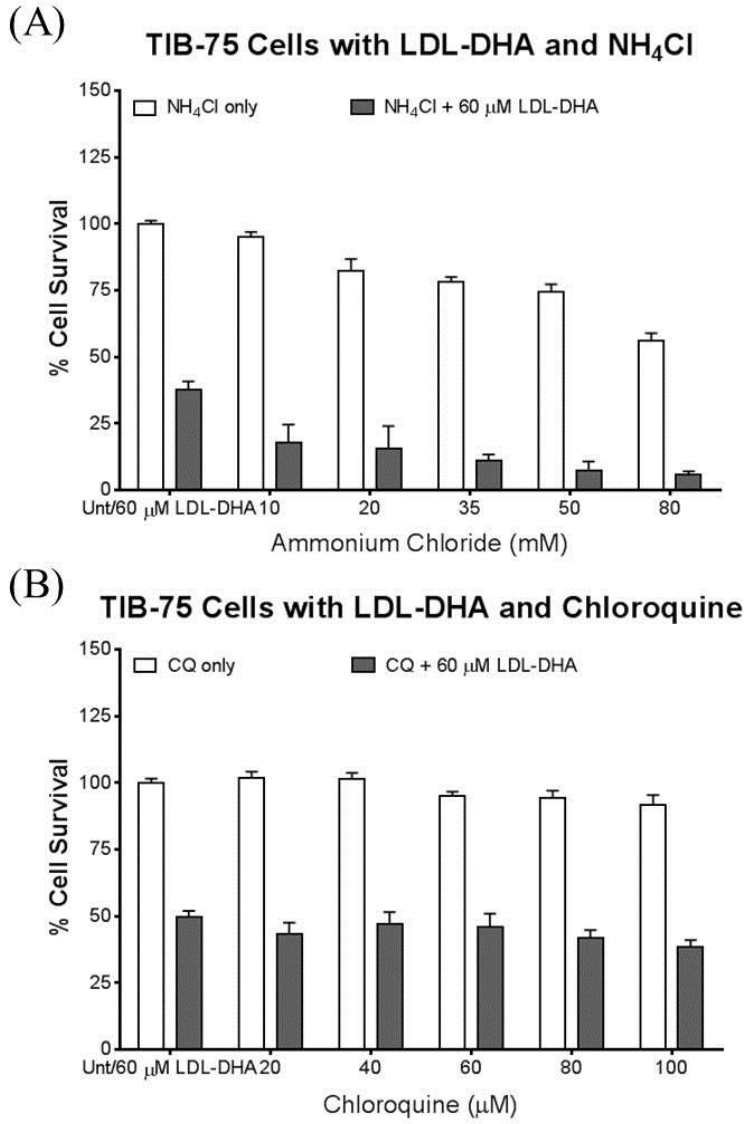

Figure 4-4-1: LDL-DHA cytotoxicity after inhibition of lysosome acidification in TIB-75 cells

TIB-75 cells were grown to 80-90% confluency in 96 well plates, serum starved overnight, and then pretreated with increasing doses of ammonium chloride **(A)** or chloroquine **(B)** to block lysosome acidification and autophagolysosome fusion. After 1 hour of pretreatment, LDL-DHA (60 μM DHA) was added to the cells. Cell viability was measured by MTS assay after 24 hours. TIB-75 cell sensitivity to LDL-DHA was not rescued by pretreatment with ammonium chloride or chloroquine.

* = p-value ≤0.05, ** = p-value ≤0.01, *** = p-value ≤0.001, **** = p-value ≤0.0001. The error bars represent the standard error of the mean.

and lysosome protein function. Surprisingly, pretreatment of TIB-75 cells with chloroquine did not protect the cells from LDL-DHA cytotoxicity (Figure 4-4-1B) indicating that LDL-DHA degradation by the lysosome is not necessary for DHA's cytotoxicity. Since there was still the possibility of endosome-phagosome fusion following inhibition with chloroquine, inhibitors of lysosome cysteine and serine proteases were examined. These inhibitors should not affect lysosome acidification and fusion of the lysosome with the endosome or phagosome. TIB-75 cells were pretreated with E-64, a lysosome cysteine protease inhibitor, before treatment with LDL-DHA but, once again, TIB-75 cells were not rescued from LDL-DHA by this protease inhibitor (Figure 4-4-2A). Administration of leupeptin, a lysosome serine protease inhibitor, prior to LDL-DHA treatment also did not rescue TIB-75 cells (Figure 4-4-2B). Another experiment that was run was the co-administration of both E-64 and leupeptin to block both cysteine and serine proteases prior to LDL-DHA treatment but this also did not rescue TIB-75 cells (data not shown). These data along with the ammonium chloride and chloroquine results suggest that LDL degradation is not necessary to elicit the cytotoxicity of LDL-DHA. Additional studies to elucidate the mechanisms governing the cytotoxicity of LDL-DHA will be further explored in later sections of this thesis.

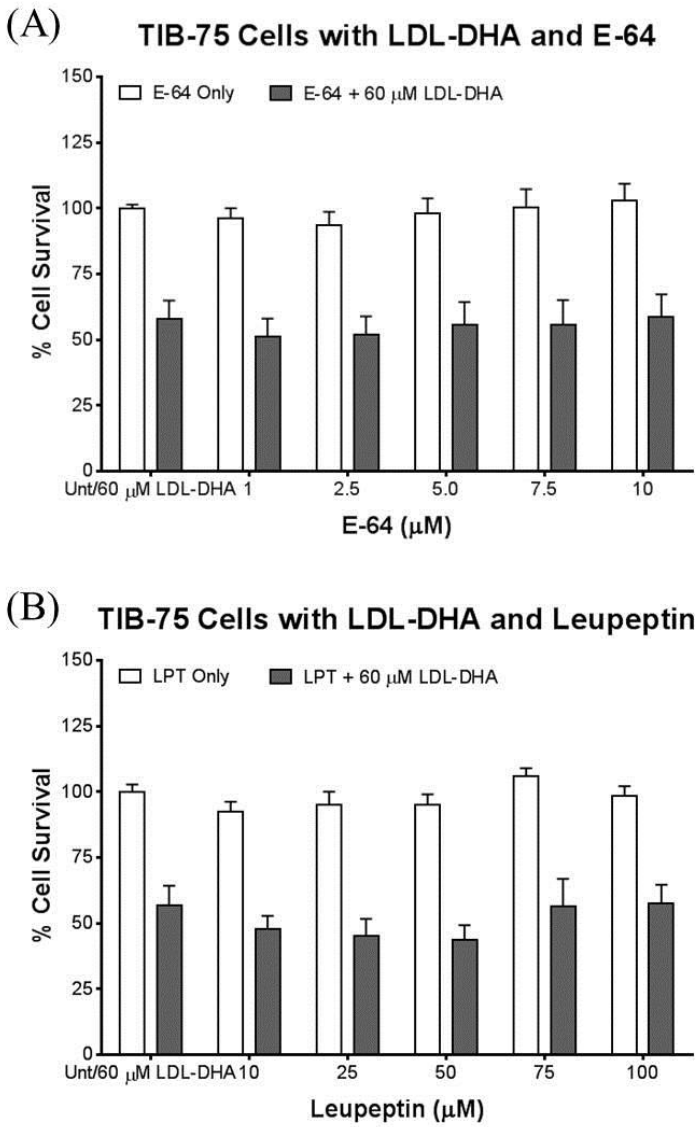

Figure 4-4-2: LDL-DHA cytotoxicity after lysosome protease inhibition in TIB-75 cells

TIB-75 cells were grown to 80-90% confluency in 96 well plates, serum starved overnight, and then pretreated with increasing doses of E-64 **(A)** or leupeptin **(B)** to block lysosomal cysteine and serine protease activity, respectively. After 1 hour of pretreatment, LDL-DHA (60 μM DHA) was added to the cells. Cell viability was measured by MTS assay after 24 hours. TIB-75 cell sensitivity to LDL-DHA was not rescued by pretreatment with E-64 or leupeptin.

* = p-value ≤0.05, ** = p-value ≤0.01, *** = p-value ≤0.001, **** = p-value ≤0.0001. The error bars represent the standard error of the mean.

LDL-DHA Is Selectively Cytotoxic to Hepatocellular Carcinoma Cells

TIB-73 cells are a nonmalignant hepatocyte cell line derived from Balb/C mice that display an epithelial morphology and cobble-stone monolayer growth pattern. TIB-75 cells, a malignant hepatocyte cell line derived from chemical transformation from TIB-73 cells, are mesenchymal in appearance and grow in chaotic overlapping layers (top images in Figure 5-1-3).

The cytotoxicity of LDL-DHA is dependent on DHA

The cytotoxicity of LDL-DHA nanoparticle was evaluated in the mouse liver cell lines TIB-73 and TIB-75. TIB-73 and TIB-75 cells were treated for 72 hours with increasing doses (0-100 μM) of LDL-DHA (Figure 5-1-1), LDL-OA (Figure 5-1-2A), or LDL-TO (Figure 5-1-2B) and cell viability was measured by MTS assay at the end of the treatment. Only treatment with LDL-DHA caused a significant decrease in TIB-75 cell viability (IC_{50} = 27.7 μM DHA). TIB-73 cells were unaffected by treatment with LDL-TO and LDL-OA and did not show appreciable cytotoxicity until 80 μM LDL-DHA (IC_{50} = 91.4 μM DHA) and in fact experienced increased growth compared to control up until 70 μM DHA. Primary hepatocytes from Balb/C mice also did not display cytotoxicity to LDL-DHA in the dose range given (IC_{50} = 148.8 μM DHA). These data indicate that DHA is the active agent resulting in cell death of the malignant TIB-75 cells and not a result of treatment with LDL since neither LDL-OA nor LDL-TO led to a significant decrease in cell viability. Furthermore, the LDL-DHA nanoparticle proved to be selectively cytotoxic towards TIB-75

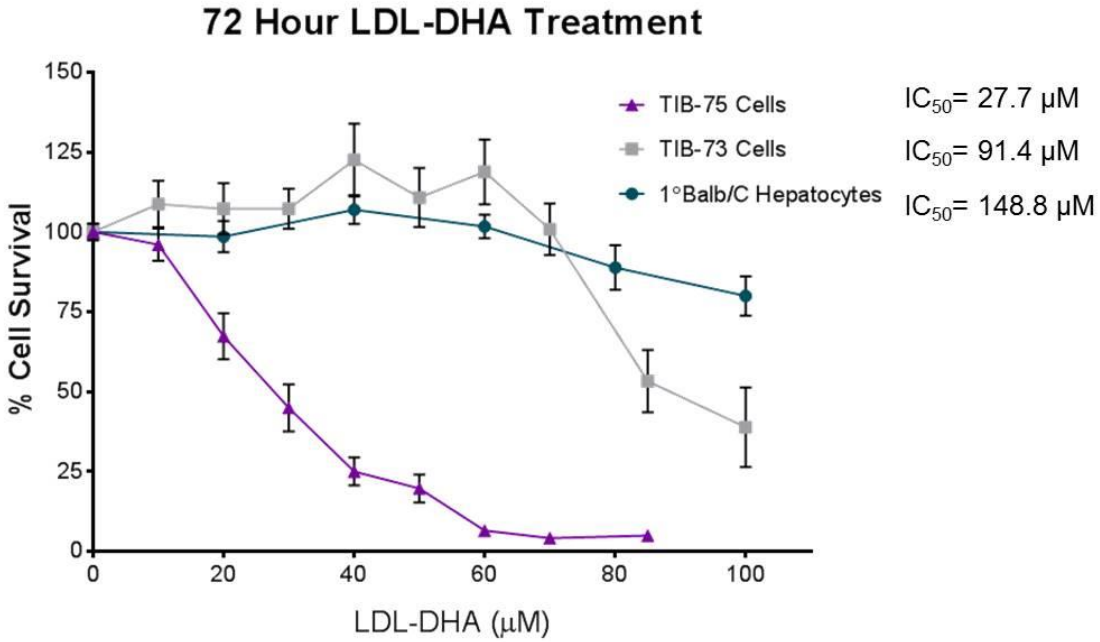

Figure 5-1-1: Cytotoxicity of LDL-DHA in TIB-73, TIB-75 and Balb/C 1° hepatocytes

TIB-73, TIB-75, and Balb/C primary hepatocytes were grown to 80-90% confluency in 96 well plates, serum starved overnight, and then treated with increasing doses of LDL-DHA (0-100 µM DHA). Cell viability was measured by MTS assay after 72 hours. TIB-75 cells were more sensitive to LDL-DHA treatment (IC_{50} = 27.7 µM DHA) than TIB-73 cells (IC_{50} = 91.4 µM DHA) and Balb/C primary hepatocytes (148.8 µM DHA).
* = p-value ≤0.05, ** = p-value ≤0.01, *** = p-value ≤0.001, **** = p-value ≤0.0001. The error bars represent the standard error of the mean.

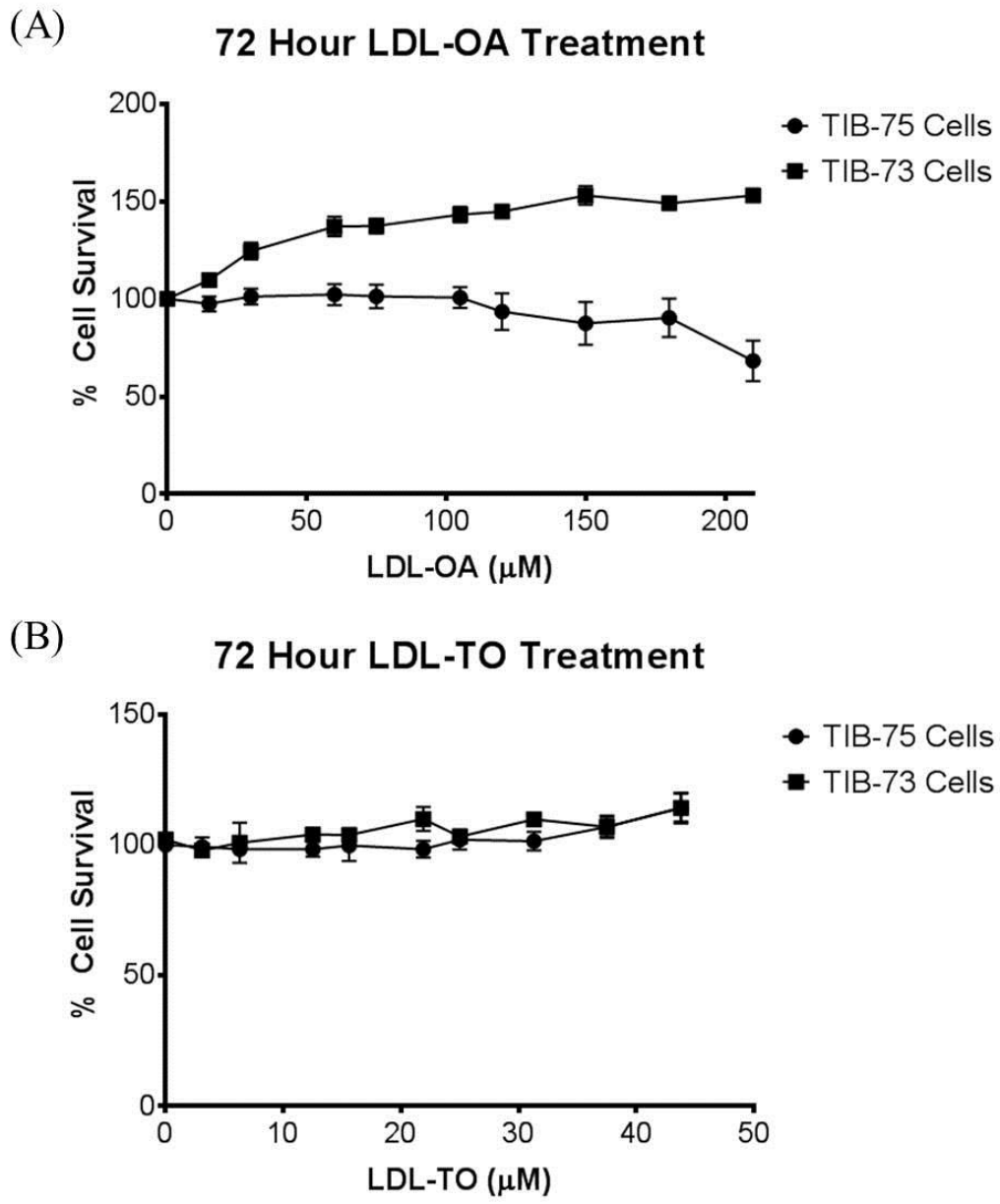

Figure 5-1-2: Cytotoxicity of LDL vehicles in TIB-73 and TIB-75 cells

TIB-73 and TIB-75 cells were grown to 80-90% confluency in 96 well plates, serum starved overnight, and then treated with increasing doses of **(A)** LDL-OA or **(B)** LDL-TO. Cell viability was measured by MTS assay after 72 hours.
* = p-value ≤0.05, ** = p-value ≤0.01, *** = p-value ≤0.001, **** = p-value ≤0.0001. The error bars represent the standard error of the mean.

cells, as it was able to kill these malignant cells at doses that were not harmful to TIB-73 or the primary mouse hepatocytes. To further examine the cancer selective cytotoxicity of LDL-DHA, TIB-73 and TIB-75 cells were grown in separate halves of the same plate and treated concurrently with 60 µM LDL-DHA or an equivalent dose of LDL-TO for 72 hours (Figure 5-1-3). The aim of this assay was to partially recapitulate conditions seen *in vivo* where both normal liver and tumor experience identical exposure to LDL-DHA treatment. Both cell lines displayed their characteristic morphologies under co-culture conditions. As expected, LDL-TO treatment did not impede the growth of TIB-73 and TIB-75 cells. Conversely with LDL-DHA treatment, only cell debris remained of TIB-75 cells after treatment with LDL-DHA, however, TIB-73 cells were not harmed and continued to grow in their characteristic cobblestone pattern on their half of the dish. The results of this co-culture assay further demonstrated that LDL-DHA was selectively cytotoxic to TIB-75 cells. Interestingly, the TIB-73 cells were not harmed by the adjacent death of the TIB-75 cells.

LDL-DHA is more cytotoxic than HSA-DHA

Since albumin functions as one of the major transporters of free fatty acids in the plasma, the efficacy of HSA-DHA to kill TIB-75 cells was evaluated (Figure 5-2A). HSA-DHA failed to induce any cytotoxicity in TIB-75 cells over a dose range of DHA up to 200 µM DHA and actually increased the viability of TIB-75 cells for most of the treatment doses of HSA-DHA. Interestingly, HSA-DHA treatment consistently reduced the viability of TIB-73 cells to 70% of the untreated controls over the entire dose range (Figure 5-2B). These data indicate that LDL rather than HSA is a better delivery vehicle for enabling the anticancer effects of DHA.

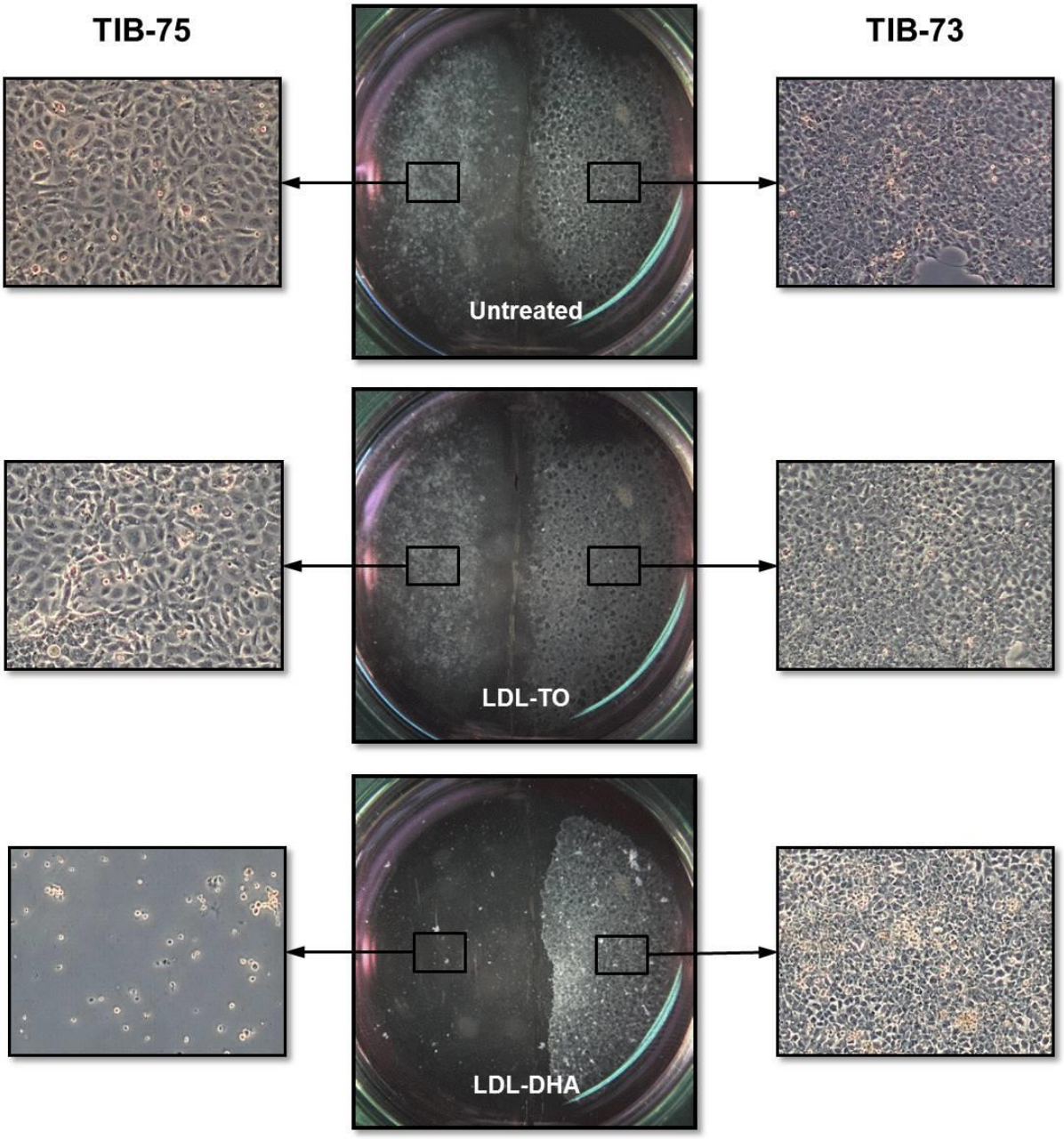

Figure 5-1-3: Selective cytotoxicity of LDL-DHA in co-culture

TIB-73 and TIB-75 cells were plated on in co-culture on separate halves of a 6-well plate until 80-90% confluent, serum starved overnight, and then treated with media, LDL-TO or 60 µM LDL-DHA for 72 hours. After treatment, the cells were imaged at 10× magnification on an inverted bright field microscope and at 0.5× magnification on a dissecting microscope.

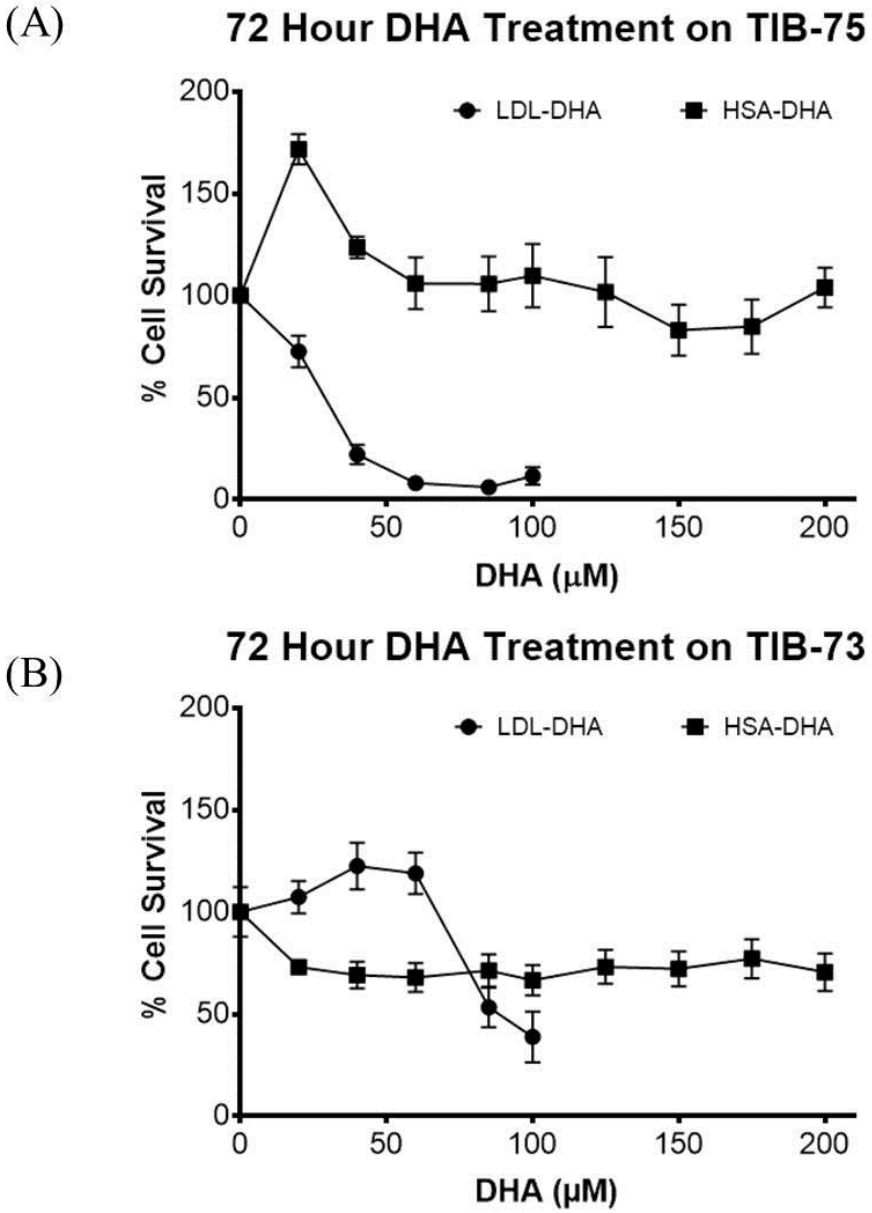

Figure 5-2: Cytotoxicity of LDL-DHA and HSA-DHA in TIB-75 and TIB-73 cells

TIB-73 and TIB-75 cells were grown to 80-90% confluency in 96 well plates, serum starved overnight, and then treated with increasing doses of LDL-DHA (0-100 μM DHA) or HSA-DHA (0-200 μM DHA) . Cell viability was measured by MTS assay after 72 hours. **(A)** TIB-75 cells were more sensitive to LDL-DHA (IC_{50} = 27.1 μM DHA) than HSA-DHA (IC_{50} = not determined). **(B)** TIB-73 cells were not significantly sensitive to HSA-DHA in the dose range tested since the IC_{50} could not be determined, but viability was consistently 70% of untreated cells.

* = p-value ≤0.05, ** = p-value ≤0.01, *** = p-value ≤0.001, **** = p-value ≤0.0001. The error bars represent the standard error of the mean.

Inhibition of different cell death pathways is not sufficient to rescue LDL-DHA cytotoxicity

Previous studies in the Corbin laboratory examined Annexin-V FITC and Propidium Iodide staining in TIB-73 and TIB-75 cells treated with LDL-DHA or LDL-TO. These experiments indicated that TIB-75 cells underwent both apoptosis and necrosis when treated with LDL-DHA (Appendix B). Additionally, time lapse microscopy of TIB-73 and TIB-75 cells showed that TIB-73 cells continue replicating while TIB-75 cells appear to die by apoptosis at lower LDL-DHA (40 µM) concentrations and by necrosis at higher concentrations (60 µM) over a 48 or 24 hour time period, respectively (data not shown).To further evaluate the cell death mechanism mediating LDL-DHA cytotoxicity, TIB-75 cells were pretreated with inhibitors of apoptosis, programmed cell necrosis, autophagy, and ferroptosis and then treated for 24 hours with 60 µM LDL-DHA. Inhibition of apoptosis using the inhibitor Z-VAD-FMK failed to rescue LDL-DHA cytotoxicity in TIB-75 cells (Figure 5-3A) and even increased sensitivity to LDL-DHA at higher doses of Z-VAD-FMK (150 µM). Attempts at inhibiting programmed cell necrosis using Necrostatin-1 also did not reduce cytotoxicity of TIB-75 cells to LDL-DHA (Figure 5-3B). It may be important that both apoptosis and necrosis are inhibited since previous Annexin-V FITC/Propidium Iodide studies implicated both pathways and inhibition of a single pathway was not sufficient to rescue TIB-75 cells. Inhibition of autophagy using Bafilomycin-A1 was also not sufficient to rescue LDL-DHA cytotoxicity and the highest dose of Bafilomycin-A1 increased TIB-75 cell sensitivity to LDL-DHA (Figure 5-3C). Finally, inhibition of ferroptosis, an iron-mediated cell death pathway, using Ferrostatin-1 was unsuccessful at inhibiting cytotoxicity of LDL-DHA (Figure 5-3D). Collectively, these results indicate that inhibiting a single cell death pathway

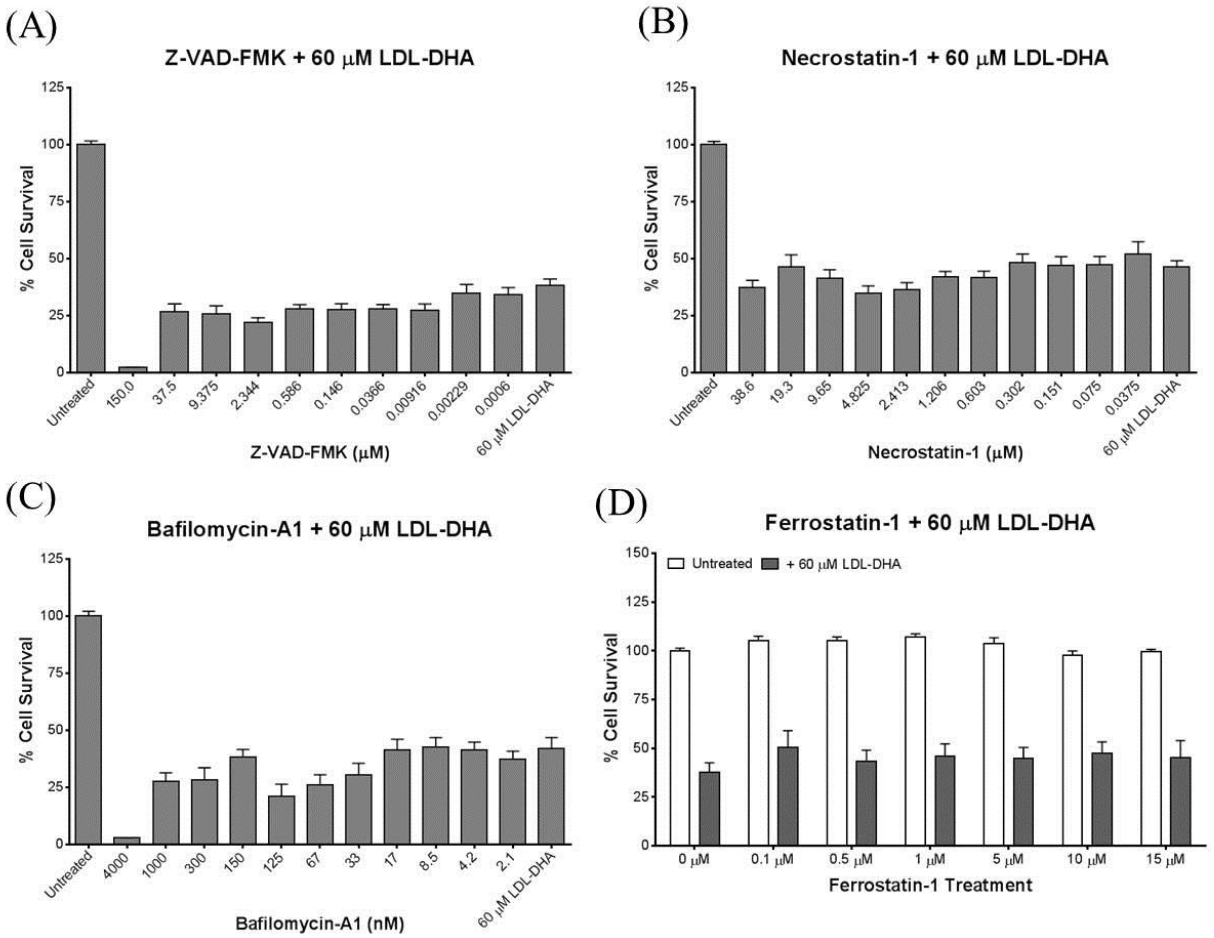

Figure 5-3: Cell death inhibitors on preventing LDL-DHA cytotoxicity in TIB-75 cells

TIB-75 cells were grown to 80-90% confluency in 96 well plates, serum starved overnight, treated with cell death inhibitors and LDL-DHA (60 μM). Cell viability was determined by MTS assay after 24 hours. **(A)** Z-VAD-FMK is an inhibitor of apoptosis. **(B)** Necrostatin-1 is an inhibitor of programmed cell necrosis. **(C)** Bafilomycin-A1 is an inhibitor of autophagy. **(D)** Ferrostatin-1is a putative inhibitor of ferroptosis, an iron-mediated cell death pathway.
* = p-value ≤0.05, ** = p-value ≤0.01, *** = p-value ≤0.001, **** = p-value ≤0.0001. The error bars represent the standard error of the mean.

is insufficient at rescuing LDL-DHA. Future experiments should look at the success of inhibiting multiple cell pathways simultaneously on preventing TIB-75 cell death from LDL-DHA. One advantage of the independence of LDL-DHA cytotoxicity on a single cell death pathway is that malignant cells may be less susceptible to developing resistance to LDL-DHA cytotoxicity which would make LDL-DHA a more effective therapeutic than traditional chemotherapies.

The Role of Reactive Oxygen Species in Sensitivity to LDL-DHA in TIB-75 Cells

An article by Reuter *et al.* reviewed the important role of increased oxidative stress and inflammation in cancer progression (Reuter *et al.*, 2010). Given that oxidative stress is known to play a key role in the initiation and progression of hepatocellular carcinoma, assays were performed to explore the inherent differences in oxidative stress and antioxidant potential between TIB-73 and TIB-75 cells at baseline. Further studies also went on to examine effects of LDL-DHA treatment on ROS generation in these two cell lines.

TIB-75 cells have lower antioxidant capability than TIB-73 cells

Baseline antioxidant enzyme protein expression in TIB-73 and TIB-75 cells was measured by western blot assay (Figure 6-1). These findings showed that TIB-75 cells have lower expression of the antioxidant enzymes catalase and glutathione peroxidase-4 (GPx-4) compared to TIB-73 cells. Superoxide dismutase-1 (SOD-1) levels were not significantly different between TIB-73 and TIB-75 cells at baseline.

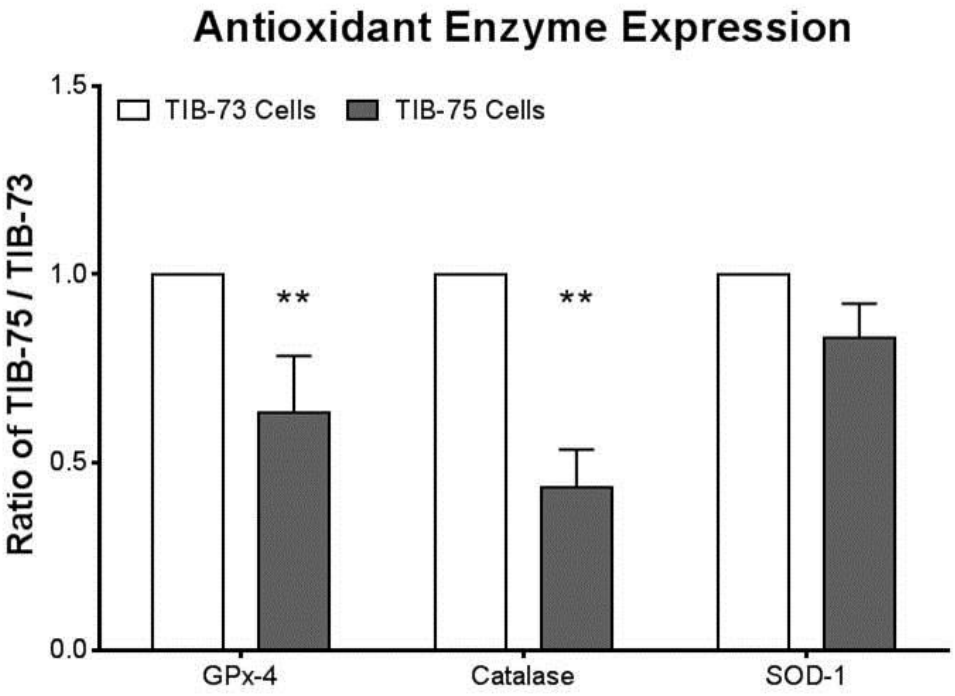

Figure 6-1: Baseline antioxidant protein levels in TIB-73 and TIB-75 cells

Antioxidant protein levels from TIB-73 and TIB-75 cell lysates were determined by Western Blot and normalized to β-actin protein. SOD-1 protein expression was not significantly different, but TIB-75 cells had significantly lower GPx-4 and catalase protein expression compared to TIB-73 cells.
* = p-value ≤0.05, ** = p-value ≤0.01, *** = p-value ≤0.001, **** = p-value ≤0.0001. The error bars represent the standard error of the mean.

Additional experiments previously completed by members of the Corbin laboratory investigated the redox-coupled systems of TIB-73 and TIB-75 cells. The first assay investigated the NADPH/$NADP^+$ ratio of the TIB-73 and TIB-75 cells at baseline as a measure of the cells reducing potential. Our studies found that both cells had equivalent NADPH/NADP+ ratios. (Figure 6-2-1). NADPH is an important player in the cell's antioxidant defense because it participates in the thioredoxin antioxidant system, reactivates catalase after hydrogen peroxide, and regenerates reduced glutathione after its oxidation (Ying, 2008). Also, the redox status of the glutathione reducing system which is closely linked to the NADPH system was examined in TIB-73 and TIB-75 cells by looking at the ratio of GSH (reduced glutathione) to GSSG (oxidized glutathione) by an enzymatic recycling method (Figure 6-2-2). It was found that the TIB-75 cells had a significantly lower GSH:GSSG ratio (≈40:1) compared to TIB-73 cells (≈115:1) . These results indicate that TIB-75 cells are more oxidized and are less capable of safely removing reactive oxygen species than TIB-73 cells.

In order to probe the importance of increased baseline reactive oxygen species in LDL-DHA cytotoxicity in TIB-75 cells, TIB-73 cells were pretreated with menadione (bisulfite salt) prior to treatment with LDL-DHA. Menadione treatment increases reactive oxygen species by interaction with NADPH cytochrome P450 reductase to form an unstable semiquinone radical that then reacts with oxygen to produce superoxide radicals, perhydroxyl radicals, hydrogen peroxide, and hydroxyl radicals that can then form lipid peroxide species

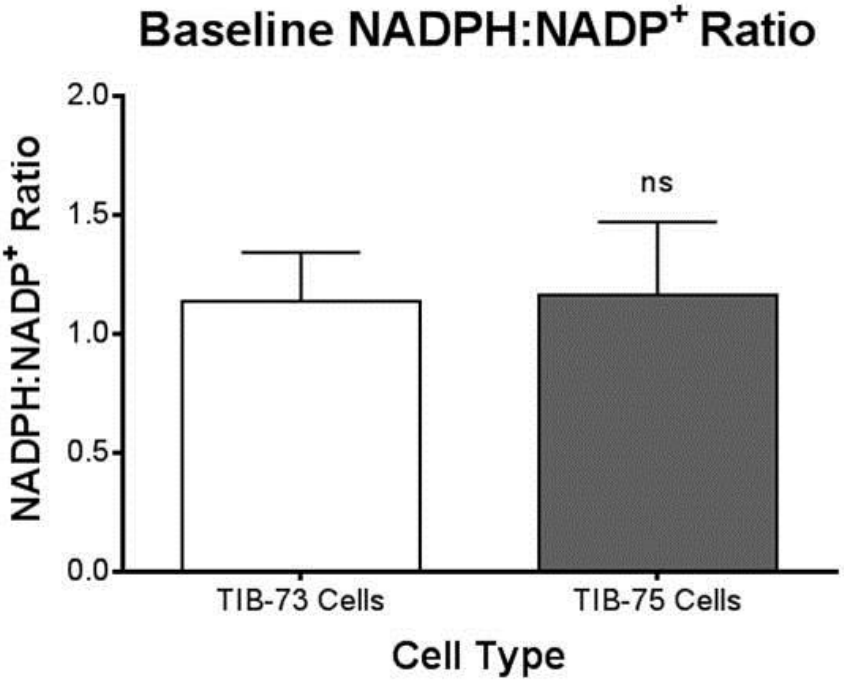

Figure 6-2-1: NADPH/NADP$^+$ ratio in TIB-73 and TIB-75 cells at baseline

TIB-73 and TIB-75 cells were grown to 80-90% confluency in 100 mm^2 dishes and then cell pellets were collected and the NADPH and NADP$^+$ levels were determined according to manufacturer's recommendations. This experiment was performed by Dr. Rohit Mulik.
* = p-value ≤0.05, ** = p-value ≤0.01, *** = p-value ≤0.001, **** = p-value ≤0.0001. The error bars represent the standard error of the mean.

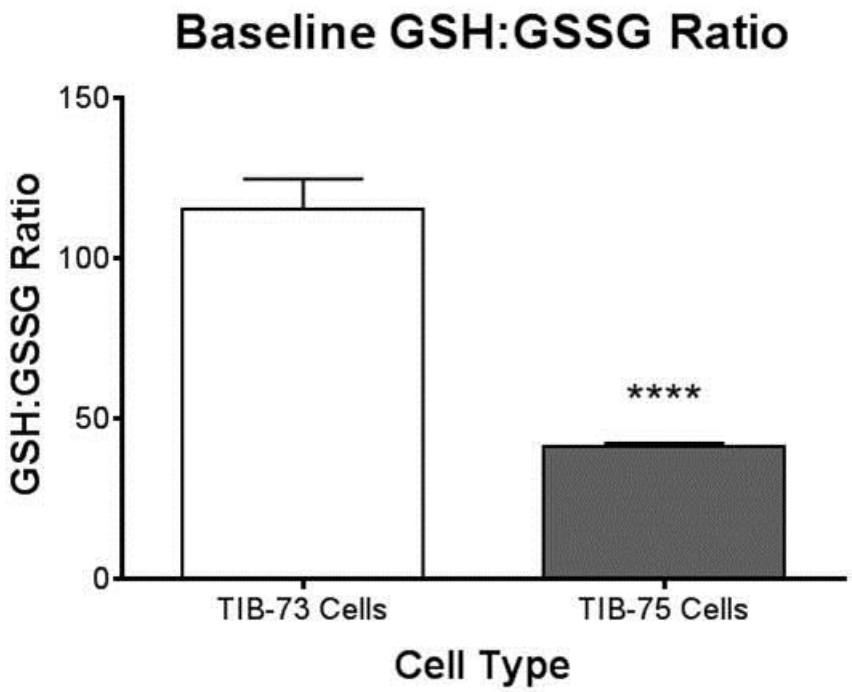

Figure 6-2-2: GSH:GSSG ratio in TIB-73 and TIB-75 cells at baseline

TIB-73 and TIB-75 cells were grown to 80-90% confluency in 100 mm^2 dishes and then cell pellets were collected and the GSH and GSSG levels were determined using an enzymatic recycling method.
* = p-value ≤0.05, ** = p-value ≤0.01, *** = p-value ≤0.001, **** = p-value ≤0.0001. The error bars represent the standard error of the mean.

(Parkinson, 2013). In the first experiment, TIB-73 cells were treated with increasing doses of menadione (0-30 µM) and then with a sublethal dose of LDL-DHA (60 µM) to establish the dose of menadione that is sufficient to induce LDL-DHA cytotoxicity without harming the cells on its own (Figure 6-3A). Even the lowest dose of menadione at 10 µM was sufficient to significantly increase sensitivity to LDL-DHA, but increased viability with menadione alone was observed with the lower menadione doses (10-20 µM). This increased viability with low doses of menadione is consistent with the literature that claims that low levels of ROS increase cell proliferation. The 25 µM menadione dose was used in the subsequent experiment because it consistently yielded significant LDL-DHA cytotoxicity while also not increasing or decreasing TIB-73 cell viability significantly from the untreated cells. TIB-73 cells were pretreated with 25 µM menadione and then treated with a dose range of LDL-DHA (0-100 µM) for twenty-four hours. The menadione pretreated TIB-73 cells experienced significantly increased sensitivity to LDL-DHA as evidenced by a drop in their IC_{50} from 131.8 µM DHA to 20.3 µM DHA (Figure 6-3B). These data show that reactive oxygen species are important in sensitizing the non-malignant TIB-73 cells to LDL-DHA.

(A)

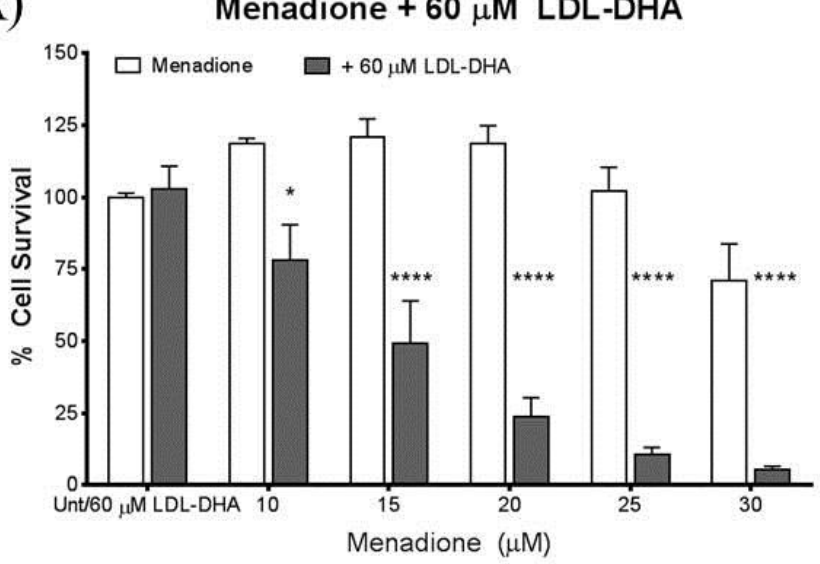

(B)

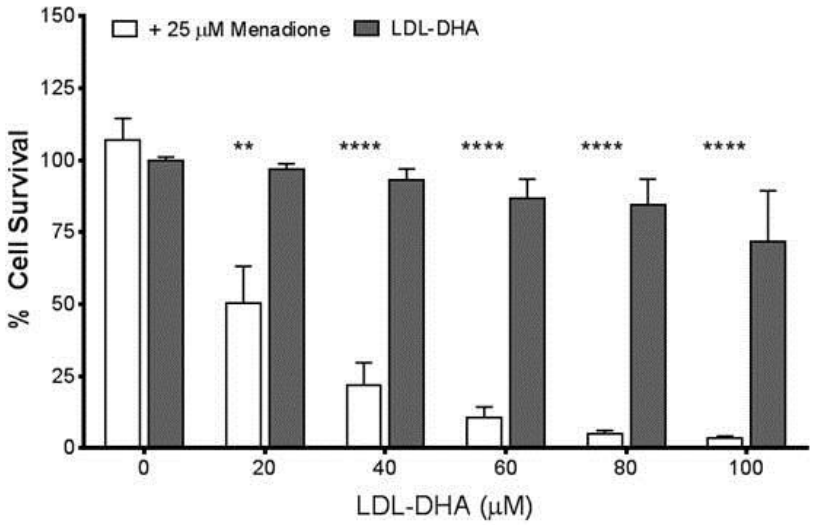

+ 25 μM Menadione IC_{50} = 20.32 μM LDL-DHA

LDL-DHA IC_{50} = 131.8 μM LDL-DHA

Figure 6-3: LDL-DHA cytotoxicity after induction of ROS by menadione bisulfite in TIB-73 cells

TIB-73 cells were grown to 80-90% confluency in 96 well plates, serum starved overnight, and then pretreated for 30 minutes with menadione bisulfite to induce intracellular ROS generation followed by the addition of LDL-DHA for 24 hours. Cell viability was analyzed by MTS assay. **(A)** To determine what dose of menadione was necessary to sensitize the cells to a sub-lethal dose of LDL-DHA, TIB-73 cells were treated with increasing doses of menadione (0-30 µM) and constant 60 µM LDL-DHA. The stars represent the significance compared to the 60 µM LDL-DHA treatment. **(B)** To determine the new IC_{50} of LDL-DHA after menadione treatment, TIB-73 cells were treated with 25 µM menadione and increasing doses of LDL-DHA (0-100 µM). The new IC_{50} after menadione pretreatment was 20.32 µM LDL-DHA compared to the original IC_{50} of 131.8 µM LDL-DHA. The stars represent the significance compared to the 25 µM menadione treatment.
* = p-value ≤0.05, ** = p-value ≤0.01, *** = p-value ≤0.001, **** = p-value ≤0.0001. The error bars represent the standard error of the mean.

Superoxide anion is not critical for LDL-DHA sensitivity

With the aim of exploring the role of superoxide species in TIB-75 cytotoxicity to LDL-DHA, experiments were performed that investigated the baseline superoxide radical levels and the effect removing superoxide radicals had on sensitivity to LDL-DHA. To answer the first of these two questions, TIB-73 and TIB-75 cells were stained with dihydroethidium (DHE) which fluoresces when oxidized by superoxide radicals and this revealed that TIB-75 cells do not have significantly higher levels of superoxide species at baseline (Figure 6-4-1). This result was consistent with the previous western blot data that showed that TIB-75 cells do not have a significant deficit in superoxide dismutase-1 enzyme. A pilot experiment was conducted that probed the question of whether LDL-DHA treatment increased superoxide radical levels in TIB-75 cells, but this showed no significant increase in superoxide after LDL-DHA (data not shown). The last question was answered by pretreating TIB-75 cells overnight with exogenous pegylated superoxide dismutase (0-500 IU) prior to treatment with 60 μM LDL-DHA for twenty-four hours. As expected, exogenous superoxide dismutase treatment did not rescue TIB-75 cells from LDL-DHA cytotoxicity (Figure 6-4-2). Cumulatively, these results led to the conclusion that superoxide radicals are not a crucial reactive oxygen species for LDL-DHA cytotoxicity in TIB-75 cells.

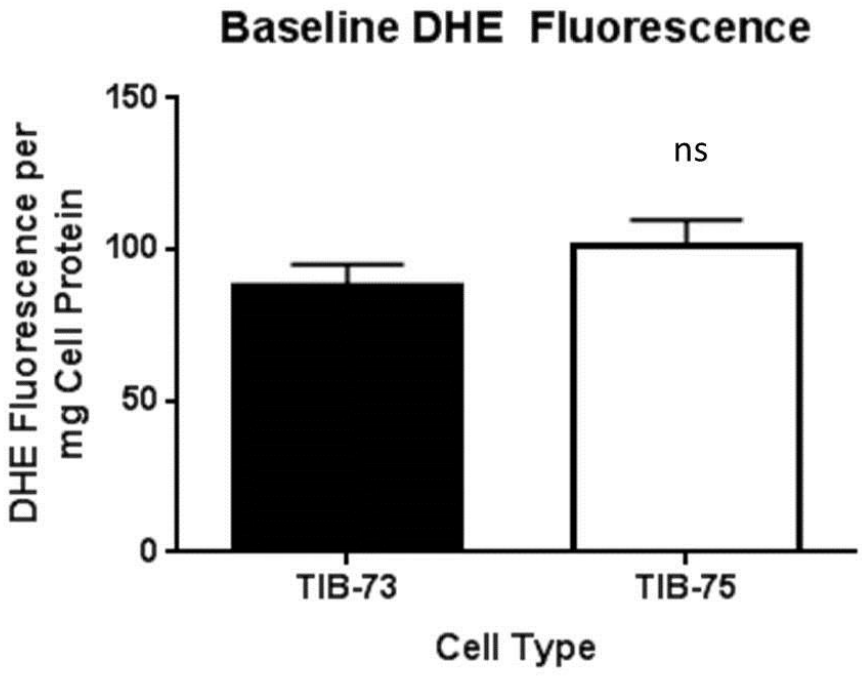

Figure 6-4-1: Baseline oxidative stress by DHE spectrophotometry in TIB-73 and TIB-75 cells

TIB-73 and TIB-75 cells were grown to 80-90% confluency in 100 mm^2 dishes. The cells were serum starved overnight and then dyed with 10 µM DHE reagent for 30 minutes at 37C. Cells were washed with PBS, collected by scraping, and lysed by sonication. The fluorescence of the cell lysate supernatant was analyzed on a Hitashi F-7000 fluorescence spectrophotometer (490 nm excitation/570 nm emission) and the protein was measured using a Bradford assay. The DHE fluorescence was normalized to cell protein and corrected for autofluorescence. There was a not significantly higher amount of superoxide levels in TIB-75 cells compared to TIB-73 cells at baseline.
* = p-value ≤0.05, ** = p-value ≤0.01, *** = p-value ≤0.001, **** = p-value ≤0.0001. The error bars represent the standard error of the mean.

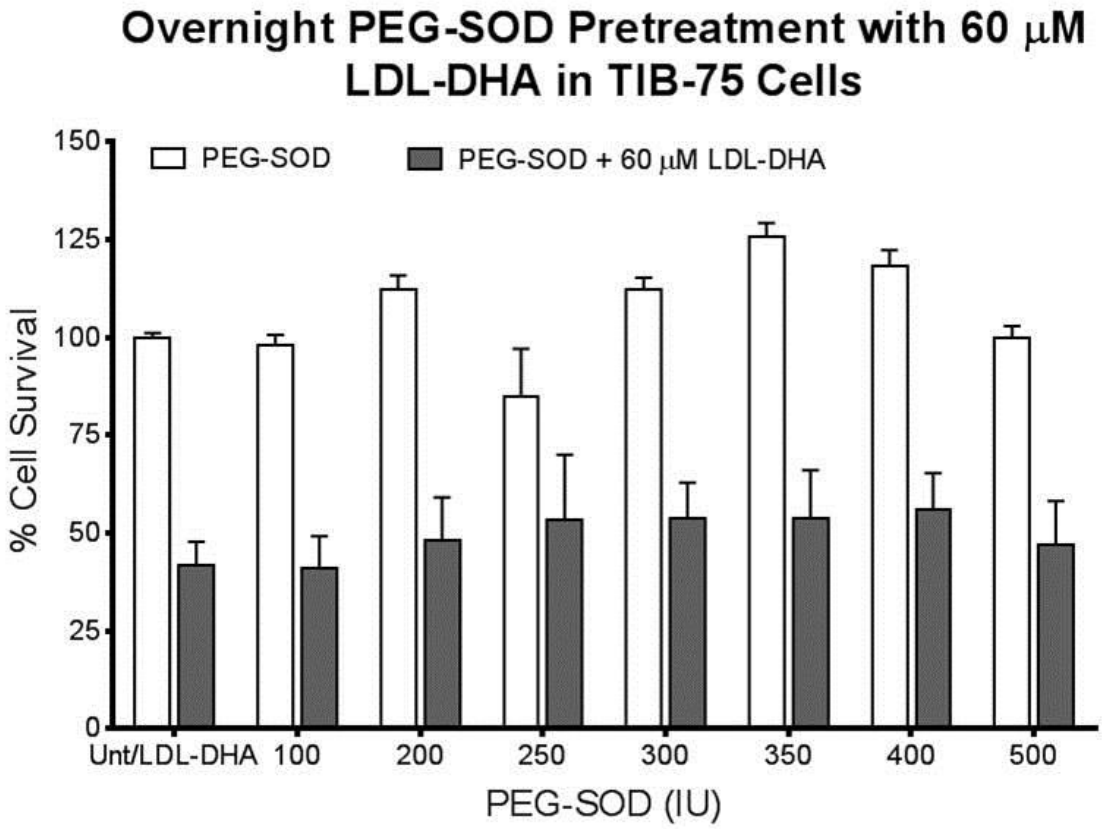

Figure 6-4-2: LDL-DHA cytotoxicity after pretreatment with PEG-superoxide dismutase in TIB-75 cells

TIB-75 cells were grown to 80-90% confluency in 96 well plates, serum starved overnight with increasing doses of PEG-SOD (0-500 IU), 60 μM LDL-DHA was added for 24 hours, and then cell viability was analyzed by MTS assay. Pretreatment with PEG-SOD to remove superoxide species did not decrease TIB-75 cell cytotoxicity to 60 μM LDL-DHA.
* = p-value ≤0.05, ** = p-value ≤0.01, *** = p-value ≤0.001, **** = p-value ≤0.0001. The error bars represent the standard error of the mean.

Hydrogen peroxide species increase with LDL-DHA treatment but inhibition is not sufficient to rescue TIB-75 cytotoxicity

The next reactive oxygen species of interest in LDL-DHA cytotoxicity was hydrogen peroxide. Hydrogen peroxide acts as an important cell signaling molecule in low levels and promotes cell proliferation but at higher levels it induces cell death. Western blots verified that TIB-75 cells have lower levels of catalase, an enzyme responsible for hydrogen peroxide removal (Figure 6-1). Subsequent experiments examining baseline hydrogen peroxide levels using the hydrogen peroxide-indicating fluorescent dye, dichlorofluoroscein (DCF), showed that TIB-75 cells have ≈4-fold higher levels of hydrogen peroxide at baseline when measured by spectrophotometry (Figure 6-5-1). When TIB-73 and TIB-75 cells were treated with 60 μM LDL-DHA or vehicle for 24 hours, DCF fluorescence increased almost 4-fold in only the LDL-DHA treated TIB-75 cells compared to untreated cells (Figure 6-5-2). LDL-TO did not increase DCF fluorescence in either cell line once again showing that DHA is the active compound capable of increasing hydrogen peroxide levels in only the malignant cells. A follow-up experiment using DCF flow cytometry assessed the time course (0-24 hours) of the rise of hydrogen peroxide levels in TIB-73 and TIB-75 cells after LDL-DHA treatment (Figure 6-5-3). This experiment again confirmed that there were baseline differences between the percentage of DCF positive TIB-73 (≈3%) and TIB-75 (≈42%) cells. The TIB-75 cells exhibited a steady increase in the percentage of DCF positive cells up to four hours, which then decreased slightly by the twenty-four hour time point. In contrast, TIB-73 cells did not

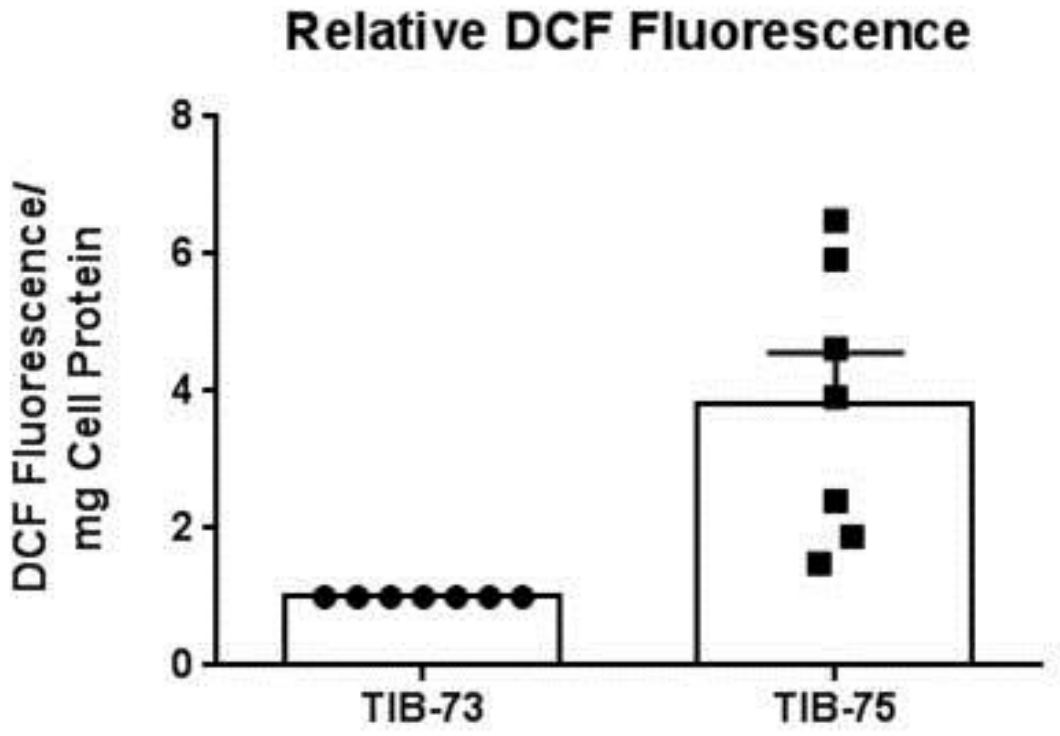

Figure 6-5-1: Oxidative stress at baseline by DCF-DA spectrophotometry in TIB-73 and TIB-75 cells

TIB-73 and TIB-75 cells were grown to 80-90% confluency in 100 mm^2 dishes. The cells were serum starved overnight, then dyed with 15 μM DCF-DA reagent for 1 hour. Cells were washed with PBS, collected by scraping, and lysed by sonication. The fluorescence of the cell lysate supernatant was analyzed on a Hitashi F-7000 fluorescence spectrophotometer (485 nm excitation/526 nm emission) and the protein was measured using a Bradford assay. The DCF fluorescence was normalized to cell protein. The fold change between TIB-73 and TIB-75 was calculated by dividing the TIB-75 sample by the corresponding TIB-73 sample. TIB-75 cells exhibited a 4-fold higher DCF fluorescence than TIB-73 cells at baseline.

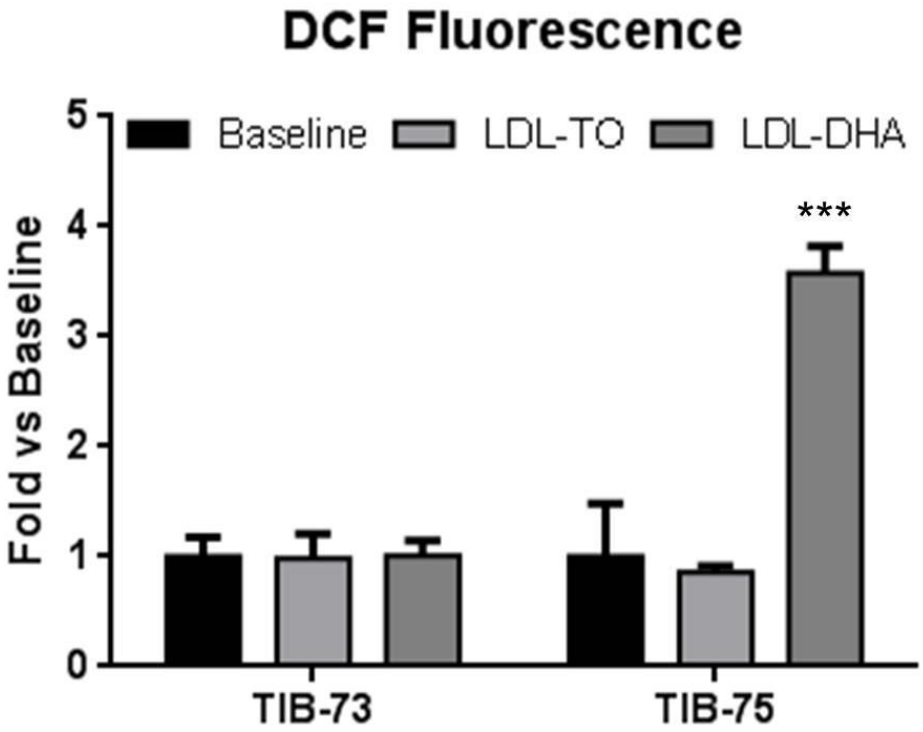

Figure 6-5-2: Oxidative stress by DCF-DA spectrophotometry in TIB-73 and TIB-75 cells following LDL-DHA treatment

TIB-73 and TIB-75 cells were grown to 80-90% confluency in 100 mm^2 dishes. The cells were serum starved overnight, treated with serum free DMEM, 60 µM LDL-TO or 60 µM LDL-DHA for 24 hours. After treatment, cells were dyed with 15 µM DCF-DA reagent for 1 hour at 37C. Cells were washed with PBS, collected by scraping, and lysed by sonication. The fluorescence of the cell lysate supernatant was analyzed on a Hitashi F-7000 fluorescence spectrophotometer (485 nm excitation/526 nm emission) and the protein was measured using a Bradford assay. The DCF fluorescence was normalized to cell protein. The fold change between TIB-73 and TIB-75 was calculated by dividing the treated samples to the corresponding untreated sample. TIB-75 cells treated with LDL-DHA exhibited almost a 4-fold higher DCF fluorescence compared to untreated TIb-73 and TIB-75 cells.
* = p-value ≤0.05, ** = p-value ≤0.01, *** = p-value ≤0.001, **** = p-value ≤0.0001. The error bars represent the standard error of the mean.

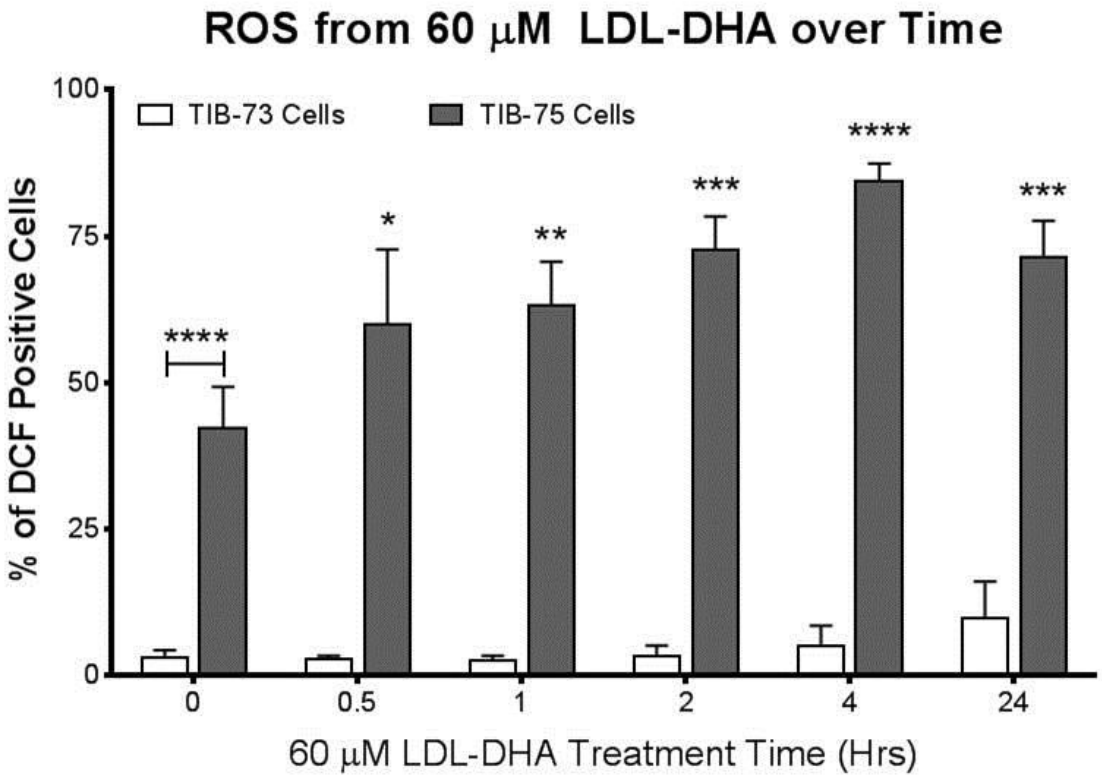

Figure 6-5-3: ROS over time by LDL-DHA treatment in TIB-73 and TIB-75 cells

TIB-73 and TIB-75 cells were grown to 80-90% confluency in 6-well plates, serum starved overnight, and then treated for different time periods with 60 μM LDL-DHA. After treatment, the cells were stained with 15 μM DCF-DA for 30 minutes at 37C, trypsinized, and washed with PBS. Increase of green fluorescence (FL1) of the cells was measured by flow cytometry to determine ROS generation. TIB-75 cells exhibited increased baseline ROS levels and ROS levels increased over time with LDL-DHA treatment compared to TIB-73 cells.
* = p-value ≤0.05, ** = p-value ≤0.01, *** = p-value ≤0.001, **** = p-value ≤0.0001. The error bars represent the standard error of the mean.

experience any significant increase in DCF positive cells for the times tested which coincides with the findings by DCF spectrophotometry.

In an effort to confirm the importance of hydrogen peroxide levels to LDL-DHA cytotoxicity in TIB-75 cells, experiments were conducted to rescue TIB-75 cells from LDL-DHA by preventing hydrogen peroxide formation and to sensitize TIB-73 cells to LDL-DHA treatment by increasing their hydrogen peroxide levels. TIB-75 cells were treated with exogenous pegylated catalase (750-1500 IU) overnight prior to treatment with 60 µM LDL-DHA (Figure 6-5-4). Pegylated catalase did not rescue TIB-75 cells from LDL-DHA cytotoxicity suggesting either that removal of hydrogen peroxide formation is not critical for LDL-DHA cytotoxicity or that the quantity of catalase added could not overcome the increased hydrogen peroxide levels generated from TIB-75 cells after LDL-DHA treatment. Additionally, treatment with exogenous hydrogen peroxide in TIB-73 cells prior to LDL-DHA dosing did not sensitize the cells to any degree to LDL-DHA treatment (Figure 6-5-5). It is possible that the intact catalase system and NADPH/$NADP^+$ ratio in TIB-73 cells allowed them to successfully remove the exogenous hydrogen peroxide before it was able to interact with DHA or significantly disturb the TIB-73 cells antioxidant defense system.

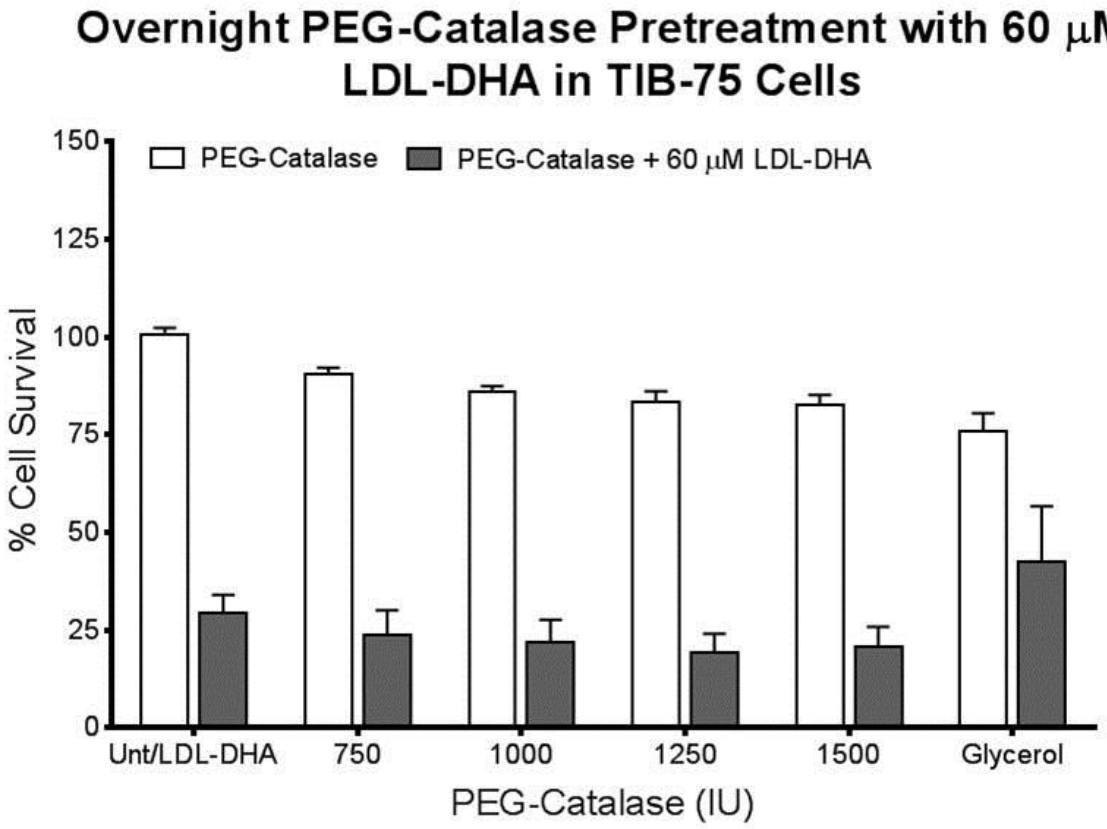

Figure 6-5-4: LDL-DHA cytotoxicity after PEG-catalase pretreatment in TIB-75 cells

TIB-75 cells were grown to 80-90% confluency in 96 well plates, serum starved overnight with increasing doses of PEG-catalase (0-1500 IU), 60 μM LDL-DHA was added for 24 hours, and then cell viability was analyzed by MTS assay. Pretreatment with PEG-catalase to remove hydrogen peroxide species did not decrease TIB-75 cell cytotoxicity to 60 μM LDL-DHA.

* = p-value ≤0.05, ** = p-value ≤0.01, *** = p-value ≤0.001, **** = p-value ≤0.0001. The error bars represent the standard error of the mean.

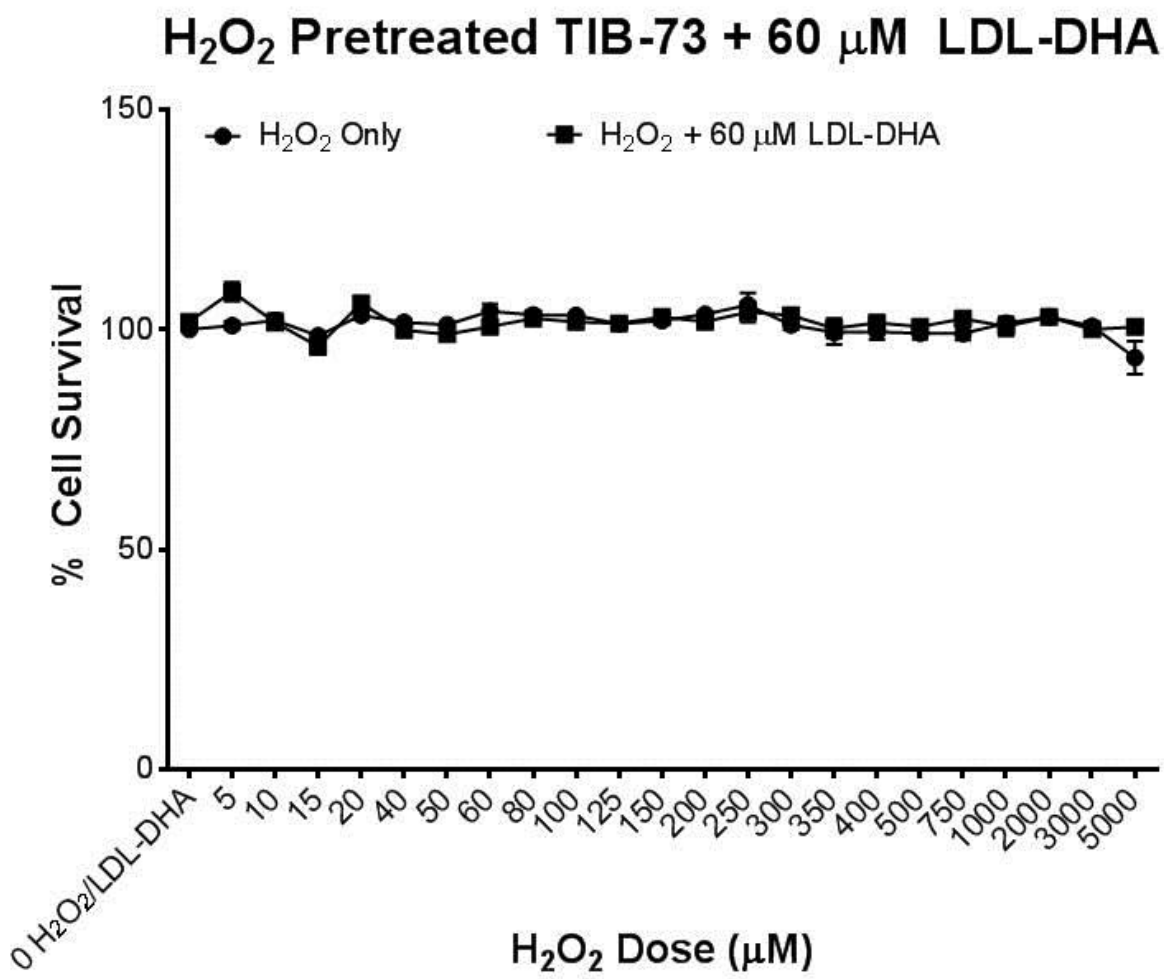

Figure 6-5-5: LDL-DHA cytotoxicity after hydrogen peroxide addition in TIB-73 cells

TIB-73 cells were grown to 80-90% confluency in 96 well plates, serum starved overnight, and then treated with 60 μM LDL-DHA for 5 hours before adding increasing doses of exogenous hydrogen peroxide. Cell viability was analyzed by MTS assay after 24 hours. Addition of exogenous hydrogen peroxide did not sensitize the TIB-73 cells to a sub-lethal dose of LDL-DHA.

* = p-value ≤0.05, ** = p-value ≤0.01, *** = p-value ≤0.001, **** = p-value ≤0.0001. The error bars represent the standard error of the mean.

Lipid peroxidation of LDL-DHA is important in TIB-75 cytotoxicity

After establishing that neither superoxide nor hydrogen peroxide species are critical reactive oxygen species to LDL-DHA cytotoxicity in TIB-75 cells, the role of lipid peroxide species was probed. Firstly, the baseline levels of LPO were measured in TIB-73 and TIB-75 cells using the TBARS assay, which measures malondialdehyde and other by-products of LPO. At baseline, TIB-75 cells have more LPO than TIB-73 cells (Figure 6-6-1). Secondly, LDL-DHA treatment significantly increased LPO in only TIB-75 cells (Figure 6-6-2). LDL-TO treatment was used as a control and did not increase LPO in either cell line (data not shown). It is noteworthy that HSA-DHA at equivalent or greater DHA doses did not significantly increase LPO compared to LDL-DHA. To confirm the findings of the TBARS assay, TIB-73 and TIB-75 cells were stained with a fatty acid analog conjugated to BODIPY (BODIPY C11 581/591) that changes colors from red to green upon oxidation of the fatty acid double bond in the dye. The stained cells were treated with LDL-DHA at different time points and the color change of the dye was monitored by flow cytometry (Figure 6-6-3). This assay showed that LDL-DHA caused a steady increase in the percentage of cells with LPO in TIB-75 cells and reached statistical significance at four hours (≈25%) and twenty-four hours (≈70%). TIB-73 cells had a slower increase in LPO that only achieved statistical significance at the twenty-four hour time point and did not reach the levels seen in TIB-75 cells. A follow-up to the flow cytometry experiment was a confocal microscopy-based experiment utilizing the same BODIPY C11 581/591 dye that demonstrated the differences in TIB-73 and TIB-75 cells' oxidative states by generating heat map images from the ratio of oxidized and

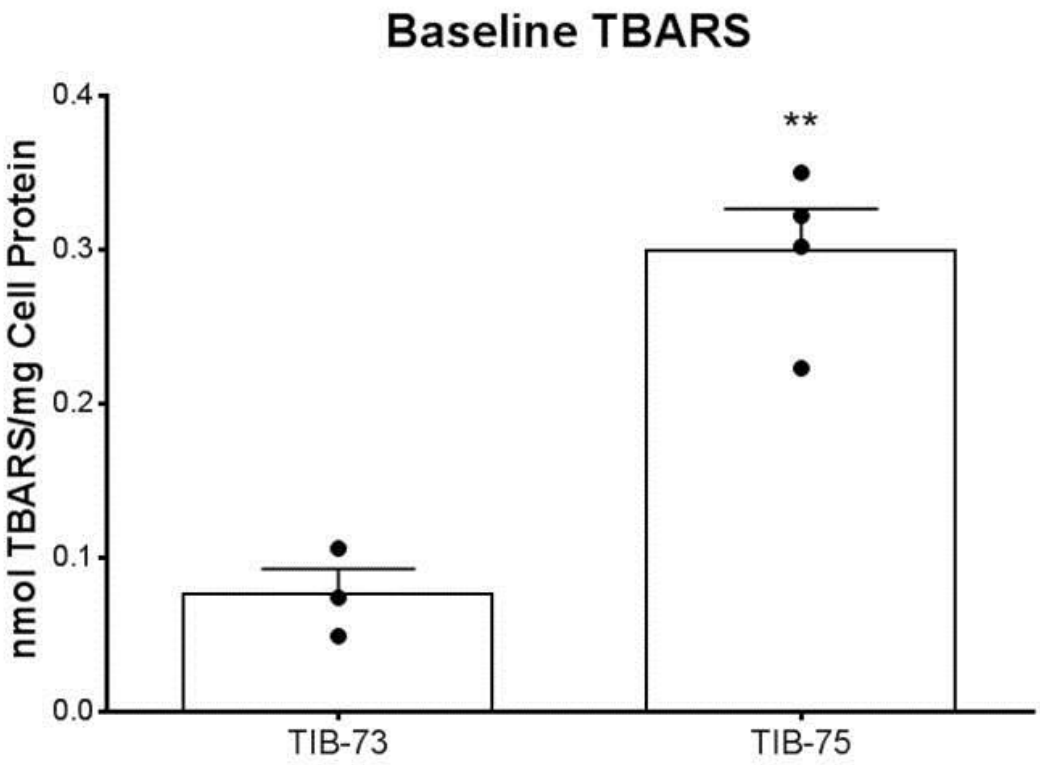

Figure 6-6-1: Lipid peroxidation at baseline by TBARS in TIB-73 and TIB-75 cells

TIB-73 and TIB-75 cells were grown to 80-90% confluency in 100 mm^2 dishes. The cells were serum starved overnight, washed with PBS, collected by scraping, and lysed by sonication. The lysate was mixed with TBARS reagent mix, incubated for 1 hour at 95C. The absorbance of the supernatant was read by plate reader at 550 nm. The protein of the cell lysate was measured by Bradford assay. The TBARS concentration (nmol) was calculated by the extinction coefficient and normalized to cell protein. TIB-75 cells had higher lipid peroxide species than TIB-73 cells at baseline.
* = p-value ≤0.05, ** = p-value ≤0.01, *** = p-value ≤0.001, **** = p-value ≤0.0001. The error bars represent the standard error of the mean.

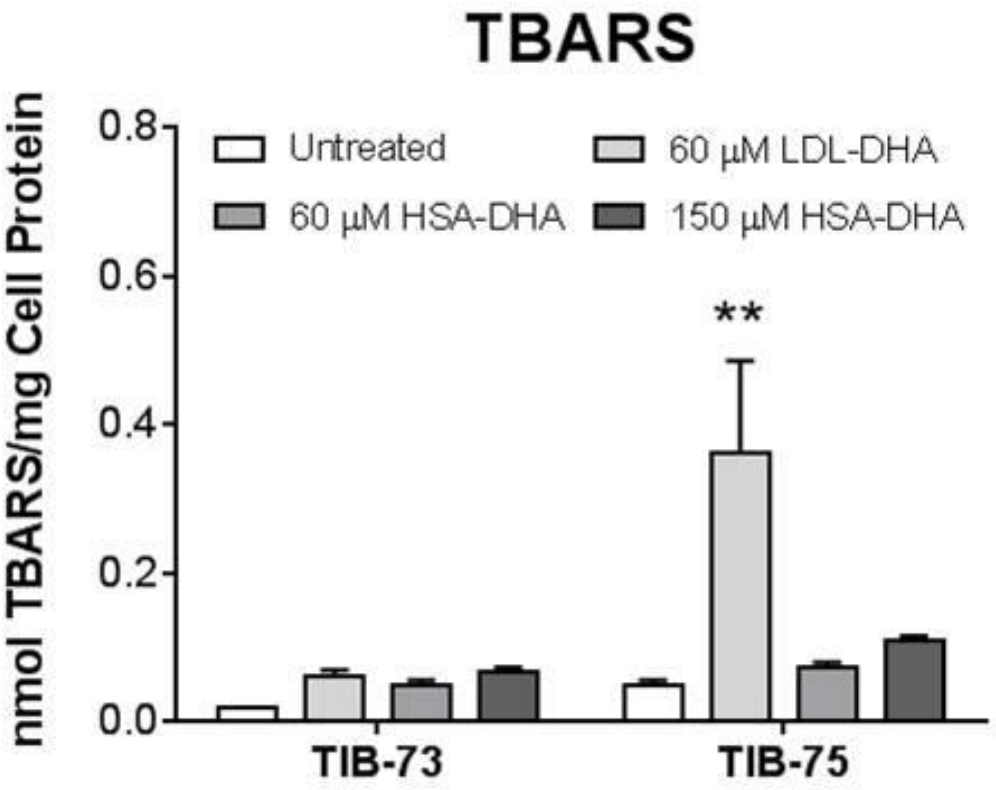

Figure 6-6-2: Lipid peroxidation after LDL-DHA or HSA-DHA treatment in TIB-73 and TIB-75 cells

TIB-73 and TIB-75 cells were grown to 80-90% confluency in 100 mm^2 dishes. The cells were serum starved overnight, treated with serum free DMEM, 60 μM LDL-TO (not shown), LDL-DHA or HSA-DHA or 150 μM HSA-DHA for 24 hours. After treatment, cells were washed with PBS, collected by scraping, and lysed by sonication. The lysate was mixed with TBARS reagent mix, incubated for 1 hour at 95°C. The absorbance of the supernatant was read by plate reader at 550 nm. The protein of the cell lysate was measured by Bradford assay. The TBARS concentration (nmol) was calculated by the extinction coefficient and normalized to cell protein. LDL-DHA treatment significantly increased lipid peroxidation in TIB-75 cells but HSA-DHA and LDL-TO treatment did not have an effect.
* = p-value ≤0.05, ** = p-value ≤0.01, *** = p-value ≤0.001, **** = p-value ≤0.0001. The error bars represent the standard error of the mean.

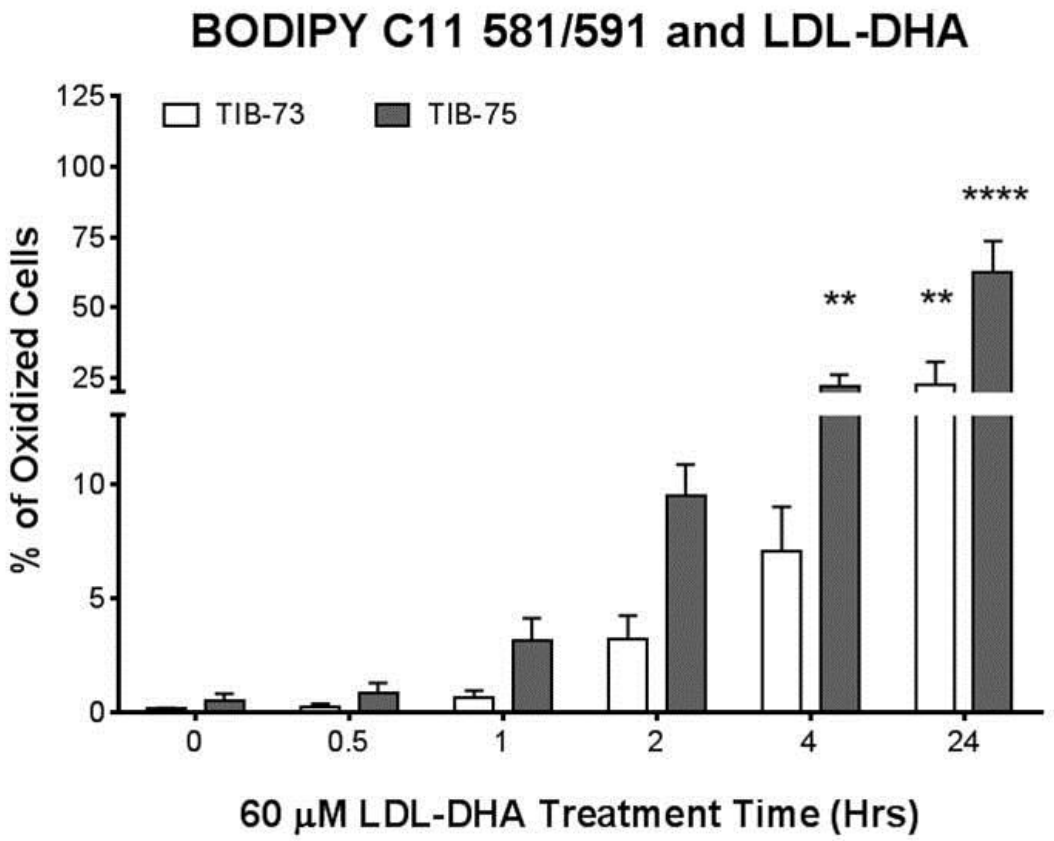

Figure 6-6-3: Lipid peroxidation over time by LDL-DHA treatment inTIB-73 and TIB-75 cells

TIB-73 and TIB-75 cells were grown to 80-90% confluency in 6-well plates, serum starved overnight, stained with 1 µM BODIPY C11 581/591dye, a lipid peroxide indicating dye, for 30 minutes at 37°C. After staining, the cells were treated for different time periods with 60 µM LDL-DHA, trypsinized, and washed with PBS. BODIPY C11 581/591 fluorescence of the cells was measured by flow cytometry where green fluorescence indicated oxidized lipid species and red fluorescence indicated unoxidized lipid species. TIB-75 cells had a higher percentage of cells with oxidized lipids following LDL-DHA treatment and that lipid oxidation increased with time.

* = p-value ≤0.05, ** = p-value ≤0.01, *** = p-value ≤0.001, **** = p-value ≤0.0001. The error bars represent the standard error of the mean.

unoxidized dye in the cells. In the top panel of Figure 6-6-4, the oxidized lipid status of the TIB-73 and TIB-75 cells is shown at baseline and after LDL-DHA treatment. TIB-75 cells at baseline exhibit enhanced lipid oxidation compared to TIB-73 cells and LDL-DHA further exacerbates this condition. TIB-75 cells. The bottom panel shows the reduced lipid state of the cells and it is evident that TIB-73 cells exhibit less oxidized lipid than TIB-75 cells at baseline and, again, after LDL-DHA. The LDL-DHA-treated TIB-73 cells remain at a lower lipid oxidation state than the baseline TIB-75 cells.

Lastly, the capacity of antioxidants to remove lipid peroxides and potentially rescue TIB-75 cell cytotoxicity to LDL-DHA was tested. TIB-75 cells were treated with increasing doses of N-acetyl-L-cysteine (1-30 mM LNAC) before dosing the cells with LDL-DHA. LNAC administration was successful at inhibiting LDL-DHA cytotoxicity in a dose-dependent manner with a 30 mM LNAC treatment recovering TIB-75 cell viability to ≈90% after LDL-DHA treatment (Figure 6-6-5). TIB-75 cells were also treated with 100 µM or 200 µM Vitamin E, a lipophilic antioxidant, prior to 40 µM LDL-DHA and, once again, removal of lipid peroxides was efficacious at preventing LDL-DHA cytotoxicity in TIB-75 cells (Figure 6-6-6). The success of these rescue experiments as well as the higher lipid peroxide levels at baseline and after LDL-DHA treatment in TIB-75 cells indicate an important role for LPO in the LDL-DHA-induced cytotoxicity of malignant cells.

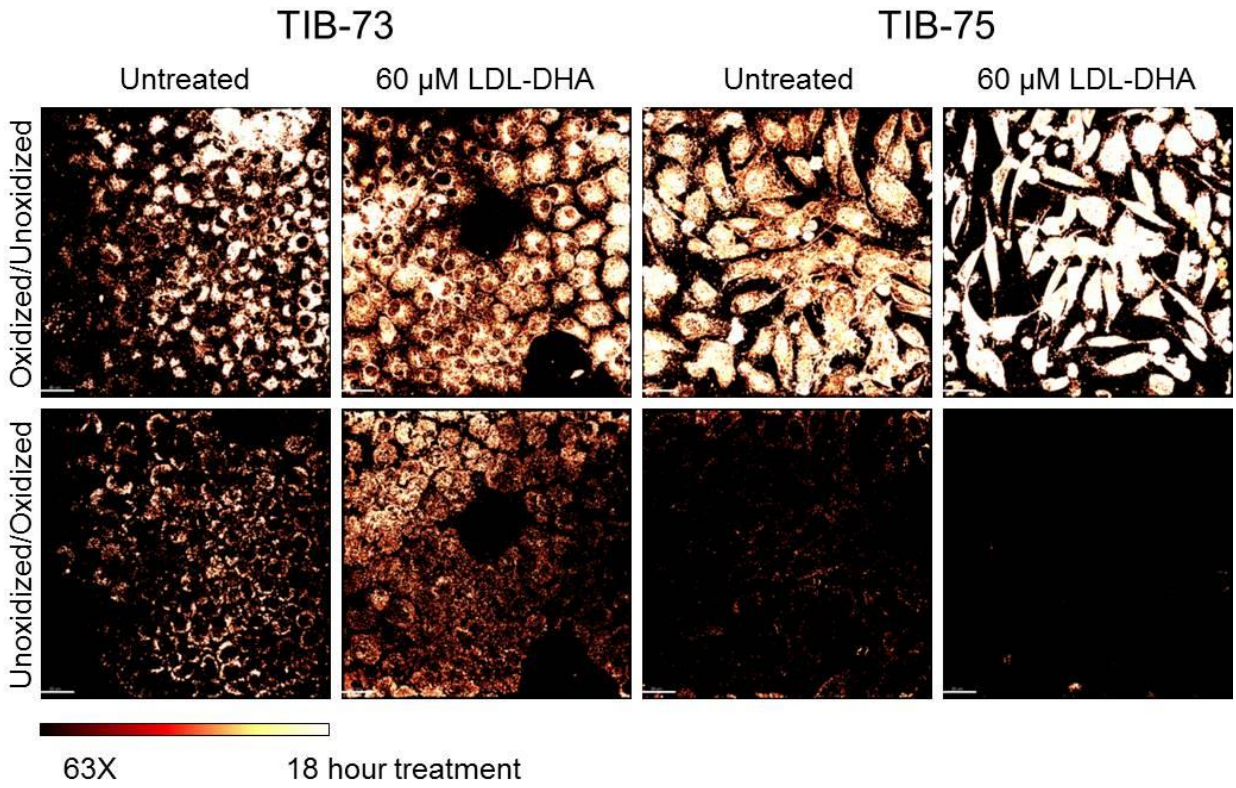

Figure 6-6-4: Lipid peroxidation by BODIPY C11 581/591 confocal microscopy in TIB-73 and TIB-75 cells

TIB-73 and TIB-75 cells were grown to 80-90% confluency in 35 mm^2 glass bottom dishes coated with 10 µg/mL fibronectin. The cells were serum starved for 8 hours, treated with serum free media or 60 µM LDL-DHA overnight, then dyed with 2 µM BODIPY C11581/591 dye, a lipid peroxide indicating dye, for 25 minutes at 37C and the media was replaced prior to imaging. Cells were imaged at 63x magnification on a Leica LP5 confocal. The green channel measured oxidized lipid dye at 488 nm excitation and 510 nm emission. The red channel measured unoxidized lipid dye at 488 nm excitation and 590 nm emission. A MatLab plug-in of the Imaris imaging software was used to create the heat map images by dividing the fluorescence intensity per pixel of the two channels. Dividing the green channel by the red channel (top) shows the oxidized state of the cellular lipids and dividing the red channel by the green channel (bottom) shows the unoxidized state of the cellular lipids. TIB-75 cells have a higher baseline oxidized state compared toTIB-73 cells and LDL-DHA treatment increases the lipid oxidation of the TIB-75 cells.

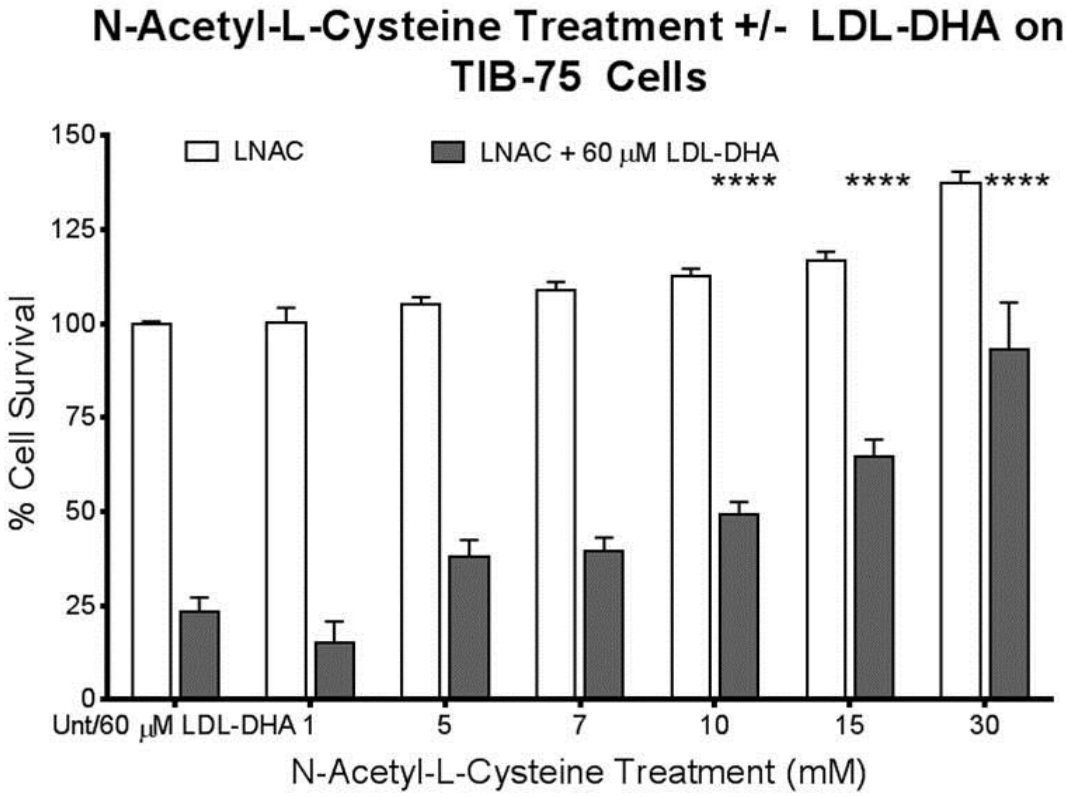

Figure 6-6-5: LDL-DHA cytotoxicity after pretreatment with N-Acetyl-L-Cysteine in TIB-75 cells

TIB-75 cells were grown to 80-90% confluency in 96 well plates, serum starved overnight, pretreated for 1 hour with increasing doses of N-acetyl-L-cysteine (0-30 mM LNAC), 60 μM LDL-DHA was added for 24 hours, and then cell viability was analyzed by MTS assay. Pretreatment with LNAC to remove lipid peroxide species did significantly rescue TIB-75 cell cytotoxicity to 60 μM LDL-DHA compared to untreated cells.
* = p-value ≤0.05, ** = p-value ≤0.01, *** = p-value ≤0.001, **** = p-value ≤0.0001. The error bars represent the standard error of the mean.

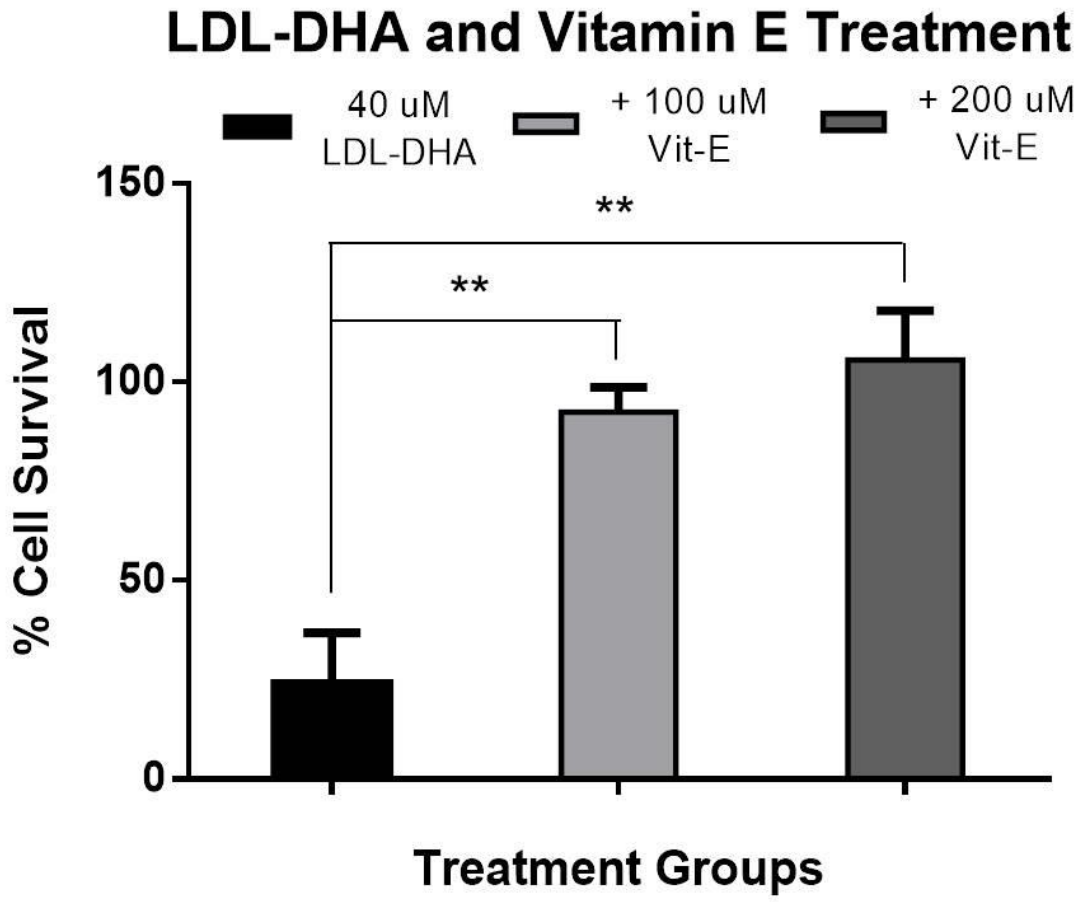

Figure 6-6-6: LDL-DHA cytotoxicity after pretreatment with vitamin E in TIB-75 cells

TIB-75 cells were grown to 80-90% confluency in 96 well plates, serum starved overnight, treated 100 or 200 μM vitamin E and 40 μM LDL-DHA. Cell viability was analyzed by MTS assay after 72 hours. Vitamin E treatment to remove lipid peroxide species rescued cytotoxicity of LDL-DHA in TIB-75 cells. The experiment was performed by Lacy Reynolds and Dr. Xiaodong Wen.

*= p-value ≤0.05, ** = p-value ≤0.01, *** = p-value ≤0.001, **** = p-value ≤0.0001. The error bars represent the standard error of the mean.

Effect of LDL-DHA Treatment on Subcellular Organelles in TIB-75 Cells

Previous experiments established that LDL-DHA enters the cell through receptor-mediated endocytosis into the lysosome and that TIB-75 cells experience significant increases in LPO following LDL-DHA treatment. Given these results, subcellular investigation starting with the lysosomes was initiated since they are the first compartment to be exposed to LDL-DHA after its receptor-mediated uptake.

LDL-DHA-induced lipid peroxidation colocalizes to lysosome compartment

Using the lipid peroxidation marker, BODIPY C11 581/591, colocalization of LPO with the lysosome was measured in TIB-73 and TIB-75 cells (Figure 7-1). The Pearson's Coefficient was greater than 0.5 in each group which shows a strong colocalization (white) of the oxidized dye (green) with the lysosome (blue). TIB-75 cells treated with LDL-DHA exhibited an even greater colocalization of oxidized lipid with the lysosome as evidenced by the increase in the Pearson's Coefficient (PC = 0.65) compared to LDL-DHA treated TIB-73 cells (PC = 0.5). Previous experiments showed that TIB-75 cells have LPO with LDL-DHA treatment (Figures 6-6-2, 3, and 4) and this experiment showed that a large amount of the LPO is located in the lysosome.

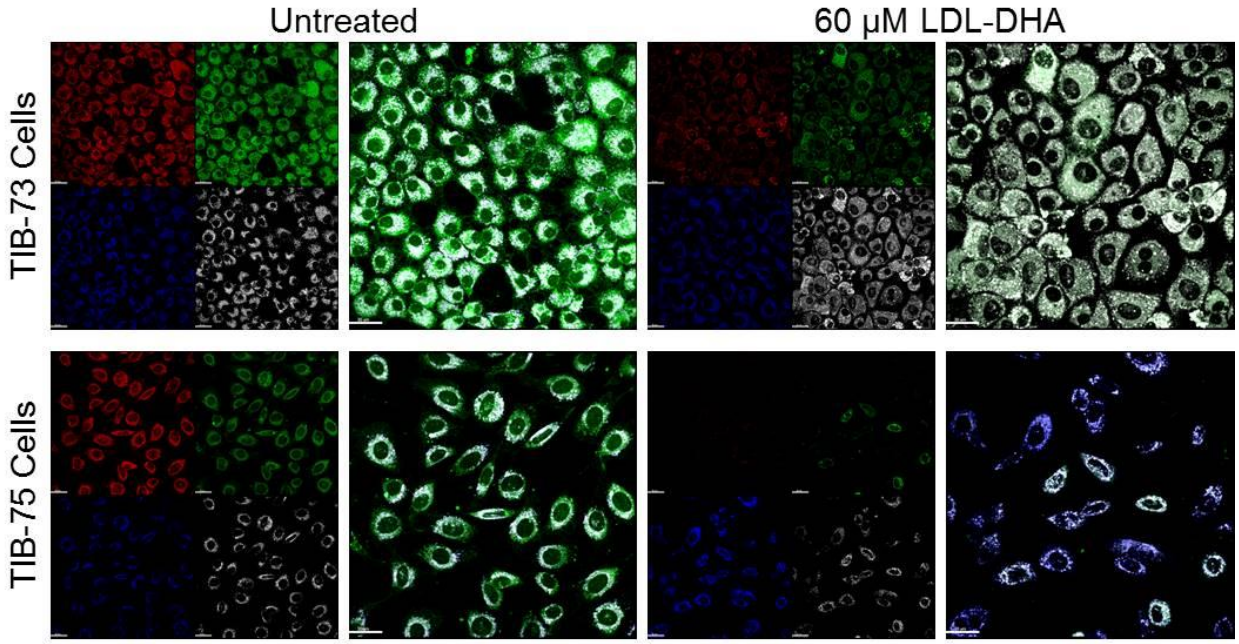

Unoxidized Lipid
Oxidized Lipid
Lysosome
Colocalization

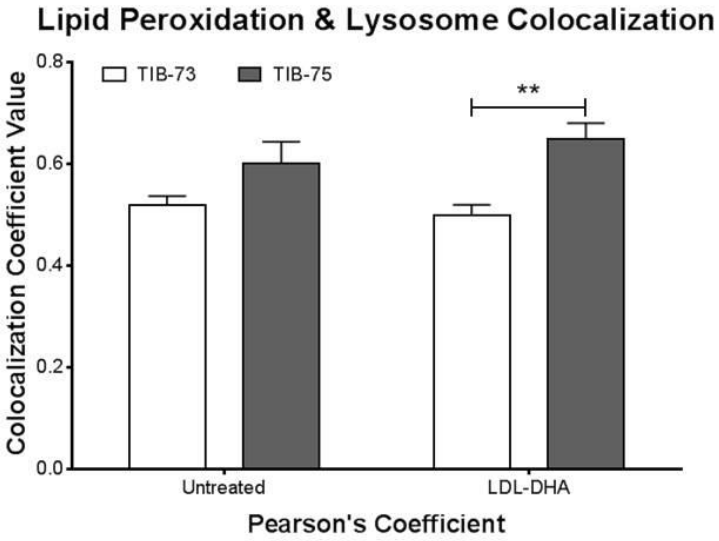

Figure 7-1: Colocalization of lysosomes and lipid peroxidation by confocal microscopy in TIB-73 and TIB-75 cells

TIB-73 and TIB-75 cells were grown to 80-90% confluency in 35 mm^2 glass bottom dishes coated with 10 µg/mL fibronectin. The cells were serum starved for overnight, dyed with 2 µM BODIPY C11 581/591 dye, a lipid peroxide indicating dye, for 25 minutes at 37C, then treated with serum free media or 60 µM LDL-DHA for 4 hours, then dyed with 75 nM LysoTracker Deep Red for 30 minutes prior to imaging. Cells were imaged at 63x magnification on a Leica LP5 confocal. The green channel measured oxidized lipid dye at 488 nm excitation and 510 nm emission. The red channel measured unoxidized lipid dye at 488 nm excitation and 590 nm emission. Imaris imaging software was used to calculate LysoTracker Deep Red colocalization with green oxidized BODIPY C11 581/591 dye in the cells.
*= p-value ≤0.05, ** = p-value ≤0.01, *** = p-value ≤0.001, **** = p-value ≤0.0001. The error bars represent the standard error of the mean.

LDL-DHA induces lysosome membrane permeability in TIB-75 cells

The effect of LDL-DHA on lysosome membrane permeability (LMP) was investigated using acridine orange staining in TIB-73 and TIB-75 cells by confocal microscopy and flow cytometry. The confocal microscopy experiment using acridine orange dye revealed that TIB-75 cells lose the red punctate fluorescence consistent with intact lysosomes and gain green cytosolic fluorescence while TIB-73 cells maintain intact lysosomes (Figure 7-2-1). Overall this staining pattern in LDL-DHA treated TIB-75 cells is consistent with lysosome leaking and an increase in lysosome membrane permeability. A follow-up experiment treating TIB-75 cells with LDL-DHA or HSA-DHA showed that HSA-DHA does not elicit the same loss of lysosome integrity as LDL-DHA at 60 μM or 150 μM DHA doses (Figure 7-2-2). In order to quantify the loss of intact lysosomes, TIB-73 and TIB-75 cells were stained with acridine orange after different time points of LDL-DHA treatment and analyzed for loss of red fluorescence by flow cytometry (Figure 7-2-3). The TIB-75 cells had a significant increase in the number of cells exhibiting leaking lysosomes after eight and twenty-four hours of LDL-DHA treatment. TIB-73 cells did not exhibit any increase in the number of cells with compromised lysosomes until the twenty-four LDL-DHA treatment and that increase was similar to that seen at eight hours in TIB-75 cells. An additional assay to confirm lysosome leaking was performed using a dye that is activated by cathepsin B activity in the lysosomes. When cells have compromised lysosomes the dye is not converted to the fluorescent form in large quantities because cathepsin B is less active outside of the acidic environment of the lysosome, thus cells will have dim and diffuse cytoplasmic staining.

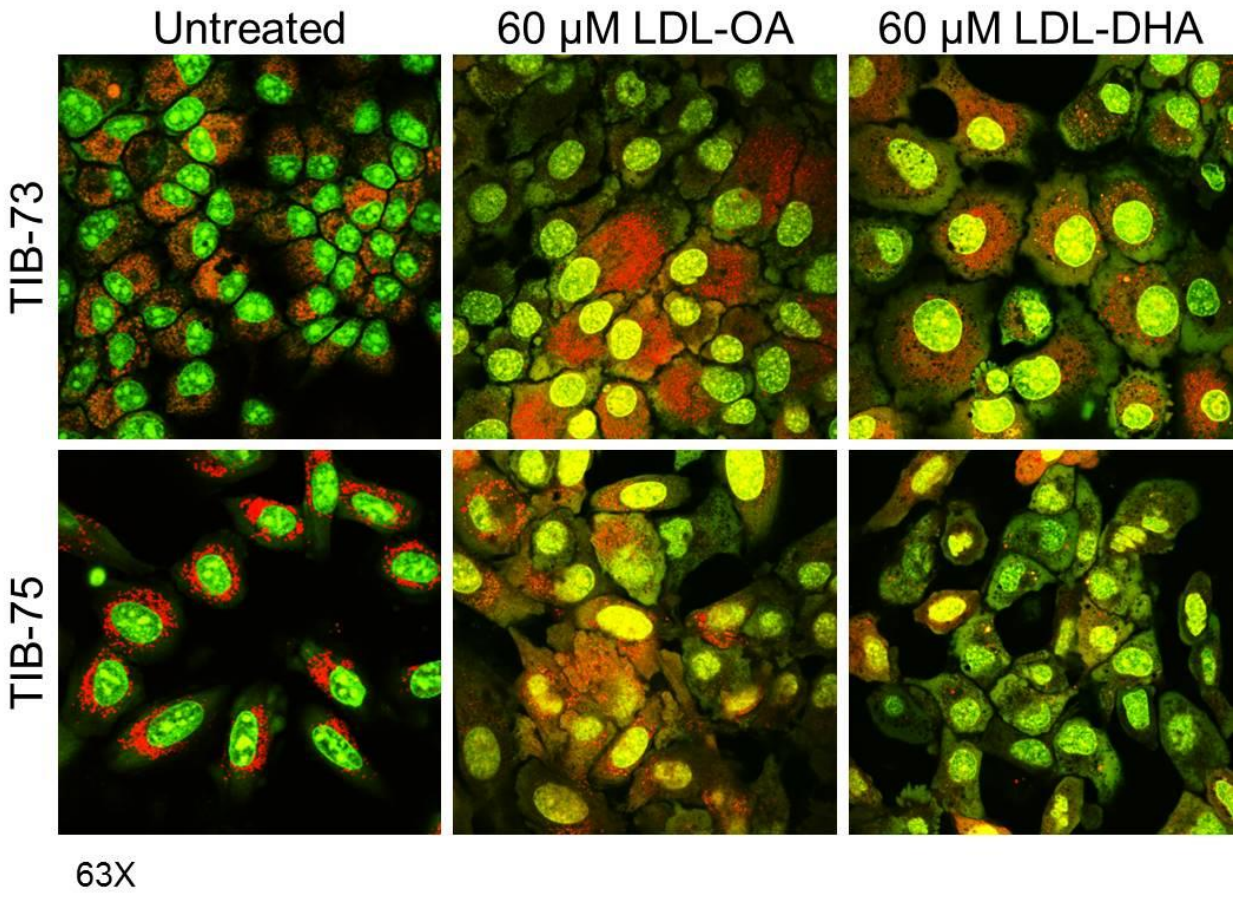

Figure 7-2-1: Lysosome membrane permeability after LDL-DHA treatment by acridine orange dye in TIB-73 and TIB-75 cells

TIB-73 and TIB-75 cells were grown to 80-90% confluency in 35 mm^2 glass bottom dishes coated with 10 µg/mL fibronectin. The cells were serum starved overnight, dyed with 5 µg/mL acridine orange for 20 minutes then treated with serum free media or 60 µM of LDL-OA or LDL-DHA for 5 hours. Cells were imaged at 63x magnification on a Leica LP5 confocal microscope using a 488 nm laser. Red punctate fluorescence (640 nm emission) indicates intact lysosomes and green diffuse fluorescence (540 nm emission) indicates leaking lysosomes. TIB-75 cells treated with LDL-DHA demonstrated loss of lysosome membrane integrity.

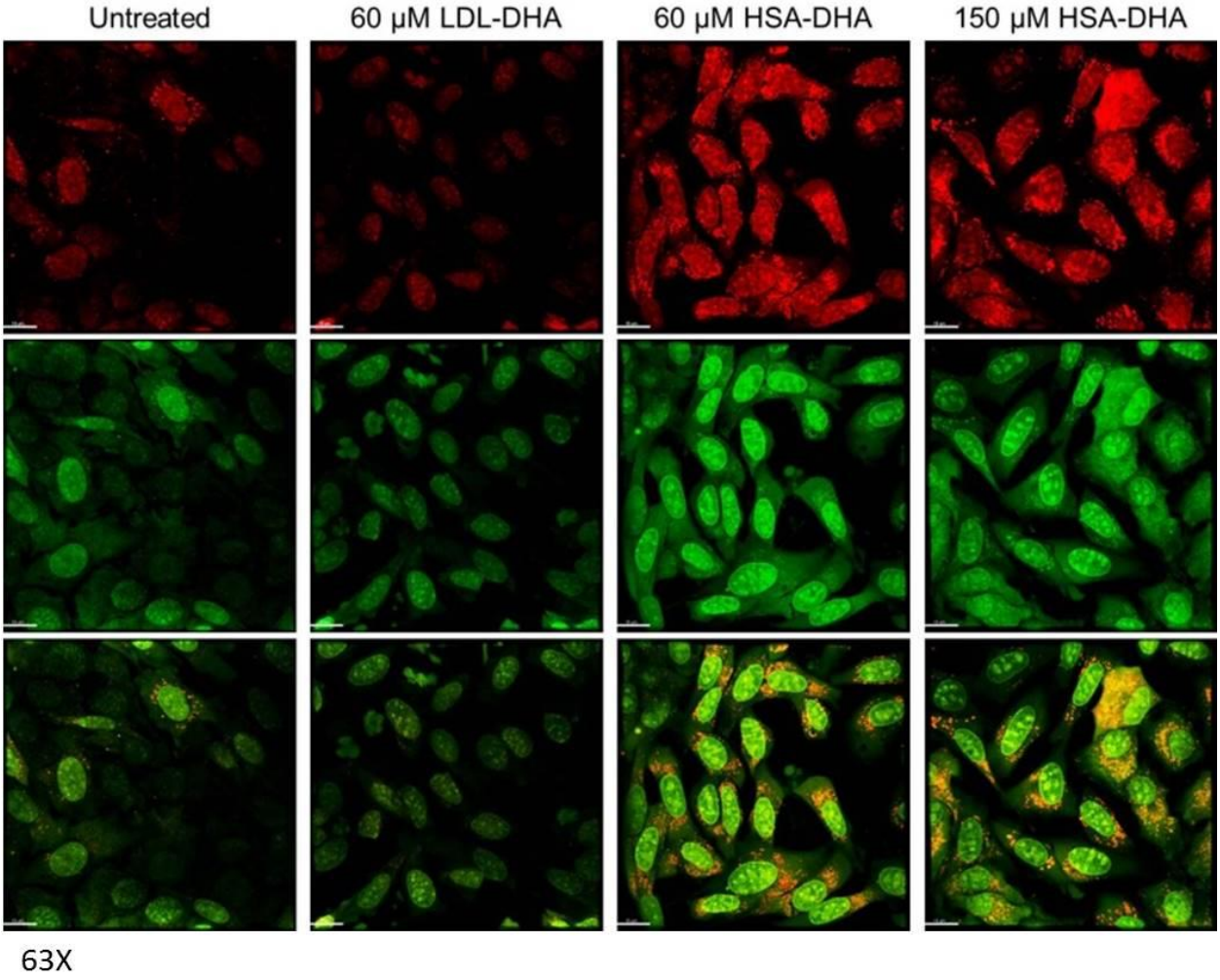

Figure 7-2-2: Lysosome membrane permeability after LDL-DHA or HSA-DHA treatment by acridine orange dye in TIB-75 cells

TIB-75 cells were grown to 80-90% confluency in 35 mm^2 glass bottom dishes coated with 10 μg/mL fibronectin. The cells were serum starved overnight, dyed with 5 μg/mL acridine orange for 20 minutes then treated with serum free media, LDL-DHA (60 μM), or HSA-DHA (60 μM and 150 μM) for 5 hours. Cells were imaged at 63x magnification on a Leica LP5 confocal microscope using a 488 nm laser. Red punctate fluorescence (640 nm emission) indicates intact lysosomes and green diffuse fluorescence (540 nm emission) indicates leaking lysosomes. TIB-75 cells treated with LDL-DHA but not HSA-DHA demonstrated loss of lysosome membrane integrity.

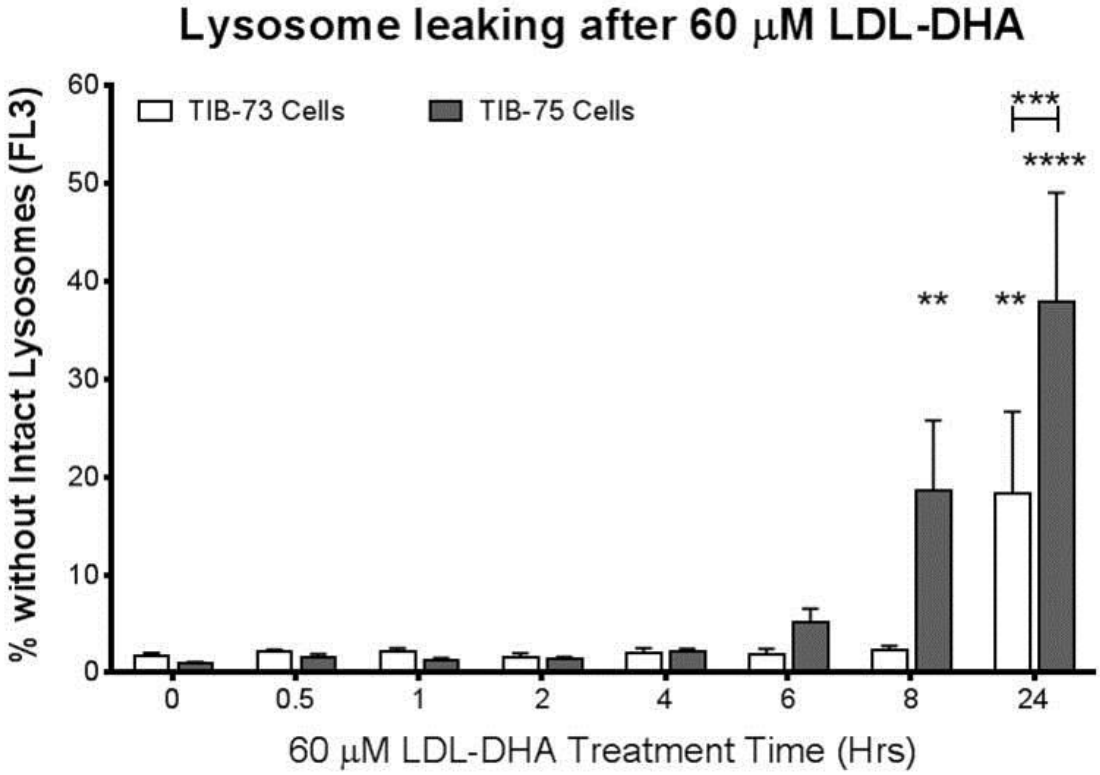

Figure 7-2-3: Lysosome membrane permeability caused over time by LDL-DHA treatment in TIB-73 and TIB-75 cells

TIB-73 and TIB-75 cells were grown to 80-90% confluency in 6-well plates, serum starved overnight, and then treated for different time periods with 60 μM LDL-DHA. After treatment, the cells were stained with 0.5 μg/mL acridine orange for 15 minutes at 37C, trypsinized, and washed with PBS. Loss of red acridine orange fluorescence (FL2) of the cells was measured by flow cytometry to determine the number of cells with loss of intact lysosomes. TIB-75 cells exhibited increased loss of intact lysosomes over time with LDL-DHA treatment compared to TIB-73 cells.

* = p-value ≤0.05, ** = p-value ≤0.01, *** = p-value ≤0.001, **** = p-value ≤0.0001. The error bars represent the standard error of the mean.

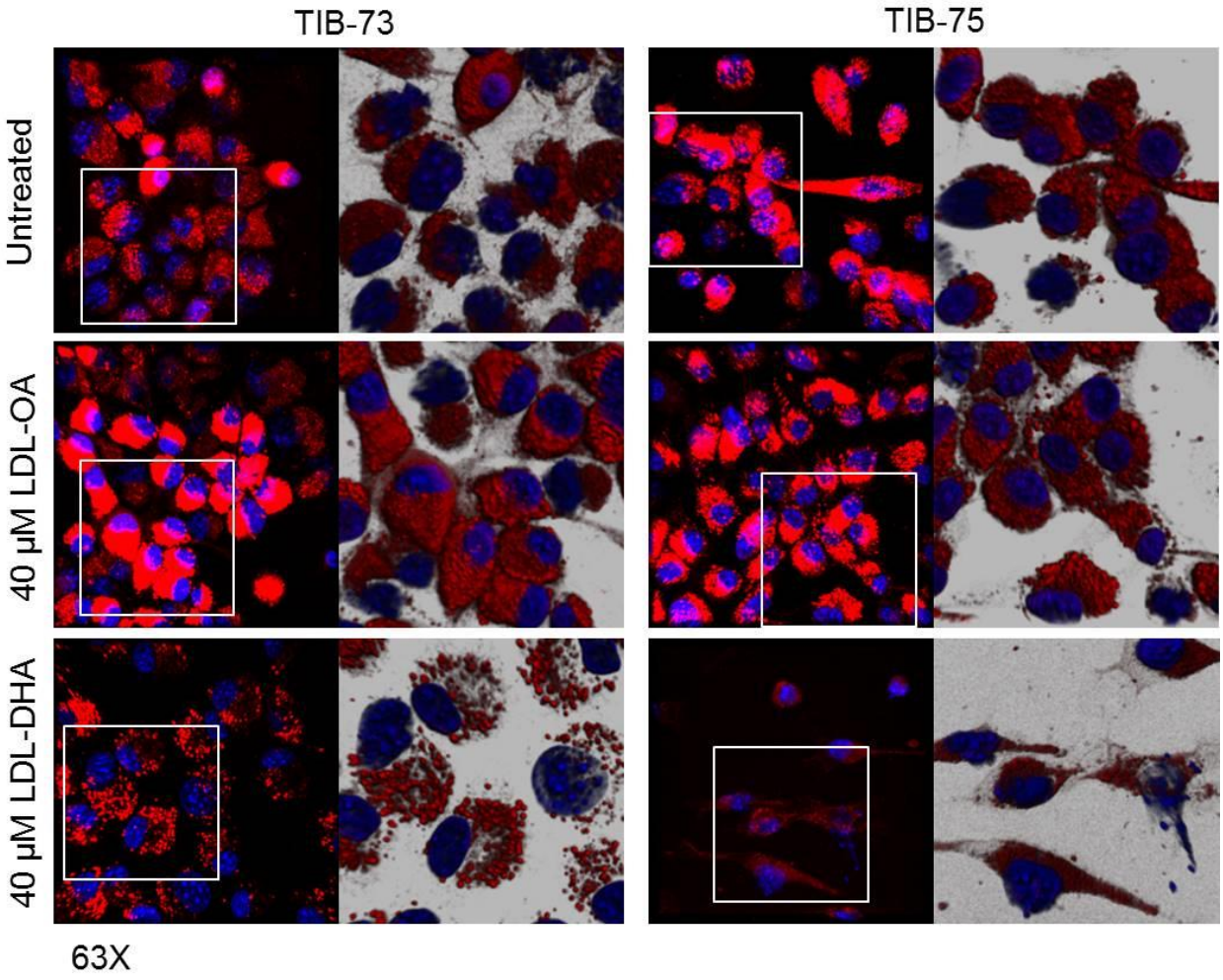

Figure 7-2-4: Lysosome membrane permeability after LDL-DHA treatment by cathepsin B activity in TIB-73 and TIB-75 cells

TIB-73 and TIB-75 cells were grown to 80-90% confluency in 35 mm^2 glass bottom dishes coated with 10 µg/mL fibronectin. The cells were serum starved overnight, treated with serum free media or 40 µM of LDL-OA or LDL-DHA overnight, then dyed with 26x Magic Red Cathepsin B reagent and NucBlue for 45 minutes. Cells were imaged at 63x magnification on a Leica LP5 confocal (561 excitation/>610 nm emission). Bright punctate fluorescence indicates intact lysosomes and dim diffuse fluorescence indicates leaking lysosomes. TIB-75 cells treated with LDL-DHA demonstrated lysosome leaking.

TIB-73 and TIB-75 cells treated overnight with media, LDL-TO, or LDL-DHA had bright punctate fluorescence consistent with intact lysosomes except for the TIB-75 cells treated with LDL-DHA, which had dim and diffuse staining indicative of leaking lysosomes (Figure 7-2-4).

LDL-DHA induces mitochondrial damage in TIB-75 cells

After ascertaining that LDL-DHA compromises lysosome integrity in TIB-75, the effect of LDL-DHA on mitochondria morphology and mitochondria membrane potential (MMP) was assessed. A Corbin Laboratory member assessed mitochondria morphology after LDL-DHA in TIB-73 and TIB-75 cells using TEM. The TEM micrographs (Figure 7-3-1) revealed that mitochondria in TIB-75 cells after LDL-DHA treatment swelled and developed tubular cristae. TIB-73 and TIB-75 cells were stained with TMRM, a fluorescent dye that monitors MMP, after an overnight LDL-DHA treatment and fluorescence was monitored by confocal microscopy. This experiment confirmed that TIB-75 cells lose MMP after LDL-DHA treatment since these cells did not stain brightly with TMRM (Figure 7-3-2A). ImageJ analysis of the images verified that only TIB-75 cells experience a significant loss of MMP following LDL-DHA treatment compared to both TIB-73 and TIB-75 untreated cells (Figure 7-3-2B). Additionally, the LDL-OA treatment does not induce the same MMP loss in either cell line. TMRM fluorescence for MMP was also monitored by flow cytometry at different times of LDL-DHA treatment (Figure 7-3-3). The TMRM flow cytometry study indicated that TIB-75 cells, but not TIB-73 gradually lose MMP with significant losses occurring at six

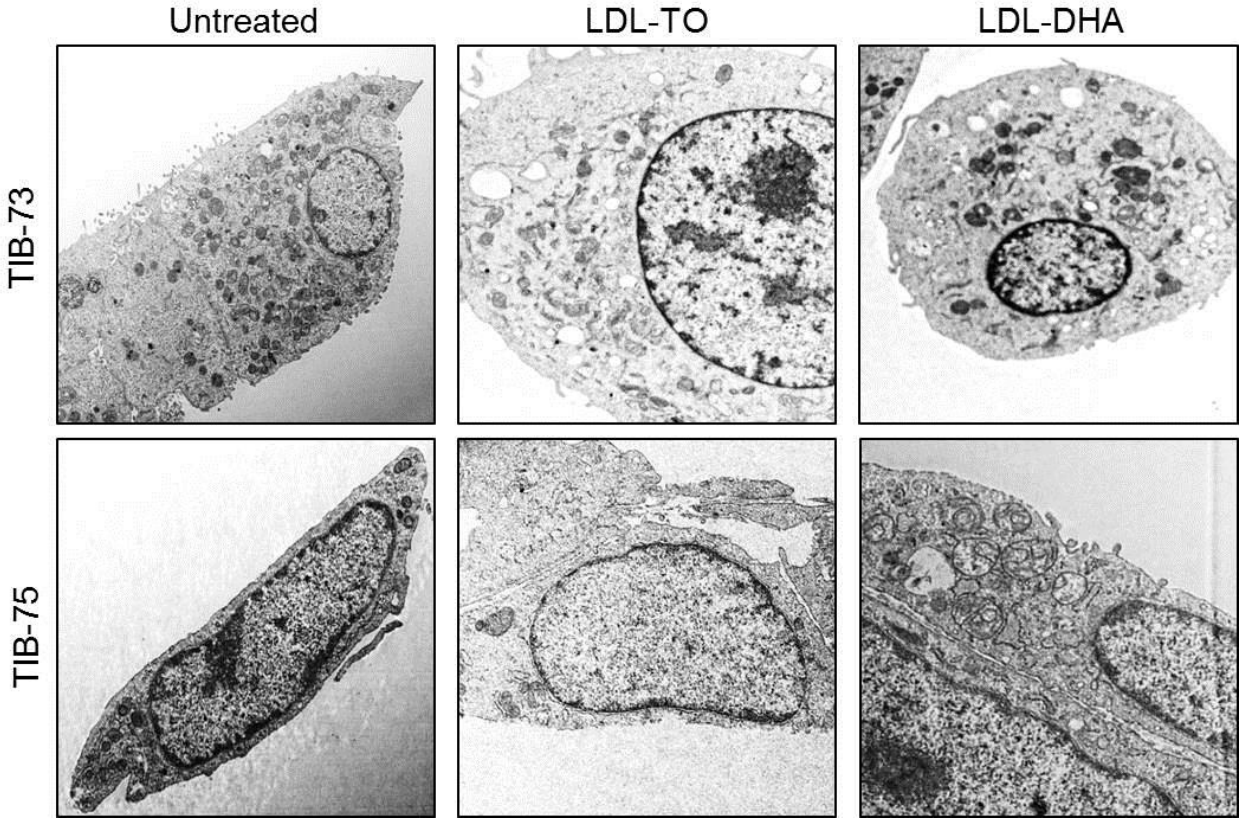

Figure 7-3-1: Mitochondrial damage after LDL-DHA treatment by TEM in TIB-73 and TIB-75 cells

TIB-73 and TIB-75 cells were grown to 80-90% confluency. The cells were serum starved overnight, treated with serum free media, LDL-TO, or LDL-DHA for 24 hours. Cells were imaged at using a Transmission Electron Microscope. TIB-75 cells treated with LDL-DHA demonstrated swollen mitochondria and other abnormal morphology. This experiment was performed by Dr. Rohit Mulik.

(A)

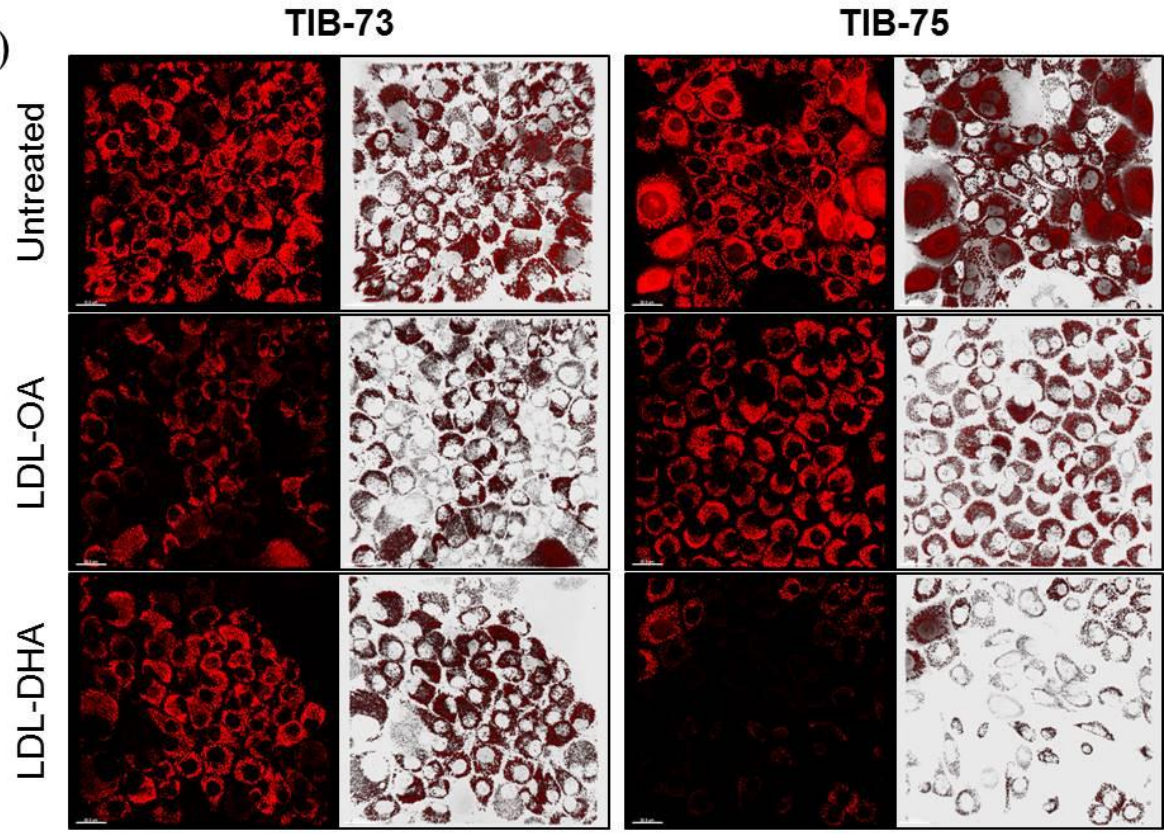
TIB-73
TIB-75
Untreated
LDL-OA
LDL-DHA

(B)

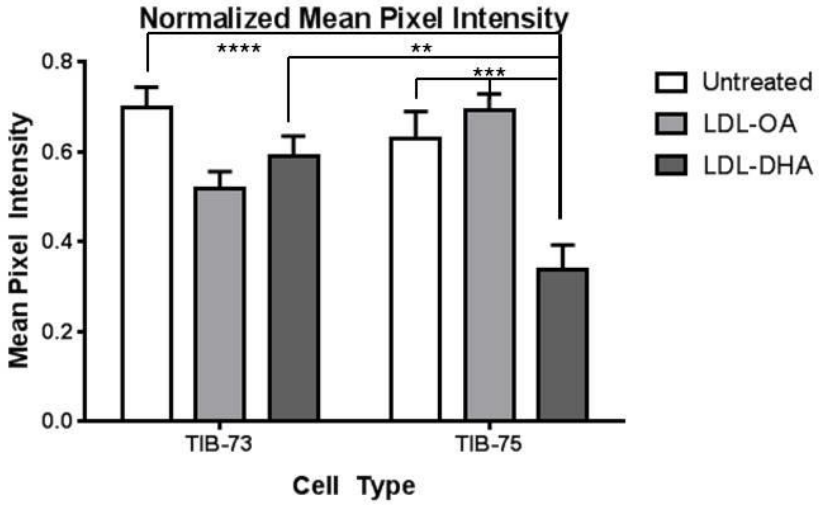
Normalized Mean Pixel Intensity
****
**
***
Mean Pixel Intensity
0.8
0.6
0.4
0.2
0.0
TIB-73
TIB-75
Cell Type
Untreated
LDL-OA
LDL-DHA

Figure 7-3-2: Mitochondrial membrane permeability after LDL-DHA treatment by TMRM fluorescence in TIB-73 and TIB-75 cells

(A) TIB-73 and TIB-75 cells were grown to 80-90% confluency in 35 mm^2 glass bottom dishes coated with 10 µg/mL fibronectin. The cells were serum starved for 8 hours, treated with serum free media or 60 µM of LDL-OA or LDL-DHA overnight, then dyed with 200 nM TMRM for 25 minutes and the media was replaced with 50 nM TMRM for imaging. Cells were imaged at 63x magnification on a Leica LP5 confocal (561 excitation/TRITC filter). Bright punctate fluorescence indicates normal/hyperpolarized mitochondrial membrane potential and dim fluorescence indicates abnormal/depolarized mitochondrial membrane potential. **(B)** The TMRM fluorescence of the cells was quantified using ImageJ software to threshold each z-stack of images to remove background fluorescence and then calculate the mean pixel intensity of the resulting image. TIB-75 cells treated with LDL-DHA demonstrated a significant loss of normal mitochondrial membrane potential.
* = p-value ≤0.05, ** = p-value ≤0.01, *** = p-value ≤0.001, **** = p-value ≤0.0001. The error bars represent the standard error of the mean.

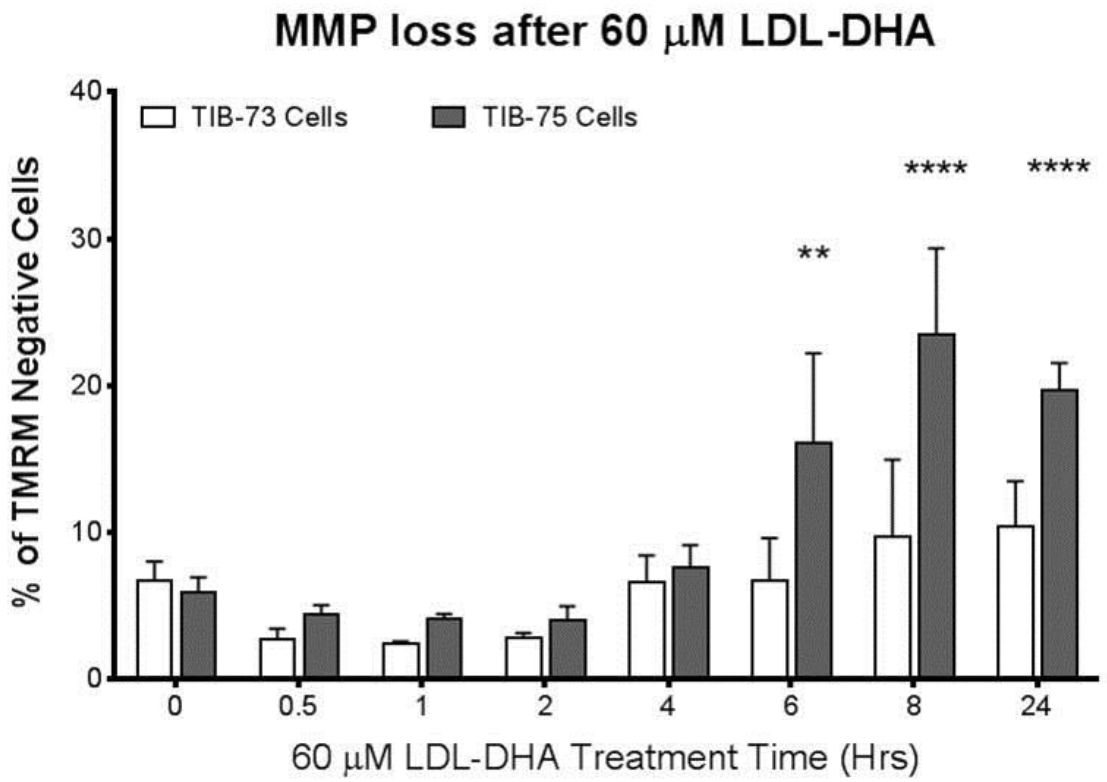

Figure 7-3-3: Loss of mitochondrial membrane potential caused by LDL-DHA treatment over time in TIB-73 and TIB-75 cells

TIB-73 and TIB-75 cells were grown to 80-90% confluency in 6-well plates, serum starved overnight, and then treated for different time periods with 60 μM LDL-DHA. After treatment, the cells were trypsinized, stained with 100 nM TMRM for 15 minutes at 37C, and washed with PBS. TMRM fluorescence of the cells was measured by flow cytometry. TIB-75 cells had a higher percentage of TMRM negative cells following LDL-DHA treatment that increased with time compared to TIB-73 cells.
* = p-value ≤0.05, ** = p-value ≤0.01, *** = p-value ≤0.001, **** = p-value ≤0.0001. The error bars represent the standard error of the mean.

hours of treatment and beyond. This study established LDL-DHA's subcellular effects are limited to the malignant TIB-75 cell line and spares the non-malignant cell line.

Mitochondrial ROS production is important in LDL-DHA sensitivity

Previous experiments comparing the mechanism of LDL-DHA cytotoxicity in TIB-73 and TIB-75 cells indicated that TIB-75 cells have higher baseline levels of ROS and that LDL-DHA exacerbates ROS production. Most ROS in the cell is produced in the mitochondria as a consequence of the citric acid cycle, and lipid peroxidation of the mitochondrial membrane can negatively affect the cycle's electron transport chain. The following experiments probed the role that LDL-DHA has on increasing mitochondrial ROS and the importance of mitochondrial baseline ROS production on sensitivity to LDL-DHA in TIB-73 and TIB-75 cells. The cells were treated overnight with 40 μM LDL-DHA, LDL-OA, or HSA-DHA and with the mitochondrial probes MitoSox and MitoTracker. Thereafter fluorescence was measured by flow cytometry in the cells (Figure 7-4-1). The TIB-75 cells treated with LDL-DHA expressed a significant increase in mitochondrial ROS production while TIB-73 cells remained unchanged. Treatment with similar concentrations of HSA-DHA did not increase mitochondrial ROS in TIB-75 cells indicating that LDL delivery of DHA is more efficacious at inducing mitochondrial dysfunction than the traditional delivery of DHA by albumin.

In order to determine if increased mitochondrial ROS production was sufficient to sensitize TIB-73 cells to LDL-DHA, TIB-73 cells were treated with increasing doses of carbonyl cyanide m-chlorophenyl hydrazone (CCCP), a mitochondria oxidative phosphorylation

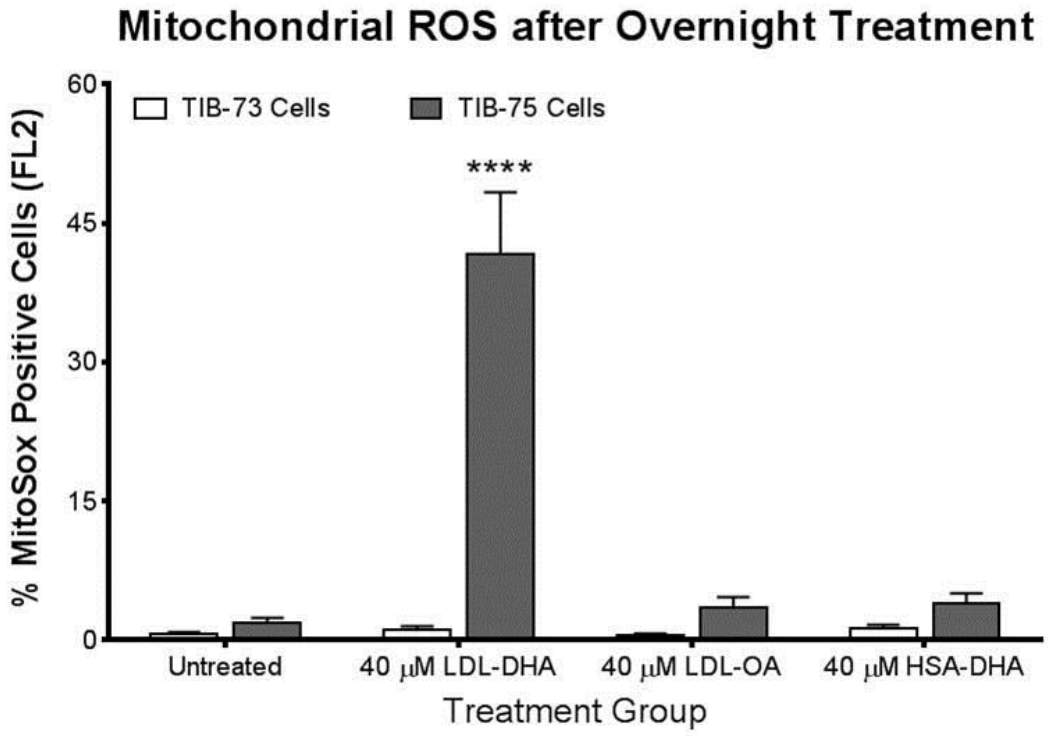

Figure 7-4-1: Mitochondrial ROS production caused by LDL-DHA treatment in TIB-73 and TIB-75 cells

TIB-73 and TIB-75 cells were grown to 80-90% confluency in 6-well plates, serum starved for 6 hours, and then treated with serum free media, 40 μM LDL-OA, LDL-DHA, or HSA-DHA overnight. After treatment, the cells were stained with 5 μM MitoSox and 0.2 μM MitoTracker Green for 15 minutes at 37°C, trypsinized, and resuspended with PBS. The MitoSox and MitoTracker fluorescence of the cells were measured by flow cytometry on the FL2 and FL1 channels, respectively. TIB-75 cells had a higher percentage of MitoSox positive cells following LDL-DHA treatment compared to TIB-73 cells. LDL-OA and HSA-DHA did not significantly increase MitoSox expression in either cell line.
* = p-value ≤0.05, ** = p-value ≤0.01, *** = p-value ≤0.001, **** = p-value ≤0.0001. The error bars represent the standard error of the mean.

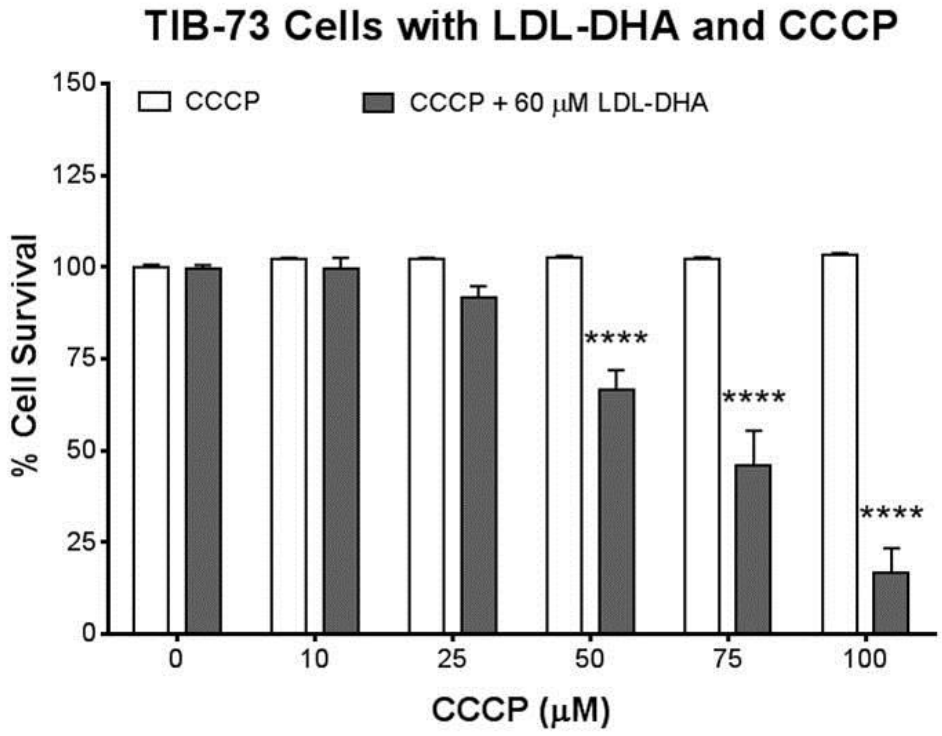

Figure 7-4-2: LDL-DHA cytotoxicity after induction of mitochondrial ROS by CCCP in TIB-73 cells

TIB-73 cells were grown to 80-90% confluency in 96-well plates, serum starved overnight, pretreated for 1 hour with increasing doses of CCCP (0-100 μM) and then treated with 60 μM LDL-DHA for 24 hours. Cell viability was determined by MTS assay. Inhibition of mitochondrial oxidative phosphorylation by CCCP sensitized TIB-73 to a sub-lethal dose of LDL-DHA in a dose-dependent manner.

* = p-value ≤0.05, ** = p-value ≤0.01, *** = p-value ≤0.001, **** = p-value ≤0.0001. The error bars represent the standard error of the mean.

inhibitor, prior to treatment with 60 µM LDL-DHA for twenty-four hours t (Figure 7-4-2). TIB-73 cells treated with CCCP or LDL-DHA alone did not experience significant cytotoxicity, but the combination of CCCP and LDL-DHA resulted in increased sensitivity to LDL-DHA in a CCCP dose-dependent manner. Treatments of TIB-73 cells with 50 µM and 75 µM CCCP and LDL-DHA yielded cytotoxicity similar to TIB-75 cells treated with only 60 µM LDL-DHA for twenty-four hours. A follow-up to the CCCP cell viability assay was to assess the mitochondrial ROS production in TIB-73 cells treated with 50 µM and 75 µM CCCP with or without 60 µM LDL-DHA using MitoSox flow cytometry (Figure 7-4-3). Untreated TIB-75 cells were also stained with MitoSox to compare the TIB-75 baseline MitoSox positive cell population (2.6 ± 0.5%) to the TIB-73 cells treated with media (1.0 ± 0.2%), 50 µM (2.2 ± 0.7%), and 75 µM CCCP only (2.9 ± 0.7%). CCCP treatment gave the TIB-73 cells a similar population of MitoSox positive cells compared to untreated TIB-75 cells. Additionally, TIB-73 cells treated with CCCP and LDL-DHA had a significant increase in the number of MitoSox positive cells compared to untreated cells. TIB-75 cells treated overnight with 40 µM LDL-DHA had a MitoSox positive population of 41.6 ± 6.8% while overnight treatment of TIB-73 cells with 75 µM CCCP and 60 µM LDL-DHA only resulted in a 10.7 ± 2.9% MitoSox positive population. The CCCP MitoSox flow cytometry data combined with the CCCP cell viability data suggest that disturbing mitochondrial function and increasing mitochondrial ROS production can sensitize TIB-73 cells to LDL-DHA treatments.

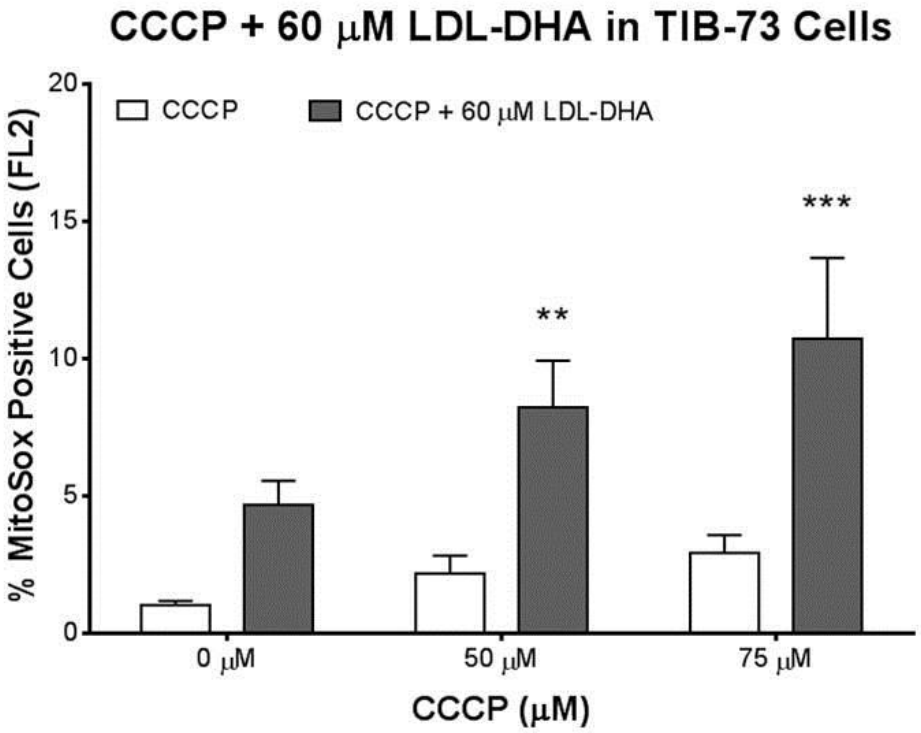

Figure 7-4-3: Mitochondrial ROS production caused by LDL-DHA treatment in TIB-73 and TIB-75 cells

TIB-73 cells were grown to 80-90% confluency in 6-well plates, serum starved for 6 hours, and then treated with 50 µM or 75 µM CCCP for 1 hour and then 60 µM LDL-DHA overnight. After treatment, the cells were stained with 5 µM MitoSox and 0.2 µM MitoTracker Green for 15 minutes at 37°C, trypsinized, and resuspended with PBS. The MitoSox and MitoTracker fluorescence of the cells were measured by flow cytometry on the FL2 and FL1 channels, respectively. Pretreatment with CCCP increased the number of MitoSox positive cells following treatment with LDL-DHA compared to the untreated control group.

* = p-value ≤0.05, ** = p-value ≤0.01, *** = p-value ≤0.001, **** = p-value ≤0.0001. The error bars represent the standard error of the mean.

LDL-DHA induces DNA damage in TIB-75 cells

The final organelle to be studied following LDL-DHA was the nucleus. Increased ROS production can cause DNA damage in cells. To study the effect of LDL-DHA on DNA damage, TIB-73 and TIB-75 cells were treated for six hours or overnight with 40 or 60 µM LDL-DHA or LDL-OA and stained with a fluorescent antibody to γ-H2AX, a protein that localizes to double strand DNA breaks. TIB-75 cells treated with 60 µM LDL-DHA for 6 hours (Figure 7-5-1) exhibited an increased number of cells with γ-H2AX foci formation. Similarly, overnight treatment with both 40 µM and 60 µM LDL-DHA (Figure 7-5-2) also significantly increased γ-H2AX foci formation in TIB-75 cells but not in TIB-73 cells. This DNA damage along with the lysosome and mitochondria changes is evidence that LDL-DHA treatment causes a multitude of subcellular changes selectively in the malignant TIB-75 cells.

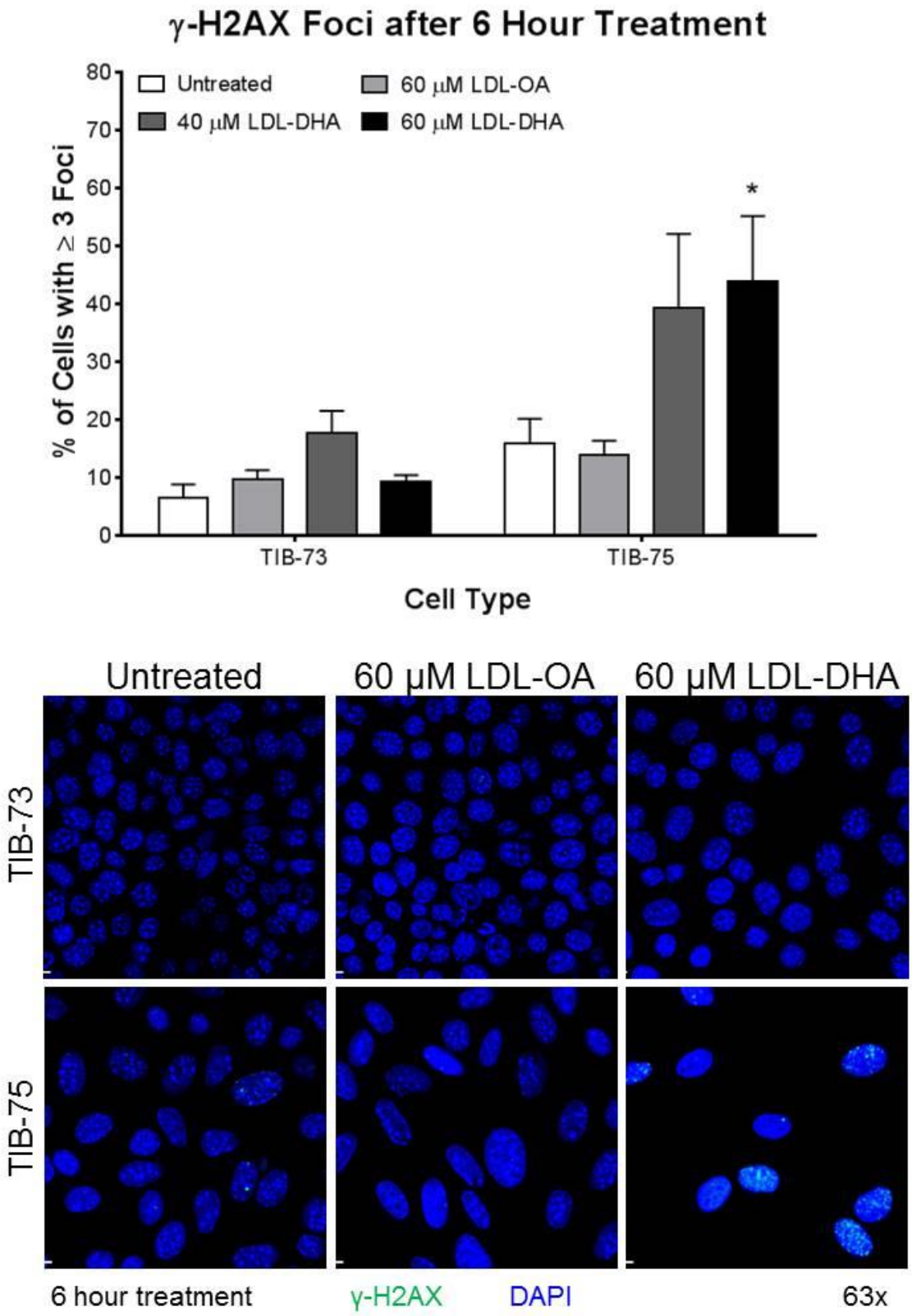
γ-H2AX Foci after 6 Hour Treatment
Untreated
60 μM LDL-OA
40 μM LDL-DHA
60 μM LDL-DHA
% of Cells with ≥ 3 Foci
80
70
60
50
40
30
20
10
0
*
TIB-73
TIB-75
Cell Type
Untreated
60 μM LDL-OA
60 μM LDL-DHA
TIB-73
TIB-75
6 hour treatment
γ-H2AX
DAPI
63x

Figure 7-5-1: γ-H2AX foci formation after LDL-DHA treatment for 6 hours in TIB-73 and TIB-75 cells

TIB-73 and TIB-75 cells were grown to 80-90% confluency in 8 chamber glass slides coated with 10 µg/mL fibronectin, serum starved, and then treated for 6 hours with serum free media, 40 µM LDL-DHA, 60 µM LDL-DHA, or 60 µM LDL-OA. After treatment, the cells were fixed with 4% paraformaldehyde, blocked with 5% BSA in PBS and probed overnight with 1:1000 Alexa 488-conjugated antibody against γ-H2AX, washed, and mounted with DAPI prolong gold. Slides were imaged at 63x on a Leica LP5 confocal microscope using the green and blue filters. Images were analyzed on Imaris imaging software and total number of cells and cells containing ≥3 γ-H2AX foci were counted using ImageJ software.
* = p-value ≤0.05, ** = p-value ≤0.01, *** = p-value ≤0.001, **** = p-value ≤0.0001. The error bars represent the standard error of the mean.

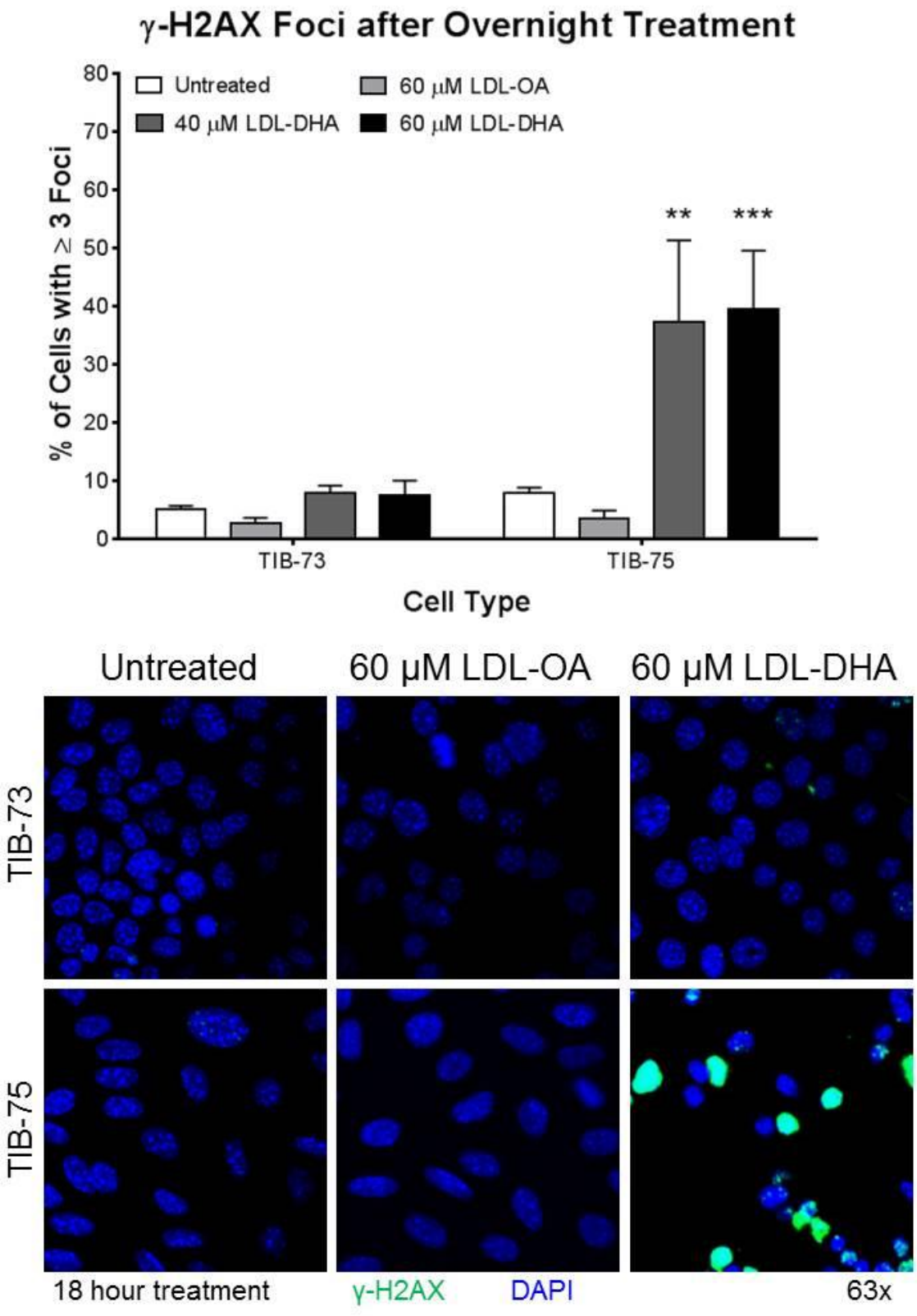
γ-H2AX Foci after Overnight Treatment
Untreated
60 μM LDL-OA
40 μM LDL-DHA
60 μM LDL-DHA
% of Cells with ≥ 3 Foci
80
70
60
50
40
30
20
10
0
**
***
TIB-73
TIB-75
Cell Type
Untreated
60 μM LDL-OA
60 μM LDL-DHA
TIB-73
TIB-75
18 hour treatment
γ-H2AX
DAPI
63x

Figure 7-5-2: γ-H2AX foci formation after LDL-DHA treatment for 18 hours in TIB-73 and TIB-75 cells

TIB-73 and TIB-75 cells were grown to 80-90% confluency in 8 chamber glass slides coated with 10 µg/mL fibronectin, serum starved, and then treated for 18 hours with serum free media, 40 µM LDL-DHA, 60 µM LDL-DHA, or 60 µM LDL-OA. After treatment, the cells were fixed with 4% paraformaldehyde, blocked with 5% BSA in PBS and probed overnight with 1:1000 Alexa 488-conjugated antibody against γ-H2AX, washed, and mounted with DAPI prolong gold. Slides were imaged at 63x on a Leica LP5 confocal microscope using the green and blue filters. Images were analyzed on Imaris imaging software and total number of cells and cells containing ≥3 γ-H2AX foci were counted using ImageJ software.
* = p-value ≤0.05, ** = p-value ≤0.01, *** = p-value ≤0.001, **** = p-value ≤0.0001. The error bars represent the standard error of the mean.

Role of Iron in LDL-DHA Cytotoxicity

In order to elucidate the cause of increased LPO following LDL-DHA cytotoxicity is TIB-75 cells, experiments were performed to investigate the role of iron as a catalyst of lipid peroxidation through the Fenton Reaction. The first aim of this line of research was to measure the levels of proteins involved in iron transport in the cells and iron levels in the TIB-73 and TIB-75 cells. The second aim was to assess whether loading TIB-73 cells with exogenous ferric chloride would increase their sensitivity to LDL-DHA. The final aim was to investigate whether removal of iron in TIB-75 cells decreases their sensitivity to LDL-DHA and the deleterious effects these cells experience after LDL-DHA treatment.

TIB-73 and TIB-75 cells have different baseline levels of iron

Protein levels of transferrin and transferrin receptor were measured by western blot in TIB-73 and TIB-75 cells at baseline. The first of these western blots showed that TIB-75 cells have lower expression of transferrin, a protein that binds iron for transport into the cell (Figure 8-1A). Lower transferrin levels are commonly seen in iron-overloading diseases such as hemochromatosis so the lower levels in TIB-75 cells may point to the down-regulation of transferrin due to high intracellular iron levels. Expression of transferrin receptor, the receptor responsible for endocytosis of iron-bound transferrin, was not significantly different between TIB-73 and TIB-75 cells (Figure 8-1B).

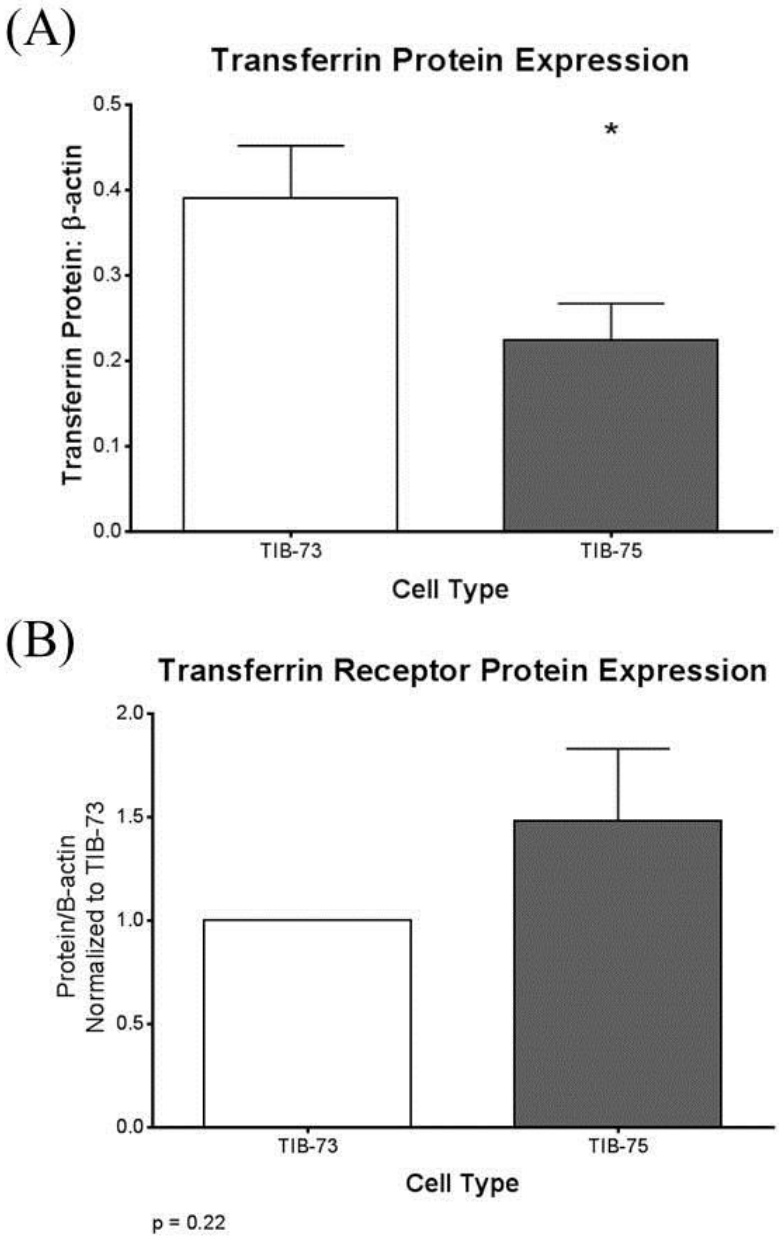

Figure 8-1: Baseline Transferrin and Transferrin Receptor protein levels in TIB-73 and TIB-75 cells

Transferrin and Transferrin Receptor protein levels from TIB-73 and TIB-75 cell lysates were determined by Western Blot and normalized to β-actin protein. TIB-75 cells had lower Transferrin levels than TIB-73 cells at baseline.
* = p-value ≤0.05, ** = p-value ≤0.01, *** = p-value ≤0.001, **** = p-value ≤0.0001. The error bars represent the standard error of the mean.

Baseline levels of intracellular iron were assayed by ferrozine assay, ICP-MS, and by microscopy using silver sulfide autometallography and IP-1, a fluorescent iron-indicating dye. Measurement of total iron levels by ferrozine assay showed that TIB-75 cells had higher iron levels than TIB-73 cells at baseline (Figure 8-2-1A). An alternate and more sensitive method to measure total iron by ICP-MS (Figure 8-2-1B) suggested that TIB-75 cells have slightly higher iron levels but the difference did not reach statistical significance (p-value = 0.075). Silver sulfide autometallography was used to qualitatively visualize the subcellular distribution and quantity of iron in the TIB-73 and TIB-75 cells. This stain showed that both TIB-73 and TIB-75 cells have delicate intracellular iron precipitation and that TIB-75 cells have slightly more iron precipitation than TIB-73 cells indicated by their darker color especially in the rounded cells (Figure 8-2-2). Finally, cells were stained with a dye that fluoresces in the presence of labile iron and with a lysosome stain to quantify labile iron levels and to determine the colocalization of the labile iron to the lysosome (Figure 8-2-3A). Labile iron colocalized very well with the lysosome in both TIB-73 and TIB-75 cells (Pearson's Coefficient > 0.7) (Figure 8-2-3B), which may have implications for labile iron's interaction with LDL-DHA. Semi-quantification of labile iron by mean pixel intensity measurements of IP-1 fluorescence did not detect a difference in iron levels between TIB-73 and TIB-75 cells (Figure 8-2-3C). The addition of deferoxamine (DFO), an iron chelator, did lower the fluorescence of IP-1 dye indicating that the IP-1 dye is selective for iron but did not change the amount of colocalization of IP-1 with the lysosome. In total, these results suggest that TIB-75 may have higher iron levels than TIB-73 cells, but further research is necessary to confirm these findings.

(A)

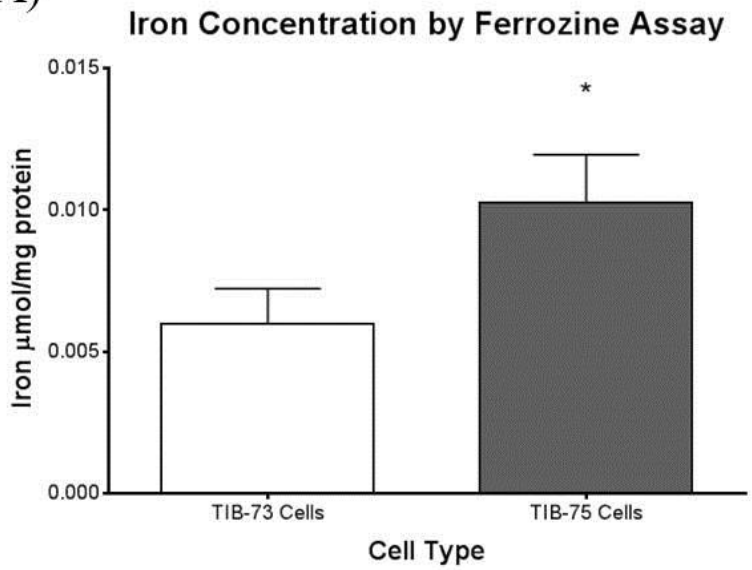
Iron Concentration by Ferrozine Assay
0.015
0.010
0.005
0.000
Iron µmol/mg protein
*
TIB-73 Cells
TIB-75 Cells
Cell Type

(B)

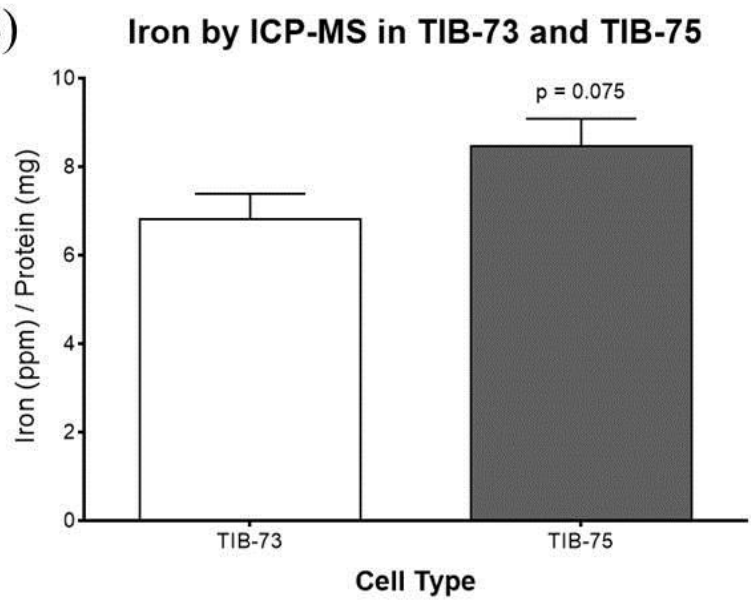
Iron by ICP-MS in TIB-73 and TIB-75
10
8
6
4
2
0
Iron (ppm) / Protein (mg)
p = 0.075
TIB-73
TIB-75
Cell Type

Figure 8-2-1: Total iron levels by ferrozine assay and ICP-MS

TIB-73 and TIB-75 cells were grown to 80-90% confluency and then scraped and pelleted. **(A)** Iron determination by the colorimetric ferrozine assay where iron is released from proteins by incubating cell lysates with 1.4 M HCl and 4.5% w/v $KMnO_4$ at 60ºC for 2 hours and then reacting the free iron with 6.5 mM ferrozine, 6.5 mM neocuproine, 2.5 M ammonium acetate, and 1 M ascorbic acid to produce a colored product that has an absorbance at 550 nm. Iron concentration of each sample was determined by comparison to a $FeCl_3$ standard curved and normalized to protein. **(B)** Iron determination by ICP-MS where the cell pellets were incubated at 90°C for 4 hours with 70% nitric acid to release iron from proteins and then run on an Agilent 7700x ICP-MS using argon carrier gas. Iron signal was detected and compared to a 10 ppm iron standard. For both assays, a portion of the cell lysate was used to measure protein by Bradford assay and iron levels were normalized to the cell protein concentration.

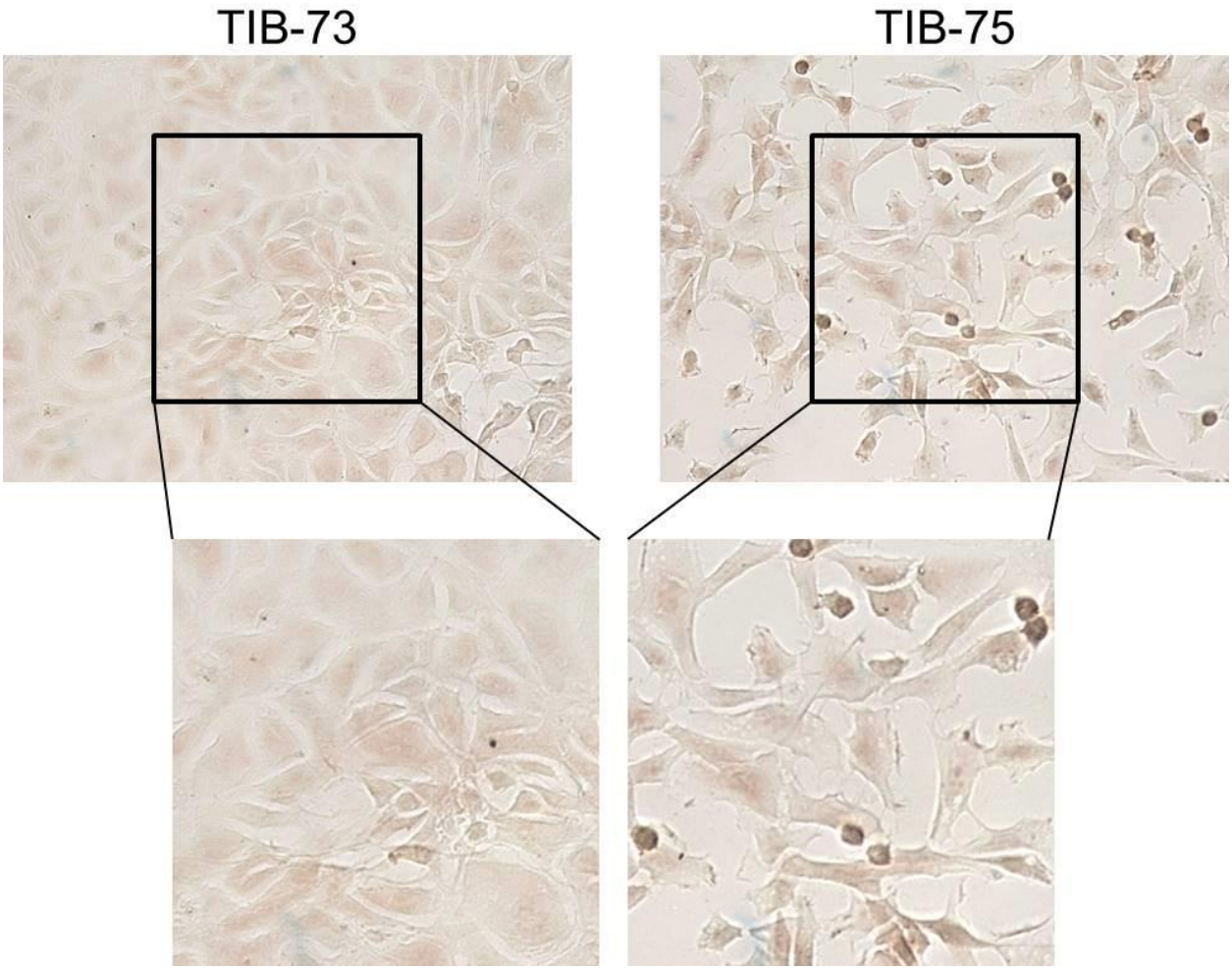

Figure 8-2-2: Iron silver sulfide autometallography staining

TIB-73 and TIB-75 cells were grown to 80-90% confluency on a 8-chamber glass slide. Cells were washed with PBS and fixed with 2% glutaraldehyde in 0.1 M Na-Cacodylate buffer with 0.1 M sucrose (pH 7.2) for 2 hours at 22°C. Cells were washed and then sulfidated using 1% (w/v) ammonium sulfide in 70% ethanol (pH ≈9) for 15 minutes at 22°C. The intracellular iron was developed using a colloid-protected reagent containing silver lactate for different time periods (the images above were developed for 10 minutes). Cells were then washed and mounted with Canada Basalm. The slides were imaged using a brightfield microscope at 20x magnification. TIB-75 cells displayed a higher amount of silver sulfide staining compared to TIB-73 cells.

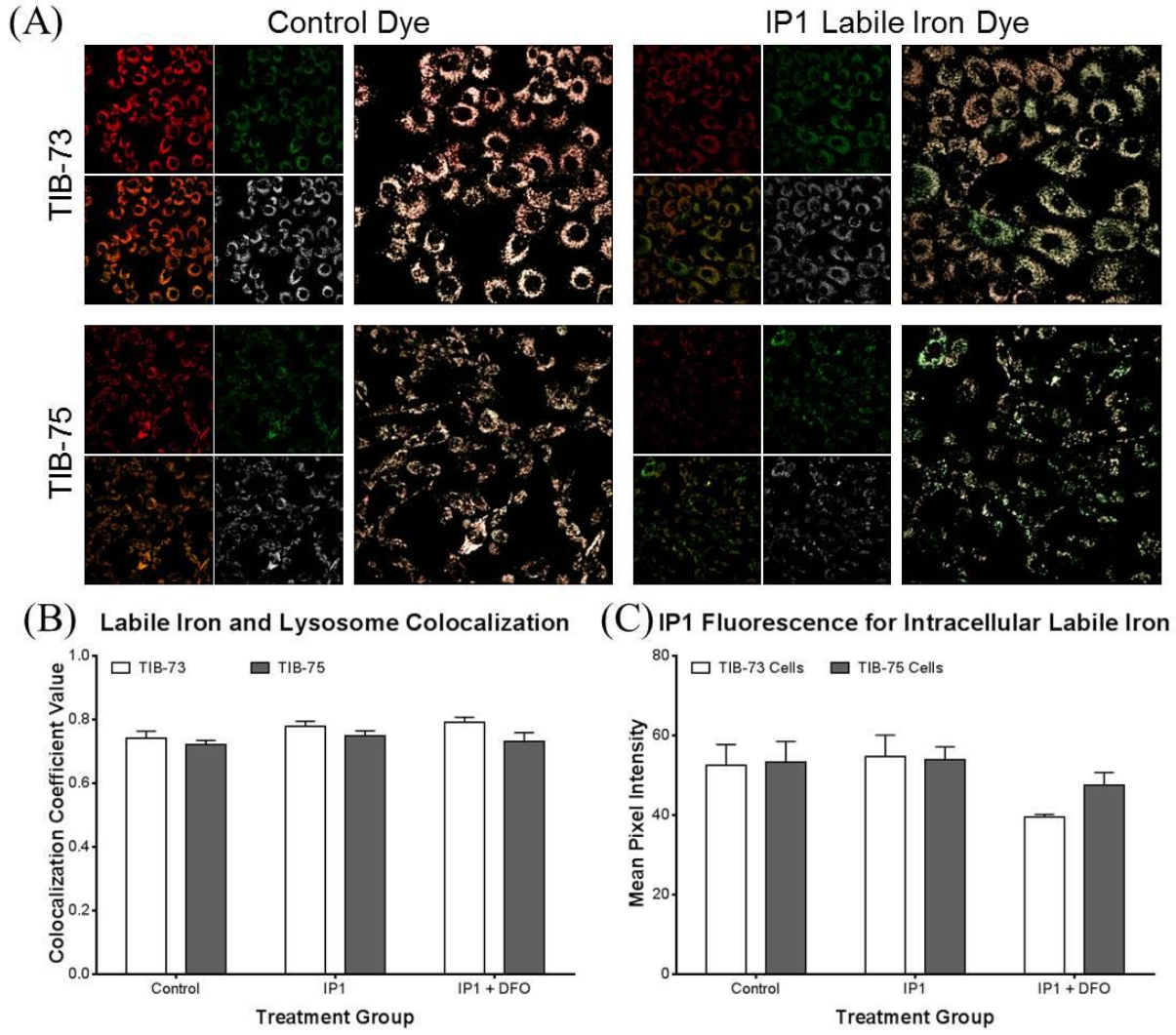

Figure 8-2-3: Fluorescent labile iron dye IP1 and lysosome colocalization

TIB-73 and TIB-75 cells were grown to 80-90% confluency in 35 mm^2 glass bottom dishes coated with 10 µg/mL fibronectin. The cells were treated with 200 µM deferoxamine (negative control for IP1 iron dye) or serum free media for 3 hours at 37°C, and then stained for 2 hours at 37°C with 500 µL of 20 µM IP1 (a dye that fluoresces green in the presence of labile iron) or 20 µM control dye (a constitutively fluorescent derivative of IP1). Cells were then dyed with 75 nM LysoTracker Deep Red for 30 minutes prior to imaging. (**A)** Cells were imaged at 63x magnification on a Leica LP5 confocal. The green channel measured IP1 or control dye fluorescence at 488 nm excitation and 510 nm emission. The red channel measured deep red fluorescence of the LysoTracker dye with 561 nm excitation and >610 nm emission. Images were deconvoluted using AutoQuant X3 software. **(B)** Imaris imaging software was used to calculate LysoTracker Deep Red colocalization with green IP1 or control dye in the cells**. (C)** ImageJ software was used to threshold the images to remove background fluorescence and then calculate the mean pixel intensity of the green channel as a semi-quantitative measure of labile iron in the cells.

Overloading TIB-73 cells with labile iron is not sufficient to induce LDL-DHA cytotoxicity

The next aim for the role of iron in LDL-DHA cytotoxicity was to see if overloading TIB-73 cells with iron would sensitize them to LDL-DHA cytotoxicity. TIB-73 cells were treated with ferric chloride for 1 hour prior to the addition of 60 µM LDL-DHA for twenty-four hours. Overloading TIB-73 cells with iron did not increase their sensitivity to LDL-DHA and they even experienced increased growth following LDL-DHA treatment (Figure 8-3). The amount of iron in the TIB-73 cells following treatment with ferric chloride was not determined so it is not known how much iron was actually taken up or where it was shuttled inside the cells.

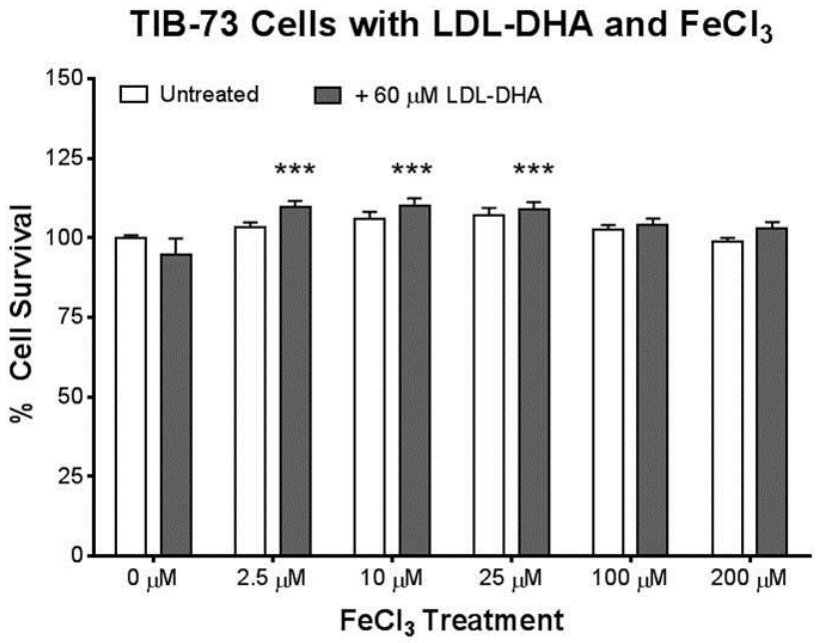

Figure 8-3: LDL-DHA cytotoxicity after ferric chloride pretreatment in TIB-73 cells

TIB-73 cells were grown to 80-90% confluency in 96-well plates, serum starved overnight, pretreated for 1 hour with increasing doses of $FeCl_3$ (0-200 µM) and then treated with 60 µM LDL-DHA for 24 hours. Cell viability was determined by MTS assay. Iron loading with $FeCl_3$ did not sensitize TIB-73 cells to LDL-DHA.
* = p-value ≤0.05, ** = p-value ≤0.01, *** = p-value ≤0.001, **** = p-value ≤0.0001. The error bars represent the standard error of the mean.

Chelation of labile iron partially rescues LDL-DHA's cytotoxicity and sequelae in TIB-75 cells

The final step in elucidating the role of iron in TIB-75 cell sensitivity to LDL-DHA was to remove labile iron using deferoxamine and study LDL-DHA cytotoxicity and its sequelae. TIB-73 and TIB-75 cells were pretreated with increasing doses of deferoxamine for three hours prior LDL-DHA treatment. As expected, TIB-73 cells did not show any cytotoxicity with LDL-DHA treatment with or without deferoxamine (Figure 8-4-1A). On the other hand, TIB-75 cells treated with deferoxamine displayed a partial rescue of LDL-DHA cytotoxicity to ≈75% of untreated cells (Figure 8-4-1B). Pretreatment with deferoxamine also reduced the amount of LPO measured by TBARS in TIB-75 cells following LDL-DHA but did not reduce LPO back to baseline levels (Figure 8-4-2). LDL-DHA-induced LPO measured by BODIPY C11 581/591 flow cytometry was reversed by pretreatment with deferoxamine (Figure 8-4-3). Furthermore, deferoxamine pretreatment also significantly reduced the number of TIB-75 cells with leaking lysosomes following LDL-DHA treatment compared to LDL-DHA treatment alone, but deferoxamine did not reduce lysosome leaking back to baseline levels (Figure 8-4-4). Deferoxamine pretreatment was not successful at preventing loss of mitochondrial membrane potential following LDL-DHA treatment (Figure 8-4-5). Deferoxamine treatment even exacerbated MMP loss in LDL-DHA treated TIB-75 cells and in TIB-73 cells. Analysis of hydrogen peroxide levels using DCF flow cytometry showed that deferoxamine treatment did not decrease the production of hydrogen peroxide following LDL-DHA treatment in TIB-75 cells (Figure 8-4-6).

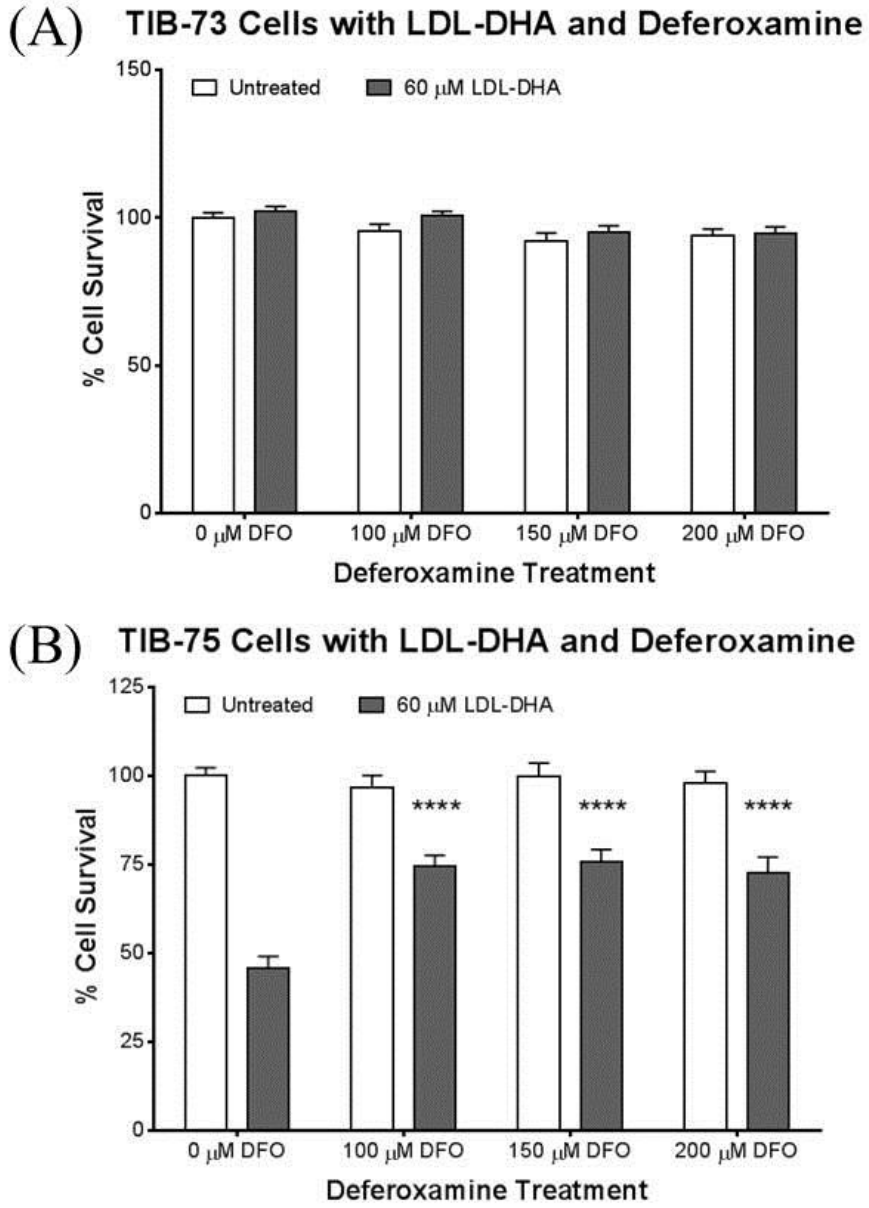

Figure 8-4-1: LDL-DHA cytotoxicity after pretreatment with deferoxamine in TIB-73 and TIB-75 cells

TIB-73 **(A)** and TIB-75 **(B)** cells were grown to 80-90% confluency in 96 well plates, serum starved overnight, pretreated for 3 hours with increasing doses of an iron chelator deferoxamine (0-200 μM), and then 60 μM LDL-DHA was added for 24 hours. Cell viability was analyzed by MTS assay. Pretreatment with deferoxamine to remove labile iron partially rescued LDL-DHA cytotoxicity in TIB-75 cells.
* = p-value ≤0.05, ** = p-value ≤0.01, *** = p-value ≤0.001, **** = p-value ≤0.0001. The error bars represent the standard error of the mean.

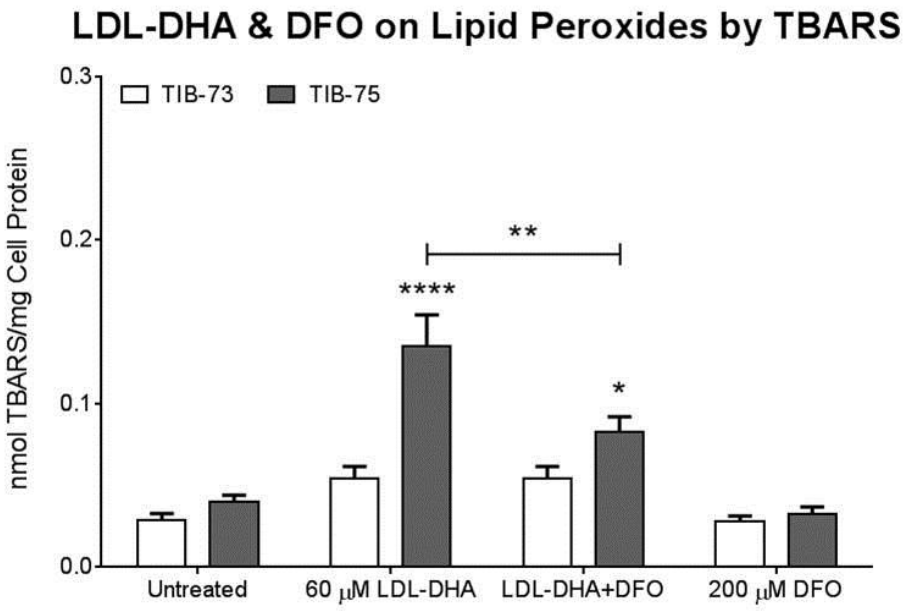

Figure 8-4-2: Lipid peroxidation by LDL-DHA after deferoxamine pretreatment by TBARS in TIB-73 and TIB-75 cells

TIB-73 and TIB-75 cells were grown to 80-90% confluency in 100 mm^2 dishes. The cells were serum starved overnight, pretreated for 3 hours with 200 µM deferoxamine. After pretreatment, 60 µM LDL-DHA was added for 24 hours. After treatment, cells were washed with PBS, collected by scraping, and lysed by sonication. The lysate was mixed with TBARS reagent mix, incubated for 1 hour at 95°C. The absorbance of the supernatant was read by plate reader at 550 nm. The protein of the cell lysate was measured by Bradford assay. The TBARS concentration (nmol) was calculated by the extinction coefficient and normalized to cell protein. Deferoxamine pretreatment to remove labile iron significantly reduced lipid peroxidation caused by LDL-DHA in TIB-75 cells, but not back to baseline levels.

* = p-value ≤0.05, ** = p-value ≤0.01, *** = p-value ≤0.001, **** = p-value ≤0.0001. The error bars represent the standard error of the mean.

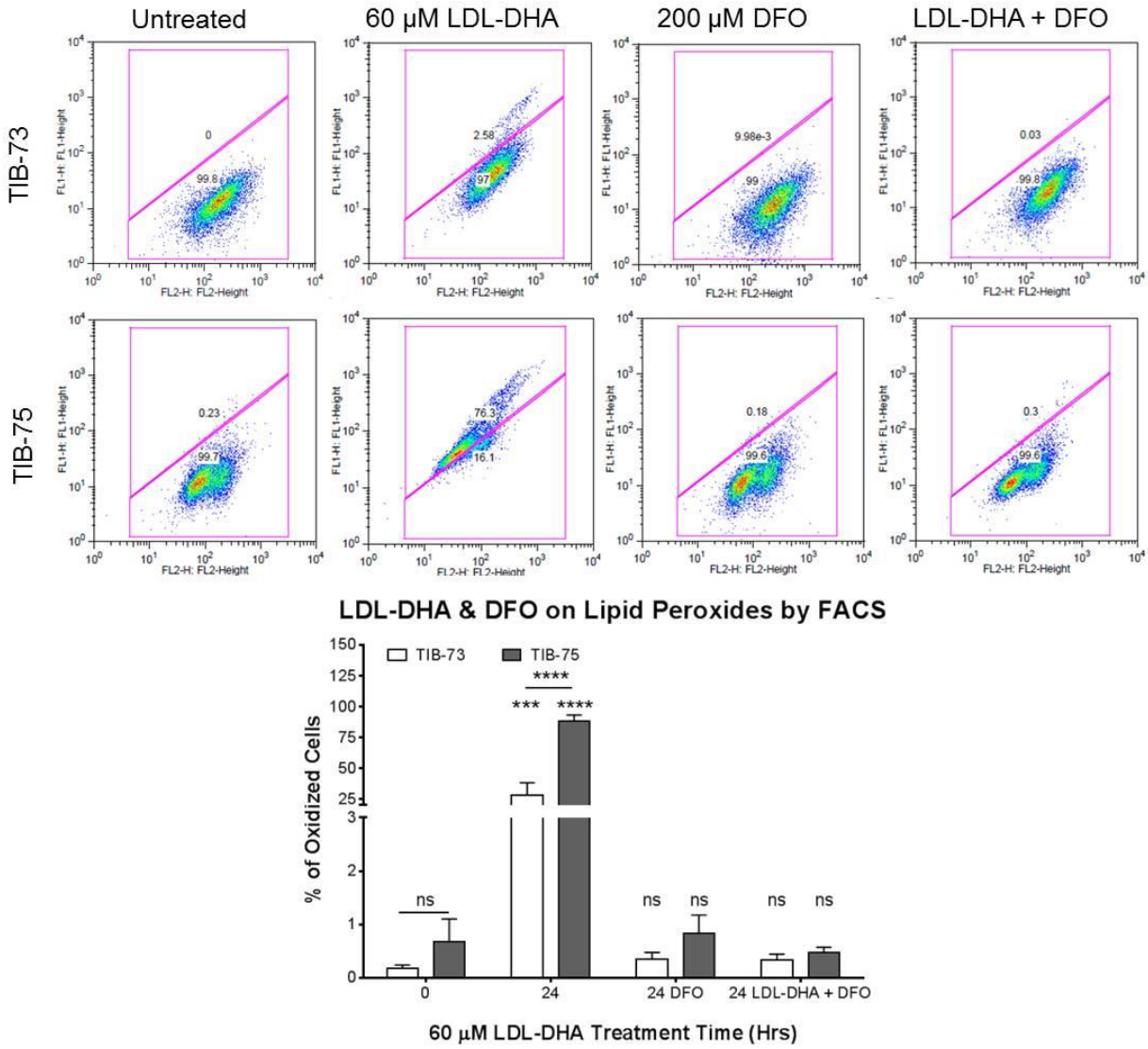

Figure 8-4-3: Lipid peroxidation by LDL-DHA after deferoxamine pretreatment by BODIPY C11 581/591 flow cytometry in TIB-73 and TIB-75 cells

TIB-73 and TIB-75 cells were grown to 80-90% confluency in 6-well plates, serum starved overnight, stained with 1 µM BODIPY C11 581/591 dye, a lipid peroxide indicating dye, for 30 minutes at 37°C. After staining, the cells were pretreated for 3 hours with 200 µM deferoxamine before adding 60 µM LDL-DHA for 24 hours. After treatment cells were trypsinized and washed with PBS. BODIPY C11 581/591 fluorescence of the cells was measured by flow cytometry where green fluorescence indicated oxidized lipid species and red fluorescence indicated unoxidized lipid species. TIB-75 cells had a higher percentage of cells with oxidized lipids following LDL-DHA treatment and that lipid oxidation was removed with deferoxamine pretreatment.

* = p-value ≤0.05, ** = p-value ≤0.01, *** = p-value ≤0.001, **** = p-value ≤0.0001. The error bars represent the standard error of the mean.

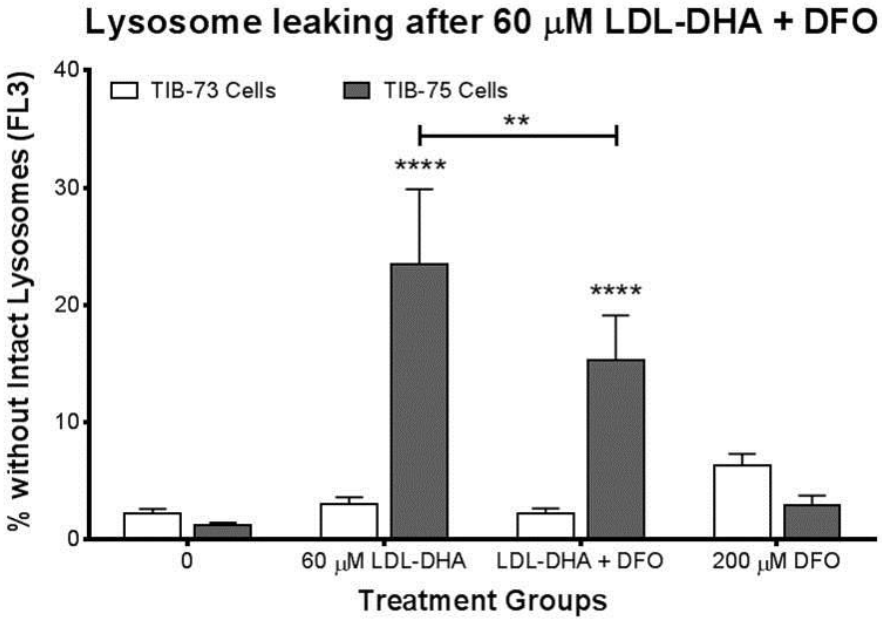

Figure 8-4-4: Rescue of LDL-DHA induced lysosome membrane permeability after deferoxamine pretreatment in TIB-73 and TIB-75 cells

TIB-73 and TIB-75 cells were grown to 80-90% confluency in 6-well plates, serum starved overnight, pretreated for 3 hours with 200 μM deferoxamine, an iron chelator, and then treated with 60 μM LDL-DHA for 24hours. After treatment, the cells were stained with 0.5 μg/mL acridine orange for 15 minutes at 37°C, trypsinized, and washed with PBS. Loss of red acridine orange fluorescence (FL2) of the cells was measured by flow cytometry to determine the number of cells with loss of intact lysosomes. Deferoxamine pretreatment was able to significantly increase the number of TIB-75 cells with intact lysosomes following LDL-DHA treatment.

* = p-value ≤0.05, ** = p-value ≤0.01, *** = p-value ≤0.001, **** = p-value ≤0.0001. The error bars represent the standard error of the mean.

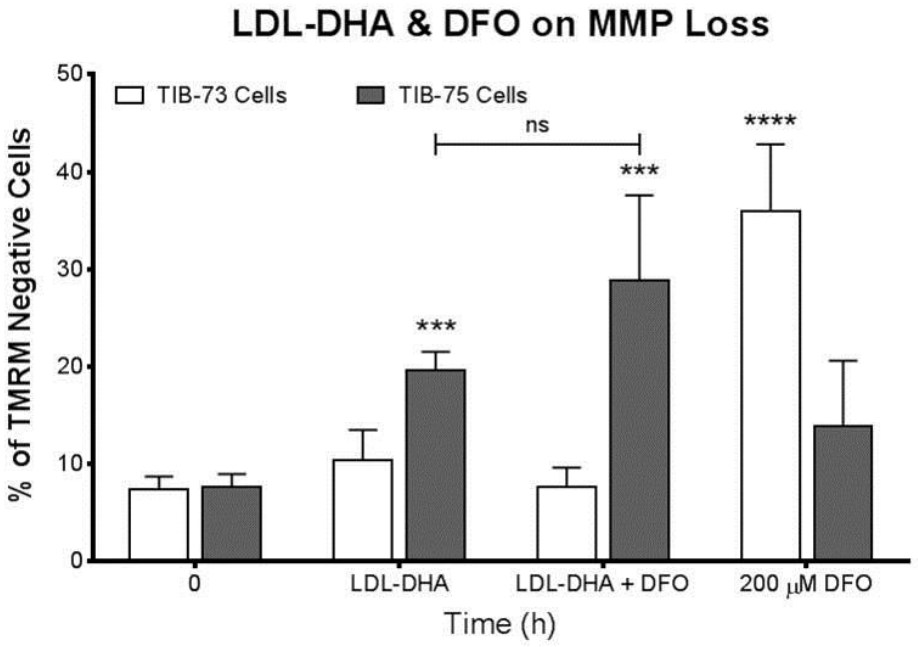

Figure 8-4-5: Mitochondrial membrane potential loss by LDL-DHA after deferoxamine pretreatment in TIB-73 and TIB-75 cells

TIB-73 and TIB-75 cells were grown to 80-90% confluency in 6-well plates, serum starved overnight, pretreated with 200 μM deferoxamine for 3 hours and then treated for 24 hours with 60 μM LDL-DHA. After treatment, the cells were trypsinized, stained with 100 nM TMRM for 15 minutes at 37°C, and washed with PBS. TMRM fluorescence of the cells was measured by flow cytometry. TIB-75 cells had a higher percentage of TMRM negative cells following LDL-DHA treatment, but deferoxamine pretreatment did not rescue loss of mitochondrial membrane potential. TIB-73 cells exhibited a deferoxamine induced loss of mitochondrial membrane potential.
* = p-value ≤0.05, ** = p-value ≤0.01, *** = p-value ≤0.001, **** = p-value ≤0.0001. The error bars represent the standard error of the mean.

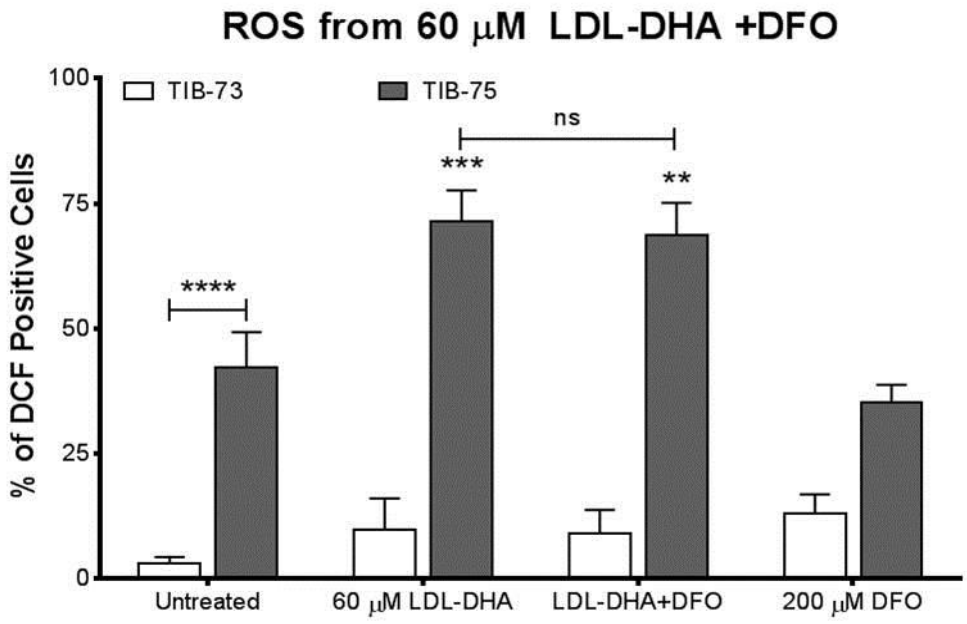

Figure 8-4-6: ROS from LDL-DHA after deferoxamine treatment by DCF flow cytometry in TIB-73 and TIB-75 cells

TIB-73 and TIB-75 cells were grown to 80-90% confluency in 6-well plates, serum starved overnight, pretreated with 200 μM deferoxamine for 3 hours and then treated for 24 hours with 60 μM LDL-DHA. After treatment, the cells were stained with 15 μM DCF-DA for 30 minutes at 37°C, trypsinized, and washed with PBS. Increase of green fluorescence (FL1) of the cells was measured by flow cytometry to determine ROS generation. TIB-75 cells had a higher percentage of DCF positive cells following LDL-DHA treatment, but deferoxamine pretreatment did not reduce the percentage of DCF positive cells.
* = p-value ≤0.05, ** = p-value ≤0.01, *** = p-value ≤0.001, **** = p-value ≤0.0001. The error bars represent the standard error of the mean.

LDL-DHA Treatment of HCC Tumors *in vivo* in Mouse HCC Models

Having documented that LDL-DHA is selectively cytotoxic to the mouse-derived hepatocellular carcinoma TIB-75 cells *in vitro*, pilot experiments looking into LDL-DHA cytotoxicity *in vivo* to hepatocellular carcinoma were initiated. TIB-75 cells injected subcutaneously into Balb/C mice were treated intratumorally with saline, LDL-OA, or LDL-DHA twice a week for two weeks. One hundred micromolar LDL-DHA treatments in this *in vivo* model did not show any reduction in tumor growth compared to the tumors treated with saline or LDL-OA (Appendix C). There were significant problems with this tumor model as consistency between initial tumor size was difficult to control. In addition, other confounding variables were present such as inconsistent or unequal nanoparticle treatment due to injection site leaking, mechanical damage to the tumor from the needle during the treatments, and unexpected mortality in treatment arms due to cage flooding or possible contamination of the LDL-OA.

Selective Cytotoxicity of LDL-DHA in Human HCC Compared to Primary Human Hepatocytes

Investigation of the cancer selective cytotoxicity of LDL-DHA was expanded to human cells *in vitro* to determine if human-derived hepatocellular carcinoma cells are selectively cytotoxic to LDL-DHA and if the mechanism of cytotoxicity in these HCC cells coincided with that observed in TIB-75 cells.

LDL-DHA is selectively cytotoxic to HCC cell lines

Primary human hepatocytes were treated for seventy-two hours with a dose response of LDL-DHA (0-200 µM DHA) or LDL-OA (0-200 µM OA). The primary human hepatocytes showed unchanged or increased survival with LDL-DHA up to 100 µM when compared to the untreated cells and did not exhibit significant cytotoxicity until 150 µM. The IC_{50} for LDL-DHA was 190.3 µM in the primary human hepatocytes (Figure 9-1A). These results are even better than those observed in the primary mouse hepatocytes treated with LDL-DHA (IC_{50} = 148.8 µM). LDL-OA treatment did not show any cytotoxicity in the primary human hepatocytes in the dose range tested (Figure 9-1B). A variety of human hepatocellular carcinoma cell lines were similarly treated with LDL-DHA or HSA-DHA (0-150 µM DHA) for seventy-two hours (Figures 9-2A, B, and C). A poorly differentiated and HBV positive cell line, FOCUS, was most sensitive to LDL-DHA treatment (IC_{50} = 20.9 µM LDL-DHA). FOCUS proved to be relatively resistant to DHA delivered by human serum albumin (IC_{50} = 112.3 µM HSA-DHA) (Figure 9-2A). Hep3B, a well-differentiated and HBV positive cell line, was treated with LDL-DHA and HSA-DHA and showed similar sensitivity to both DHA delivery modalities (IC_{50} = 35.0 µM LDL-DHA and 34.7 µM HSA-DHA) (Figure 9-2B). DHA treatment of a well-differentiated and HBV negative Huh7 cell line showed sensitivity to LDL-DHA (IC_{50} = 41.2 µM) but to a lesser degree than FOCUS and Hep3B (Figure 9-2C). Like FOCUS, Huh7 cells were not as sensitive to HSA-DHA (IC_{50} = 96.3 µM) as LDL-DHA. Most important to note is that LDL-DHA showed selective cytotoxicity to the HCC cells compared to the primary human hepatocytes as evidenced by the therapeutic window observed in their IC_{50} values (>150 µM LDL-DHA).

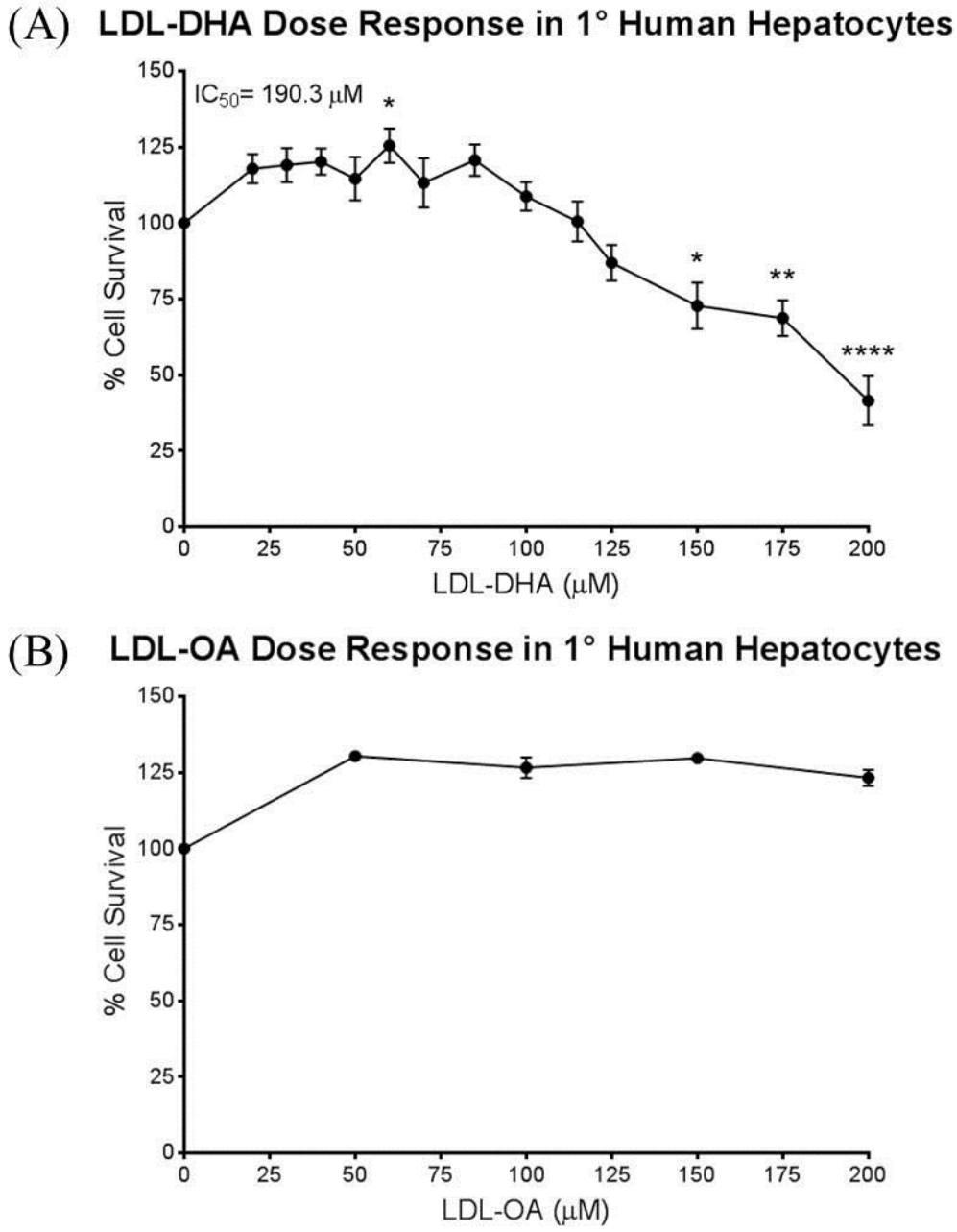

Figure 9-1: Cytotoxicity of LDL-DHA and LDL-OA in primary human hepatocytes

Primary human hepatocytes were plated to 80-90% confluency in collagen-coated 96 well plates for 24 hours and then treated with increasing doses of LDL-OA or LDL-DHA (0-200 μM DHA). Cell viability was measured by MTS assay after 72 hours. The primary hepatocytes were resistant to LDL-DHA induced cytotoxicity up to 150 μM and not sensitive at all to LDL-OA.

* = p-value ≤0.05, ** = p-value ≤0.01, *** = p-value ≤0.001, **** = p-value ≤0.0001. The error bars represent the standard error of the mean.

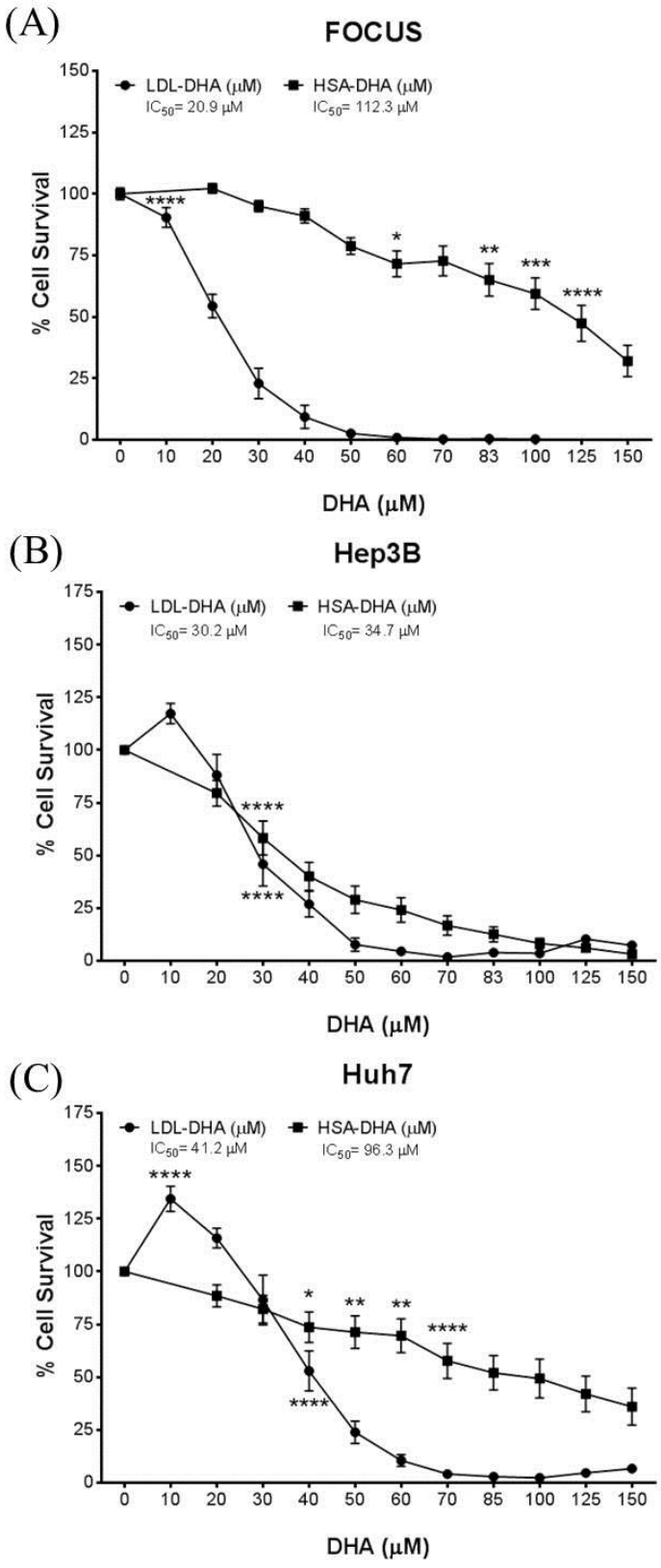
(A)
FOCUS
LDL-DHA (μM)
IC50= 20.9 μM
HSA-DHA (μM)
IC50= 112.3 μM
% Cell Survival
DHA (μM)
(B)
Hep3B
LDL-DHA (μM)
IC50= 30.2 μM
HSA-DHA (μM)
IC50= 34.7 μM
% Cell Survival
DHA (μM)
(C)
Huh7
LDL-DHA (μM)
IC50= 41.2 μM
HSA-DHA (μM)
IC50= 96.3 μM
% Cell Survival
DHA (μM)

Figure 9-2: Cytotoxicity of LDL-DHA and HSA-DHA in human FOCUS, Hep3B, and Huh7 HCC cells

Human HCC cells (FOCUS, Hep3B, and Huh7) were grown to 80-90% confluency in 96 well plates, serum starved overnight, and then treated with increasing doses of LDL-DHA or HSA-DHA (0-200 μM DHA). Cell viability was measured by MTS assay after 72 hours. With the exception of Hep3B, the HCC cell lines were more sensitive to LDL-DHA than HSA-DHA. * = p-value ≤0.05, ** = p-value ≤0.01, *** = p-value ≤0.001, **** = p-value ≤0.0001. The error bars represent the standard error of the mean.

ROS production and subcellular organelle damage is evident in human HCC cells after LDL-DHA treatment

The mechanism of LDL-DHA cytotoxicity was examined in FOCUS, Hep3B, and Huh7 cells. The primary hepatocytes were not studied in the following experiments due to the excessive cost of the hepatocytes and confounding variables that could affect the results such as the lack of *in vitro* proliferation and special media needed by the primary hepatocytes. The dose of 40 µM LDL-DHA was chosen for the following treatments because it was at or above the IC_{50} of each cell line after the 72 hour dose response. Firstly, superoxide levels were assessed by DHE flow cytometry after 24 hour treatment with 40 µM LDL-DHA or LDL-OA (Figure 9-3). This experiment showed that there was no significant difference in superoxide production between untreated and LDL-DHA-treated HCC cells, which was observed previously in the TIB-73 and TIB-75 cells. DCF flow cytometry also showed no significant increase in ROS production after LDL-DHA treatment in any of the HCC cell lines (Figure 9-4). In fact, all of the human HCC cell lines had very high baseline DCF fluorescence (>85% of cells), which is different from the results observed in untreated TIB-75 cells (≈42% of cells). When levels of lipid peroxidation after LDL-DHA treatment were measured, all three HCC cell lines treated with LDL-DHA, but not LDL-OA, showed a significant increase in TBARS compared to untreated cells (Figure 9-5). These results again indicate an important role for lipid peroxidation in the cytotoxicity of LDL-DHA in both TIB-75 cells and human HCC cells. LDL-DHA treatment also caused lysosome membrane permeability in human HCC cells after five hours with 40 µM LDL-DHA as observed by

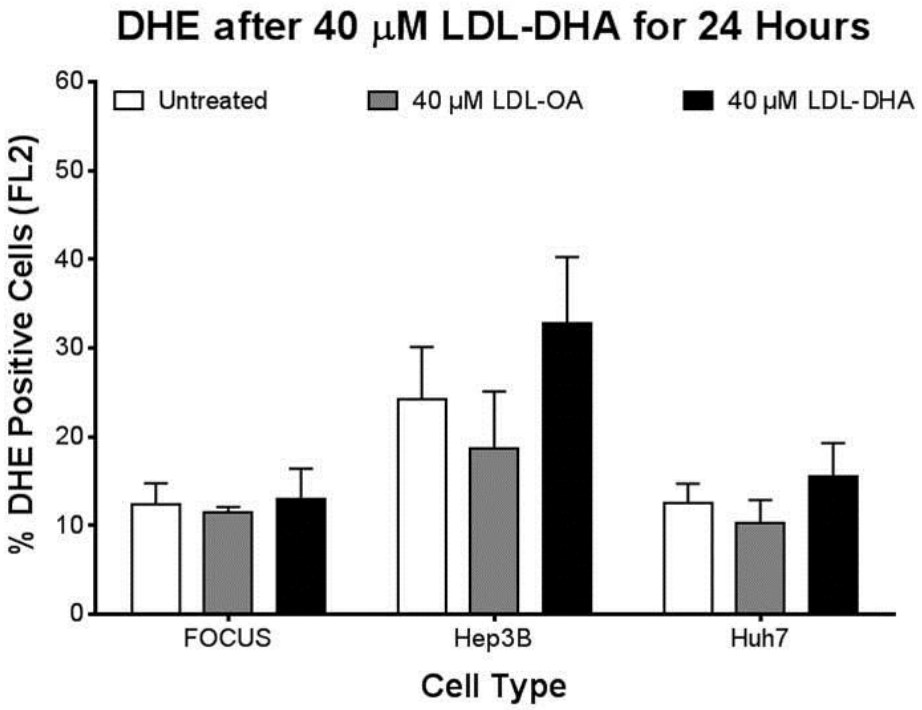

Figure 9-3: DHE flow cytometry after LDL-DHA treatment in FOCUS, Hep3B, and Huh7 cells

FOCUS, Hep3B, and Huh7 cells were grown to 80-90% confluency in 12-well plates, serum starved overnight, and then treated for different time periods with 40 μM LDL-DHA. After treatment, the cells were trypsinized, stained with 10 μM DHE for 30 minutes at 37°C in PBS. Increase of red fluorescence (FL2) of the cells was measured by flow cytometry to determine ROS generation.
* = p-value ≤0.05, ** = p-value ≤0.01, *** = p-value ≤0.001, **** = p-value ≤0.0001. The error bars represent the standard error of the mean.

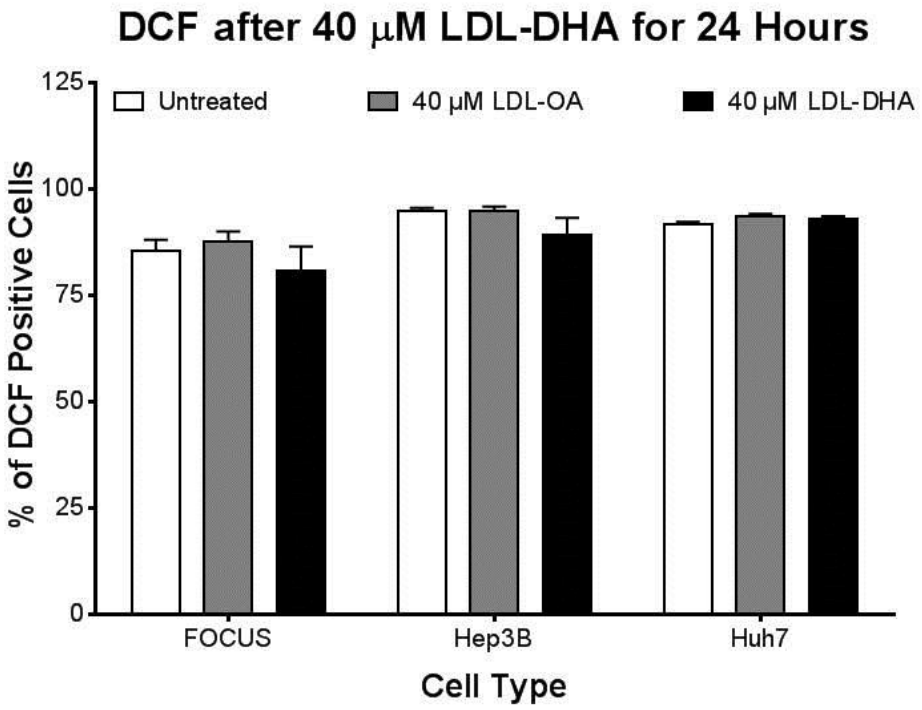

Figure 9-4: DCF flow cytometry after LDL-DHA treatment in FOCUS, Hep3B, and Huh7 cells

FOCUS, Hep3B, and Huh7 cells were grown to 80-90% confluency in 12-well plates, serum starved overnight, and then treated for different time periods with 40 μM LDL-DHA. After treatment, the cells were stained with 10 μM DCF-DA for 15 minutes at 37°C, trypsinized, and washed with PBS. Increase of green fluorescence (FL1) of the cells was measured by flow cytometry to determine ROS generation.
* = p-value ≤0.05, ** = p-value ≤0.01, *** = p-value ≤0.001, **** = p-value ≤0.0001. The error bars represent the standard error of the mean.

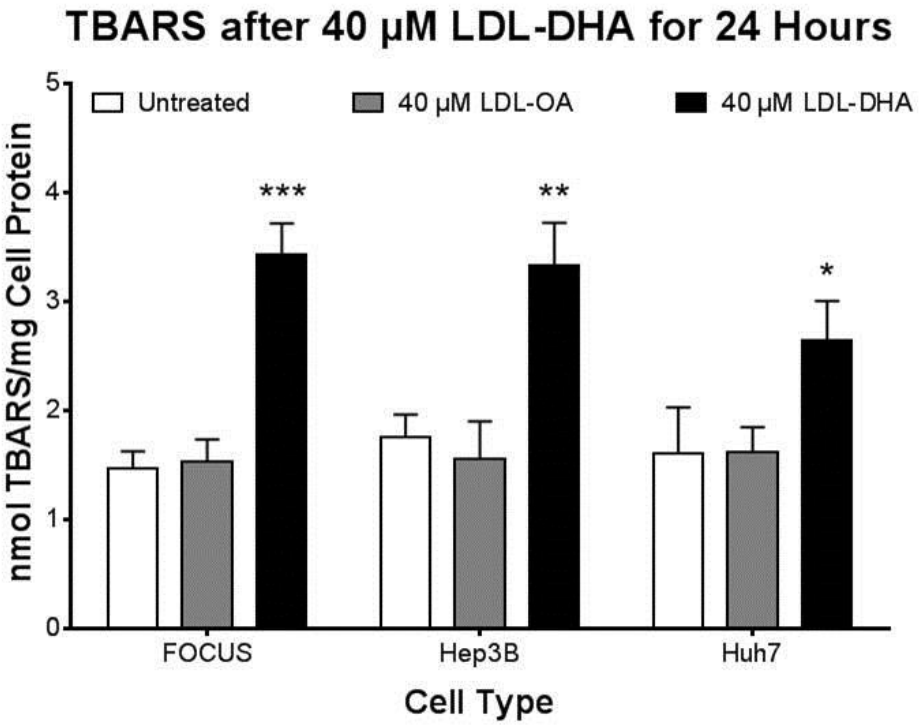

Figure 9-5: Lipid peroxidation by TBARS in FOCUS, Hep3B, and Huh7 cells

FOCUS, Hep3B, and Huh7 cells were grown to 80-90% confluency in 100 mm^2 dishes. The cells were serum starved overnight, treated with serum free DMEM, 40 µM LDL-TO or 40 µM LDL-DHA for 24 hours. After treatment, cells were washed with PBS, collected by scraping, and lysed by sonication. The lysate was mixed with TBARS reagent mix, incubated for 1 hour at 95C. The absorbance of the supernatant was read by plate reader at 550 nm. The protein of the cell lysate was measured by Bradford assay. The TBARS concentration (nmol) was calculated by the extinction coefficient and normalized to cell protein.
* = p-value ≤0.05, ** = p-value ≤0.01, *** = p-value ≤0.001, **** = p-value ≤0.0001. The error bars represent the standard error of the mean.

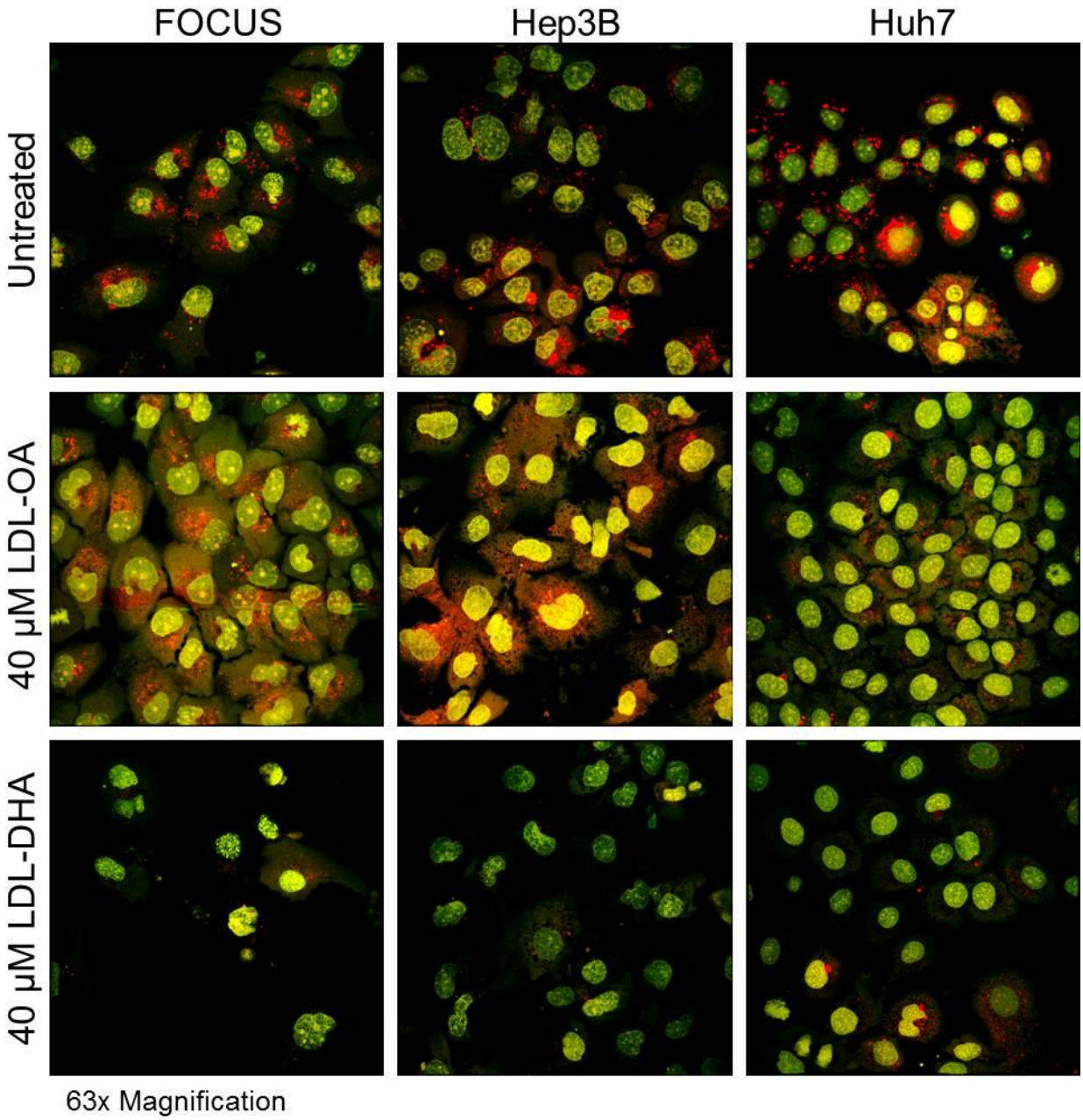

Figure 9-6: Lysosome membrane permeability after LDL-DHA treatment in FOCUS, Hep3B, and Huh7 cells

FOCUS, Hep3B, and Huh7 cells were grown to 80-90% confluency in 35 mm^2 glass bottom dishes coated with 10 µg/mL fibronectin. The cells were serum starved overnight, dyed with 5 µg/mL acridine orange for 20 minutes then treated with serum free media or 40 µM of LDL-OA or LDL-DHA for 5 hours. Cells were imaged at 63x magnification on a Leica LP5 confocal microscope using a 488 nm laser. Red punctate fluorescence (640 nm emission) indicates intact lysosomes and green diffuse fluorescence (540 nm emission) indicates leaking lysosomes.

acridine orange confocal microscopy (Figure 9-6). Huh7 cells had a less distinct loss of lysosome integrity as a small number of intact lysosomes were present in some cells in each field of view, but there was still fewer observable intact lysosomes in Huh7 cells when compared to the untreated and LDL-OA cells. The last experiment was to determine if LDL-DHA was able to cause mitochondrial dysfunction in the human HCC cells. To this end, the effect of LDL-DHA in human HCC cells on mitochondrial ROS production was examined by MitoSox flow cytometry after a twenty-four hour treatment (Figure 9-7). This experiment showed that FOCUS had a higher percentage of cells with MitoSox fluorescence at baseline in comparison to Hep3B and Huh7 cells and that LDL-OA had no effect on mitochondrial ROS in comparison to untreated cells. LDL-DHA treatment significantly increased the population of MitoSox positive cells in both FOCUS and Hep3B cells, but there was no observable increase in MitoSox in Huh7 cells at 40 μM LDL-DHA. Overall these experiments showed that LDL-DHA is selectively cytotoxic to human HCC cells and that lipid peroxidation, lysosome leaking and mitochondrial dysfunction play a role in that cytotoxicity, which corroborates the experiments described previously with the TIB-73 and TIB-75 mouse cells.

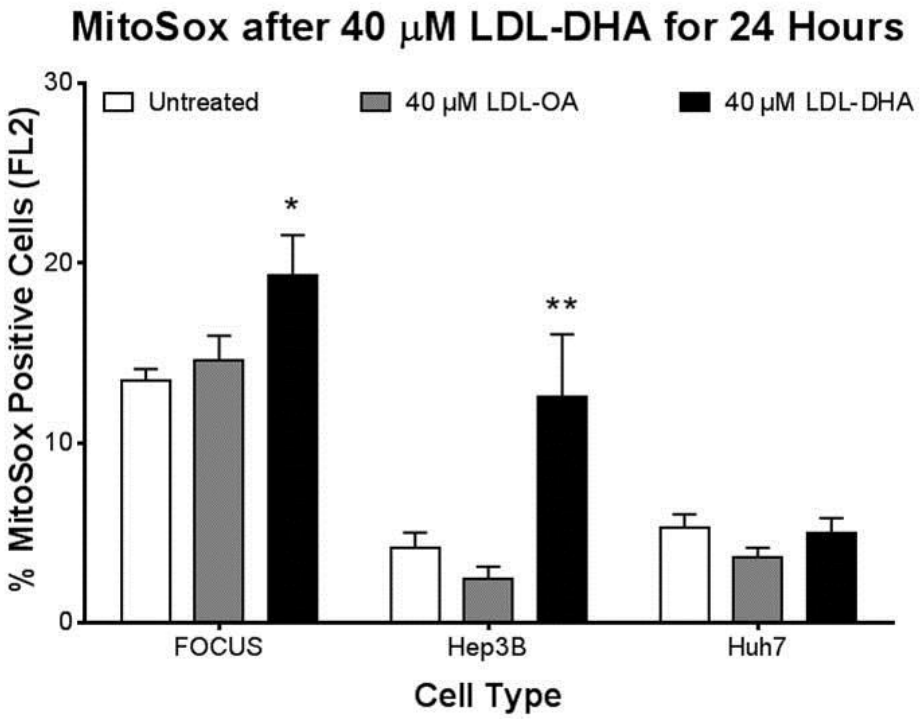

Figure 9-7: Mitochondrial ROS production caused by LDL-DHA treatment in FOCUS, Hep3B, and Huh7 cells

FOCUS, Hep3B, and Huh7 cells were grown to 80-90% confluency in 12-well plates, serum starved overnight, and then treated with 40 μM LDL-DHA or LDL-OA for 24 hours. After treatment, the cells were stained with 5 μM MitoSox and 0.2 μM MitoTracker Green for 15 minutes at 37°C, trypsinized, and resuspended with PBS. The MitoSox and MitoTracker fluorescence of the cells were measured by flow cytometry on the FL2 and FL1 channels, respectively.

* = p-value ≤0.05, ** = p-value ≤0.01, *** = p-value ≤0.001, **** = p-value ≤0.0001. The error bars represent the standard error of the mean.

CHAPTER FIVE
Conclusions and Recommendations

LDL-DHA NANOPARTICLE IS A PROMISING ANTI-CANCER THERAPEUTIC

LDL Can Be Reconstituted with Free Fatty Acids and Maintain Its LDLR Binding Affinity

LDL-DHA has similar physicochemical properties to native LDL

Low Density Lipoprotein (LDL) has been proposed as a drug delivery vehicle for chemotherapeutics such as doxorubicin, paclitaxel, and vincristine since the 1980's, however these LDL-drug complexes have suffered from poor stability, altered ApoB-100 conformation, drug leaking, and low drug loading (Firestone, 1994; Hammel *et al.*, 2003; Kader *et al.*, 1998; Masquelier *et al.*, 2000; Shaw & Shaw, 1991) . The *in vivo* delivery of drugs via LDL has had limited advancement due to these problems. Edwards and colleagues, from Wake Forest University, were the first group to investigate the anti-cancer cytotoxicity of ω-3 PUFAs associated with LDL or albumin delivery. This group used a very inefficient method to obtain PUFA enriched LDL (≈22 mol % of EPA/DHA) by feeding African Green monkeys a fish-oil-enriched diet for five years (Edwards *et al.*, 2004). The LDL reconstitution method described herein proved to be much more efficient as it takes only 2 days to complete and yields LDL with over 1400 molecules of PUFA per particle. These results were validated by analytical HPLC and high resolution NMR spectroscopy. Furthermore, the LDL-DHA nanoparticles had similar physicochemical properties to native

LDL. The only changes observed in LDL-DHA or LDL-OA nanoparticles compared to native LDL, apart from the lipid cargo, was a more electronegative surface charge and lower phospholipid content. These differences in surface charge and phospholipid content may be due to incorporation of ionized DHA (or OA) into the phospholipid membrane as triolein, a neutral triglyceride of oleic acid, had surface charge and phospholipid measurements more similar to native LDL. Studies are ongoing in the Corbin Laboratory to confirm this hypothesis. Despite these changes in surface charge and phospholipid content, the secondary structure of the ApoB-100 protein is not significantly affected by incorporation of DHA or OA into LDL. Stability studies previously published by the Corbin Laboratory have shown that DHA stabilizes the LDL structure and improves the stability and long-term storage of the LDL nanoparticle (Reynolds *et al.*, 2014). Further studies are ongoing to characterize the physical structure of LDL-DHA as there is some evidence that suggests that bilayer structures may be formed during the reconstitution procedure with DHA.

LDL-DHA binds to LDL receptor and it is transported to the lysosome

Changes in LDL receptor binding affinity can result when the ApoB-100 structure is affected by changes in surface charge, number of active lysine residues, and particle diameter (Lund-Katz *et al.*, 1998). In order to confirm that reconstitution of LDL with DHA did not hinder LDL's ability to bind LDL receptor (LDLR) and be endocytosed, LDLR binding affinity and specificity binding assays were conducted. Prior to the start of the binding studies, Western blots were performed to document the expression of LDLR in TIB-73 and TIB-75 cells. Both cell lines expressed LDL receptor to a similar degree. Although malignant cells typically

express more LDLR and take up more LDL, in the present study LDL/LDL nanoparticle uptake by TIB-75 cells was equal or slightly less than the TIB-73 cells. Further investigation revealed that in each cell line LDL-DHA nanoparticles were taken up in lower quantities compared to native LDL. Furthermore, competition with excess unlabeled LDL was able to partially block the uptake of LDL-DHA in the TIB-73 cells, however, under these conditions no change was seen in the uptake of LDL-DHA in TIB-75 cells. Additional studies went on to examine the LDLR binding properties in the TIB-73 and TIB-75 cells. In the TIB-73 cells, the LDLR displayed traditional saturable kinetics, LDLR kinetics in the TIB-75 cells differed in that saturable binding was not achieved over the dose range tested. Collectively, these results indicate both TIB-73 and TIB-75 cells are able to internalize LDL-DHA, although to a lesser degree than native LDL, and that additional receptors (eg. lipoprotein binding site, LDL receptor-related protein 6) (Truong *et al.*, 2000; Ye *et al.*, 2012) may participate in the uptake of LDL nanoparticles in the TIB-75 cells. A study examining LDL binding in normal mouse hepatocytes showed that LDLR was responsible for approximately half of the LDL binding observed while an unknown secondary "lipoprotein binding site" was responsible for the other half. They hypothesized that the "lipoprotein binding site" was binding LDL for cholesterol ester selective uptake (Truong *et al.*, 2000). If this is true, LDL-DHA could bind to this lipoprotein binding site, in addition to LDLR, and DHA could be taken into the cell in place of cholesterol. If DHA can also be taken up by a non-LDLR pathway in TIB-75 cells, then blocking lysosomal degradation of LDL may not rescue the TIB-75 cell cytotoxicity to LDL-DHA. This could explain the depressed LDLR-mediated LDL-DHA uptake by TIB-75 cells seen in the receptor binding affinity studies. Attempts to block LDL degradation using

chloroquine, ammonium chloride, and cysteine and protease inhibitors were unsuccessful at rescuing LDL-DHA cytotoxicity in TIB-75 cells. Given these results, binding of LDL-DHA by non-LDLR mechanisms should be explored in more depth in future studies.

Because there was positive evidence of LDL-DHA binding and internalization by LDLR in both TIB-73 and TIB-75 cells, studies were performed to confirm that LDL-DHA did enter into the lysosome of these cells. If receptor-mediated endocytosis is utilized for LDL and LDL-DHA uptake, then most of the nanoparticle should be in the lysosome (Manders M_1), but it is not expected that all lysosomes will contain nanoparticles (Manders M_2). Colocalization of fluorescently labeled LDL and LDL-DHA with lysosomes labeled with LysoSensor showed that both LDL and LDL-DHA are being endocytosed and transported to the lysosomes in TIB-73 and TIB-75 cells. Interestingly, LDL-DHA colocalization with the lysosome (Manders M_1 Coefficient) was not significantly different than the colocalization of native LDL with the lysosome indicating that similar proportions of LDL-DHA and LDL are entering the cells via the lysosome. The Manders M_2 Coefficient indicated that not all of the lysosomes contained nanoparticle in both cell types with either LDL or LDL-DHA treatment. This was expected to occur given the low dose of nanoparticle administered (10 μg/mL) relative to the equilibrium binding constant of LDL receptor ($K_D \approx 16.67$ μg/mL in TIB-73 cells) meaning the lysosome capacity was not saturated.. Importantly, this experiment showed that in both cell lines native LDL and LDL-DHA are both internalized into the lysosome with high Manders M_1 coefficients. It is important to note that similar colocalization with the lysosome between LDL-DHA and LDL does not provide any

indication about the actual quantity of LDL-DHA and LDL taken up by the cells, so the LDLR binding affinity results showing reduced LDL-DHA internalization is still consistent with the colocalization findings.

DHA is able to exert its cytotoxicity without LDL degradation

It was expected that since LDL-DHA is being taken up into the lysosomes, blocking LDL degradation in the lysosome would prevent DHA's escape into the cytosol and prevent its cytotoxicity to TIB-75 cells. Previous studies showed that LDL degradation by the lysosome was largely dependent on the activity of hydrolytic enzymes, especially the cathepsin proteases, in the acidic environment of the lysosome (Goldstein & Brown, 1974, 1979; Linke *et al.*, 2006). The studies conducted during this research project blocked lysosome acidification in TIB-75 cells prior to LDL-DHA, using chloroquine and ammonium chloride and neither of these agents was able to rescue TIB-75 cell cytotoxicity. Hart and Young claim that ammonium chloride's inhibition of lysosome-phagosome fusion concurrently induces cells to undergo a direct endosome-phagosome fusion (Hart & Young, 1991); therefore, LDL-DHA may be delivered directly to the phagosome from the endosome for degradation without the necessity of lysosome acidity, which could explain why TIB-75 cells are not rescued by ammonium chloride treatment. Inhibition of serine and cysteine proteases using leupeptin and E-64, respectively, prior to LDL-DHA treatment was also not able to rescue TIB-75 cell cytotoxicity. Supposing that there may be redundancy in the LDL degradation capability of serine and cysteine proteases, TIB-75 cells were treated with both leupeptin and E-64 to block both serine and cysteine proteases and this combination still

failed to rescue TIB-75 cells from LDL-DHA cytotoxicity. A review of the literature on LDL degradation revealed that Cathepsin S, a cysteine protease, remains catalytically active at neutral pH and it is capable of degrading LDL (Linke *et al.*, 2006). Blocking lysosome acidification using chloroquine and ammonium chloride would not inhibit LDL degradation by Cathepsin S; neither would blocking cysteine protease activity with E-64 be sufficient to block the activity of all the other lysosomal enzymes capable of degrading LDL. Future experiments should look at the cytotoxicity of LDL-DHA in TIB-75 cells after chemical inhibition of lysosome proteases, especially Cathepsin S with E-64, and simultaneous inhibition of lysosome acidification. One hypothesis for why LDL degradation would not be necessary for LDL-DHA cytotoxicity is the permeabilization of LDL following oxidation caused by the higher likelihood of the Fenton ($Fe^{2+} + H_2O_2 \rightarrow Fe^{3+} + OH\bullet + OH^-$) and Haber-Weiss reactions ($O_2\bullet^- + H_2O_2 \rightarrow O_2 + OH\bullet + OH^-$ and $Fe^{3+} + O_2\bullet^- \rightarrow Fe^{2+} + O_2$) (Valko *et al.*, 2007) occurring in the lysosomes of cancer cells. This hypothesis could be tested by incubating LDL-DHA with labile iron and exogenous hydrogen peroxide and measuring oxidation of the LDL nanoparticle and its subsequent release of DHA and other lipid components. Clearly, further experiments are needed to determine whether LDL degradation is necessary for LDL-DHA cytotoxicity and how that degradation might occur.

The LDL-DHA Nanoparticle Shows Selective Cytotoxicity to HCC Cells

LDL-DHA is more cytotoxic than HSA-DHA

The anti-cancer properties of free or albumin-bound DHA have been studied extensively *in vitro* by other research groups, but all these groups failed to suggest how cytotoxic doses of DHA could be obtained *in vivo* as dietary DHA peaks at 12.5 μM in plasma after high levels of consumption (Arterburn *et al.*, 2006; Conquer & Holub, 1998); alternatively, ω-3 PUFA-enriched emulsions fair only slightly better (Garaiova *et al.*, 2007; Raatz *et al.*, 2009; Schuchardt & Hahn, 2013). In addition to DHA's poor bioavailability *in vivo*, the antioxidant capacity of albumin may negate DHA's cytotoxicity to cancer cells if DHA is delivered solely by its association with albumin (Kanno *et al.*, 2011; Roche *et al.*, 2008). Given the inherent difficulties of achieving cytotoxic doses of DHA *in vivo* without a carrier, DHA delivery by LDL was tested for its cytotoxicity compared to albumin by the Corbin Laboratory in HCC cells. These studies showed that not only was LDL-DHA selectively cytotoxic to TIB-75 cells and not TIB-73 or primary Balb/C hepatocytes, but DHA delivered by LDL was significantly more cytotoxic (IC_{50} = 27.1 μM DHA) to TIB-75 cells than equivalent doses of DHA delivered by albumin (IC_{50} > 200 μM). When this experiment was expanded to human HCC cell lines (FOCUS, Hep3B, and Huh7), all the cell lines showed cytotoxicity to LDL-DHA treatment while primary human hepatocytes were not sensitive to LDL-DHA treatment. Interestingly, the different human HCC cell lines had varied responses to albumin DHA delivery. Hep3B cells showed equivalent sensitivity to LDL-DHA and HSA-DHA treatment, whereas the poorly differentiated FOCUS cell line had a large discrepancy in IC_{50} between LDL-DHA (20.9 μM DHA) and HSA-DHA (112.3 μM DHA) cytotoxicity.

In order to tease apart why there are differences in sensitivity to LDL-DHA versus HSA-DHA in these cell lines, additional experiments should be performed. The first experiment should examine the endogenous albumin production of these cell lines as upregulation or downregulation of albumin production confers resistance or sensitivity, respectively, to DHA in HCC cells (Kanno *et al.*, 2011). Albumin production differences in Hep3B and FOCUS cells may explain their differences in sensitivity. If Hep3B cells are producing less albumin, then they would be more dependent upon exogenous albumin leading to increased HSA-DHA uptake than a cell that has sufficient endogenous albumin production. Furthermore, cells with low albumin production would have less endogenous albumin available to buffer DHA's harmful intracellular effects. Adding exogenous albumin or siRNA knockdown of endogenous albumin production should change the sensitivity of the HCC cells to HSA-DHA and confirm the hypothesis that endogenous albumin production is important to HSA-DHA sensitivity in TIB-73, TIB-75, Hep3B, FOCUS, and Huh7 cells. From an *in vivo* standpoint, albumin production may be an important factor influencing the side effects and therapeutic window of LDL-DHA treatment in HCC and liver tissue. If low albumin levels promote cytotoxicity of DHA, then diseased liver cells may be more sensitive to DHA by HSA or LDL delivery as low serum albumin levels are a common finding in patients with liver disease. It will be important to test if HSA-DHA is more cytotoxic to cancer cells with low endogenous albumin production because these cells would take up more of the HSA-DHA and thus receive a higher DHA dose or if lack of endogenous albumin reduces these cells antioxidant capability to buffer DHA's cytotoxic effects. If the latter is the case, then diseased liver tissue may be more prone to cytotoxicity caused by DHA. In the future,

nonmalignant primary hepatocytes derived from livers with cirrhosis or chronic hepatitis should be treated with LDL-DHA and HSA-DHA to determine their sensitivity.

Additional experiments to parse out why there are differences in HSA-DHA sensitivity between the human HCC cell lines should examine LDL receptor levels and uptake, free fatty acid uptake by diffusion, and differences in metabolism of DHA delivered by HSA or LDL. Looking at LDL receptor levels and uptake is important to determining whether FOCUS cells are more sensitive to LDL-DHA than HSA-DHA because of higher DHA exposure by increased LDL uptake. It is not expected that Hep3B cells would have high LDL receptor uptake because its sensitivity to LDL-DHA is consistent with TIB-75, Huh7, and FOCUS cells. However, Hep3B cells might have more uptake of DHA by diffusion across the cell membrane either because they lack the fatty acid transport proteins to export free fatty acids out of the cell, they have greater association of albumin with putative albumin binding receptors on the cell surface, or they have high Acyl-CoA activity to trap fatty acids intracellularly (Kamp & Hamilton, 2006). To determine if there are differences in metabolism of DHA in Hep3B cells, an experiment could be performed to develop Hep3B cells that are resistant to HSA-DHA treatment by growing them continually in moderate doses of HSA-DHA and then comparing the DHA metabolism of the resistant and sensitive Hep3B populations. If there are differences in DHA metabolism between DHA sensitive and resistant Hep3B cells, then seeing if FOCUS and Huh7 cells utilize similar mechanisms could explain their resistance to HSA-DHA.

LDL-DHA cytotoxicity is not blocked by classical cell death pathway inhibitors

When the mechanism of LDL-DHA-induced cell death was explored in TIB-75 cells using inhibitors of classical cell death pathways, it was surprising to observe that LDL-DHA is not killing cells via apoptosis, programmed necrosis, or autophagy. Previous studies by other groups indicated that DHA was able to kill a variety of cancer cell lines *in vitro* by induction of apoptosis using caspase cleavage, PARP cleavage, cytochrome *c* release, and changes in the ratio of pro-apoptotic and anti-apoptotic Bcl-2 family members (Chiu *et al.*, 2004; Lee *et al.*, 2009; Miura *et al.*, 2004; H. Sun *et al.*, 2013; S. N. Sun *et al.*, 2013; Toit-Kohn *et al.*, 2009; Yamagami *et al.*, 2009). Morphological features of apoptosis, such as blebbing, were evident on time-lapse microscopy and on TEM micrographs of TIB-75 cells treated with 40 μM LDL-DHA for 48 hours. Despite morphological observations of apoptosis in TIB-75 cells, pretreatment with Z-VAD-FMK, a pan caspase cleavage inhibitor, was unable to rescue cytotoxicity of 60 μM LDL-DHA in TIB-75 cells indicating that apoptosis is not solely responsible for TIB-75 cell death.

TIB-75 cells may experience caspase-independent cell death (CICD) following LDL-DHA treatment if caspase activity is blocked. One form of CICD, termed “necroptosis”, is initiated in cells if their caspase activity is blocked and this process starts with death receptor activation by TNF-α or FasL. RIP-1 (Receptor-interacting protein-1), an adaptor protein with kinase activity, modulates the induction of necroptosis by unknown means though evidence suggests that RIP-1can interfere with the interaction of adenine nucleotide translocase and cyclophilin D resulting in mitochondria dysfunction or autophagy-related cell death (Tait &

Green, 2008). Necrostatin-1, an inhibitor of necroptosis, was also unable to rescue TIB-75 cells treated with 60 µM LDL-DHA though it may be possible that inhibition of both apoptosis and necroptosis is necessary to prevent TIB-75 cell death. A second form of CICD is initiated by mitochondrial outer membrane permeabilization (MOMP) resulting in a slow leak of apoptosis-inducing factor-1 (AIF-1) which then translocates to the nucleus and mediates chromatin condensation (Tait & Green, 2008). Future experiments should inhibit AIF-1 nuclear translocation and MOMP in TIB-75 cells after LDL-DHA treatment to see if this form of CICD is being utilized.

It is possible that LDL-DHA doses above 40 µM induce necrosis rather than apoptosis as time-lapse microscopy of TIB-75 cells treated with 60 µM LDL-DHA for 24 hours showed cell rupturing more consistent with death by necrosis. In favor of this theory are the observations by other groups that acute ROS induction in cells causes necrosis rather than apoptosis (Ozben, 2007). Data collected by other members of the Corbin Laboratory, stained TIB-73 and TIB-75 cells with fluorescent markers of apoptosis (Annexin-V) and necrosis (propidium iodide) following LDL-DHA treatment and showed that the TIB-75 cells stained positively for both apoptosis and necrosis induction. It is difficult to selectively inhibit necrosis because it is an uncontrolled process characterized by cell and organelle swelling, plasma membrane rupture, and loss of intracellular contents. Recently a group from Japan has developed a small molecule IM-54 that selectively inhibits oxidative stress-induced necrosis (Sodeoka & Dodo, 2010). In the future, TIB-75 cells can be treated with IM-54 to determine if LDL-DHA induced cytotoxicity is caused by ROS-induced necrosis.

Inhibition of cell death by autophagy was also inhibited prior to LDL-DHA treatment in TIB-75 cells using Bafilomycin-A1 and, once again, no rescue in LDL-DHA cytotoxicity was observed. Interestingly, the highest dose of Bafilomycin-A1 (4000 nM) increased TIB-75 cell cytotoxicity to LDL-DHA. Some cancer cells depend on autophagy to remove dysfunctional mitochondria to prevent excessive ROS production and cell death (Wallace, 2012). It is possible that TIB-75 cells similarly rely on autophagy and the use of Bafilomycin-A1 had a cytotoxic effect independent of LDL-DHA treatment. It will be important to treat TIB-75 cells with Bafilomycin-A1 alone to determine if they are autophagy-dependent. Additional future experiments should explore if HSA-DHA treatment in TIB-75 cells uses any of these cell death pathways and what pathways are used after LDL-DHA and HSA-DHA treatment in the human HCC cells.

LDL-DHA cytotoxicity is not blocked by Ferrostatin-1

A final attempt to rescue LDL-DHA cytotoxicity in TIB-75 cells was undertaken by pretreating TIB-75 cells with Ferrostatin-1 (FST), a putative inhibitor of a novel iron-dependent cell death pathway called "ferroptosis". Erastin and Ras-Selective Lethal-3 (RSL3) drugs were able to initiate a ferroptosis, a non-apoptotic, non-necrotic, non-autophagic form of cell death in Ras-driven tumor cells (Dixon *et al.*, 2012). In general, ferroptosis induced by erastin or RSL3 is associated with the dysregulation of the cell's redox homeostasis by blocking the cystine uptake necessary for GSH production, which makes the cells more susceptible to iron-induced ROS and lipid peroxidation (Dixon *et al.*, 2012;

Skouta *et al.*, 2014). The role of iron in ferroptosis is unclear as it may be necessary to catalyze ROS production via the Fenton reaction or it may be an essential cofactor of some as yet unidentified enzyme that promotes ROS (Dixon *et al.*, 2012; Skouta *et al.*, 2014). Because DHA may be able to induce ferroptosis by participating in the Fenton reaction to form lipid peroxides, an attempt to rescue TIB-75 cell death with FST was made. FST works as a potent antioxidant to prevent lipid peroxidation and PUFA destruction rather than by changing cystine or GSH levels. Prevention of lipid peroxidation by FST may help cells avoid ferroptosis by maintaining their membrane integrity or by preventing the toxic aldehyde by-products of lipid peroxidation (Skouta *et al.*, 2014). Unfortunately, pretreatment of TIB-75 cells with FST did not ameliorate LDL-DHA (60 µM) cytotoxicity indicating that ferroptosis is not critical for LDL-DHA cytotoxicity.

Lipid Peroxidation Is Critical for LDL-DHA Cytotoxicity in HCC Cells

Overall, low to moderate levels of reactive oxygen species and lipid peroxidation promote tumorigenesis, cell cycle progression, cell-to-cell adhesion, metabolism, motility, angiogenesis, proliferation, and survival in cancer cells (Liou & Storz, 2010; Ozben, 2007). Cancer cells can either increase ROS production or reduce antioxidant capacity or use a combination of the two strategies to maintain an ‘optimal redox state’ that promotes proliferation and tumorigenesis (Martindale & Holbrook, 2002; Ozben, 2007; Pelicano *et al.*, 2004; Sotgia *et al.*, 2011; Valko *et al.*, 2007). Experiments were conducted to determine the baseline levels of different reactive oxygen species in TIB-73 and TIB-75 cells and the

antioxidant capacity of each cell line. Important antioxidants that remove intracellular ROS are both enzymatic (superoxide dismutase, catalase, glutathione peroxidase) and non-enzymatic (NADPH, GSH, thioredoxin, vitamin E, and vitamin C) systems (Valko *et al.*, 2007). The cellular pool of NADPH is important in maintaining several antioxidant defense systems in the cell including the glutathione (GSH) system. Through the actions of glutathione reductase, NADPH is used as an electron donor to regenerate GSH from GSSG, GSH is then in turn necessary for glutathione peroxidase and glutathione-S transferase activity (Ying, 2008). NADPH is also required to maintain the hydrogen peroxide detoxifying enzyme, catalase in its active form. Although TIB-73 and TIB-75 cells had similar NADPH:$NADP^+$ ratios, TIB-75 cells had a significantly lower GSH:GSSG ratio (≈40:1) compared to TIB-73 cells (≈115:1). These results indicate that TIB-75 cells are more oxidized and are less capable of safely removing reactive oxygen species than TIB-73 cells. GSH protects against oxidative stress by reducing disulfide bonds back to cysteine on oxidized proteins, regenerating vitamin C and E back to their active forms, protecting against ROS-induced DNA damage, and removing ROS species either directly (hydroxyl radicals and singlet oxygen) or indirectly (hydrogen peroxide and lipid peroxides) through GPx and glutathione S-transferase (Liou & Storz, 2010; Valko *et al.*, 2007). Published values suggest that resting cells will have a GSH:GSSG ratio in excess of 100:1, but that oxidative stress decreases those values to 10:1 or even 1:1(Zitka *et al.*, 2012). Indeed, measurement of baseline ROS levels showed that TIB-75 cells have higher levels of hydrogen peroxide and lipid peroxidation, compared to TIB-73 cells. Furthermore, Western blot analysis showed that TIB-75 cells had lower GPx-4 and catalase protein expression than TIB-73 cells at

baseline. On the whole, these experiments indicate that TIB-75 cells have an inferior antioxidant defense system, which may be exploited by LDL-DHA treatment. The highly unsaturated structure of DHA is prone to oxidation (Hardman *et al.*, 2002; Kubo *et al.*, 1997; Schonfeld & Wojtczak, 2008; Stoll, 2002). This, in addition to the lower levels of GPx-4, in TIB-75 cells would significantly hinder their capacity to detoxify lipid peroxide species from DHA peroxidation. Thus, with lower antioxidant capability and higher baseline levels of ROS, TIB-75 would be more susceptible to LDL-DHA-induced cell death mediated by lipid peroxidation and ROS. The human HCC cell lines also showed similar perturbations after LDL-DHA treatment. Although elevated ROS were not prominent in the human HCC cells after treatment, all cell lines showed significant increases in lipid peroxidation after LDL-DHA treatment. These findings suggest LDL-DHA induced similar cancer killing mechanisms among the murine and human cells.

Superoxide production and removal are not critical for LDL-DHA induced cytotoxicity

Superoxide is generally considered the main ROS produced in cells as other ROS are generated by metal- or enzyme- catalyzed reactions with superoxide (Valko *et al.*, 2007). Most superoxide is produced in the mitochondria due to the leaking of electrons in the ETC at Complex I and Complex III (Valko *et al.*, 2007). NADPH oxidase (Nox) and xanthine oxidase enzymes are additional sources of superoxide generation (Kumar *et al.*, 2008; Valko *et al.*, 2007). Superoxide dismutase reduces superoxide in the cytosol (SOD-1) and mitochondria (SOD-2) to hydrogen peroxide and oxygen and expression can be

downregulated, upregulated, or unchanged in cancer cells (Ding *et al.*, 2004; Pelicano *et al.*, 2004).

TIB-73 and TIB-75 cells showed no difference in baseline protein expression of SOD-1 or in their baseline superoxide radical levels as measured by DHE fluorescence. Furthermore, LDL-DHA treatment did not increase superoxide production as measured by DHE fluorescence. Interestingly, LDL-DHA treatment increased mitochondrial superoxide production in TIB-75 cells as revealed by MitoSox, a mitochondrial specific DHE dye. Future studies should look at the baseline protein expression of SOD-2 to see if lower SOD-2 levels could explain the increased mitochondrial superoxide production following LDL-DHA treatment.

The importance of ROS generation in LDL-DHA cytotoxicity was tested in TIB-73 cells after treating them with an ROS-generating agent, menadione bisulfite (MD-B). MD-B is a quinone that is reduced by enzymes in the microsome (NADPH-cytochrome P450 reductase) or mitochondria (NADH-ubiquinone oxidoreductase/Complex I) to an unstable semiquinone. This semiquinone enters the redox cycle when molecular oxygen is present causing generation of ROS species ($O^{-\cdot} \rightarrow HO_2^{\cdot} \rightarrow H_2O_2 \rightarrow HO^{\cdot}$) and reformation of the original quinone, which can be reduced and enter the redox cycle again (Figure 10-1). Since the enzymes responsible for generating the semiquinone utilize NAD(P)H as an electron donor, repeated cycling of MD-B generates ROS and depletes cellular NAD(P)H reserves. ROS

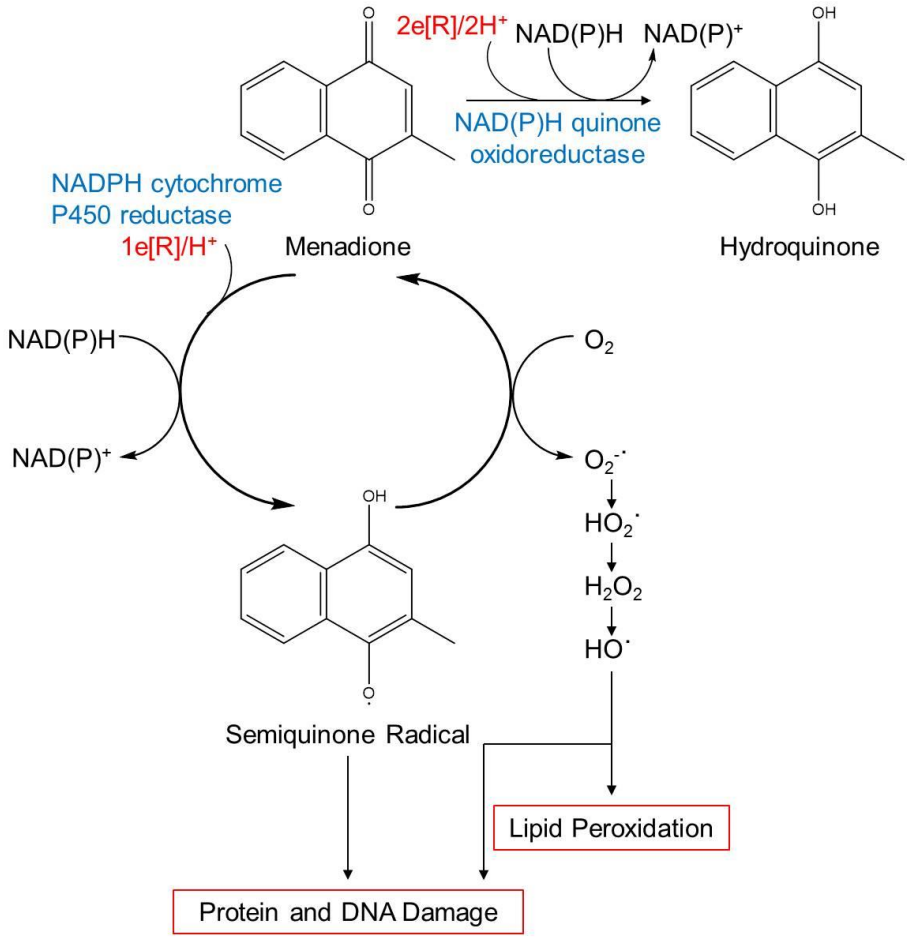

Figure 10-1: ROS generation by menadione bisulfite

Menadione bisulfite has two possible cellular fates. In the first, menadione bisulfite is reduced to an unstable semiquinone by NADPH-cytochrome P450 reductase that enters the redox cycle to generate ROS and reform the quinone that can be reduced again. In cells with NAD(P)H quinone reductase, menadione bisulfite is metabolized by a two electron reduction to a stable hydroquinone which does not generate ROS.

generation can be mitigated if the cell contains NAD(P)H quinone oxidoreductase 1 (NQO1), which metabolizes quinones via a two electron reduction to a stable hydroquinone without generating ROS though it still utilizes NAD(P)H (Criddle *et al.*, 2006; Parkinson, 2013). When TIB-73 cells were pretreated with increasing concentrations of menadione bisulfite, their sensitivity to 60 µM LDL-DHA increased in a dose-dependent manner. Similarly, treatment with 25 µM MD-B drastically lowered the LDL-DHA IC_{50} in TIB-73 cells from 131.8 µM to 20.3 µM. Because MD-B generates many ROS species and depletes NAD(P)H, it is difficult to conclude if superoxide alone was responsible for sensitizing TIB-73 cells to LDL-DHA. However, overnight pretreatment of TIB-75 cells with exogenous pegylated-SOD to remove superoxide anions did not improve LDL-DHA cytotoxicity. Overall, these data suggest that increased ROS generation sensitizes TIB-73 cells to LDL-DHA, but removal of superoxide anions alone is not sufficient to rescue LDL-DHA cytotoxicity in TIB-75 cells. Future experiments should measure changes in superoxide and hydrogen peroxide levels and in the NAD(P)H:$NAD(P)^+$ ratio in TIB-73 cells treated with MD-B with or without LDL-DHA treatment to determine how MD-B is sensitizing TIB-73 cells to LDL-DHA.

Hydrogen peroxide levels increase with LDL-DHA treatment but this is not sufficient for LDL-DHA cytotoxicity

Hydrogen peroxide is produced intracellularly by reduction of superoxide radicals by superoxide dismutase or produced directly in the peroxisomes. Instability of the peroxisomes can increase hydrogen peroxide leaking into the cytosol (Valko *et al.*, 2007). Hydrogen

peroxide is able to diffuse a large distance within the cell or be transported across membranes by aquaporins and is thus able to act intercellularly to distant locations (Toyokuni, 2014). Catalase is the antioxidant enzyme used to remove hydrogen peroxide intracellularly by converting it to water and oxygen. Both hydrogen peroxide and superoxide function as secondary messengers in the cell and are able to activate several receptor kinases members (Akt/PI3K, Erk1/2, protein kinases C, Src and Jak), growth factors (PDGF, EGF, VEGF), nuclear transcription factors directly or indirectly (NF-κB, AP-1, HIF-1, and others), and inactivate protein tyrosine phosphatases (Finkel, 2011; Martindale & Holbrook, 2002; Valko *et al.*, 2007). Baseline ROS levels in TIB-73 and TIB-75 cells were compared using DCF fluorescence spectrophotometry and flow cytometry and these assays both showed that TIB-75 cells have significantly higher baseline DCF fluorescence than TIB-73 cells. DCF fluorescence also increased in a time-dependent manner in TIB-75 cells treated with 60 μM LDL-DHA for up to twenty four hours. It was also observed that human HCC cells had a large percentage of cells with high DCF fluorescence (>80%) and LDL-DHA treatment for twenty four hours did little in any cell line to increase this percentage. Important information has come to light about the lack of specificity of DCF fluorescence for ROS generation (Karlsson *et al.*, 2010). H_2DCF-DA, a lipophilic precursor to DCF, crosses cell membranes where it is rapidly cleaved by cytosolic esterases in the cell to a non-fluorescent hydrophilic H_2DCF. It was generally assumed that H_2DCF evenly distributed in the cell, and was then oxidized by ROS species, especially hydrogen peroxide, to a fluorescent DCF moiety (Wang & Joseph, 1999). Recent studies have shown that H_2DCF is actually oxidized to DCF by hydroxyl radicals resulting from the Fenton reaction rather than by hydrogen peroxide

(Karlsson *et al.*, 2010). Furthermore, mitochondria may have weak baseline oxidation of H_2DCF due to cytochrome *c* activity and due to the Fenton reaction in the dual presence of hydrogen peroxide and labile iron in the mitochondria. In general, large cytosolic increases in DCF fluorescence are now presumed to reflect lysosome membrane permeabilization (LMP) due to the release of catalytic iron into the cytosol or cytochrome *c* release from the mitochondria rather than hydrogen peroxide production in the cell (Karlsson *et al.*, 2010). Experiments will need to be conducted in the future to measure hydrogen peroxide production in TIB-73, TIB-75, and the human HCC cells treated with LDL-DHA without using DCF fluorescence. Despite the fact that hydrogen peroxide production was not accurately measured in TIB-73 and TIB-75 cells after LDL-DHA treatment, attempts to induce cytotoxicity to LDL-DHA in TIB-73 cells using exogenous hydrogen peroxide were unsuccessful. Additionally, pretreatment with exogenous pegylated-catalase was unable to rescue TIB-75 cells from LDL-DHA cytotoxicity. Both of these results suggest that hydrogen peroxide may not be the reactive oxygen species responsible for LDL-DHA cytotoxicity in this HCC model.

Lipid peroxidation is necessary for LDL-DHA cytotoxicity in HCC cells

Hydroxyl radicals are the neutral form of the hydroxide ion and this very reactive radical has a very short half-life (10^{-9} s) so it interacts with proteins or lipids close to its production site. Hydroxyl radicals are produced by the Fenton ($Fe^{2+} + H_2O_2 \rightarrow Fe^{3+} + OH\bullet + OH^-$) and Haber-Weiss Reactions ($O_2\bullet^- + H_2O_2 \rightarrow O_2 + OH\bullet + OH^-$ and $Fe^{3+} + O_2\bullet^- \rightarrow Fe^{2+} + O_2$). These reactions are also important in the formation of LPO. Hydroxyl radicals are removed

by the glutathione antioxidant system while LPO species are removed by glutathione peroxidase-4 (Valko *et al.*, 2007). Hydroxyl radicals are also responsible for damaging the purine and pyrimidine bases of DNA leading to mutagenesis. Both hydroxyl radicals and LPO can exert protumorigenic effects by destabilizing DNA to promote mutations, and by disrupting mitochondria to increase ROS generation (Liou & Storz, 2010; Valko *et al.*, 2007). Lipid peroxides can inhibit NADPH formation in the mitochondria by oxidizing isocitrate dehydrogenase (Yang *et al.*, 2004) and the lipid peroxide metabolites malondialdehyde (MDA) and 4-hydroxynonenal (HNE) are mutagenic and cytotoxic in themselves (Ryter *et al.*, 2007; Valko *et al.*, 2007; Ying, 2008). LPO is likely to occur following LDL-DHA treatment because DHA is delivered to the lysosomes. The lysosomes are important vesicles for the Fenton and Haber-Weiss reactions to occur because they store large quantities of iron from degraded iron-containing proteins and organelles (Kurz *et al.*, 2006; Kurz *et al.*, 2008). Importantly, the low pH of the lysosome combined with the presence of reducing agents (superoxide, cysteine, ascorbic acid, or glutathione) easily reduces Fe^{3+} to Fe^{2+} (Kurz *et al.*, 2006; Kurz *et al.*, 2008), thus facilitating its participation in the Fenton reaction. Lysosomes also lack glutathione peroxidase and catalase enzymes necessary to remove the lipid and hydrogen peroxide species that form inside them (Kurz *et al.*, 2006). Importantly, cancer cells have higher metabolic demands, which increases intralysosomal labile iron storage and ROS production (Boya & Kroemer, 2008), which could make the lysosomes of cancer cells more susceptible to the Fenton reaction.

When TIB-73 and TIB-75 cells were treated with LDL-DHA, increased LPO was observed by multiple assays. In the first assay, lipid peroxidation was measured by flow cytometry using BODIPY C11 581/591, which contains a polyunsaturated butadienyl moiety that changes fluorescence from red to green in response to oxidation. This assay showed that lipid peroxidation increases in a time-dependent manner in TIB-75 cells following LDL-DHA treatment and thatTIB-73 cells have a delayed and smaller increase in LPO compared to TIB-75 cells. These findings indicate that TIB-75 cells are more sensitive to LPO induced by LDL-DHA. When the same dye was used to monitor the intracellular location of LPO formation in TIB-73 and TIB-75 cells, colocalization of the lysosome and LPO signal was observed in both cell lines confirming that the lysosome is a site of LPO generation following LDL-DHA treatment. There was also more colocalization of LPO with the lysosome in TIB-75 cells than TIB-73 cells following LDL-DHA treatment. The heat map image of oxidized/unoxidized dye indicated that TIB-75 cells have higher LPO at baseline than TIB-73 cells and that LDL-DHA further increased LPO formation in the TIB-75 cells. The TBARS assay, which measures aldehyde metabolites of LPO, also confirmed these results by showing that TIB-75 cells have higher baseline LPO than TIB-73 cells and that LDL-DHA treatment increased LPO formation only in the TIB-75 cells. Similar results were observed in the human HCC cell lines where treatment with 40 μM LDL-DHA increased TBARS levels relative to untreated controls in FOCUS, Hep3B, and Huh7 cells. Interestingly, HSA-DHA, even at 150 μM doses, did not increase LPO formation in TIB-75 cells indicating that the lysosomal environment that DHA is exposed to by LDL delivery is more conducive to LPO formation than entry by diffusion. The formation of LPO likely

explains why LDL-DHA is more cytotoxic to TIB-75 cells than HSA-DHA. In the future, TBARS production caused by HSA-DHA treatment in FOCUS, Hep3B, and Huh7 should be measured to determine if LPO formation in each cell line correlates with their sensitivity to HSA-DHA (e.g. Hep3B cells are anticipated to have high LPO while FOCUS would have low LPO).

In order to test the importance of LPO formation on cytotoxicity to LDL-DHA, TIB-73 and TIB-75 cells were pretreated with N-acetyl-L-Cystein (LNAC) or Vitamin E, which are antioxidants that specifically remove LPO, prior to LDL-DHA treatment. Both LNAC and Vitamin E were able to rescue LDL-DHA cytotoxicity in TIB-75 cells in a dose-dependent manner indicating that LPO formation is important in LDL-DHA cytotoxicity in TIB-75 cells. Future experiments should look at the effect of LPO removal on the cytotoxicity of LDL-DHA and HSA-DHA in FOCUS, Hep3B, and Huh7 cell lines to confirm the importance of LPO in DHA-induced cell death in human HCC cells. Additional experiments that could be performed to probe the role of LPO in DHA-induced cell death would be to look at the effect GSH depletion or addition has on increasing or decreasing sensitivity to LDL-DHA because TIB-75 cells have a lower GSH:GSSG ratio at baseline that may explain their inability to cope with LPO. GSH is an important antioxidant to directly remove hydroxyl radicals, and it is necessary for GPx-4 to function (Liou & Storz, 2010; Valko *et al.*, 2007) . Additionally, susceptibility to ferroptosis has been linked to GSH depletion secondary to blocking the cystine/glutamate antiporter in cancer cells by erastin and RSL3 such that co-treatment of HCC cells with erastin and LDL-DHA may have a synergistic

effect on cytotoxicity (Dixon *et al.*, 2012; Skouta *et al.*, 2014). A second experiment should look at the subcellular location of LPO production beyond the lysosome to see if membranes in the mitochondria, endoplasmic reticulum, or nucleus are affected. Metabolomic studies could also be performed to determine the relative generation of DHA- or non-DHA derived lipid peroxidation products and aldehyde metabolites in normal and HCC cells as these products have potent cellular and molecular affects in both normal and cancer cells (Calder, 2006; Gao *et al.*, 2007; Gonzalez-Periz *et al.*, 2006; S. Hong *et al.*, 2003; Sato *et al.*, 2011; Shaikh *et al.*, 2009; Siddiqui *et al.*, 2008; Skender *et al.*, 2012; Weylandt *et al.*, 2011).

LDL-DHA Induces LMP, Mitochondrial Dysfunction, and DNA Damage

As mentioned previously, the Fenton reaction generates hydroxyl radicals and LPO which are both very damaging to cellular membranes, especially in the lysosome and mitochondria. Additionally, both can cause damage to the DNA in the mitochondria and nucleus (Liou & Storz, 2010; Valko *et al.*, 2007).

LDL-DHA increases lysosome membrane permeability in HCC cells

Lysosomes are double membrane-bound organelles that use proton-pumping ATPases to maintain an acidic pH (4.6 to 5.0) for the digestion of macromolecules and damaged organelles using a wide range of acid hydrolase enzymes (Johansson *et al.*, 2010; Luzio *et al.*, 2007). Recently, the induction of lysosome membrane permeability (LMP) has been studied for its role in activating cell death either by apoptosis, autophagy, or necrosis (Boya

& Kroemer, 2008; Johansson *et al.*, 2010). LMP can be triggered by many stimuli including death receptor activation, endoplasmic reticulum stress, oxidative stress, DNA damage, osmotic stress, and growth factor starvation (Johansson *et al.*, 2010). Important mediators of LMP-induced cell death are the lysosome proteases Cathepsin B, D, and L, all of which are active at normal pH (Almaguel *et al.*, 2010; Boya & Kroemer, 2008). These cathepsins may be released in small quantities into the cytosol at the onset of LMP, by caspase recruitment to the lysosome (caspases 2, 8, and 9), by death receptor activation (TRAIL and TNF-α) or by inactivation of cell pathways (Erk and PI3K) (Boya & Kroemer, 2008; Johansson *et al.*, 2010; Kurz *et al.*, 2006). Importantly, cytosolic cathepsin initiates the recruitment of Bcl-2 family members (Bax, Bim, and/or Bid) to the lysosome where they further permeabilize the lysosome (Boya & Kroemer, 2008). The activated Bcl-2 family members can also initiate mitochondrial pore formation, activation of AIF-1, and cytochrome *c* release and thus cause a positive feedback loop to the lysosome though mitochondrial involvement is not necessary for LMP cell death (Johansson *et al.*, 2010). In order to monitor the integrity of the lysosomes after LDL-DHA treatment in TIB-73, TIB-75, and the human HCC cell lines, the cells were stained with acridine orange prior to LDL-DHA treatment which will fluoresce bright red in intact lysosomes and fluoresce dim green in the cytosol. Monitoring acridine orange fluorescence by confocal microscopy showed that LDL-DHA treatment was able to cause LMP in TIB-75 cells after a five hour treatment and TIB-73 cells maintained intact lysosomes. The human HCC cell lines FOCUS, Hep3B, and Huh7 also exhibited signs of LMP by acridine orange staining after five hours. The LMP observed in Huh7 cells was less severe than that seen in FOCUS and Hep3B, which could be due to the decreased sensitivity

of Huh7 cells to LDL-DHA cytotoxicity and treatment with a higher LDL-DHA might strengthen the LMP effect. Importantly, LDL-OA was not able to cause LMP in any cell line indicating that free fatty acid lipotoxicity is not the cause of the LMP but rather lipid peroxidation of DHA. An additional experiment was performed in TIB-75 cells to determine if HSA-DHA treatment has the same ability as LDL-DHA treatment to induce LMP. This experiment showed that HSA-DHA (60 and 150 μ M) was not able to induce LMP during the same time period as LDL-DHA, which is not surprising considering the previous findings showed that HSA-DHA does not increase lipid peroxidation in TIB-75 cells after a twenty four hour treatment. The results of the acridine orange confocal microscopy experiment were confirmed using a Magic Red dye that is activated by cathepsin B cleavage in the lysosome. TIB-75 cells treated with LDL-DHA showed reduced cathepsin B activity and a diffuse staining pattern that is consistent with cathepsin B release into the cytosol where it has lower activity in neutral pH. Interestingly, an overnight treatment with LDL-DHA was necessary to see reduction in cathepsin B activity in TIB-75 cells compared to a 5 five hour treatment to see LMP by acridine orange. This discrepancy may be due to the differences in sensitivity of the dyes in detecting LMP. An acridine orange flow cytometry experiment using TIB-73 and TIB-75 cells treated with LDL-DHA at different time points was also performed to monitor how quickly LMP occurs in TIB-75 cells after LDL-DHA treatment. Detectable increases in the percentage of TIB-75 cells with LMP were observed at six hours which is consistent with the acridine orange confocal microscopy results, but the increases were not statistically significant until eight hours. After twenty four hours, the TIB-73 cells had a significant increase in LMP after LDL-DHA treatment similar to that seen at eight hours in TIB-75 cells

which was unexpected. Despite the increase in LMP, TIB-73 cells do not experience cytotoxicity from LDL-DHA at the dose given (60 μM) so they must able to buffer the effects of LMP and protect themselves from cytotoxicity. One possibility for this resistance to LMP-induced cell death in TIB-73 cells could be due in part to maintenance of normal mitochondrial function after LDL-DHA treatment or that the slower increase in LMP is not sufficient to initiate a death-signaling cascade. Additional experiments should be performed to explore these processes in greater detail. These results show that DHA delivered into the lysosome by LDL rather than by diffusion is particularly susceptible to lipid peroxidation in HCC cells, which can then initiate a cell death cascade induced by LMP.

Future experiments should examine whether LMP is caused by peroxidation of DHA, by peroxidation of the fatty acids in the phospholipid membrane of the lysosome, or by a combination of DHA and phospholipid fatty acid peroxidation that results in increased fluidity of the lysosome membrane. Experiments should also be conducted to block lipid peroxidation using LNAC to see if this prevents LMP in TIB-75 cells following LDL-DHA treatment. Additionally, differences in the lysosomes of the TIB-73 and TIB-75 should be examined to determine why TIB-75 lysosomes are more susceptible to LMP by LDL-DHA treatment. Previous research by others has shown that lysosome membrane integrity is compromised by many factors including increased lysosome diameter, localization next to ROS producing mitochondria, decreased lysosome-associated membrane proteins (LAMP) concentration, and decreased cholesterol in the lysosome membrane (Boya & Kroemer, 2008; Johansson *et al.*, 2010). The lysosomes of cancer cells undergo many changes that

affect their size, iron storage, intracellular localization, cathepsin expression, and enzymatic activity (Boya & Kroemer, 2008). Interestingly, extralysosomal cathepsin is upregulated in cancer cells and promotes a malignant phenotype by its extracellular excretion to promote angiogenesis, metastasis, and invasion, and cathepsin B upregulation is associated with decreased LAMP proteins in the lysosome (Boya & Kroemer, 2008; Johansson *et al.*, 2010). It has been suggested that Heat Shock Protein-70 (Hsp70) localizes to the lysosome in cancer cells and stabilizes the lysosome membrane to a certain extent under stress even in the presence of cytosolic cathepsin (Nylandsted *et al.*, 2004). Additionally, DHA may reduce the cholesterol content of the lysosome membrane, as it is known to have that effect in the plasma membrane of the cell (Stillwell *et al.*, 2005), and make lysosomes more susceptible to LMP by that mechanism. There are still many avenues of research to explore to determine why the lysosomes of cancer cells are more sensitive to LMP with LDL-DHA treatments.

LDL-DHA increases loss of MMP and increases mitochondrial ROS production in TIB-75 cells

Lipid peroxidation, incorporation of DHA into cardiolipin, and LMP can all have effects on mitochondria function in normal and cancer cells. The phospholipids of the mitochondrial membrane, especially cardiolipin, are susceptible to lipid peroxidation caused by increased ROS production. Lipid peroxidation of the mitochondrial membranes will affect the functioning of the ETC proteins and the membrane's structural integrity making them more likely to release cytochrome *c* and calcium to induce apoptosis (Gogvadze *et al.*, 2008). DHA's incorporation into cardiolipin in the mitochondria may increase mitochondria

membrane lipid peroxidation, mitochondrial ‘leakiness’, and induction of apoptosis (M. Y. Hong *et al.*, 2002; Ng *et al.*, 2005; Siddiqui *et al.*, 2008; Watkins *et al.*, 1998). LMP can activate pro-apoptotic Bcl-2 family members to initiate mitochondrial pore formation, activation of AIF-1, and cytochrome *c* release and thus cause a positive feedback loop to the lysosome and induce apoptosis in this manner (Johansson *et al.*, 2010). Cancer cells must keep a tight check on mitochondrial ROS production because even though increased ROS production promotes proliferation, too much ROS will induce apoptosis.

The effect of LDL-DHA on the mitochondria of TIB-73 and TIB-75 cells was examined by two main methods: first, mitochondrial membrane potential (MMP) by TMRM as a measure of overall mitochondrial function; and second, mitochondrial ROS production by MitoSox fluorescence. TMRM confocal microscopy of TIB-73 and TIB-75 cells following an overnight treatment with LDL-DHA showed that only TIB-75 cells treated with LDL-DHA experience significant MMP loss indicative of mitochondria dysfunction. When TMRM fluorescence was analyzed by flow cytometry at different times after LDL-DHA treatment, MMP loss was not observed in cells until six hours and the number of cells with MMP loss increased further at eight and twenty four hours. Unlike the LMP studies, TIB-73 cells did not have a significant loss of MMP after LDL-DHA treatment which could explain their resistance to LMP-induced cytotoxicity. Experiments should be conducted in the future to examine the incorporation of DHA into cardiolipin in the mitochondria, mitochondrial respiration before and after LDL-DHA treatment, SOD-2 protein expression and activity, and

whether mitochondria release of cytochrome *c* or other pro-apoptotic factors occur following LDL-DHA treatment.

Mitochondrial ROS production was also measured in TIB-73 and TIB-75 cells. Baseline levels of mitochondrial ROS were similar between the two cell lines, after LDL-DHA treatment significant increases in mitochondrial ROS were detected in TIB-75 cells only. HSA-DHA was not able to increase mitochondrial ROS in either cell line, even though DHA addition to cardiolipin is possible via albumin transport. HSA-DHA's inability to increase mitochondrial ROS suggests that lipid peroxidation in the mitochondria and/or LMP rather than incorporation of DHA into cardiolipin are the more likely causes of LDL-DHA's effects on mitochondria dysfunction. The mitochondrial ROS production in the human HCC cells was also measured and both FOCUS and Hep3B showed significant increases in MitoSox positive cells following LDL-DHA treatment. Huh7 cells did not have a significant increase with the 40 μM LDL-DHA dose and a higher dose should be used in future measures. Since an increase in mitochondrial ROS was observed in TIB-75 cells with LDL-DHA treatment, an experiment was conducted to determine if inducing mitochondrial ROS in TIB-73 cells sensitizes these cells to LDL-DHA. TIB-73 cells were pretreated with increasing doses of CCCP, a mitochondrial decoupler, and then treated with a sublethal dose of LDL-DHA overnight. CCCP treatment increased TIB-73 cell sensitivity to LDL-DHA in a dose dependent manner. Subsequent measurement of MitoSox by flow cytometry showed that CCCP treatment alone caused a non-significant increase in mitochondrial ROS compared to untreated cells, the addition of LDL-DHA, however, caused a significant rise in

mitochondrial ROS over untreated cells and those treated with LDL-DHA alone. This experiment showed that small, seemingly insignificant increases in mitochondrial ROS production are sufficient to sensitize non-malignant cells to LDL-DHA treatment. This may have important ramifications in using LDL-DHA as *in vivo* therapeutic in HCC as hepatocytes from the diseased liver may be more sensitive to LDL-DHA if their mitochondrial ROS production is increased. On the other hand, drugs targeted to the tumor cells could be given to increase their sensitivity to LDL-DHA by increasing their mitochondrial dysfunction to widen the therapeutic window. Additional experiments should be performed to determine exactly how DHA increases mitochondrial ROS production.

LDL-DHA treatment increases DNA damage in HCC cells

DNA damage in the cell can occur when hydroxyl radicals damage the purine and pyrimidine bases of DNA or when lipid peroxides form lipid-DNA adducts. Both hydroxyl radical and LPO induced DNA damage can be mutagenic in small quantities promoting tumorigenesis, but in large quantities they are genotoxic and result in cell death (Cao *et al.*, 1995; Valko *et al.*, 2007). Cathepsin B, a lysosomal cysteine protease that is released by LMP, has also been shown to translocate to the nucleus and cause DNA damage (Boya & Kroemer, 2008). In normal cells, DHA-derived lipid intermediates termed resolvins (17*S*-hydroxy-DHA) and protectins (protectin-D1) can conversely prevent liver damage by inhibiting DNA damage, COX-2 mRNA transcription, proinflammatory prostaglandin-E2 production and LPO (Calder, 2006; Gonzalez-Periz *et al.*, 2006). These protective effects of DHA were demonstrated *in vitro* when CC-1 hepatocytes were challenged with hydrogen peroxide, as

well as *in vivo* in mice with acute treatments of carbon tetrachloride (Gonzalez-Periz *et al.*, 2006). These studies illustrate how DHA may have opposite effects on DNA damage in normal and malignant cells.

The effect of LDL-DHA treatment on TIB-73 and TIB-75 cells was measured by quantification of γ-H2AX foci following a six hour or overnight treatment with 40 or 60 μM LDL-DHA or LDL-OA. The six-hour and eighteen-hour treatments showed a significant increase in the number of TIB-75 cells with γ-H2AX foci with 60 μM LDL-DHA, but only the eighteen-hour treatment was significant with the 40 μM LDL-DHA treatment. In contrast, no increase in foci formation was seen with LDL-DHA in TIB-73 cells or with LDL-OA treatments in either cell type or time point. The reason behind the increase in DNA damage in TIB-75 cells following LDL-DHA treatment is not known. Future experiments should examine the mechanism of DNA damage formation in TIB-75 cells by looking for 8-OH-G DNA lesion formation caused by hydroxyl radicals, lipid-DNA adduct formation caused by lipid peroxides, MDA-DNA adduct formation (Valko *et al.*, 2007), or ROS-induced p53 inactivation (Pelicano et al., 2004). In cancer cells, p53 loss promotes glycolysis, increased ROS production, inhibits apoptosis by multiple mechanisms (Gogvadze *et al.*, 2008). Loss of p53 can also make cancer cells more resistant to glutathione depletion because p53 normally suppresses SLC7A11, a cystine/glutamate antiporter component (Jiang *et al.*, 2015). Experiments conducted by other researchers have shown that TIB-75 cells have wild-type p53 expression (Gonzales *et al.*, 1998; Ogunwobi & Liu, 2011). Future experiments should also look at DNA damage in the human HCC cell lines as well as these

cells have different transcription and mutations of p53 that may alter their ability to respond to DNA damage (Bressac *et al.*, 1990; Kanno *et al.*, 2011; Puisieux *et al.*, 1993). Additionally, HBV infection status may affect the human HCC cell's ability to repair and respond to DNA damage as HBV can reduce nucleotide excision repair and block p53 induced cell death (Hussain *et al.*, 2007).

Iron Chelation Partially Rescues LDL-DHA Cytotoxicity

The last series of experiments looked at the role of iron in causing the cytotoxicity, LMP, and mitochondrial defects observed in TIB-75 cells following LDL-DHA treatment. Labile iron is a critical catalyst of the Fenton reaction, which generates hydroxyl radicals, hydrogen peroxide, and lipid peroxide species. Hypothetically, removing the pool of labile iron in the cell, especially in the lysosome, should protect TIB-75 cells from the deleterious effects of the ROS and LPO produced by the Fenton reaction. Other researchers have shown that iron chelation is sufficient to stop ferroptosis and LMP in cancer cells treated with cytotoxic agents (Dixon *et al.*, 2012; Kurz *et al.*, 2006). First, tests were conducted to examine the relative levels of iron in TIB-73 and TIB-75 cells, and overall the results suggest that TIB-75 cells have more iron than TIB-73 cells (ferrozine assay, silver sulfide autometallography staining, ICP-MS approaching significance at p-value = 0.075). This difference, however, was just an incremental increase in the levels of iron in TIB-75 cells. Importantly, the IP-1 fluorescent dye that measures labile iron strongly colocalized with the lysosome and TIB-75 cells, also, displayed a silver sulfide staining consistent with lysosomal iron accumulation.

These results are consistent with those found by other researchers that labile iron is stored predominantly in the lysosome of cells (Boya & Kroemer, 2008; Johansson *et al.*, 2010; Kurz *et al.*, 2006; Kurz *et al.*, 2008). To test the hypothesis that blocking the Fenton reaction with iron chelating agents can prevent LDL-DHA cytotoxicity, TIB-73 and TIB-75 cells were pretreated for three hours with the iron chelator, deferoxamine (DFO), prior to a twenty-four hour LDL-DHA treatment. DFO treatment partially rescued TIB-75 cells (viability maintained at≈75% of untreated cells) from LDL-DHA cytotoxicity. Interestingly, overloading TIB-73 cells using $FeCl_3$ did not increase their sensitivity to LDL-DHA cytotoxicity. In the future, TIB-73 cells may be sensitized to LDL-DHA treatment via iron-overloading if they are pretreated with Fe-nitrolotriacetate, which has four iron ligands making it an extremely potent catalyst of the Fenton reaction (Toyokuni, 2014). The effects of DFO iron chelation with LDL-DHA treatment on LPO production was also examined by BODIPY C11 581/591 flow cytometry and TBARS. The flow cytometry experiments showed that DFO was able to completely reverse LPO production in LDL-DHA treated TIB-73 and TIB-75 cells back to baseline. Iron chelation also significantly lowered TBARS levels following LDL-DHA treatment in TIB-75 cells, but it was not a full reversal of LPO when compared to untreated controls. The differences in the BODIPY C11 581/591 flow cytometry and TBARS results could be a result of the inherent differences in how the assays work. TBARS provides a global measure of aldehyde by-products of LPO while BODIPY C11 581/591 provides a local read out of active lipid peroxidation whereever the dye may distribute in the cell. These results indicate that lysosomal iron chelation by DFO is able to reduce LPO formation induced by LDL-DHA in TIB-75 cells. When lysosomal integrity of

TIB-75 cells was examined following DFO and LDL-DHA treatment, it was found that LMP was partially prevented as acridine orange red fluorescence was retained but not to the level of untreated cells. Next MMP loss was studied in TIB-73 and TIB-75 cells after iron chelation by DFO, the number of cells with MMP loss increased following DFO treatment with LDL-DHA in TIB-73 and TIB-75 cells. Surprisingly, TIB-73 cells experienced MMP loss with DFO treatment alone indicating that DFO may have deleterious off-target effects on the mitochondria. One hypothesis is that iron is necessary for cell viability because of its vital role as a cofactor in components of the ETC, antioxidant enzymes, and ROS-producing enzymes (Dixon & Stockwell, 2014; Toyokuni, 2014). Iron chelation by DFO may deplete TIB-73 cells of iron and cause mitochondrial dysfunction. However, TIB-73 cell viability was not negatively affected by DFO treatment so the mitochondrial dysfunction they experience may be at a level that is not harmful to their viability. Regardless, DFO did not prevent MMP loss in TIB-75 cells treated with LDL-DHA and even seemed to increase MMP loss. DFO pretreatment also did not lower DCF fluorescence in TIB-75 cells treated with LDL-DHA. Because DCF fluorescence may be increased by hydroxyl radical formation or cytochrome *c* release from the mitochondria, it is feasible DCF fluorescence was increased by the negative effects caused by DFO on the mitochondria. Treatment of TIB-73 and TIB-75 cells with a lipophilic iron chelator, salicyl-aldehyde isonicotinoyl hydrazone (SIH), may give a better indication of the effect of iron chelation on LDL-DHA cytotoxicity because SIH can freely diffuse in the cell and does not have deleterious effects on cell viability that have been observed with DFO (Dixon *et al.*, 2012; Kurz *et al.*, 2006). These experiments on the role of labile iron in LDL-DHA should be expanded in the future to the human HCC cell

lines to determine if Fenton reaction ROS and LPO production are important mediators in their LDL-DHA cytotoxicity. Additionally, the role of iron chelation on blocking LDL-DHA induced DNA damage should also be explored in normal and HCC cell lines. Sorafenib, a RAF kinase inhibitor that is FDA-approved for treatment of HCC, was able to induce ferroptosis independent of its kinase inhibitory capacity by blocking the cystine/glutamate antiporter (Lachaier *et al.*, 2014). Sorafenib's ability to induce ferroptosis is intriguing because a combination treatment of sorafenib and LDL-DHA may produce a synergistic induction of cell death by multiple pathways in HCC cells and this warrants further study.

Based on the studies contained herein, a model of LDL-DHA cytotoxicity in HCC cells can be proposed (Figure 11-1). HCC cells have increased lysosomal iron storage and ROS production creating a site for the Fenton reaction to occur. When HCC cells are treated with LDL-DHA that is taken into the lysosome by LDLR endocytosis, DHA is attacked by hydroxyl radicals generated in the Fenton reaction leading to large increases in DHA lipid peroxidation. These DHA lipid peroxides permeabilize the lysosome membrane, cause loss of mitochondrial membrane potential, increase mitochondrial ROS production, and DNA damage. These subcellular changes caused by LDL-DHA peroxidation cause cytotoxicity of the HCC cells.

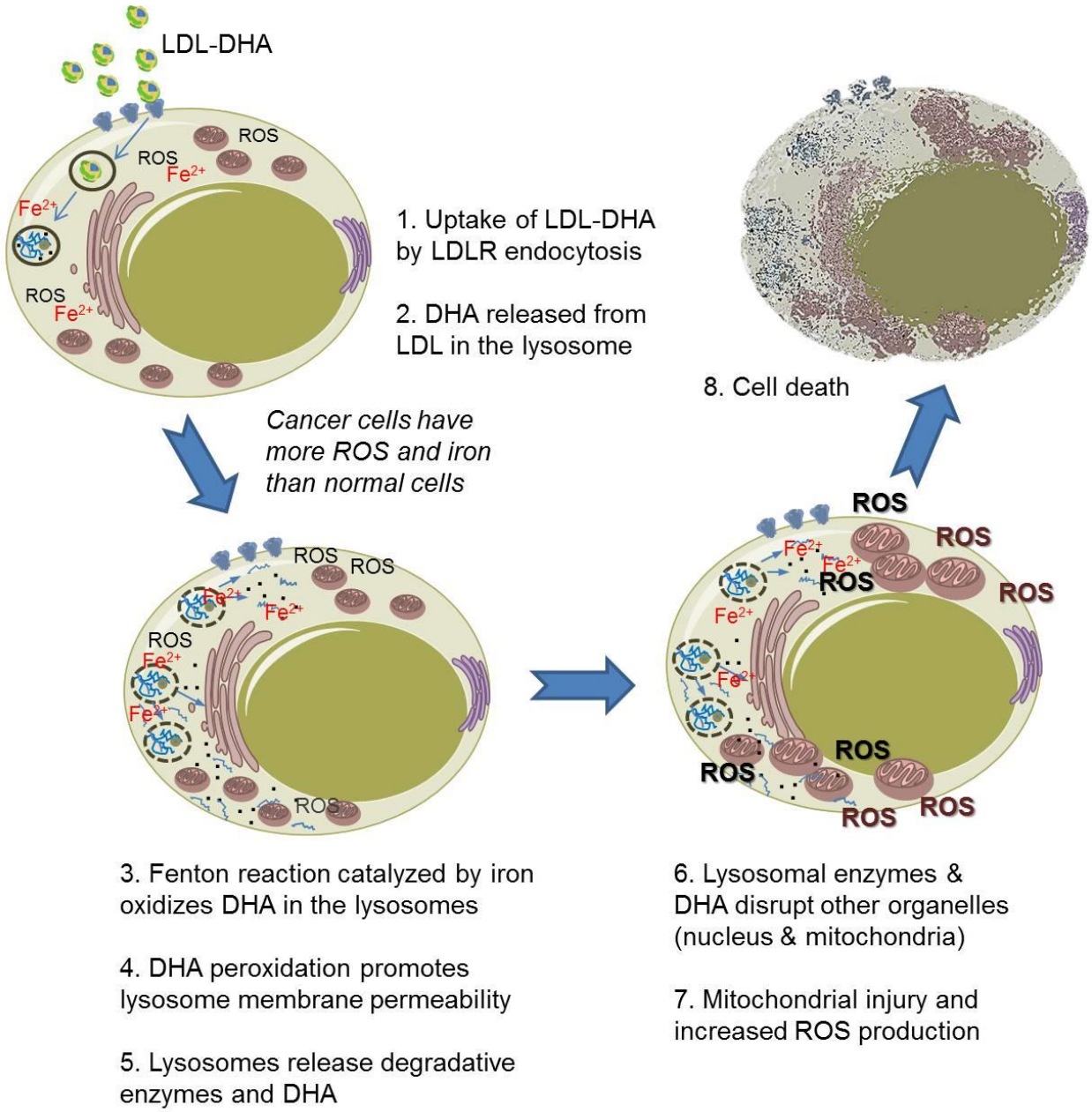

Figure 11-1: Conceptual figure of LDL-DHA induced cytotoxicity in HCC cells

LDL-DHA binds to LDLR and is endocytosed to the lysosome where DHA is released from LDL. DHA is oxidized by iron and hydrogen peroxide in the Fenton reaction. DHA peroxidation promotes lysosome membrane permeability and release of lysosomal enzymes to the cytosol. Lysosome membrane permeabilization, DHA peroxides, and ROS species promote organelle damage in the nucleus (DNA damage) and mitochondria. The mitochondrial injury promotes more ROS production. Eventually, the downstream actions of LDL-DHA result in HCC cell death.

Potential Challenges with LDL-DHA Therapy *in vivo*

The results of this research have shown the *in vitro* efficacy of LDL-DHA in selective cytotoxicity of HCC over normal hepatocytes. Pilot studies into the *in vivo* efficacy LDL-DHA in mice was explored as part of this research. Balb/C mice injected subcutaneously with TIB-75 cells were treated with intratumoral injection of 100 μM LDL-DHA/kg biweekly for two weeks. This pilot study was difficult for many reasons. One major problem was the difficulty in growing tumors of equivalent mass in the mice. Also, intratumoral injection of the nanoparticle caused leaking out of the injection site so the dose of LDL-DHA or LDL-OA was inconsistent between injections and between animals. Repeated injections of the tumor with a needle created mechanical damage of the tumor and scar tissue formation. There were also difficulties in being able to consistently measure tumor size; only length and width were measured to calculate volume, but some tumors were flat while others were very bulbous so the depth of the tumor played a significant part on the volume of the tumor that was not controlled for in this study. Based on these problems, any conclusions on the *in vivo* efficacy on TIB-75 tumors would be premature. Previous experiments conducted by other members of the Corbin laboratory showed *in vivo* efficacy of LDL-DHA in an orthotopic HCC model in rats where single transarterial treatments of LDL-DHA (2 mg/kg) impeded tumor cell proliferation as measured by Ki67 immunohistological staining, increased TBARS, and caused near complete necrosis of the tumors three or seven days after the treatment (data not shown). Studies are ongoing in the Corbin laboratory to study LDL-DHA cytotoxicity in mice with genetically-induced Myc-driven HCC.

It is also important to explore the potential difficulties in transitioning LDL-DHA HCC treatment into humans. One shortfall to using LDL as the DHA carrier is that the LDL-DHA must compete with endogenous LDL *in vivo* for LDLR binding and internalization. Fortunately, cancer patients usually present with low plasma LDL levels because their endogenous LDL supply is being exhausted by the needs of the tumor. If needed, native LDL levels could be suppressed by other means (eg. plasmapheresis) or LDLR levels and activity in the liver and adrenals could be suppressed to improve tumor uptake (Firestone, 1994). One study has even found that free fatty acids can upregulate LDLR protein expression in HepG2cells independent of SREBP-1(Yu-Poth *et al.*, 2005) such that DHA delivery by LDL may further increase LDLR expression, DHA uptake, and DHA's cytotoxicity in cancer cells. This research showed that LDLR overexpression in tumors is not necessary for LDL-DHA cytotoxicity as TIB-73 and TIB-75 cells have similar LDLR expression and uptake, but LDL can be targeted to other cellular receptors, such as the folate receptor, by modifying the lysine residues of ApoB-100 on LDL to increase its specificity for particular types of tumors (Zheng *et al.*, 2005).

Other potential problems with LDL-DHA treatment of HCC in humans are that the livers of these patients are diseased to some extent either by cirrhosis, fibrosis, steatohepatitis, hepatitis, or any combination of these. Hepatitis and other liver damage cause an accumulation of iron in hepatocytes over time as lipofuscin (Kurz *et al.*, 2008). This means that some patients, especially older men, are going to have livers with excess iron storage even if iron uptake is properly regulated. Women have menstrual cycles to reduce iron

accumulation over their lifetimes so excess iron storage in the liver is not as much of a concern in female patients (Kurz *et al.*, 2008). Excess iron storage in the hepatocytes makes them more susceptible to oxidative stress damage. Lipofuscin accumulation in the lysosomes of hepatocytes reduces autophagy, leading to accumulation of damaged organelles, especially mitochondria, which can increase ROS production. Overall, ageing and liver damage could sensitize the non-malignant liver tissue to LDL-DHA cytotoxicity due to excess iron accumulation and increased ROS production. In addition to iron accumulation, liver disease also has many genetic alterations that may be important in modulating LDL-DHA cytotoxicity. All of the studies conducted herein and in the Corbin laboratory have looked at LDL-DHA cytotoxicity to normal, healthy hepatocytes or in animals with healthy livers. It will be important to study the cytotoxicity of LDL-DHA in non-malignant, diseased hepatocytes. The diethyl nitrosamine (DEN) rat model of HCC would offer a good opportunity to study the safety of LDL-DHA treatment in diseased livers as this model develops HCC on a background of liver cirrhosis. Additionally, primary hepatocytes could be collected and studied from rodents treated with various hepatotoxins (eg. carbon tetrachloride or thioacetamide). Liver damage from HCV or HBV infection can be studied in a variety of transgenic and chimeric mouse models which are reviewed in Liu *et al.* (2013) and primary hepatocytes from these mice models could be tested for LDL-DHA sensitivity. The safety regulations needed for a laboratory to work with live HCV and HBV are strict and might make studying some of these models difficult to initiate. NAFLD and NASH are now considered one of the most common causes of liver dysfunction and can result in HCC development. There are also many mouse models (genetic, diet-induced, or a combination of

genetic and diet) that can be utilized to study LDL-DHA cytotoxicity in hepatocytes with NAFLD and NASH. Genetic models of NAFLD (eg. ob/ob mice) result from deficiencies in leptin signaling leading to obesity and insulin resistance and spontaneous occurrence of hepatic steatosis and Type II diabetes (Liu *et al.*, 2013). Mice with a liver-specific PTEN deletion develop NASH which will spontaneously progress to HCC and this model may be ideal to study the *in vivo* cytotoxicity of LDL-DHA against HCC on a diseased liver background (Horie *et al.*, 2004). LDL-DHA cytotoxicity in alcohol-induced liver disease could be studied in mice fed a 5% ethanol liquid diet for ten days and then given a bolus of ethanol by gavage (the chronic-binge model) as these mice develop severe liver injury, fatty livers, and elevated ALT and AST levels (Liu *et al.*, 2013). There are many mouse models available to determine LDL-DHA cytotoxicity in non-malignant hepatocytes with chronic liver disease. These models could also be used to determine if LDL-DHA treatment can ameliorate the chronic liver disease as DHA has been shown to aid cirrhosis, hepatic steatosis, and NAFLD (Fernandez *et al.*, 1997; Gonzalez-Periz *et al.*, 2006; Huang *et al.*, 2013; Jump *et al.*, 2008; Masterton *et al.*, 2010; Sekiya *et al.*, 2003; Takayama *et al.*, 2010; Valenzuela *et al.*, 2012; Videla *et al.*, 2004; Weylandt *et al.*, 2011).

Future studies should explore the efficacy of LDL-DHA *in vivo* on HCC tumor tissue as the *in vitro* studies contained herein showed very promising results. Further research should also be done into how LDL-DHA treatment can be expanded into treatment with other malignancies. Additionally, mass-production methods for LDL-DHA should be investigated to promote its rapid appropriation into clinical use.

APPENDIX A
LDL and LDL-DHA Transmission Electron Microscopy Micrographs

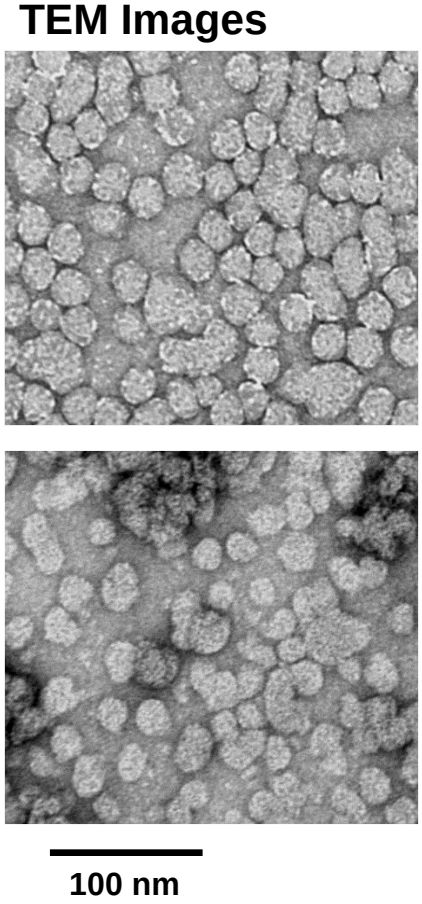

Appendix A: TEM of native LDL and LDL-DHA nanoparticles

Images of LDL (top) and LDL-DHA (bottom) obtained by Transmission Electron Microscopy (experiment performed by Dr. Rohit Mulik).

APPENDIX B
Annexin V-FITC/PI Staining

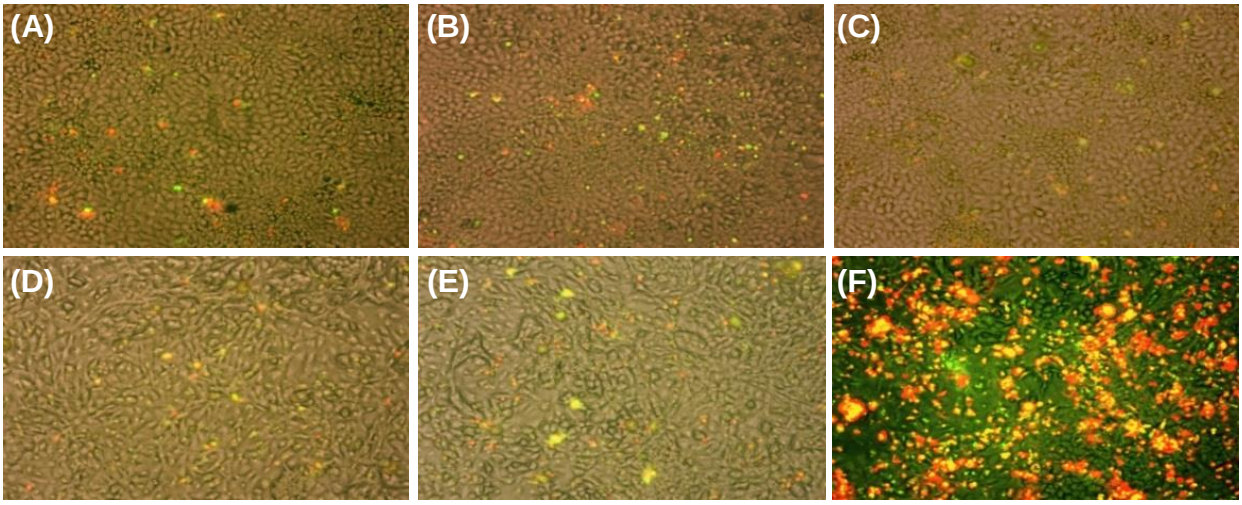

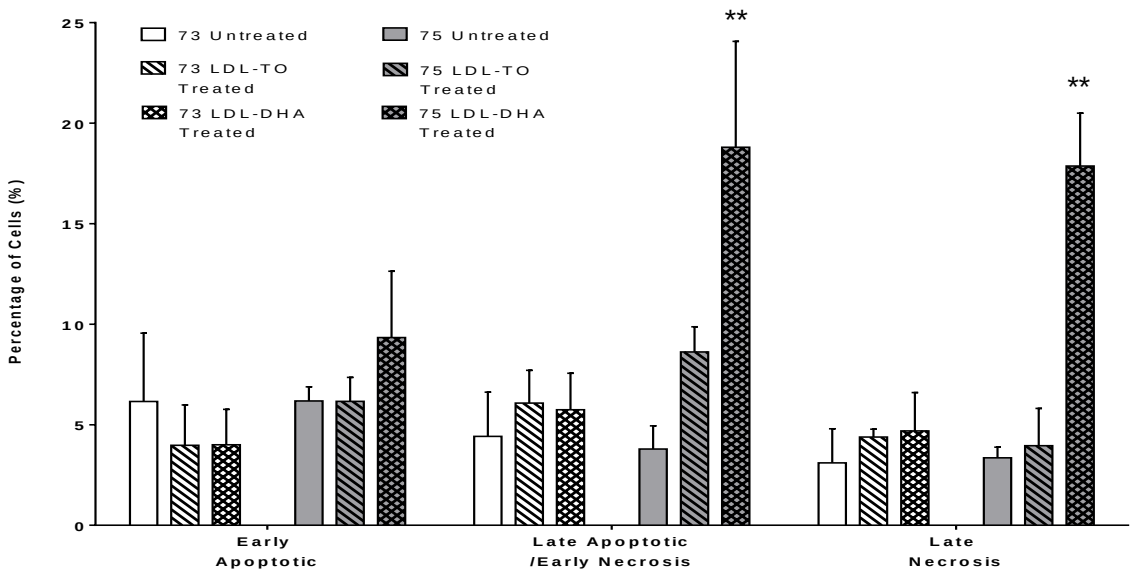

Appendix B: Annexin-V/PI fluorescent imaging and flow cytometry

(A–F) Fluorescence microscopy of TIB-73 and TIB-75 cells following a 72 hour treatment with LDL nanoparticles (40 μM). The mode of cell death was assessed by staining the cells with annexin V-fluorescein isothiocyanate to detect apoptosis (green) and propidium iodide to detect necrosis (red). Concurrent apoptosis and necrosis coregistered as yellow fluorescence. The treatment groups are as follows: **(A)** TIB-73 untreated; **(B)** TIB-73 LDL-TO treated; **(C)** TIB-73 LDL-DHA nanoparticle treated; **(D)** TIB-75 untreated; **(E)** TIB-75 LDL-TO treated; and **(F)** TIB-75 LDL-DHA nanoparticle treated. **(G)** Quantitative analysis of the same treatment groups was performed by FACS analysis using two-color flow cytometric measurements. Quadrant gating was used to determine the percentage of cells in different stages of apoptosis and necrosis. Results are expressed as percentage of total cell population.

* = p-value ≤0.05, ** = p-value ≤0.01, *** = p-value ≤0.001, **** = p-value ≤0.0001. The error bars represent the standard error of the mean. The experiment was performed by Dr. Rohit Mulik.

APPENDIX C
Subcutaneous TIB-75 Tumor Treatment

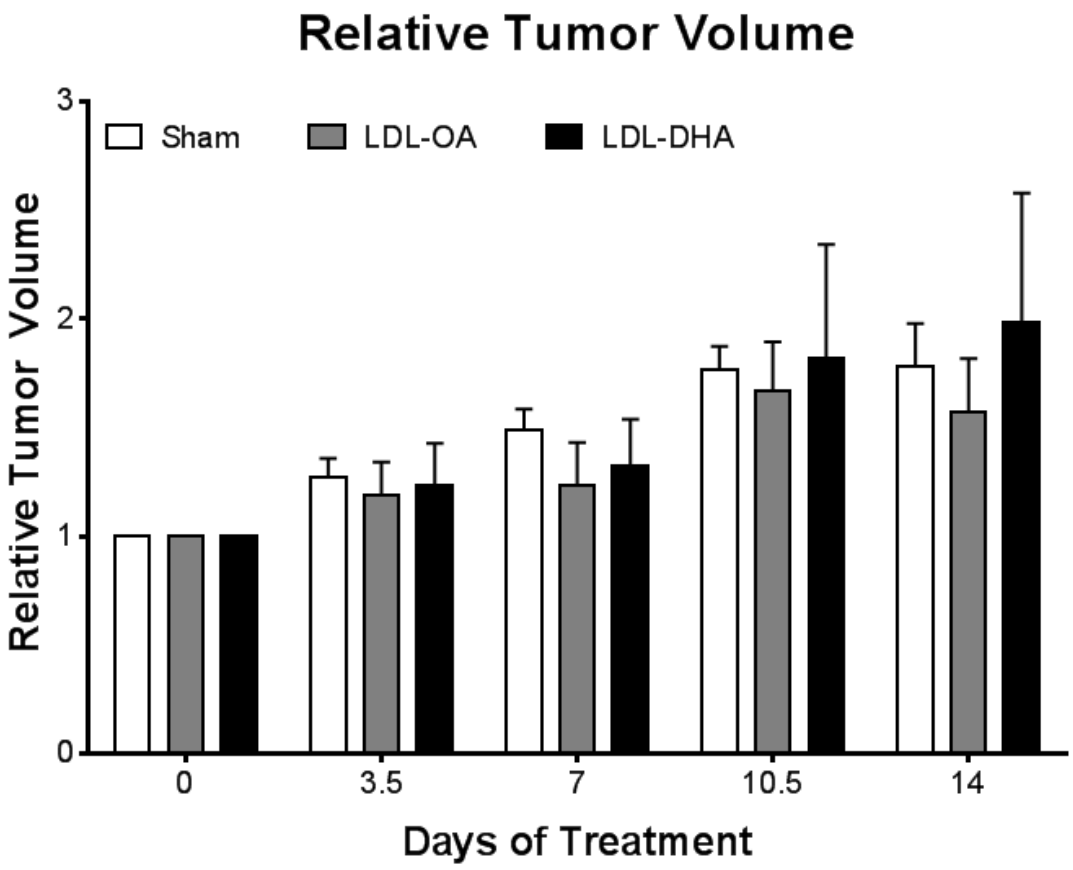

Appendix C: Relative tumor volume of TIB-75 subcutaneous tumors after LDL-DHA treatment

Balb/C mice were injected subcutaneously with TIB-75 cells and then treated with 100 μM LDL-DHA or LDL-OA twice a week for two weeks. Relative tumor volume was calculated as the size of the tumor after treatment divided by the initial size of the tumor. There was no significant change in relative tumor volume in LDL-DHA treated tumors and tumors treated with vehicle.

BIBLIOGRAPHY

Almaguel, F. G., Liu, J. W., Pacheco, F. J., De Leon, D., Casiano, C. A., & De Leon, M. (2010). Lipotoxicity-mediated cell dysfunction and death involve lysosomal membrane permeabilization and cathepsin L activity. *Brain Res, 1318*, 133-143. doi: 10.1016/j.brainres.2009.12.038

Altekruse, S. F., Henley, S. J., Cucinelli, J. E., & McGlynn, K. A. (2014). Changing hepatocellular carcinoma incidence and liver cancer mortality rates in the United States. *Am J Gastroenterol, 109*(4), 542-553. doi: 10.1038/ajg.2014.11

Arab, K., Rossary, A., Flourie, F., Tourneur, Y., & Steghens, J. P. (2006). Docosahexaenoic acid enhances the antioxidant response of human fibroblasts by upregulating gamma-glutamyl-cysteinyl ligase and glutathione reductase. *Br J Nutr, 95*(1), 18-26.

Arterburn, L. M., Hall, E. B., & Oken, H. (2006). Distribution, interconversion, and dose response of n-3 fatty acids in humans. *Am J Clin Nutr, 83*(6 Suppl), 1467S-1476S.

Au-Yeung, H. Y., Chan, J., Chantarojsiri, T., & Chang, C. J. (2013). Molecular imaging of labile iron(II) pools in living cells with a turn-on fluorescent probe. *J Am Chem Soc, 135*(40), 15165-15173. doi: 10.1021/ja4072964

Berg, J. M., Timoczko, John L., Stryer, Lubert. (2007). Fatty Acid Metabolism. In P. Zimmerman (Ed.), *Biochemistry* (6th ed., pp. 617-648). New York: W. H. Freeman and Company.

Berquin, I. M., Edwards, I. J., & Chen, Y. Q. (2008). Multi-targeted therapy of cancer by omega-3 fatty acids. *Cancer Lett, 269*(2), 363-377. doi: 10.1016/j.canlet.2008.03.044

Biondo, P. D., Brindley, D. N., Sawyer, M. B., & Field, C. J. (2008). The potential for treatment with dietary long-chain polyunsaturated n-3 fatty acids during chemotherapy. *J Nutr Biochem, 19*(12), 787-796. doi: 10.1016/j.jnutbio.2008.02.003

Bougnoux, P., Hajjaji, N., Ferrasson, M. N., Giraudeau, B., Couet, C., & Le Floch, O. (2009). Improving outcome of chemotherapy of metastatic breast cancer by docosahexaenoic acid: a phase II trial. *Br J Cancer, 101*(12), 1978-1985. doi: 10.1038/sj.bjc.6605441

Boya, P., & Kroemer, G. (2008). Lysosomal membrane permeabilization in cell death. *Oncogene, 27*(50), 6434-6451. doi: 10.1038/onc.2008.310

Bressac, B., Galvin, K. M., Liang, T. J., Isselbacher, K. J., Wands, J. R., & Ozturk, M. (1990). Abnormal structure and expression of p53 gene in human hepatocellular carcinoma. *Proc Natl Acad Sci U S A, 87*(5), 1973-1977.

Bruix, J., Boix, L., Sala, M., & Llovet, J. M. (2004). Focus on hepatocellular carcinoma. *Cancer Cell, 5*(3), 215-219.

Bruno, M. J., Koeppe, R. E., 2nd, & Andersen, O. S. (2007). Docosahexaenoic acid alters bilayer elastic properties. *Proc Natl Acad Sci U S A, 104*(23), 9638-9643. doi: 10.1073/pnas.0701015104

Calder, P. C. (2006). n-3 polyunsaturated fatty acids, inflammation, and inflammatory diseases. *Am J Clin Nutr, 83*(6 Suppl), 1505S-1519S.

Calviello, G., Resci, F., Serini, S., Piccioni, E., Toesca, A., Boninsegna, A., . . . Palozza, P. (2007). Docosahexaenoic acid induces proteasome-dependent degradation of beta-catenin, down-regulation of survivin and apoptosis in human colorectal cancer cells not expressing COX-2. *Carcinogenesis, 28*(6), 1202-1209. doi: 10.1093/carcin/bgl254

Cao, E. H., Liu, X. Q., Wang, L. G., Wang, J. J., & Xu, N. F. (1995). Evidence that lipid peroxidation products bind to DNA in liver cells. *Biochim Biophys Acta, 1259*(2), 187-191.

Cepinskas, G., Kvietys, P. R., & Aw, T. Y. (1994). Omega 3-lipid peroxides injure CaCo-2 cells: relationship to the development of reduced glutathione antioxidant systems. *Gastroenterology, 107*(1), 80-86.

Chen, Z. Y., & Istfan, N. W. (2000). Docosahexaenoic acid is a potent inducer of apoptosis in HT-29 colon cancer cells. *Prostaglandins Leukot Essent Fatty Acids, 63*(5), 301-308. doi: 10.1054/plef.2000.0218

Cheng, A. S., Chan, H. L., Leung, N. W., Liew, C. T., To, K. F., Lai, P. B., & Sung, J. J. (2002). Expression of cyclooxygenase-2 in chronic hepatitis B and the effects of anti-viral therapy. *Aliment Pharmacol Ther, 16*(2), 251-260.

Chiu, L. C., Wong, E. Y., & Ooi, V. E. (2004). Docosahexaenoic acid from a cultured microalga inhibits cell growth and induces apoptosis by upregulating Bax/Bcl-2 ratio in human breast carcinoma MCF-7 cells. *Ann N Y Acad Sci, 1030*, 361-368. doi: 10.1196/annals.1329.045

Conquer, J. A., & Holub, B. J. (1998). Effect of supplementation with different doses of DHA on the levels of circulating DHA as non-esterified fatty acid in subjects of Asian Indian background. *J Lipid Res, 39*(2), 286-292.

Corbin, I. R., Ng, K., & Zheng, G. (2011). 18. Lipoprotein-Based Nanoplatforms for Cancer Molecular Imaging. In X. Chen (Ed.), *Nanoplatform-Based Molecular Imaging* (X. Chen ed.). Hoboken, NJ, USA: John Wiley & Sons, Inc.

Corsetto, P. A., Montorfano, G., Zava, S., Jovenitti, I. E., Cremona, A., Berra, B., & Rizzo, A. M. (2011). Effects of n-3 PUFAs on breast cancer cells through their incorporation in plasma membrane. *Lipids Health Dis, 10*, 73. doi: 10.1186/1476-511X-10-73

Criddle, D. N., Gillies, S., Baumgartner-Wilson, H. K., Jaffar, M., Chinje, E. C., Passmore, S., . . . Petersen, O. H. (2006). Menadione-induced reactive oxygen species generation via redox cycling promotes apoptosis of murine pancreatic acinar cells. *J Biol Chem, 281*(52), 40485-40492. doi: 10.1074/jbc.M607704200

Crosby, A. J., Wahle, K. W., & Duthie, G. G. (1996). Modulation of glutathione peroxidase activity in human vascular endothelial cells by fatty acids and the cytokine interleukin-1 beta. *Biochim Biophys Acta, 1303*(3), 187-192.

Danscher, G. (1981). Histochemical demonstration of heavy metals. A revised version of the sulphide silver method suitable for both light and electronmicroscopy. *Histochemistry, 71*(1), 1-16.

Das, U. N., & Madhavi, N. (2011). Effect of polyunsaturated fatty acids on drug-sensitive and resistant tumor cells in vitro. *Lipids Health Dis, 10*, 159. doi: 10.1186/1476-511X-10-159

Ding, W. Q., & Lind, S. E. (2007). Phospholipid hydroperoxide glutathione peroxidase plays a role in protecting cancer cells from docosahexaenoic acid-induced cytotoxicity. *Mol Cancer Ther, 6*(4), 1467-1474. doi: 10.1158/1535-7163.MCT-06-0608

Ding, W. Q., Vaught, J. L., Yamauchi, H., & Lind, S. E. (2004). Differential sensitivity of cancer cells to docosahexaenoic acid-induced cytotoxicity: the potential importance of down-regulation of superoxide dismutase 1 expression. *Mol Cancer Ther, 3*(9), 1109-1117.

Dixon, S. J., Lemberg, K. M., Lamprecht, M. R., Skouta, R., Zaitsev, E. M., Gleason, C. E., . . . Stockwell, B. R. (2012). Ferroptosis: an iron-dependent form of nonapoptotic cell death. *Cell, 149*(5), 1060-1072. doi: 10.1016/j.cell.2012.03.042

Dixon, S. J., & Stockwell, B. R. (2014). The role of iron and reactive oxygen species in cell death. *Nat Chem Biol, 10*(1), 9-17. doi: 10.1038/nchembio.1416

Edwards, I. J., Berquin, I. M., Sun, H., O'Flaherty J, T., Daniel, L. W., Thomas, M. J., . . . Chen, Y. Q. (2004). Differential effects of delivery of omega-3 fatty acids to human cancer cells by low-density lipoproteins versus albumin. *Clin Cancer Res, 10*(24), 8275-8283. doi: 10.1158/1078-0432.CCR-04-1357

El-Serag, H. B., Marrero, J. A., Rudolph, L., & Reddy, K. R. (2008). Diagnosis and treatment of hepatocellular carcinoma. *Gastroenterology, 134*(6), 1752-1763. doi: 10.1053/j.gastro.2008.02.090

Erdahl, W. L., Krebsbach, R. J., & Pfeiffer, D. R. (1991). A comparison of phospholipid degradation by oxidation and hydrolysis during the mitochondrial permeability transition. *Arch Biochem Biophys, 285*(2), 252-260.

Farazi, P. A., & DePinho, R. A. (2006). Hepatocellular carcinoma pathogenesis: from genes to environment. *Nat Rev Cancer, 6*(9), 674-687. doi: 10.1038/nrc1934

Fauser, J. K., Prisciandaro, L. D., Cummins, A. G., & Howarth, G. S. (2011). Fatty acids as potential adjunctive colorectal chemotherapeutic agents. *Cancer Biol Ther, 11*(8), 724-731.

Fernandez, M. I., Torres, M. I., Gil, A., & Rios, A. (1997). Steatosis and collagen content in experimental liver cirrhosis are affected by dietary monounsaturated and polyunsaturated fatty acids. *Scand J Gastroenterol, 32*(4), 350-356.

Finkel, T. (2011). Signal transduction by reactive oxygen species. *J Cell Biol, 194*(1), 7-15. doi: 10.1083/jcb.201102095

Firestone, R. A. (1994). Low-density lipoprotein as a vehicle for targeting antitumor compounds to cancer cells. *Bioconjug Chem, 5*(2), 105-113.

Gao, L., Wang, J., Sekhar, K. R., Yin, H., Yared, N. F., Schneider, S. N., . . . Freeman, M. L. (2007). Novel n-3 fatty acid oxidation products activate Nrf2 by destabilizing the association between Keap1 and Cullin3. *J Biol Chem, 282*(4), 2529-2537. doi: 10.1074/jbc.M607622200

Garaiova, I., Guschina, I. A., Plummer, S. F., Tang, J., Wang, D., & Plummer, N. T. (2007). A randomised cross-over trial in healthy adults indicating improved absorption of omega-3 fatty acids by pre-emulsification. *Nutr J, 6*, 4. doi: 10.1186/1475-2891-6-4

Gogvadze, V., Orrenius, S., & Zhivotovsky, B. (2008). Mitochondria in cancer cells: what is so special about them? *Trends Cell Biol, 18*(4), 165-173. doi: 10.1016/j.tcb.2008.01.006

Goldstein, J. L., & Brown, M. S. (1974). Binding and degradation of low density lipoproteins by cultured human fibroblasts. Comparison of cells from a normal subject and from a patient with homozygous familial hypercholesterolemia. *J Biol Chem, 249*(16), 5153-5162.

Goldstein, J. L., & Brown, M. S. (1979). The LDL receptor locus and the genetics of familial hypercholesterolemia. *Annu Rev Genet, 13*, 259-289. doi: 10.1146/annurev.ge.13.120179.001355

Gomaa, A. I., Khan, S. A., Toledano, M. B., Waked, I., & Taylor-Robinson, S. D. (2008). Hepatocellular carcinoma: epidemiology, risk factors and pathogenesis. *World J Gastroenterol, 14*(27), 4300-4308.

Gonzales, A. J., Goldsworthy, T. L., & Fox, T. R. (1998). Chemical transformation of mouse liver cells results in altered cyclin D-CDK protein complexes. *Carcinogenesis, 19*(6), 1093-1102.

Gonzalez-Periz, A., Planaguma, A., Gronert, K., Miquel, R., Lopez-Parra, M., Titos, E., . . . Claria, J. (2006). Docosahexaenoic acid (DHA) blunts liver injury by conversion to protective lipid mediators: protectin D1 and 17S-hydroxy-DHA. *FASEB J, 20*(14), 2537-2539. doi: 10.1096/fj.06-6250fje

Gotoh, Y., Noda, T., Iwakiri, R., Fujimoto, K., Rhoads, C. A., & Aw, T. Y. (2002). Lipid peroxide-induced redox imbalance differentially mediates CaCo-2 cell proliferation and growth arrest. *Cell Prolif, 35*(4), 221-235.

Guo, W., Huang, N., Cai, J., Xie, W., & Hamilton, J. A. (2006). Fatty acid transport and metabolism in HepG2 cells. *Am J Physiol Gastrointest Liver Physiol, 290*(3), G528-534. doi: 10.1152/ajpgi.00386.2005

Hammel, M., Laggner, P., & Prassl, R. (2003). Structural characterisation of nucleoside loaded low density lipoprotein as a main criterion for the applicability as drug delivery system. *Chem Phys Lipids, 123*(2), 193-207.

Hanahan, D., & Weinberg, R. A. (2011). Hallmarks of cancer: the next generation. *Cell, 144*(5), 646-674. doi: 10.1016/j.cell.2011.02.013

Hardman, W. E., Munoz, J., Jr., & Cameron, I. L. (2002). Role of lipid peroxidation and antioxidant enzymes in omega 3 fatty acids induced suppression of breast cancer xenograft growth in mice. *Cancer Cell Int, 2*(1), 10.

Hart, P. D., & Young, M. R. (1991). Ammonium chloride, an inhibitor of phagosome-lysosome fusion in macrophages, concurrently induces phagosome-endosome fusion, and opens a novel pathway: studies of a pathogenic mycobacterium and a nonpathogenic yeast. *J Exp Med, 174*(4), 881-889.

He, L., Isselbacher, K. J., Wands, J. R., Goodman, H. M., Shih, C., & Quaroni, A. (1984). Establishment and characterization of a new human hepatocellular carcinoma cell line. *In Vitro, 20*(6), 493-504.

Hevonoja, T., Pentikainen, M. O., Hyvonen, M. T., Kovanen, P. T., & Ala-Korpela, M. (2000). Structure of low density lipoprotein (LDL) particles: basis for

understanding molecular changes in modified LDL. *Biochim Biophys Acta, 1488*(3), 189-210.

Hong, M. Y., Chapkin, R. S., Barhoumi, R., Burghardt, R. C., Turner, N. D., Henderson, C. E., . . . Lupton, J. R. (2002). Fish oil increases mitochondrial phospholipid unsaturation, upregulating reactive oxygen species and apoptosis in rat colonocytes. *Carcinogenesis, 23*(11), 1919-1925.

Hong, S., Gronert, K., Devchand, P. R., Moussignac, R. L., & Serhan, C. N. (2003). Novel docosatrienes and 17S-resolvins generated from docosahexaenoic acid in murine brain, human blood, and glial cells. Autacoids in anti-inflammation. *J Biol Chem, 278*(17), 14677-14687. doi: 10.1074/jbc.M300218200

Horie, Y., Suzuki, A., Kataoka, E., Sasaki, T., Hamada, K., Sasaki, J., . . . Nakano, T. (2004). Hepatocyte-specific Pten deficiency results in steatohepatitis and hepatocellular carcinomas. *J Clin Invest, 113*(12), 1774-1783. doi: 10.1172/JCI20513

Hussain, S. P., Schwank, J., Staib, F., Wang, X. W., & Harris, C. C. (2007). TP53 mutations and hepatocellular carcinoma: insights into the etiology and pathogenesis of liver cancer. *Oncogene, 26*(15), 2166-2176. doi: 10.1038/sj.onc.1210279

Ichihara, H., Zako, K., Komizu, Y., Goto, K., & Ueoka, R. (2011). Therapeutic effects of hybrid liposomes composed of phosphatidylcholine and docosahexaenoic acid on the hepatic metastasis of colon carcinoma along with apoptosis in vivo. *Biol Pharm Bull, 34*(6), 901-905.

Jenski, L. J., Zerouga, M., & Stillwell, W. (1995). Omega-3 fatty acid-containing liposomes in cancer therapy. *Proc Soc Exp Biol Med, 210*(3), 227-233.

Jiang, L., Kon, N., Li, T., Wang, S. J., Su, T., Hibshoosh, H., . . . Gu, W. (2015). Ferroptosis as a p53-mediated activity during tumour suppression. *Nature, 520*(7545), 57-62. doi: 10.1038/nature14344

Johansson, A. C., Appelqvist, H., Nilsson, C., Kagedal, K., Roberg, K., & Ollinger, K. (2010). Regulation of apoptosis-associated lysosomal membrane permeabilization. *Apoptosis, 15*(5), 527-540. doi: 10.1007/s10495-009-0452-5

Jump, D. B., Botolin, D., Wang, Y., Xu, J., Demeure, O., & Christian, B. (2008). Docosahexaenoic acid (DHA) and hepatic gene transcription. *Chem Phys Lipids, 153*(1), 3-13. doi: 10.1016/j.chemphyslip.2008.02.007

Kader, A., Davis, P. J., Kara, M., & Liu, H. (1998). Drug targeting using low density lipoprotein (LDL): physicochemical factors affecting drug loading into LDL particles. *J Control Release, 55*(2-3), 231-243.

Kader, A., & Pater, A. (2002). Loading anticancer drugs into HDL as well as LDL has little affect on properties of complexes and enhances cytotoxicity to human carcinoma cells. *J Control Release, 80*(1-3), 29-44.

Kafrawy, O., Zerouga, M., Stillwell, W., & Jenski, L. J. (1998). Docosahexaenoic acid in phosphatidylcholine mediates cytotoxicity more effectively than other omega-3 and omega-6 fatty acids. *Cancer Lett, 132*(1-2), 23-29.

Kamp, F., & Hamilton, J. A. (2006). How fatty acids of different chain length enter and leave cells by free diffusion. *Prostaglandins Leukot Essent Fatty Acids, 75*(3), 149-159. doi: 10.1016/j.plefa.2006.05.003

Kang, K. S., Wang, P., Yamabe, N., Fukui, M., Jay, T., & Zhu, B. T. (2010). Docosahexaenoic acid induces apoptosis in MCF-7 cells in vitro and in vivo via reactive oxygen species formation and caspase 8 activation. *PLoS One, 5*(4), e10296. doi: 10.1371/journal.pone.0010296

Kanno, S., Kurauchi, K., Tomizawa, A., Yomogida, S., & Ishikawa, M. (2011). Albumin modulates docosahexaenoic acid-induced cytotoxicity in human hepatocellular carcinoma cell lines. *Toxicol Lett, 200*(3), 154-161. doi: 10.1016/j.toxlet.2010.11.009

Karlsson, M., Kurz, T., Brunk, U. T., Nilsson, S. E., & Frennesson, C. I. (2010). What does the commonly used DCF test for oxidative stress really show? *Biochem J, 428*(2), 183-190. doi: 10.1042/BJ20100208

Katsura, N., Ikai, I., Mitaka, T., Shiotani, T., Yamanokuchi, S., Sugimoto, S., . . . Yamaoka, Y. (2002). Long-term culture of primary human hepatocytes with preservation of proliferative capacity and differentiated functions. *J Surg Res, 106*(1), 115-123.

Kennedy, A. S., & Salem, R. (2010). Radioembolization (yttrium-90 microspheres) for primary and metastatic hepatic malignancies. *Cancer J, 16*(2), 163-175. doi: 10.1097/PPO.0b013e3181d7e8cf

Kim, J., Lim, S. Y., Shin, A., Sung, M. K., Ro, J., Kang, H. S., . . . Lee, E. S. (2009). Fatty fish and fish omega-3 fatty acid intakes decrease the breast cancer risk: a case-control study. *BMC Cancer, 9*, 216. doi: 10.1186/1471-2407-9-216

Kim, Y. J., & Chung, H. Y. (2007). Antioxidative and anti-inflammatory actions of docosahexaenoic acid and eicosapentaenoic acid in renal epithelial cells and macrophages. *J Med Food, 10*(2), 225-231. doi: 10.1089/jmf.2006.092

Komatsu, W., Ishihara, K., Murata, M., Saito, H., & Shinohara, K. (2003). Docosahexaenoic acid suppresses nitric oxide production and inducible nitric oxide synthase expression in interferon-gamma plus lipopolysaccharide-stimulated murine macrophages by inhibiting the oxidative stress. *Free Radic Biol Med, 34*(8), 1006-1016.

Krieger, M. (1986). Reconstitution of the hydrophobic core of low-density lipoprotein. *Methods Enzymol, 128*, 608-613.

Krieger, M., Brown, M. S., Faust, J. R., & Goldstein, J. L. (1978). Replacement of endogenous cholesteryl esters of low density lipoprotein with exogenous cholesteryl linoleate. Reconstitution of a biologically active lipoprotein particle. *J Biol Chem, 253*(12), 4093-4101.

Krieger, M., McPhaul, M. J., Goldstein, J. L., & Brown, M. S. (1979). Replacement of neutral lipids of low density lipoprotein with esters of long chain unsaturated fatty acids. *J Biol Chem, 254*(10), 3845-3853.

Kuan, C. Y., Walker, T. H., Luo, P. G., & Chen, C. F. (2011). Long-chain polyunsaturated fatty acids promote paclitaxel cytotoxicity via inhibition of the

MDR1 gene in the human colon cancer Caco-2 cell line. *J Am Coll Nutr, 30*(4), 265-273.

Kubo, K., Saito, M., Tadokoro, T., & Maekawa, A. (1997). Changes in susceptibility of tissues to lipid peroxidation after ingestion of various levels of docosahexaenoic acid and vitamin E. *Br J Nutr, 78*(4), 655-669.

Kumar, B., Koul, S., Khandrika, L., Meacham, R. B., & Koul, H. K. (2008). Oxidative stress is inherent in prostate cancer cells and is required for aggressive phenotype. *Cancer Res, 68*(6), 1777-1785. doi: 10.1158/0008-5472.CAN-07-5259

Kurz, T., Gustafsson, B., & Brunk, U. T. (2006). Intralysosomal iron chelation protects against oxidative stress-induced cellular damage. *FEBS J, 273*(13), 3106-3117. doi: 10.1111/j.1742-4658.2006.05321.x

Kurz, T., Terman, A., Gustafsson, B., & Brunk, U. T. (2008). Lysosomes in iron metabolism, ageing and apoptosis. *Histochem Cell Biol, 129*(4), 389-406. doi: 10.1007/s00418-008-0394-y

Kusunoki, C., Yang, L., Yoshizaki, T., Nakagawa, F., Ishikado, A., Kondo, M., . . . Maegawa, H. (2013). Omega-3 polyunsaturated fatty acid has an anti-oxidant effect via the Nrf-2/HO-1 pathway in 3T3-L1 adipocytes. *Biochem Biophys Res Commun, 430*(1), 225-230. doi: 10.1016/j.bbrc.2012.10.115

Lachaier, E., Louandre, C., Godin, C., Saidak, Z., Baert, M., Diouf, M., . . . Galmiche, A. (2014). Sorafenib induces ferroptosis in human cancer cell lines originating from different solid tumors. *Anticancer Res, 34*(11), 6417-6422.

Larsson, S. C., Kumlin, M., Ingelman-Sundberg, M., & Wolk, A. (2004). Dietary long-chain n-3 fatty acids for the prevention of cancer: a review of potential mechanisms. *Am J Clin Nutr, 79*(6), 935-945.

Le Borgne, F. D., Jean. (2012). Interaction Between Peroxisomes and Mitochondria in Fatty Acid Metabolism. *Open Journal of Molecular and Integrative Physiology, 2*, 27-33. doi: 10.4236/ojmip.2012.210005

Lee, C. Y., Sit, W. H., Fan, S. T., Man, K., Jor, I. W., Wong, L. L., . . . Wan, J. M. (2010). The cell cycle effects of docosahexaenoic acid on human metastatic hepatocellular carcinoma proliferation. *Int J Oncol, 36*(4), 991-998.

Lee, S. E., Lim, J. W., & Kim, H. (2009). Activator protein-1 mediates docosahexaenoic acid-induced apoptosis of human gastric cancer cells. *Ann N Y Acad Sci, 1171*, 163-169. doi: 10.1111/j.1749-6632.2009.04716.x

Leu, G. Z., Lin, T. Y., & Hsu, J. T. (2004). Anti-HCV activities of selective polyunsaturated fatty acids. *Biochem Biophys Res Commun, 318*(1), 275-280. doi: 10.1016/j.bbrc.2004.04.019

Lien, E. L. (2009). Toxicology and safety of DHA. *Prostaglandins Leukot Essent Fatty Acids, 81*(2-3), 125-132. doi: 10.1016/j.plefa.2009.05.004

Lim, K., Han, C., Dai, Y., Shen, M., & Wu, T. (2009). Omega-3 polyunsaturated fatty acids inhibit hepatocellular carcinoma cell growth through blocking beta-catenin and cyclooxygenase-2. *Mol Cancer Ther, 8*(11), 3046-3055. doi: 10.1158/1535-7163.MCT-09-0551

Linke, M., Gordon, R. E., Brillard, M., Lecaille, F., Lalmanach, G., & Bromme, D. (2006). Degradation of apolipoprotein B-100 by lysosomal cysteine cathepsins. *Biol Chem, 387*(9), 1295-1303. doi: 10.1515/BC.2006.160

Liou, G. Y., & Storz, P. (2010). Reactive oxygen species in cancer. *Free Radic Res, 44*(5), 479-496. doi: 10.3109/10715761003667554

Liu, Y., Meyer, C., Xu, C., Weng, H., Hellerbrand, C., ten Dijke, P., & Dooley, S. (2013). Animal models of chronic liver diseases. *Am J Physiol Gastrointest Liver Physiol, 304*(5), G449-468. doi: 10.1152/ajpgi.00199.2012

Llovet, J. M., & Bruix, J. (2008). Novel advancements in the management of hepatocellular carcinoma in 2008. *J Hepatol, 48 Suppl 1*, S20-37. doi: 10.1016/j.jhep.2008.01.022

Llovet, J. M., Ricci, S., Mazzaferro, V., Hilgard, P., Gane, E., Blanc, J. F., . . . Bruix, J. (2008). Sorafenib in advanced hepatocellular carcinoma. *N Engl J Med, 359*(4), 378-390. doi: 10.1056/NEJMoa0708857

Lund-Katz, S., Laplaud, P. M., Phillips, M. C., & Chapman, M. J. (1998). Apolipoprotein B-100 conformation and particle surface charge in human LDL subspecies: implication for LDL receptor interaction. *Biochemistry, 37*(37), 12867-12874. doi: 10.1021/bi980828m

Luzio, J. P., Pryor, P. R., & Bright, N. A. (2007). Lysosomes: fusion and function. *Nat Rev Mol Cell Biol, 8*(8), 622-632. doi: 10.1038/nrm2217

Madsen, L., Rustan, A. C., Vaagenes, H., Berge, K., Dyroy, E., & Berge, R. K. (1999). Eicosapentaenoic and docosahexaenoic acid affect mitochondrial and peroxisomal fatty acid oxidation in relation to substrate preference. *Lipids, 34*(9), 951-963.

Martindale, J. L., & Holbrook, N. J. (2002). Cellular response to oxidative stress: signaling for suicide and survival. *J Cell Physiol, 192*(1), 1-15. doi: 10.1002/jcp.10119

Masquelier, M., Vitols, S., Palsson, M., Mars, U., Larsson, B. S., & Peterson, C. O. (2000). Low density lipoprotein as a carrier of cytostatics in cancer chemotherapy: study of stability of drug-carrier complexes in blood. *J Drug Target, 8*(3), 155-164. doi: 10.3109/10611860008996861

Massaro, M., Habib, A., Lubrano, L., Del Turco, S., Lazzerini, G., Bourcier, T., . . . De Caterina, R. (2006). The omega-3 fatty acid docosahexaenoate attenuates endothelial cyclooxygenase-2 induction through both NADP(H) oxidase and PKC epsilon inhibition. *Proc Natl Acad Sci U S A, 103*(41), 15184-15189. doi: 10.1073/pnas.0510086103

Masterton, G. S., Plevris, J. N., & Hayes, P. C. (2010). Review article: omega-3 fatty acids - a promising novel therapy for non-alcoholic fatty liver disease. *Aliment Pharmacol Ther, 31*(7), 679-692. doi: 10.1111/j.1365-2036.2010.04230.x

Merendino, N., Costantini, L., Manzi, L., Molinari, R., D'Eliseo, D., & Velotti, F. (2013). Dietary omega -3 polyunsaturated fatty acid DHA: a potential adjuvant in the treatment of cancer. *Biomed Res Int, 2013*, 310186. doi: 10.1155/2013/310186

Merendino, N., Loppi, B., D'Aquino, M., Molinari, R., Pessina, G., Romano, C., & Velotti, F. (2005). Docosahexaenoic acid induces apoptosis in the human PaCa-44

pancreatic cancer cell line by active reduced glutathione extrusion and lipid peroxidation. *Nutr Cancer, 52*(2), 225-233. doi: 10.1207/s15327914nc5202_12

Miura, Y., Takahara, K., Murata, Y., Utsumi, K., Tada, M., & Takahata, K. (2004). Docosahexaenoic acid induces apoptosis via the Bax-independent pathway in HL-60 cells. *Biosci Biotechnol Biochem, 68*(11), 2415-2417.

Mori, T. A. (2004). Effect of fish and fish oil-derived omega-3 fatty acids on lipid oxidation. *Redox Rep, 9*(4), 193-197. doi: 10.1179/135100004225005200

Murphy, R. A., Mourtzakis, M., Chu, Q. S., Baracos, V. E., Reiman, T., & Mazurak, V. C. (2011). Supplementation with fish oil increases first-line chemotherapy efficacy in patients with advanced nonsmall cell lung cancer. *Cancer, 117*(16), 3774-3780. doi: 10.1002/cncr.25933

Ng, Y., Barhoumi, R., Tjalkens, R. B., Fan, Y. Y., Kolar, S., Wang, N., . . . Chapkin, R. S. (2005). The role of docosahexaenoic acid in mediating mitochondrial membrane lipid oxidation and apoptosis in colonocytes. *Carcinogenesis, 26*(11), 1914-1921. doi: 10.1093/carcin/bgi163

Nylandsted, J., Gyrd-Hansen, M., Danielewicz, A., Fehrenbacher, N., Lademann, U., Hoyer-Hansen, M., . . . Jaattela, M. (2004). Heat shock protein 70 promotes cell survival by inhibiting lysosomal membrane permeabilization. *J Exp Med, 200*(4), 425-435. doi: 10.1084/jem.20040531

Ogunwobi, O. O., & Liu, C. (2011). Hepatocyte growth factor upregulation promotes carcinogenesis and epithelial-mesenchymal transition in hepatocellular carcinoma via Akt and COX-2 pathways. *Clin Exp Metastasis, 28*(8), 721-731. doi: 10.1007/s10585-011-9404-x

. Omegaven (1999). In Oley (Ed.).

Ozben, T. (2007). Oxidative stress and apoptosis: impact on cancer therapy. *J Pharm Sci, 96*(9), 2181-2196. doi: 10.1002/jps.20874

Park, K. S., Lim, J. W., & Kim, H. (2009). Inhibitory mechanism of omega-3 fatty acids in pancreatic inflammation and apoptosis. *Ann N Y Acad Sci, 1171*, 421-427. doi: 10.1111/j.1749-6632.2009.04887.x

Parkinson, A. P. B. W. O. D. B. B. F. K. M. C. O. (2013). Chapter 6: Biotransformation of Xenobiotics. In C. D. Klaassen (Ed.), *Casaratt and Doull's Toxicology:The Basic Science of Poisons* (8th ed.). New York: McGraw Hill Professional.

Patek, P. Q., Collins, J. L., & Cohn, M. (1978). Transformed cell lines susceptible or resistant to in vivo surveillance against tumorigenesis. *Nature, 276*(5687), 510-511.

Pelicano, H., Carney, D., & Huang, P. (2004). ROS stress in cancer cells and therapeutic implications. *Drug Resist Updat, 7*(2), 97-110. doi: 10.1016/j.drup.2004.01.004

Peshavariya, H. M., Dusting, G. J., & Selemidis, S. (2007). Analysis of dihydroethidium fluorescence for the detection of intracellular and extracellular superoxide produced by NADPH oxidase. *Free Radic Res, 41*(6), 699-712. doi: 10.1080/10715760701297354

Puisieux, A., Galvin, K., Troalen, F., Bressac, B., Marcais, C., Galun, E., . . . Ozturk, M. (1993). Retinoblastoma and p53 tumor suppressor genes in human hepatoma cell lines. *FASEB J, 7*(14), 1407-1413.

Quilliot, D., Walters, E., Bohme, P., Lacroix, B., Bonte, J. P., Fruchart, J. C., . . . Ziegler, O. (2003). Fatty acid abnormalities in chronic pancreatitis: effect of concomitant diabetes mellitus. *Eur J Clin Nutr, 57*(3), 496-503. doi: 10.1038/sj.ejcn.1601556

Raatz, S. K., Redmon, J. B., Wimmergren, N., Donadio, J. V., & Bibus, D. M. (2009). Enhanced absorption of n-3 fatty acids from emulsified compared with encapsulated fish oil. *J Am Diet Assoc, 109*(6), 1076-1081. doi: 10.1016/j.jada.2009.03.006

Rahman, I., Kode, A., & Biswas, S. K. (2006). Assay for quantitative determination of glutathione and glutathione disulfide levels using enzymatic recycling method. *Nat Protoc, 1*(6), 3159-3165. doi: 10.1038/nprot.2006.378

Research, A. A. o. C. (2011). AACR Cancer Progress Report 2011 (pp. 1-84).

Reuter, S., Gupta, S. C., Chaturvedi, M. M., & Aggarwal, B. B. (2010). Oxidative stress, inflammation, and cancer: how are they linked? *Free Radic Biol Med, 49*(11), 1603-1616. doi: 10.1016/j.freeradbiomed.2010.09.006

Reynolds, L., Mulik, R. S., Wen, X., Dilip, A., & Corbin, I. R. (2014). Low-density lipoprotein-mediated delivery of docosahexaenoic acid selectively kills murine liver cancer cells. *Nanomedicine (Lond), 9*(14), 2123-2141. doi: 10.2217/nnm.13.187

Ringbom, T., Huss, U., Stenholm, A., Flock, S., Skattebol, L., Perera, P., & Bohlin, L. (2001). Cox-2 inhibitory effects of naturally occurring and modified fatty acids. *J Nat Prod, 64*(6), 745-749.

Roche, M., Rondeau, P., Singh, N. R., Tarnus, E., & Bourdon, E. (2008). The antioxidant properties of serum albumin. *FEBS Lett, 582*(13), 1783-1787. doi: 10.1016/j.febslet.2008.04.057

Ryter, S. W., Kim, H. P., Hoetzel, A., Park, J. W., Nakahira, K., Wang, X., & Choi, A. M. (2007). Mechanisms of cell death in oxidative stress. *Antioxid Redox Signal, 9*(1), 49-89. doi: 10.1089/ars.2007.9.49

Sakurai, T., He, G., Matsuzawa, A., Yu, G. Y., Maeda, S., Hardiman, G., & Karin, M. (2008). Hepatocyte necrosis induced by oxidative stress and IL-1 alpha release mediate carcinogen-induced compensatory proliferation and liver tumorigenesis. *Cancer Cell, 14*(2), 156-165. doi: 10.1016/j.ccr.2008.06.016

Salem, R., Lewandowski, R. J., Kulik, L., Wang, E., Riaz, A., Ryu, R. K., . . . Mulcahy, M. F. (2011). Radioembolization results in longer time-to-progression and reduced toxicity compared with chemoembolization in patients with hepatocellular carcinoma. *Gastroenterology, 140*(2), 497-507 e492. doi: 10.1053/j.gastro.2010.10.049

Sampath, H., & Ntambi, J. M. (2005). Polyunsaturated fatty acid regulation of genes of lipid metabolism. *Annu Rev Nutr, 25*, 317-340. doi: 10.1146/annurev.nutr.25.051804.101917

Sato, S. B., Sato, S., Kawamoto, J., & Kurihara, T. (2011). Differential roles of internal and terminal double bonds in docosahexaenoic acid: Comparative study of cytotoxicity of polyunsaturated fatty acids to HT-29 human colorectal tumor cell line. *Prostaglandins Leukot Essent Fatty Acids, 84*(1-2), 31-37. doi: 10.1016/j.plefa.2010.09.006

Sawada, N., Inoue, M., Iwasaki, M., Sasazuki, S., Shimazu, T., Yamaji, T., . . . Japan Public Health Center-Based Prospective Study, G. (2012). Consumption of n-3 fatty acids and fish reduces risk of hepatocellular carcinoma. *Gastroenterology, 142*(7), 1468-1475. doi: 10.1053/j.gastro.2012.02.018

Scheffer, P. G., Bakker, S. J., Heine, R. J., & Teerlink, T. (1998). Measurement of LDL particle size in whole plasma and serum by high performance gel-filtration chromatography using a fluorescent lipid probe. *Clin Chem, 44*(10), 2148-2151.

Schley, P. D., Jijon, H. B., Robinson, L. E., & Field, C. J. (2005). Mechanisms of omega-3 fatty acid-induced growth inhibition in MDA-MB-231 human breast cancer cells. *Breast Cancer Res Treat, 92*(2), 187-195. doi: 10.1007/s10549-005-2415-z

Schonfeld, P., & Wojtczak, L. (2007). Fatty acids decrease mitochondrial generation of reactive oxygen species at the reverse electron transport but increase it at the forward transport. *Biochim Biophys Acta, 1767*(8), 1032-1040. doi: 10.1016/j.bbabio.2007.04.005

Schuchardt, J. P., & Hahn, A. (2013). Bioavailability of long-chain omega-3 fatty acids. *Prostaglandins Leukot Essent Fatty Acids, 89*(1), 1-8. doi: 10.1016/j.plefa.2013.03.010

Sekiya, M., Yahagi, N., Matsuzaka, T., Najima, Y., Nakakuki, M., Nagai, R., . . . Shimano, H. (2003). Polyunsaturated fatty acids ameliorate hepatic steatosis in obese mice by SREBP-1 suppression. *Hepatology, 38*(6), 1529-1539. doi: 10.1016/j.hep.2003.09.028

Serini, S., Trombino, S., Oliva, F., Piccioni, E., Monego, G., Resci, F., . . . Calviello, G. (2008). Docosahexaenoic acid induces apoptosis in lung cancer cells by increasing MKP-1 and down-regulating p-ERK1/2 and p-p38 expression. *Apoptosis, 13*(9), 1172-1183. doi: 10.1007/s10495-008-0246-1

Shaikh, S. R., Rockett, B. D., Salameh, M., & Carraway, K. (2009). Docosahexaenoic acid modifies the clustering and size of lipid rafts and the lateral organization and surface expression of MHC class I of EL4 cells. *J Nutr, 139*(9), 1632-1639. doi: 10.3945/jn.109.108720

Shaw, J. M., & Shaw, K. V. (1991). Key issues in the delivery of pharmacological agents using lipoproteins: design of a synthetic apoprotein-lipid carrier. *Targeted Diagn Ther, 5*, 351-383.

Shen, B. W., Scanu, A. M., & Kezdy, F. J. (1977). Structure of human serum lipoproteins inferred from compositional analysis. *Proc Natl Acad Sci U S A, 74*(3), 837-841.

Shimazawa, M., Nakajima, Y., Mashima, Y., & Hara, H. (2009). Docosahexaenoic acid (DHA) has neuroprotective effects against oxidative stress in retinal ganglion cells. *Brain Res, 1251*, 269-275. doi: 10.1016/j.brainres.2008.11.031

Siddiqui, R. A., Harvey, K., & Stillwell, W. (2008). Anticancer properties of oxidation products of docosahexaenoic acid. *Chem Phys Lipids, 153*(1), 47-56. doi: 10.1016/j.chemphyslip.2008.02.009

Skender, B., Vaculova, A. H., & Hofmanova, J. (2012). Docosahexaenoic fatty acid (DHA) in the regulation of colon cell growth and cell death: a review. *Biomed Pap Med Fac Univ Palacky Olomouc Czech Repub, 156*(3), 186-199. doi: 10.5507/bp.2012.093

Skotland, T., Iversen, T. G., & Sandvig, K. (2014). Development of nanoparticles for clinical use. *Nanomedicine (Lond), 9*(9), 1295-1299. doi: 10.2217/nnm.14.81

Skouta, R., Dixon, S. J., Wang, J., Dunn, D. E., Orman, M., Shimada, K., . . . Stockwell, B. R. (2014). Ferrostatins inhibit oxidative lipid damage and cell death in diverse disease models. *J Am Chem Soc, 136*(12), 4551-4556. doi: 10.1021/ja411006a

Sneddon, A. A., Wu, H. C., Farquharson, A., Grant, I., Arthur, J. R., Rotondo, D., . . . Wahle, K. W. (2003). Regulation of selenoprotein GPx4 expression and activity in human endothelial cells by fatty acids, cytokines and antioxidants. *Atherosclerosis, 171*(1), 57-65.

Sodeoka, M., & Dodo, K. (2010). Development of selective inhibitors of necrosis. *Chem Rec, 10*(5), 308-314. doi: 10.1002/tcr.201000031

Sotgia, F., Martinez-Outschoorn, U. E., & Lisanti, M. P. (2011). Mitochondrial oxidative stress drives tumor progression and metastasis: should we use antioxidants as a key component of cancer treatment and prevention? *BMC Med, 9*, 62. doi: 10.1186/1741-7015-9-62

Stillwell, W., Ehringer, W., & Jenski, L. J. (1993). Docosahexaenoic acid increases permeability of lipid vesicles and tumor cells. *Lipids, 28*(2), 103-108.

Stillwell, W., Shaikh, S. R., Zerouga, M., Siddiqui, R., & Wassall, S. R. (2005). Docosahexaenoic acid affects cell signaling by altering lipid rafts. *Reprod Nutr Dev, 45*(5), 559-579. doi: 10.1051/rnd:2005046

Stoll, B. A. (2002). N-3 fatty acids and lipid peroxidation in breast cancer inhibition. *Br J Nutr, 87*(3), 193-198. doi: 10.1079/BJNBJN2001512

Sun, H., Hu, Y., Gu, Z., Owens, R. T., Chen, Y. Q., & Edwards, I. J. (2011). Omega-3 fatty acids induce apoptosis in human breast cancer cells and mouse mammary tissue through syndecan-1 inhibition of the MEK-Erk pathway. *Carcinogenesis, 32*(10), 1518-1524. doi: 10.1093/carcin/bgr132

Sun, H., Meng, X., Han, J., Zhang, Z., Wang, B., Bai, X., & Zhang, X. (2013). Anti-cancer activity of DHA on gastric cancer--an in vitro and in vivo study. *Tumour Biol, 34*(6), 3791-3800. doi: 10.1007/s13277-013-0963-0

Sun, S. N., Jia, W. D., Chen, H., Ma, J. L., Ge, Y. S., Yu, J. H., & Li, J. S. (2013). Docosahexaenoic acid (DHA) induces apoptosis in human hepatocellular carcinoma cells. *Int J Clin Exp Pathol, 6*(2), 281-289.

Sun, Y., Tang, X. M., Half, E., Kuo, M. T., & Sinicrope, F. A. (2002). Cyclooxygenase-2 overexpression reduces apoptotic susceptibility by inhibiting the cytochrome c-dependent apoptotic pathway in human colon cancer cells. *Cancer Res, 62*(21), 6323-6328.

Tait, S. W., & Green, D. R. (2008). Caspase-independent cell death: leaving the set without the final cut. *Oncogene, 27*(50), 6452-6461. doi: 10.1038/onc.2008.311

Takahashi, M., Tsuboyama-Kasaoka, N., Nakatani, T., Ishii, M., Tsutsumi, S., Aburatani, H., & Ezaki, O. (2002). Fish oil feeding alters liver gene expressions to defend against PPARalpha activation and ROS production. *Am J Physiol Gastrointest Liver Physiol, 282*(2), G338-348. doi: 10.1152/ajpgi.00376.2001

Tanaka, Y., Goto, K., Matsumoto, Y., & Ueoka, R. (2008). Remarkably high inhibitory effects of docosahexaenoic acid incorporated into hybrid liposomes on the growth

of tumor cells along with apoptosis. *Int J Pharm, 359*(1-2), 264-271. doi: 10.1016/j.ijpharm.2008.03.045

Toit-Kohn, J. L., Louw, L., & Engelbrecht, A. M. (2009). Docosahexaenoic acid induces apoptosis in colorectal carcinoma cells by modulating the PI3 kinase and p38 MAPK pathways. *J Nutr Biochem, 20*(2), 106-114. doi: 10.1016/j.jnutbio.2007.12.005

Toyokuni, S. (2014). Iron and thiols as two major players in carcinogenesis: friends or foes? *Front Pharmacol, 5*, 200. doi: 10.3389/fphar.2014.00200

Truong, T. Q., Auger, A., Denizeau, F., & Brissette, L. (2000). Analysis of low-density lipoprotein catabolism by primary cultures of hepatic cells from normal and low-density lipoprotein receptor knockout mice. *Biochim Biophys Acta, 1484*(2-3), 307-315.

Tuller, E. R., Beavers, C. T., Lou, J. R., Ihnat, M. A., Benbrook, D. M., & Ding, W. Q. (2009). Docosahexaenoic acid inhibits superoxide dismutase 1 gene transcription in human cancer cells: the involvement of peroxisome proliferator-activated receptor alpha and hypoxia-inducible factor-2alpha signaling. *Mol Pharmacol, 76*(3), 588-595. doi: 10.1124/mol.109.057430

Valenzuela, R., Espinosa, A., Gonzalez-Manan, D., D'Espessailles, A., Fernandez, V., Videla, L. A., & Tapia, G. (2012). N-3 long-chain polyunsaturated fatty acid supplementation significantly reduces liver oxidative stress in high fat induced steatosis. *PLoS One, 7*(10), e46400. doi: 10.1371/journal.pone.0046400

Valko, M., Leibfritz, D., Moncol, J., Cronin, M. T., Mazur, M., & Telser, J. (2007). Free radicals and antioxidants in normal physiological functions and human disease. *Int J Biochem Cell Biol, 39*(1), 44-84. doi: 10.1016/j.biocel.2006.07.001

VanRollins, M., Baker, R. C., Sprecher, H. W., & Murphy, R. C. (1984). Oxidation of docosahexaenoic acid by rat liver microsomes. *J Biol Chem, 259*(9), 5776-5783.

Vibet, S., Goupille, C., Bougnoux, P., Steghens, J. P., Gore, J., & Maheo, K. (2008). Sensitization by docosahexaenoic acid (DHA) of breast cancer cells to anthracyclines through loss of glutathione peroxidase (GPx1) response. *Free Radic Biol Med, 44*(7), 1483-1491. doi: 10.1016/j.freeradbiomed.2008.01.009

Videla, L. A., Rodrigo, R., Araya, J., & Poniachik, J. (2004). Oxidative stress and depletion of hepatic long-chain polyunsaturated fatty acids may contribute to nonalcoholic fatty liver disease. *Free Radic Biol Med, 37*(9), 1499-1507. doi: 10.1016/j.freeradbiomed.2004.06.033

Visioli, F., Giordano, E., Nicod, N. M., & Davalos, A. (2012). Molecular targets of omega 3 and conjugated linoleic Fatty acids - "micromanaging" cellular response. *Front Physiol, 3*, 42. doi: 10.3389/fphys.2012.00042

Wallace, D. C. (2012). Mitochondria and cancer. *Nat Rev Cancer, 12*(10), 685-698. doi: 10.1038/nrc3365

Wang, H., & Joseph, J. A. (1999). Quantifying cellular oxidative stress by dichlorofluorescein assay using microplate reader. *Free Radic Biol Med, 27*(5-6), 612-616.

Wang, X. W., Hussain, S. P., Huo, T. I., Wu, C. G., Forgues, M., Hofseth, L. J., . . . Harris, C. C. (2002). Molecular pathogenesis of human hepatocellular carcinoma. *Toxicology, 181-182*, 43-47.

Ward, P. S., & Thompson, C. B. (2012). Metabolic reprogramming: a cancer hallmark even warburg did not anticipate. *Cancer Cell, 21*(3), 297-308. doi: 10.1016/j.ccr.2012.02.014

Watkins, S. M., Carter, L. C., & German, J. B. (1998). Docosahexaenoic acid accumulates in cardiolipin and enhances HT-29 cell oxidant production. *J Lipid Res, 39*(8), 1583-1588.

Weylandt, K. H., Krause, L. F., Gomolka, B., Chiu, C. Y., Bilal, S., Nadolny, A., . . . Kang, J. X. (2011). Suppressed liver tumorigenesis in fat-1 mice with elevated omega-3 fatty acids is associated with increased omega-3 derived lipid mediators and reduced TNF-alpha. *Carcinogenesis, 32*(6), 897-903. doi: 10.1093/carcin/bgr049

Wu, Q., Yu, J. C., Liu, Y. Q., Kang, W. M., & Guo, W. D. (2010). [Effect of combination of docosahexaenoic acid and fluorouracil on human gastric carcinoma cell strain MGC803]. *Zhongguo Yi Xue Ke Xue Yuan Xue Bao, 32*(1), 65-70. doi: 10.3881/j.issn.1000-503X.2010.01.016

Xue, M., Wang, Q., Zhao, J., Dong, L., Ge, Y., Hou, L., . . . Zheng, Z. (2014). Docosahexaenoic acid inhibited the Wnt/beta-catenin pathway and suppressed breast cancer cells in vitro and in vivo. *J Nutr Biochem, 25*(2), 104-110. doi: 10.1016/j.jnutbio.2013.09.008

Yamagami, T., Porada, C. D., Pardini, R. S., Zanjani, E. D., & Almeida-Porada, G. (2009). Docosahexaenoic acid induces dose dependent cell death in an early undifferentiated subtype of acute myeloid leukemia cell line. *Cancer Biol Ther, 8*(4), 331-337.

Yang, W. S., SriRamaratnam, R., Welsch, M. E., Shimada, K., Skouta, R., Viswanathan, V. S., . . . Stockwell, B. R. (2014). Regulation of ferroptotic cancer cell death by GPX4. *Cell, 156*(1-2), 317-331. doi: 10.1016/j.cell.2013.12.010

Ying, W. (2008). NAD+/NADH and NADP+/NADPH in cellular functions and cell death: regulation and biological consequences. *Antioxid Redox Signal, 10*(2), 179-206. doi: 10.1089/ars.2007.1672

Yu-Poth, S., Yin, D., Kris-Etherton, P. M., Zhao, G., & Etherton, T. D. (2005). Long-chain polyunsaturated fatty acids upregulate LDL receptor protein expression in fibroblasts and HepG2 cells. *J Nutr, 135*(11), 2541-2545.

Zakim, D. (1996). Fatty acids enter cells by simple diffusion. *Proc Soc Exp Biol Med, 212*(1), 5-14.

Zakim, D. (2000). Thermodynamics of fatty acid transfer. *J Membr Biol, 176*(2), 101-109.

Zheng, G., Chen, J., Li, H., & Glickson, J. D. (2005). Rerouting lipoprotein nanoparticles to selected alternate receptors for the targeted delivery of cancer diagnostic and therapeutic agents. *Proc Natl Acad Sci U S A, 102*(49), 17757-17762. doi: 10.1073/pnas.0508677102

Zhu, A. X. (2006). Systemic therapy of advanced hepatocellular carcinoma: how hopeful should we be? *Oncologist*, *11*(7), 790-800. doi: 10.1634/theoncologist.11-7-790

Zitka, O., Skalickova, S., Gumulec, J., Masarik, M., Adam, V., Hubalek, J., . . . Kizek, R. (2012). Redox status expressed as GSH:GSSG ratio as a marker for oxidative stress in paediatric tumour patients. *Oncol Lett*, *4*(6), 1247-1253. doi: 10.3892/ol.2012.931